OECD/MCCI-2004-TR05

OECD MCCI Project

2-D Core Concrete Interaction (CCI) Tests:

CCI-2 Test Data Report-Thermalhydraulic Results

Rev. 0 October 15, 2004

by:

M. T. Farmer, S. Lomperski, D. J. Kilsdonk, and R. W. Aeschlimann
Nuclear Engineering Division
Argonne National Laboratory
9700 S. Cass Avenue
Argonne, IL 60439 USA

S. Basu
Project Manager
U.S. Nuclear Regulatory Commission

Table of Contents

Page

1.0 INTRODUCTION 1

2.0 FACILITY DESCRIPTION 3

2.1 Test Apparatus 3

2.2 Water Supply System 12

2.3 Quench System 13

2.4 Test Section Pressure Relief System 15

2.5 Off Gas System 15

2.6 Cover Gas System 16

2.7 Power Supply 18

2.8 Concrete Sidewalls and Basemat 18

2.9 Corium Composition 19

2.10 Instrumentation and Data Acquisition 20

3.0 TEST PROCEDURES 28

3.1 Pretest Operations 28

3.2 Test Operations 30

4.0 TEST RESULTS 36

4.1 Electric Power 36

4.2 Melt Temperatures 38

4.3 Concrete Basemat and Sidewall Ablation Rates 42

4.4 Test Section Water Inlet Conditions 46

4.5 Crust Lance Data 49

4.6 Corium Quench Rate 51

4.7 Electrode Current Monitoring System Data 54

4.8 Posttest Debris Examinations 55

5.0 REFERENCES 63

APPENDIX A: Data Acquisition System Channel Assignments 64

APPENDIX B: Test Data 77

List of Figures

Figure		Page
2-1	Key Elements of the CCI-2 Test Apparatus	4
2-2	Overview Photograph of CCI Test Facility	4
2-3	Details of the CCI-2 Test Section	5
2-4	Top View of Lower Test Section	5
2-5	Side View of Lower Test Section Showing Inert MgO Sidewall Sections	6
2-6	Side View of Lower Test Section Showing Concrete Sidewall Sections	6
2-7	Photograph Showing Lower Section Sidewall Components after Fabrication	7
2-8	Illustration of the CCI-2 Thermite Powder Loading Scheme	8
2-9	Photograph Showing Electrodes Installed in Clamps	9
2-10	Details of the Top Test Section Showing Water Weirs	9
2-11	Illustration of CCI-2 Crust Lance Assembly Installed in Test Section	10
2-12	Details of Crust Lance Loading Device	11
2-13	Illustration of CCI-2 Test Section Mounted on ZPR-9 Reactor Bed	11
2-14	Illustration of Test Section Clamping Bars	12
2-15	Test Section Water Supply System	13
2-16	CCI-2 Quench and Overflow Tanks	14
2-17	CCI-2 Spray Tank System	14
2-18	CCI-2 Test Section Pressure Relief System	16
2-19	CCI-2 Off Gas System	17
2-20	CCI-2 Cover Gas System	17
2-21	Data Acquisition System Setup for CCI-2	21
2-22	Plan View of Basemat Instrumentation Layout (dimensions are in cm)	22
2-23	Elevation View of Basemat Type C Thermocouple Locations	22
2-24	CCI-2 Test Section Sidewall Instrumentation (View from West)	23
2-25	Thermocouple Arrays Installed in Basemat Concrete Form	24
2-26	CCI-2 Test Section Sidewall Instrumentation (View from South)	24
2-27	CCI-2 Test Section Pressure Transducer Layout	25
2-28	Illustration of CCI-2 Electrode Current Monitoring System Layout	27

List of Figures (Contd.)

Figure		Page
3-1	Illustration of Thermite Sample Train Installed in Test Section	29
3-2	Voltage Reading across Thermite Igniter Shunt	33
3-3	Bulk Melt Temperature Data Over the First 5 Minutes of the Interaction	34
4-1	Power Supply Voltage	36
4-2	Power Supply Current	37
4-3	Total DEH Input Power	37
4-4	Melt Temperature Data from Basemat Type C “WCL” Array	38
4-5	Melt Temperature Data from Basemat Type C “WNW” Array	39
4-6	Melt Temperature Data from Basemat Type C “WNE” Array	39
4-7	Melt Temperature Data from Basemat Type C “WSE” Array	40
4-8	Melt Temperature Data from Basemat Type C “WSW” Array	40
4-9	Melt Temperature Data from North Sidewall Type C “NW” Array	41
4-10	Melt Temperature Data From North Sidewall Type C “SW” Array	41
4-11	Data From all 36 Melt Temperature Thermocouples	42
4-12	Thermal Response of the Concrete Basemat at the Centerline (“A” Array)	43
4-13	North Concrete Sidewall Thermal Response at +10.0 cm (“SWI” Array)	43
4-14	South Concrete Sidewall Thermal Response at +10.0 cm (“SWJ” Array)	44
4-15	Basemat Axial Ablation Front Location	44
4-16	North Sidewall Radial Ablation Front Location	45
4-17	South Sidewall Radial Ablation Front Location	45
4-18	Maximum Axial and Radial Ablation Depths Versus Time	46
4-19	Cavity Erosion Profile Based on TC Data and Posttest Examinations	47
4-20	Test Section Water Inlet and Quench Tank Coil Water Flow Rates	48
4-21	Water Supply Tank Water Volume	48
4-22	Water Head Over Melt	49
4-23	Load Force Exerted on Crust vs. Time	50
4-24	Lance Tip Elevation over Initial Concrete Surface	50
4-25	Quench System Tank Water Volume Data	52

List of Figures (Contd.)

Figure		Page
4-26	Cumulative Quench System Water Volume	52
4-27	Melt-Water Heat Flux Based on Steam Formation Rate	53
4-28	Selected Quench System Temperatures during Water Flooding Stage	53
4-29	Voltage Drop Across Selected Electrodes on the West Side	54
4-30	Voltage Drop Across Selected Electrodes on the East Side	55
4-31	West View of Debris Top Surface After Removal of the Middle Sidewall Section	56
4-32	Topographical Map Showing Key Debris Upper Surface Elevations	56
4-33	Crust Mantle Adhering to East Sidewall (after removal of bridge crust)	57
4-34	Non-Electrode Sidewall View of the Solidified Debris	57
4-35	Solidified Corium and Concrete Sidewalls (View From Southeast)	59
4-36	Solidified Corium and Concrete Sidewalls (View From Northwest)	59
4-37	Picture of the Core Hole Drilled Near the Test Section Centerline	60
4-38	Core Sample Remnants (Core-concrete interface is to the right)	60
4-39	View of Solidified Corium Remaining Over the Basemat	61
4-40	View of the South Concrete Sidewall after Removal	62
B-1	Compensator Temperature, Channels B01-B49 and B50-B99	78
B-2	Basemat Type C “WCL” Array Data	78
B-3	Basemat Type C “WNW” Array Data	79
B-4	Basemat Type C “WNE” Array Data	79
B-5	Basemat Type C “WSE” Array Data	80
B-6	Basemat Type C “WSW” Array Data	80
B-7	North Sidewall Type C “NW” Array Data	81
B-8	South Sidewall Type C “WS” Array Data	81
B-9	Basemat Type K “A” Array Data	82
B-10	Basemat Type K “B” Array Data	82
B-11	Basemat Type K “C” Array Data	83
B-12	Basemat Type K “D” Array Data	83
B-13	Basemat Type K “E” Array Data	84

List of Figures (Contd.)

Figure		Page
B-14	North Sidewall Type K "SWA" Array Data	84
B-15	South Sidewall Type K "SWB" Array Data	85
B-16	North Sidewall Type K "SWC" Array Data	85
B-17	South Sidewall Type K "SWD" Array Data	86
B-18	North Sidewall Type K "SWE" Array Data	86
B-19	South Sidewall Type K "SWF" Array Data	87
B-20	North Sidewall Type K "SWG" Array Data	87
B-21	South Sidewall Type K "SWH" Array Data	88
B-22	North Sidewall Type K "SWI" Array Data	88
B-23	South Sidewall Type K "SWJ" Array Data	89
B-24	North Sidewall Type K "SWK" Array Data	89
B-25	South Sidewall Type K "SWL" Array Data	90
B-26	Thermocouple Compensator Data for Channels Q01-Q49 and Q50-Q99	90
B-27	Test Section Sidewall Heat Loss Data at -15.0 cm Elevation	91
B-28	Test Section Sidewall Heat Loss Data at -5.0 cm Elevation	91
B-29	Test Section Sidewall Heat Loss Data at +5.0 cm Elevation	92
B-30	Test Section Sidewall Heat Loss Data at +15.0 cm Elevation	92
B-31	Test Section Sidewall Heat Loss Data at +70.0 cm and +84.7 cm Elevations	93
B-32	Test Section Sidewall Heat Loss Data at +94.7 cm and +124.9 cm Elevations	93
B-33	Test Section Sidewall Heat Loss Data at +151.3 cm and +174.7 cm Elevations	94
B-34	Test Section Mainline Thermocouple Data	94
B-35	Test Section Plenum and Insertable Water Level Probe Thermocouple Data	95
B-36	Quench Tank Water Temperature Data	95
B-37	Quench Tank Coil Inlet and Outlet Temperature Data	96
B-38	Supply, Overflow, Spray, and Auxiliary Tank Water Temperature Data	96
B-39	Gas Temperature in Off Gas System	97
B-40	Crust Lance Load Cell Data	97
B-41	Lance Position Indicator Data	98

List of Figures (Contd.)

Figure		Page
B-42	Total Power Supply Power	98
B-43	Power Supply Voltage Data	99
B-44	Total Power Supply Current Data	99
B-45	Power Supply Current Transformer Data	100
B-46	Hall Effect Meter Data	100
B-47	Voltage across Igniter Shunt	101
B-48	Pressure Transducer Power Supply Voltages	101
B-49	Quench System Tank Water Volume Data	102
B-50	Water Supply Tank Water Volume Data	102
B-51	Supply and Quench System Tank Head Data (Backup)	103
B-52	Water Head Over Melt	103
B-53	Water Supply Tank Pressure	104
B-54	Various System Pressures	104
B-55	Water Flow Rates	105
B-56	Test Section Helium Cover Gas Flow Rates	105
B-57	Final Off Gas Flow Rate	106

List of Tables

Table		Page
1-1	Specifications for CCI-2	2
2-1	Chemical Composition of Castable MgO	7
2-2	Engineering Composition of CCI-2 LCS Concrete Basemat and Sidewalls	18
2-3	Estimated Chemical Composition of LCS Concrete	19
2-4	Post-Reaction Bulk Composition for CCI-2 Thermite	20
2-5	Detailed Pre- and Post-Reaction Compositions for CCI-2 Thermite	20
3-1	CCI-2 Event Sequence (times relative to melt contact with basemat)	32
4-1	Masses of Various Debris Regions	58
A-1	"Basemat" DAS Channel Assignments for CCI-2	65
A-2	"Power" DAS Channel Assignments for CCI-2	69
A-3	"Quench" DAS Channel Assignments for CCI-2	73

1.0 INTRODUCTION

The Melt Attack and Coolability Experiments (MACE) program addressed the issue of the ability of water to cool and thermally stabilize a molten core-concrete interaction when the reactants are flooded from above. These tests provided data regarding the nature of corium interactions with concrete, the heat transfer rates from the melt to the overlying water pool, and the role of noncondensable gases in the mixing processes that contribute to melt quenching. As a follow-on program to MACE, The Melt Coolability and Concrete Interaction Experiments (MCCI) project is conducting reactor material experiments and associated analysis to achieve the following objectives:

i. resolve the ex-vessel debris coolability issue through a program that focuses on providing both confirmatory evidence and test data for the coolability mechanisms identified in MACE integral effects tests, and

ii. address remaining uncertainties related to long-term two-dimensional molten core-concrete interactions under both wet and dry cavity conditions.

Achievement of these two program objectives will demonstrate the efficacy of severe accident management guidelines for existing plants, and provide the technical basis for better containment designs for future plants.

In terms of satisfying these objectives, the Management Board (MB) approved the conduct of two long-term 2-D Core-Concrete Interaction (CCI) experiments designed to provide information in several areas, including: i) lateral vs. axial power split during dry core-concrete interaction, ii) integral debris coolability data following late phase flooding, and iii) data regarding the nature and extent of the cooling transient following breach of the crust formed at the melt-water interface.

This data report provides thermal hydraulic test results from the CCI-2 experiment, which was conducted on August 24, 2004. Test specifications for CCI-2 are provided in Table 1-1. This experiment investigated the interaction of a fully oxidized 400 kg PWR core melt, initially containing 8 wt % Limestone/Common Sand (LCS) concrete, with a specially designed two-dimensional LCS concrete test section with an initial cross-sectional area of 50 cm x 50 cm. The report begins by providing a summary description of the CCI-2 test apparatus and operating procedures, followed by presentation of the thermal-hydraulic results. Detailed posttest debris examination results will be provided in a subsequent publication. Observations drawn within this report regarding the overall cavity erosion behavior may be subject to revision once the posttest examinations are completed, since these examinations will fully reveal the final cavity shape.

Table 1-1. Specifications for CCI-2.

Parameter	Specification
Corium	100 % oxidized PWR with 8 wt % limestone/common sand concrete
Concrete type	limestone/common sand concrete
Initial basemat dimension	50 cm x 50 cm
Initial melt mass (depth[a])	400 kg (25 cm)
Test section sidewall construction	Nonelectrode walls: concrete Electrode walls: MgO protected by UO_2 pellet layer.
Radial ablation limit	35 cm
Axial ablation limit	35 cm
System operating pressure	Atmospheric
Melt formation technique (timescale)	Chemical reaction (~30 seconds)
Initial melt temperature	2000 ºC
Melt heating technique	Direct Electrical (Joule) Heating
Power supply operation prior to water addition	Constant power at 120 kW
Criteria for water addition	1) 5.5 hours of operation with DEH input, or 2) radial or axial ablation reaches 30 cm
Inlet water temperature	20 ºC
Inlet water flow rate (2 MW/m^2 equivalent quench rate)	2 liters/second
Sustained water depth over melt	50 ± 5 cm
Power supply operation after water addition	Constant voltage
Test termination criteria	1) Melt temperature falls below concrete solidus, 2) concrete ablation is arrested, or 3) maximum radial/axial ablation limit of 35 cm is reached.

[a]Based on an assumed melt density of 6500 kg/m^3

2.0 FACILITY DESCRIPTION

The CCI test facility consists of a test apparatus, a power supply for Direct Electrical Heating (DEH) of the corium, a water supply system, two steam condensation (quench) tanks, an off gas system to filter and vent the off-gases, and a Data Acquisition System (DAS). A schematic illustration of facility is provided in Figure 2-1, while an overview photograph showing key elements of the facility is provided in Figure 2-2. Test specifications for CCI-2 are summarized in Table 1-1. With the exception of the DAS, the entire system is housed in an explosion-rated containment cell. DEH input power, water supply, and gas flows are remotely controlled from the experimenter's console located outside the containment. The various elements of the facility are described in sequence below.

2.1 Test Apparatus

The apparatus for containment of the core material consists of a test section that is ~ 3.4 m tall with a square internal cross-section which initially measures 50 cm x 50 cm. The principal components of the apparatus, shown in Figure 2-3, consist of a bottom support plate, three sidewall sections, and an upper enclosure lid. The lower sidewall section contains the corium melt and structural concrete components that are intended to undergo ablation. A top view of the lower section is shown in Figure 2-4, while cross-sectional views of the electrode and non-electrode sidewalls are provided in Figures 2-5 and 2-6, respectively. The concrete basemat is initially 55 cm deep, so that up to 35 cm of axial ablation can safely be accommodated with this design.

As shown in Figure 2-4, the electrode sidewalls of the lower section are fabricated from castable MgO[a] refractory, while the non-electrode sidewalls are fabricated from Limestone/Common Sand (LCS) concrete. A photograph showing these components after fabrication is provided in Figure 2-7. The middle sidewall section is also fabricated from castable MgO, while the upper section and lid are made from locally obtained LCS concrete. The chemical composition of the cast MgO is shown in Table 2-1, while the detailed composition of the LCS concrete basemat and sidewalls is provided later in this section. The concrete and MgO are contained within flanged 11 gauge steel forms that secure the lower section to the balance of the existing test section components with an aluminum transition plate. The lower section is fabricated with vertical, flanged casting seams between the MgO and concrete so that the sidewalls can be disassembled to reveal the solidified corium following the test. The MgO sections are intended to be reusable, while the concrete sidewall remnants are disposed of as radioactive waste.

A layer of crushed UO_2 pellets is used to protect the interior surface of the MgO sidewalls against thermo-chemical attack by the corium. In the event that the UO_2 layer does not provide adequate protection, 3.2 mm thick tungsten back-up plates are embedded in these sidewalls as a final barrier to terminate sidewall attack. The plates are instrumented to provide an indication of corium contact with either of these two surfaces during the test. As illustrated in Figure 2-5, multi-junction Type C thermocouple assemblies are also cast within the MgO sidewalls. These thermocouples allow the time-dependent heat loss from the melt to be estimated from the local temperature gradient and the thermal conductivity of the MgO through stand inverse heat conduction techniques.

[a] Periclase Permanente 98-AF; from National Refractories and Minerals, Columbiana, OH.

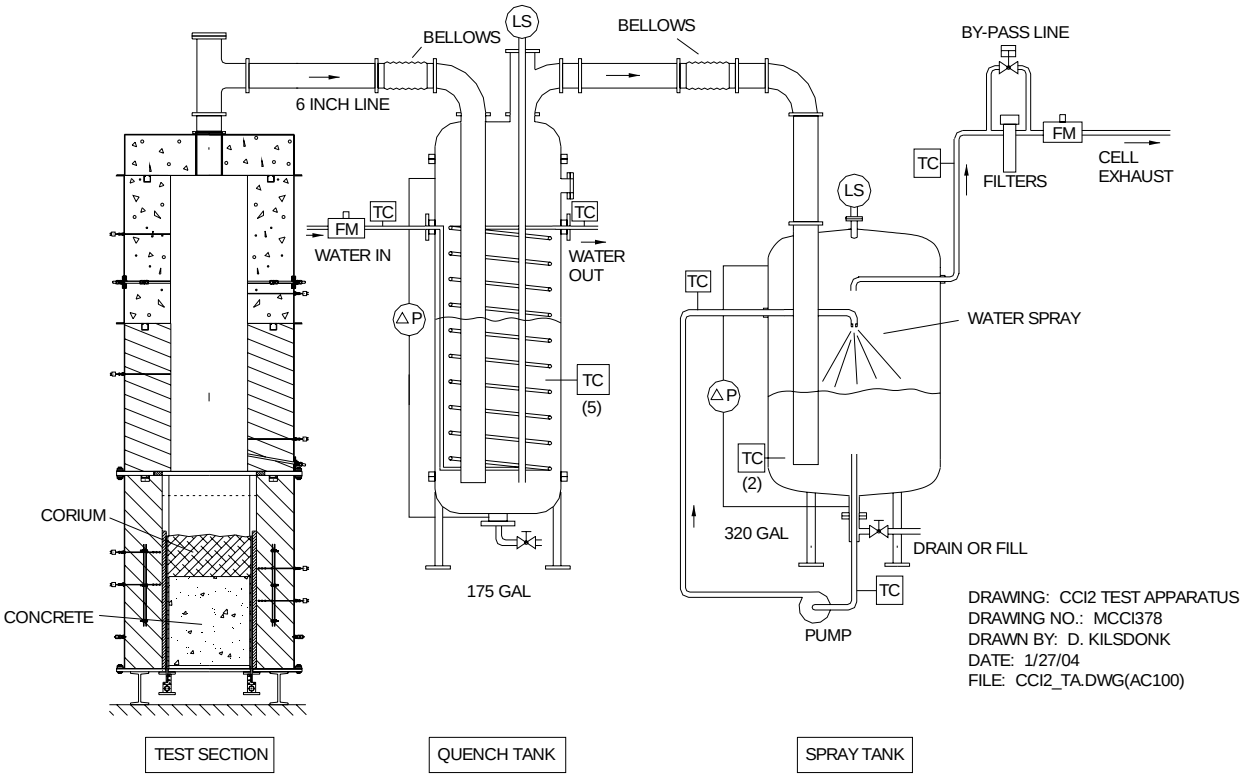

Figure 2-1. Key Elements of the CCI-2 Test Apparatus.

Figure 2-2. Overview Photograph of CCI Test Facility.

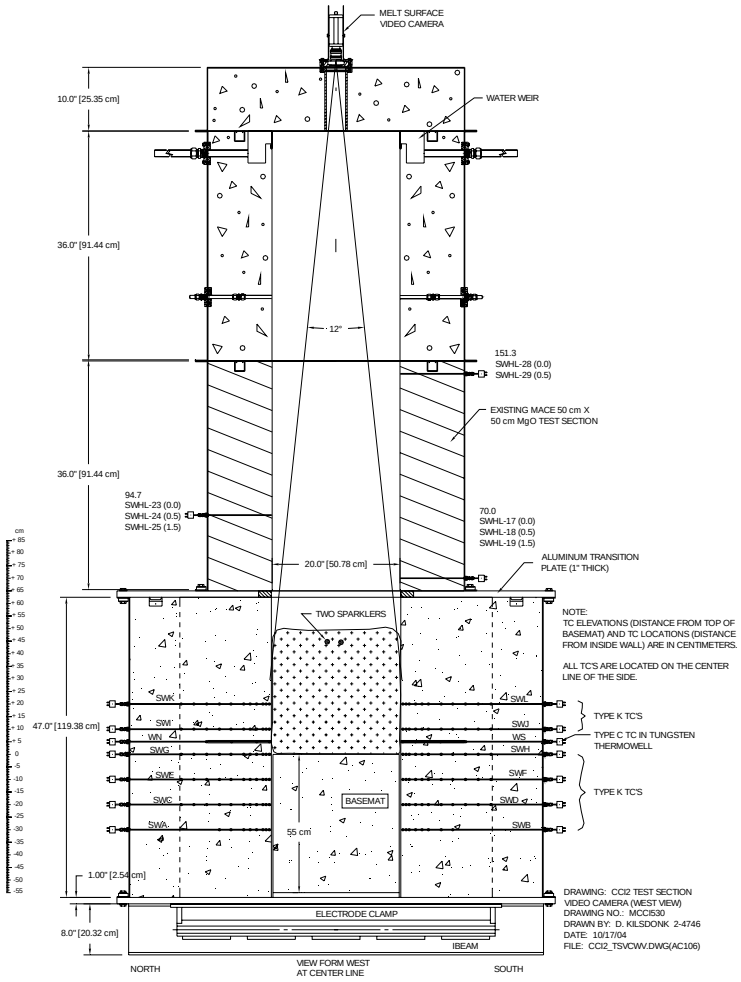

Figure 2-3. Details of the CCI-2 Test Section.

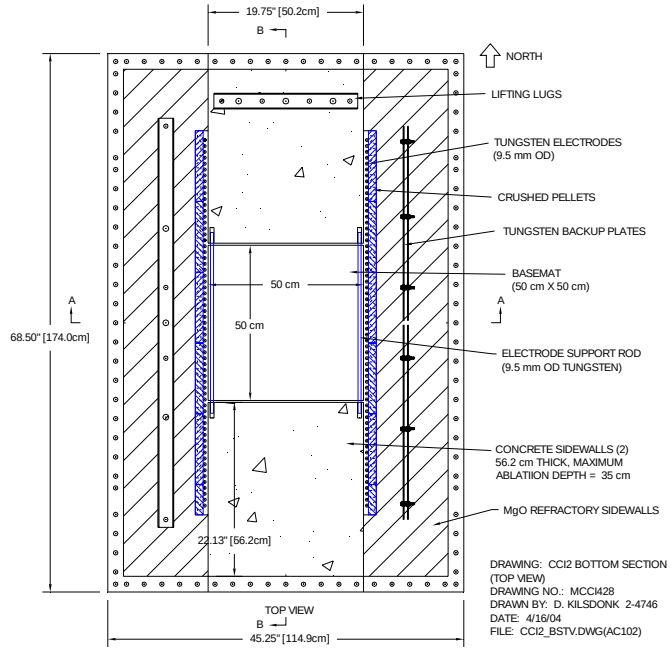

Figure 2-4. Top View of Lower Test Section.

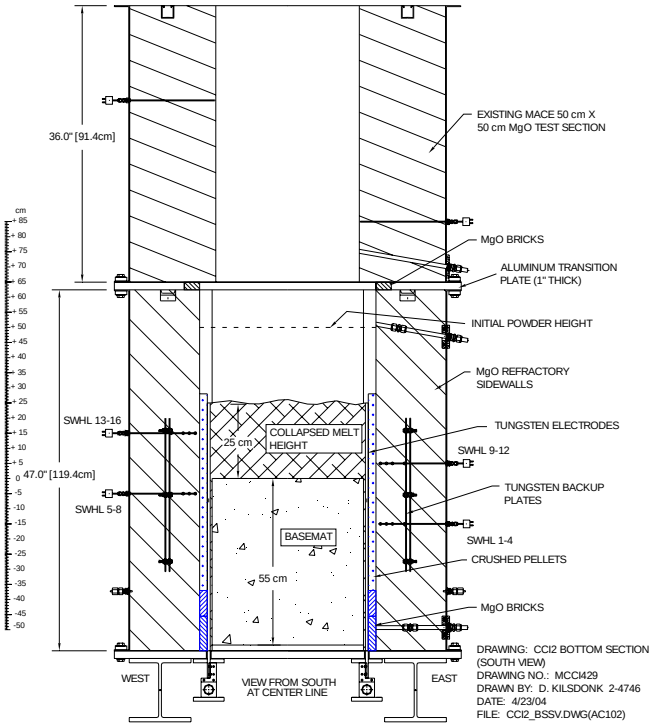

Figure 2-5. Side View of Lower Test Section Showing Inert MgO Sidewall Sections.

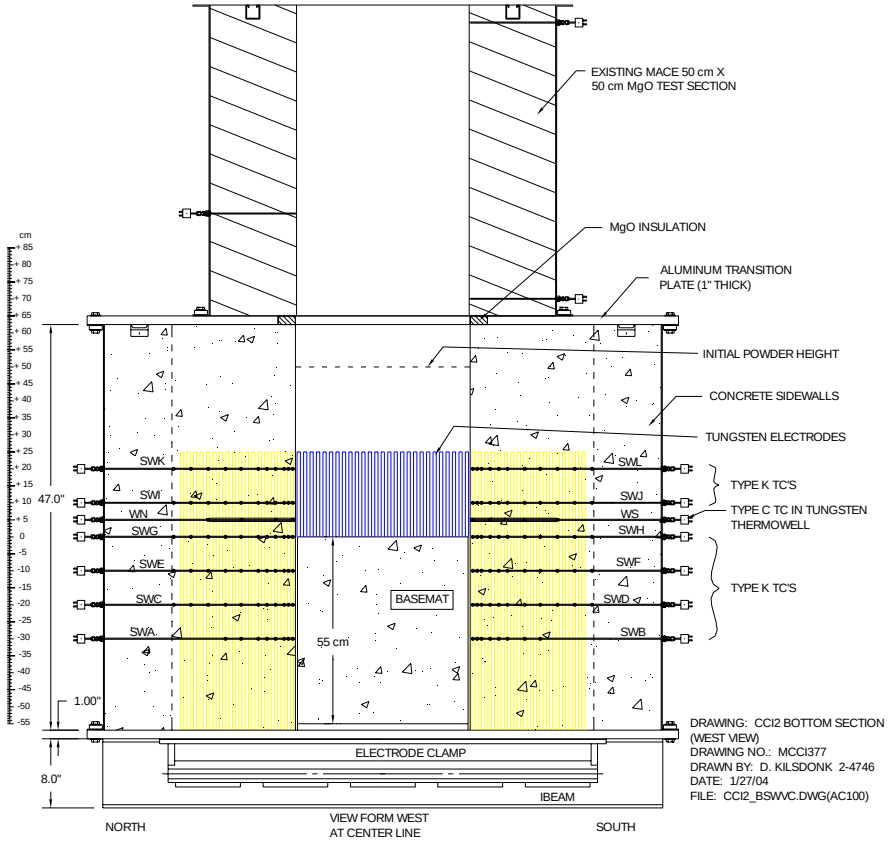

Figure 2-6. Side View of Lower Test Section Showing Concrete Sidewall Sections.

Figure 2-7. Photograph Showing Lower Section Sidewall Components After Fabrication.

Table 2-1. Chemical Composition of Castable MgO.

Element (Oxide Form)	Mass %	
	Element	Oxide
Al (Al_2O_3)	0.24	0.45
B (B_2O_3)	0.12	0.39
Ca (CaO)	0.58	0.81
Fe (Fe_2O_3)	0.14	0.20
Mg (MgO)	58.4	96.8
Mn (MnO)	0.038	0.049
Si (SiO_2)	0.24	0.51
Ti (TiO_2)	0.002	0.003
Zr (ZrO_2)	0.038	0.023
Total		99.24

Melt pool generation in this test is achieved through an exothermic "thermite" chemical reaction that produces the target initial melt mass over a timescale of ~ 30 seconds. A depiction of the powder loading scheme is provided in Figure 2-8. As is evident from the figure, two iron/alumina sparklers, wrapped with nichrome starter wire, are positioned a few centimeters below the top of the corium charge near the centerline of the test section. One of these sparklers is used to initiate the thermite reaction by heating the neighboring powder to the ignition point. (The thermite composition is described in detail later in this section). The second sparkler is provided as a backup in case the first fails to ignite the material.

After the chemical reaction, DEH is supplied to the melt to simulate decay heat through two banks of tungsten electrodes that line the interior surfaces of the opposing MgO sidewalls. As illustrated in Figures 2-5 and 2-6, the copper electrode clamps are attached to a 2.5 cm thick

aluminum bottom support plate that forms the foundation for the apparatus. A total of sixty three 91 cm long, 0.95 cm diameter tungsten electrodes are attached to each electrode clamp at a pitch of 1.9 cm. A photograph showing the electrodes after installation in the clamps but prior to placement of the lower section sidewalls is provided in Figure 2-9. The clamps are attached with water-cooled buss bars to a 560 kW AC power supply. As shown in Figure 2-4, each electrode bank is vertically restrained by a horizontally mounted, 0.95 cm diameter tungsten rod which is recessed into the concrete sidewalls near the tops of the electrodes. These restraints are provided to prevent slumping of the electrodes away from the sidewalls, as occurred in the MACE Scoping Test[1].

As illustrated in Figure 2-4, the electrodes span a total width of 120 cm on each sidewall of the lower section. At the start of the experiment, the electrical current is drawn through the center 50 cm lateral span of electrodes that are in direct contact with the melt. As the test progresses and the concrete sidewalls erode, additional electrodes are exposed to the corium. Electrical current is drawn through these newly exposed heating elements, thereby maintaining a uniform heating pattern in the melt over the course of the experiment. Given the overall electrode span of 120 cm, up to 35 cm of radial sidewall ablation can be accommodated in this design while maintaining uniform heat input. As shown in Figure 2-4, the concrete sidewalls are 56 cm thick, which provides ~ 20 cm of remaining sidewall thickness once the 35 cm radial ablation limit has been reached.

Water is introduced into the test section through weirs located in the upper sidewall section just beneath the lid of the apparatus. The layout for the weirs is shown in Figure 2-10. A total of nine penetrations are cast into the upper lid of the test section. Of these penetrations, six were utilized for Test CCI-2: one stationary lid video camera view port, a port for an insertable water level depth probe, a 15 cm main steam line to the quench system, two light ports, and a port for an insertable crust lance. An illustration of the stationary lid camera installed in the test section is shown in Figure 2-3.

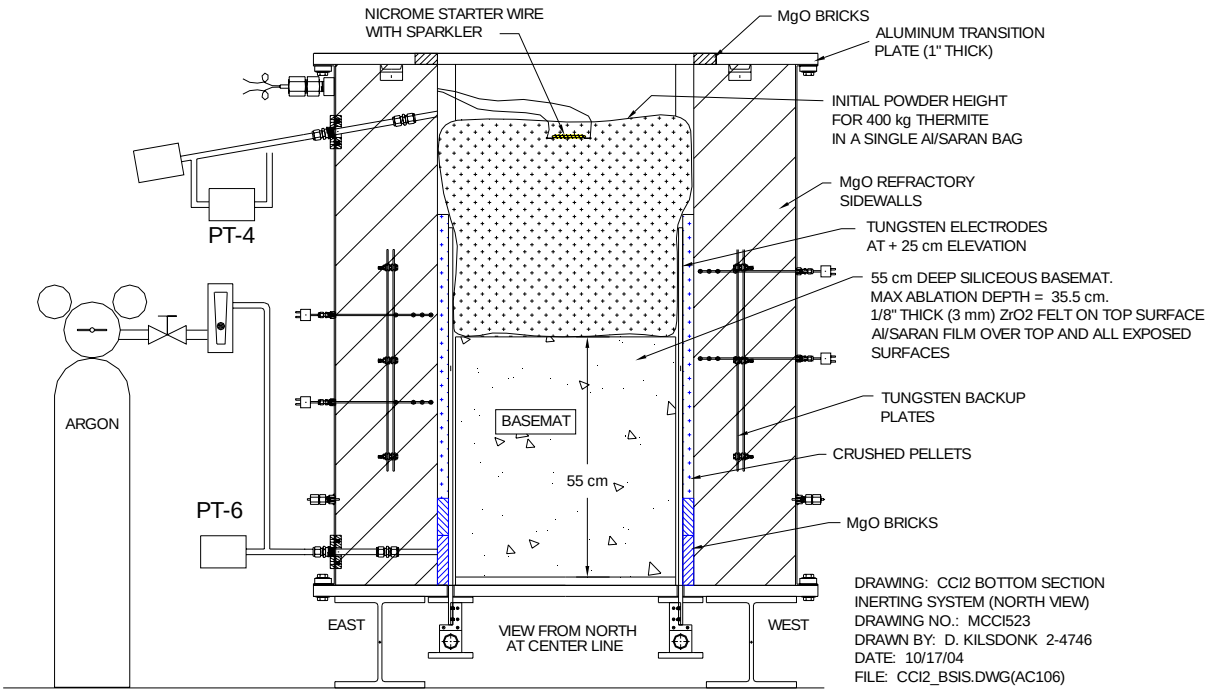

Figure 2-8. Illustration of the CCI-2 Thermite Powder Loading Scheme.

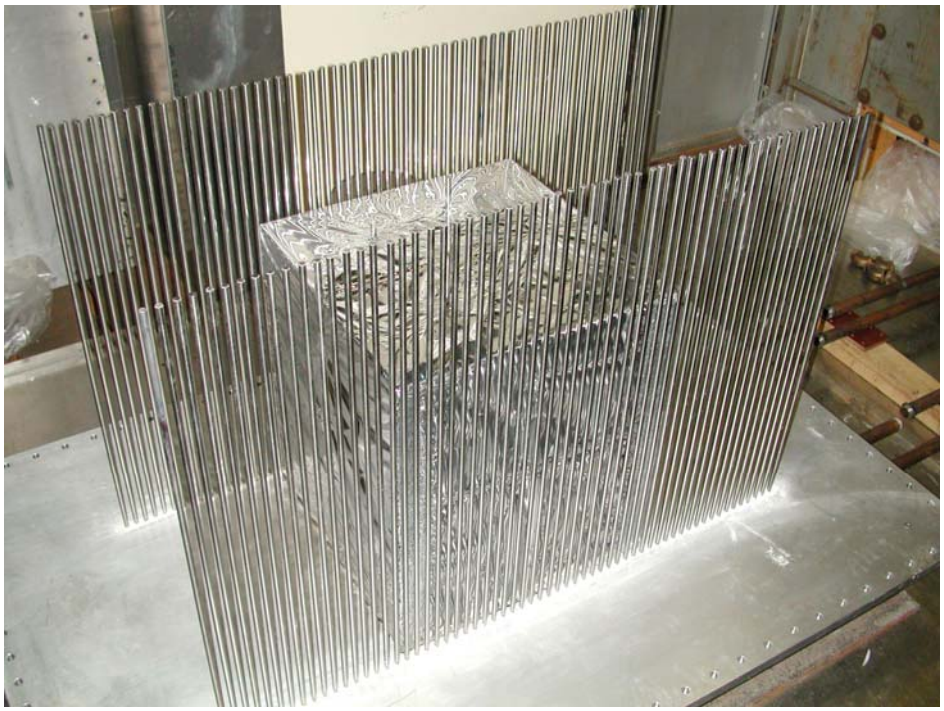

Figure 2-9. Photograph Showing Electrodes Installed in Clamps.

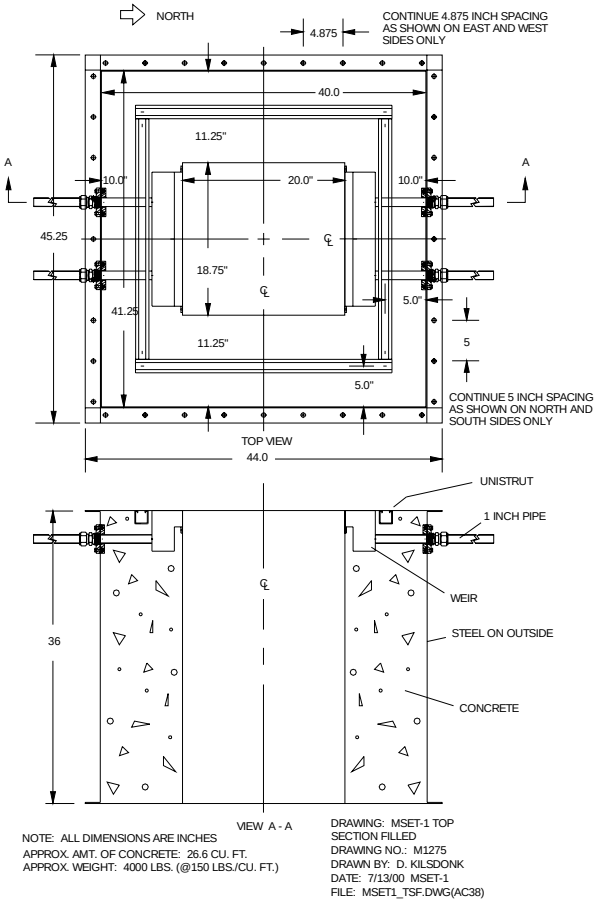

Figure 2-10. Details of the Top Test Section Showing Water Weirs.

The insertable crust lance is designed to fail the crust formed at the melt/water interface in order to obtain data on the transient crust breach cooling mechanism. An illustration of the crust lance installed in the test section is shown in Figure 2-11, while details of the lance loading device are provided in Figure 2-12. The lance is made from 2.54 cm diameter, 304 stainless steel rod with a pointed tip. The lance contains an electrical isolation hub so that there is no need to terminate DEH power input during the crust loading procedure. As shown in Figure 2-12, the driving force for the lance is simply a 450 kg dead weight that is remotely lowered with the crane during the test. The lance assembly is equipped with a load cell and displacement transducer to record load vs. position data as the force is applied to the crust.

The test section components are bolted together on the stationary half of the ZPR-9 reactor bed. Zirconia felt and silicon gasket material are used to seal the flanges. An illustration is provided in Figure 2-13. Installation and torquing of test section flange bolts is performed according to an approved procedure to ensure uniform preload on the flange surfaces. Additional reinforcement of each test section component is provided by clamping bars installed in both the North-South and East-West directions. A diagram illustrating the complete flange bolt and clamping bar layout is provided in Figure 2-14.

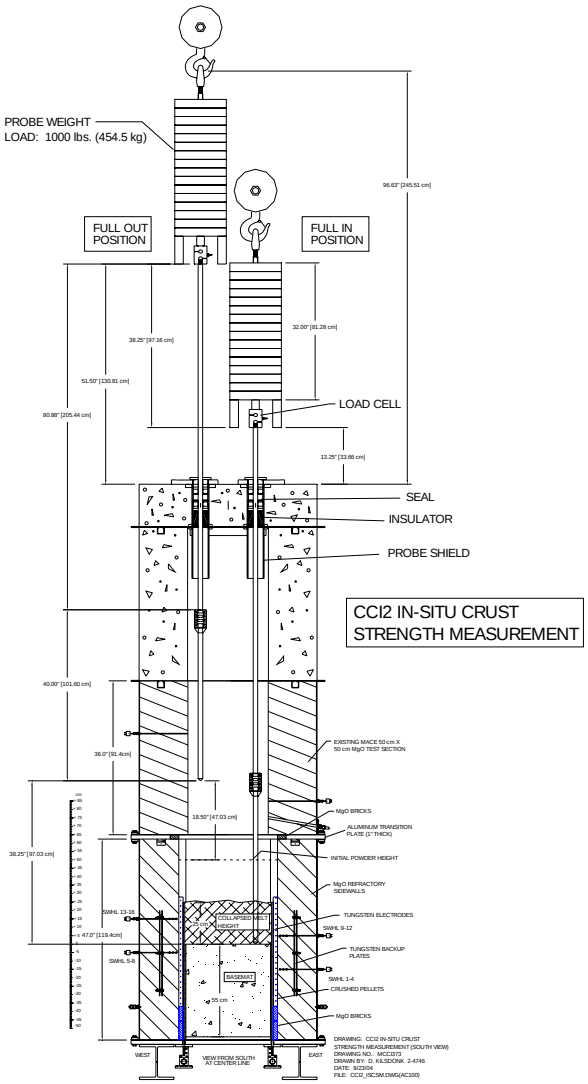

Figure 2-11. Illustration of CCI-2 Crust Lance Assembly Installed in Test Section.

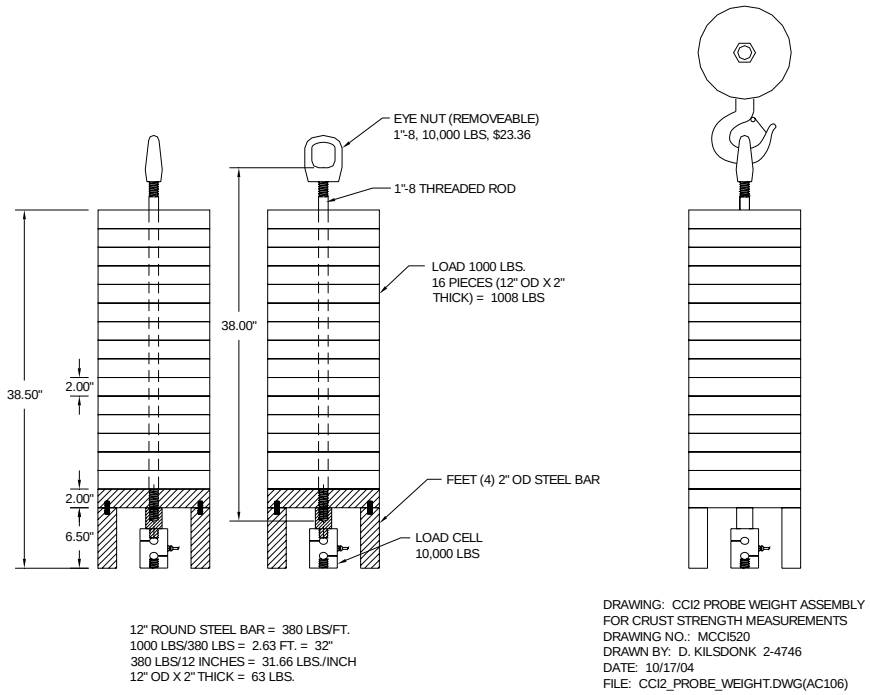

Figure 2-12. Details of Crust Lance Loading Device.

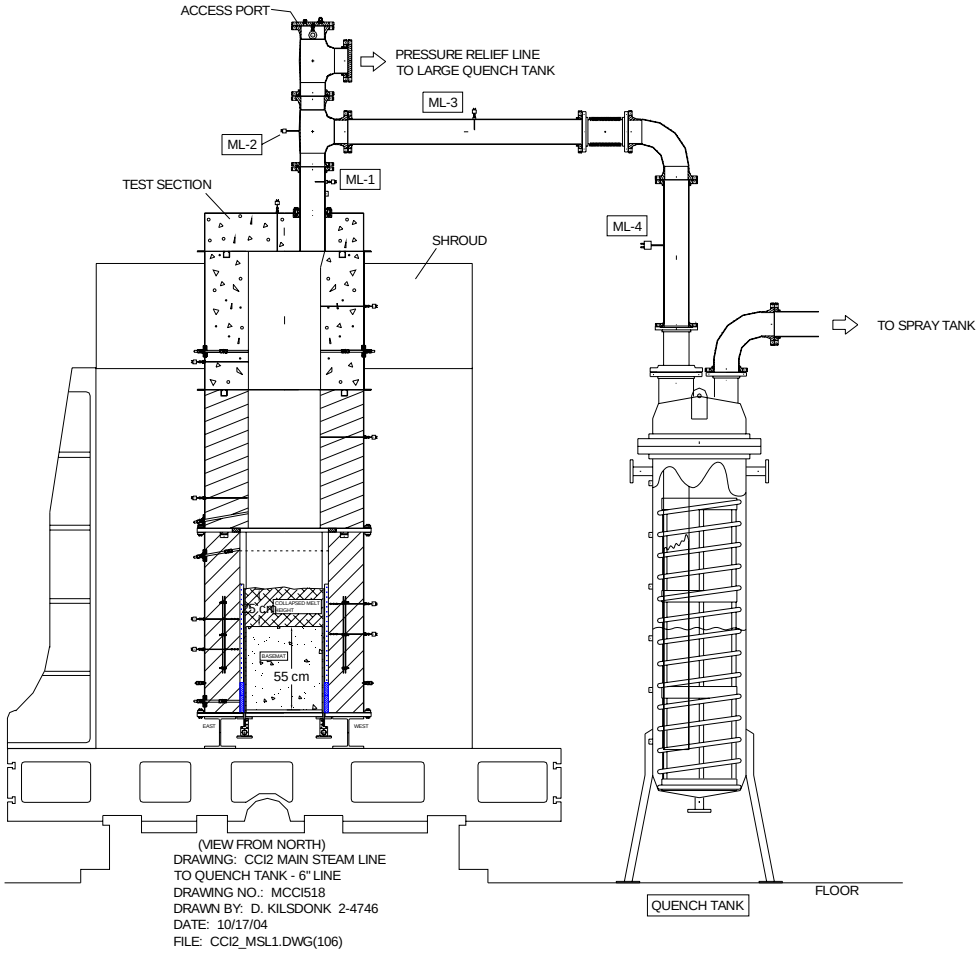

Figure 2-13. Illustration of CCI-2 Test Section Mounted on ZPR-9 Reactor Bed.

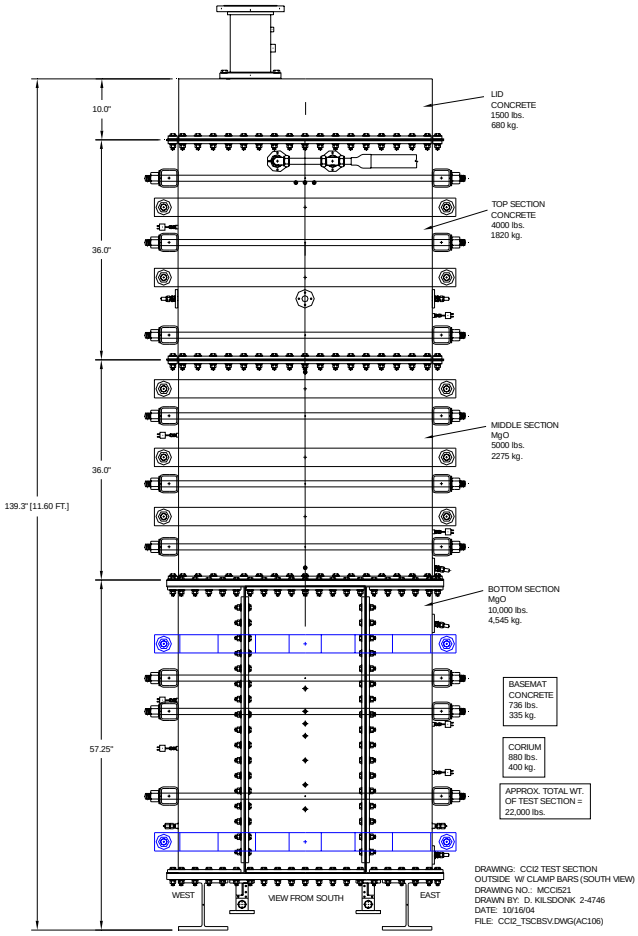

Figure 2-14. Illustration of Test Section Clamping Bars.

2.2 Water Supply System

The water supply system consists of a 1900 l capacity tank connected to the flooding weirs in the north and south sidewalls of the top test section through a valve-controlled supply line that provides water to the test section at a specified flow rate. A schematic illustration of the supply system is provided in Figure 2-15; details of the flooding weirs are shown in Figure 2-10. The supply system flowmeter, pressure transducer, level sensor, and thermocouple instrumentation locations are also shown in Figure 2-15. Water flow through the system is driven by an 80 kPa differential pressure in the supply tank at a nominal flow rate of 120 lpm (2 l/s). The inlet water flow rate of 120 lpm corresponds to a melt/water heat flux of approximately 20 MW/m^2 based on a specific enthalpy of 2.6 MJ/kg for saturated steam at atmospheric pressure, assuming heat transfer occurs through boiling of the overlying coolant. The inlet water flow rate to the test section is monitored with a paddlewheel flowmeter. Both the initial water inventory (125 l) and makeup are provided through pneumatic ball valve RV-1, which is opened as needed at the control console to maintain the water volume inside the test section constant at 125 ± 13 l (50 ± 5 cm). A redundant supply line, activated by pneumatic ball valve RV-2, is provided in case RV-1 fails to open during the test. A third pneumatic valve, RV-3, is provided in case RV-1 or RV-2 fail in the open position. The test is initiated with valve RV-3 in the open position.

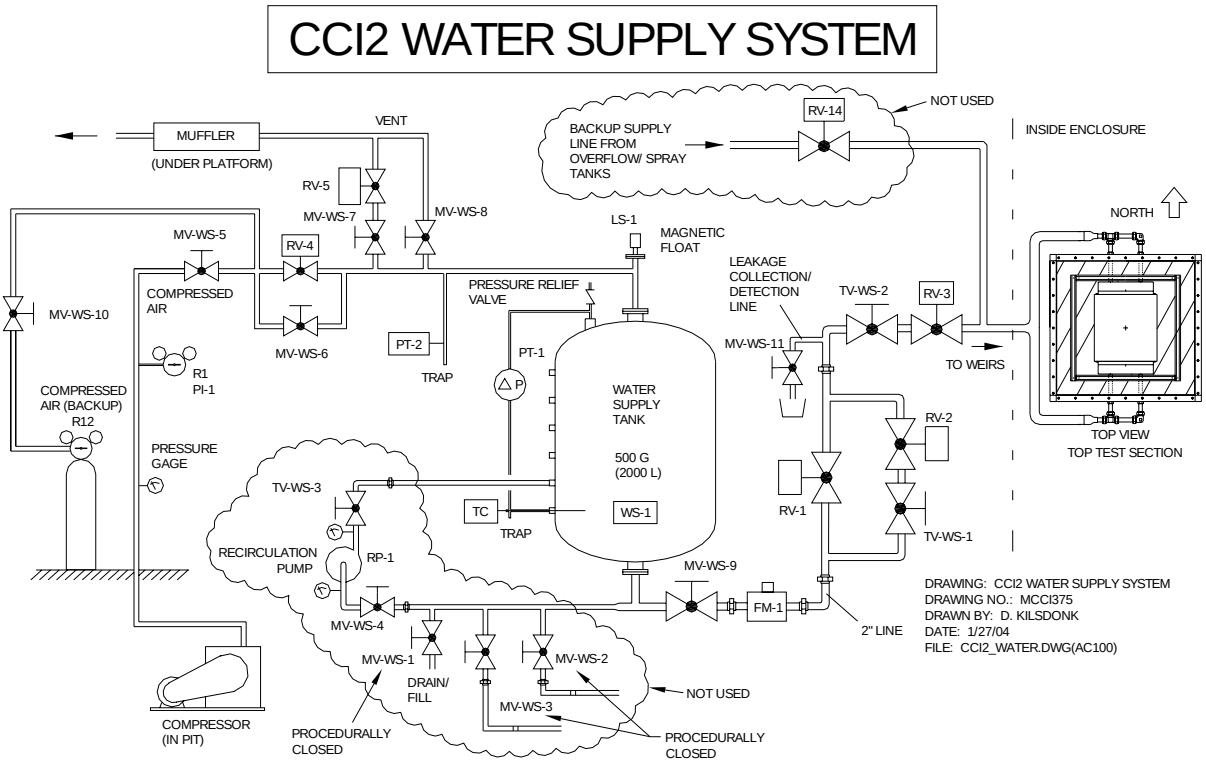

Figure 2-15. Test Section Water Supply System.

Note from Figure 2-15 that the supply line to the test section contains a manual bypass valve downstream of water injection valves RV-1 and RV-2. This valve is vented to a catch pan equipped with an alarmed water detector. During pretest procedures, this valve is left in the open position to divert any water leakage away from the test section. The alarm is intended to notify personnel that a leak is present so that corrective action can be taken. This valve is closed as one of the final steps of pretest operations just prior to evacuation of the cell.

2.3 Quench System

The quench system, shown in Figure 2-16 and 2-17, consists of a primary quench tank, a secondary spray tank, and a condensate overflow tank. The quench system flowmeter, pressure transducer, level sensor, and thermocouple instrumentation locations are also shown in these two figures. Steam and concrete decomposition gases pass from the test section through a 16.1 cm ID stainless steel pipe into the 680 l capacity, 60 cm ID primary quench tank. This tank contains an initial water inventory of 250 l. With this amount of water, a pool void fraction of ~ 60% can initially be accommodated before the voided water height reaches the top of the tank. The quench tank is equipped with a 1.9 cm diameter cooling coil to remove heat from steam condensation, thereby maintaining a subcooled state. The water supply to the cooling coil is drawn from the building supply system. The coil water flow rate is throttled to 30 lpm, which corresponds to a heat removal rate of 170 kW assuming a heat capacity of 4200 J/kg•K for water and a temperature rise of 80 °C across the coil. Should the condensate level in the quench tank rise to a level of 560 l, spillover into the adjacent 930 l overflow tank will occur through a 2.5 cm ID pipe. The quench tank and interconnecting piping between the test section and quench tank are insulated to minimize heat losses.

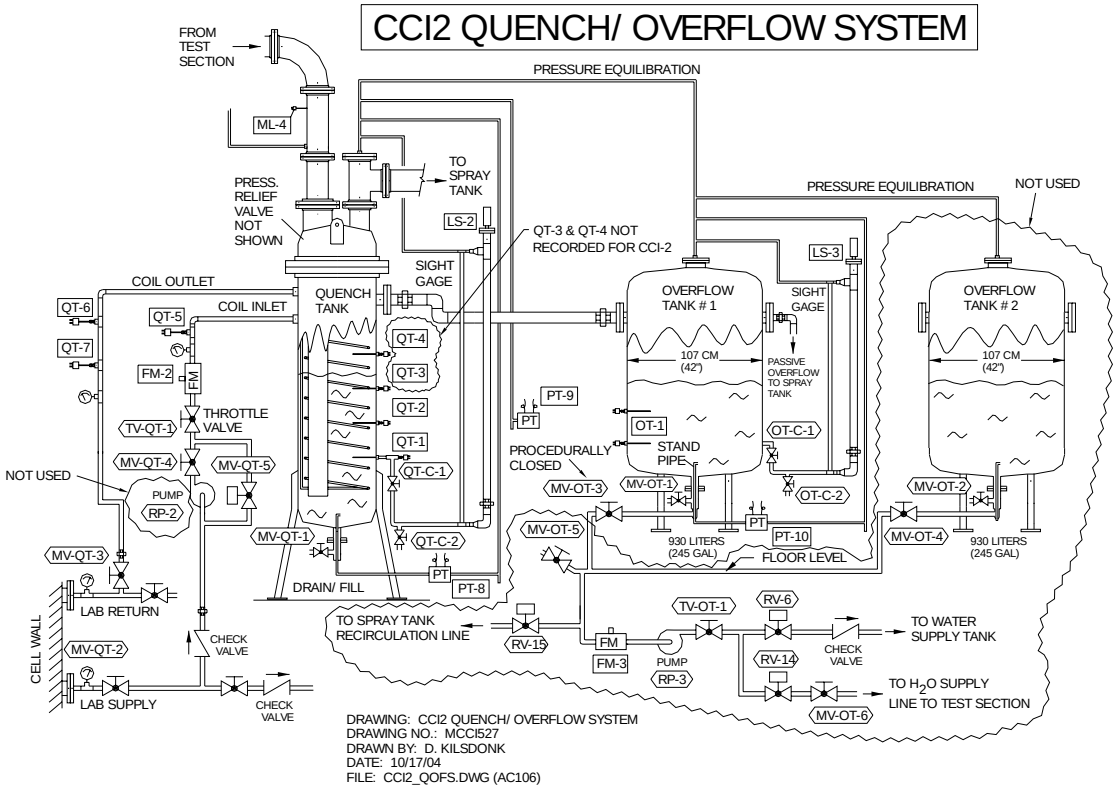

Figure 2-16. CCI-2 Quench and Overflow Tanks.

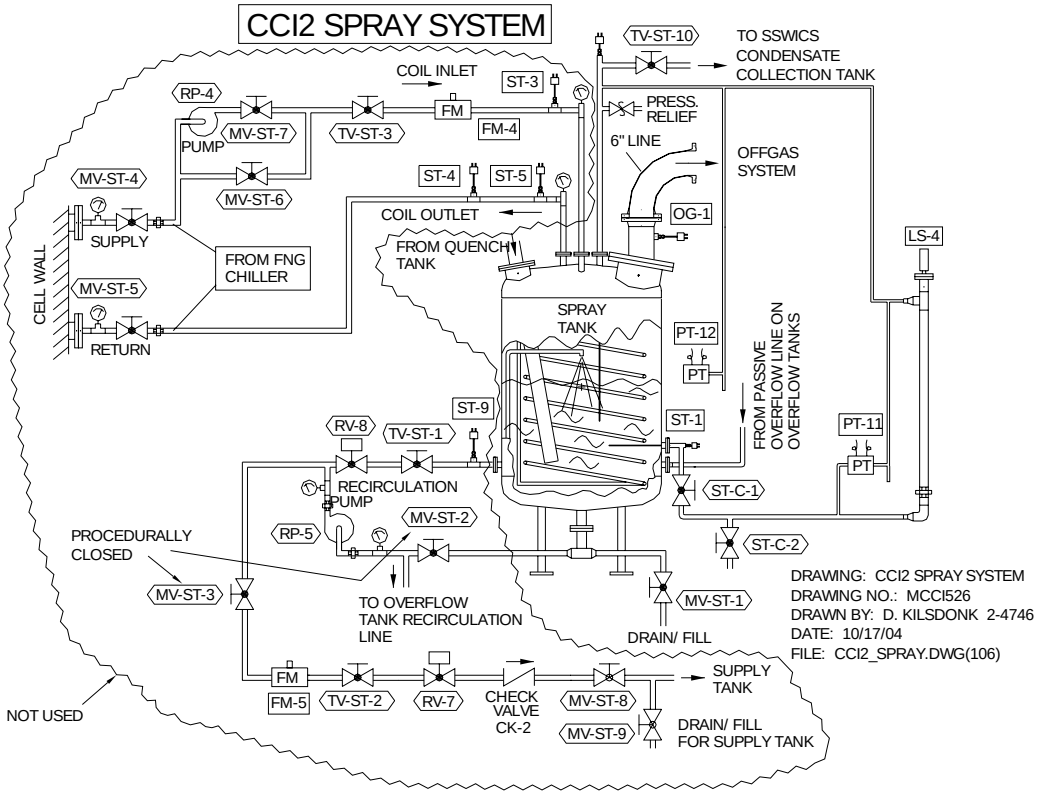

Figure 2-17. CCI-2 Spray Tank System.

The secondary 1230 l capacity spray tank is connected to the quench tank by a 16.1 cm ID stainless steel pipe. In the event that the steam generation rate overwhelms the primary quench tank, the secondary spray tank serves to condense the remaining steam. This tank contains an initial water inventory of 375 l. With this amount of water, a pool void fraction in excess of 60% can be accommodated before the voided water height reaches the top of the tank. The spray tank and interconnecting piping between the spray and quench tanks is also insulated to minimize heat losses.

2.4 Test Section Pressure Relief System

A pressure relief system is provided to prevent over-pressurization and possible failure of the test section. A schematic illustration of the system is shown in Figure 2-18. The system consists of a 16.1 cm vent line from the test section to an auxiliary tank containing a nominal initial water inventory of 1100 l. The auxiliary tank has an inside diameter of 1.22 m and a capacity of 4100 l. The tank is open to the atmosphere. The pressure relief line to the tank is equipped with a passive, counter-weighted check valve set to open at a differential pressure of nominally 68 kPa. A rupture diaphragm (68 ± 13.4 kPa differential failure pressure) upstream from the check valve prevents any flow through the line unless the pressure in the test section exceeds the design value of 68 kPa differential. As shown in Figure 2-18, the relief line is also equipped with a 7.5 cm vacuum breaker valve. This valve is provided to prevent water hammer from occurring due to stream condensation should the pressure relief valve open and then reseat after water has been introduced into the test section.

The initial 400 l water inventory in the auxiliary tank is provided to cool gases from the test section and to remove aerosols before any noncondensables present in the gas stream pass into the cell atmosphere. The tank is instrumented with a Type K thermocouple to measure water temperature and a differential pressure transducer to measure water depth. The instrumentation locations are shown in Figure 2-18. Water depth and temperature instrumentation is provided for the auxiliary tank so that the steam condensation rate can be determined should the pressure relief valve open during the test. In this manner, there is no loss of data should the pressure relief system activate.

2.5 Off Gas System

An illustration of the off gas system is provided in Figure 2-19. Thermocouple and flowmeter instrumentation locations are also shown in this figure. This system filters and exhausts the noncondensable concrete decomposition gases to the cell exhaust. The decomposition gases (H_2, CO, CO_2 and the cover gas) exit the spray tank and pass through a flow separator. The cleanup efficiency of the separator is 99% of all entrained solid and liquid when the particle size exceeds 10 microns. After passing through the flow separator, the flow can potentially split into the two parallel off gas system lines. One line is constructed from 7.5 cm piping, while the second is made from 10.0 cm piping. The system was designed with the capacity to accommodate large-scale (up to 120 cm x 120 cm) tests. Since CCI-2 uses a reduced scale 50 cm x 50 cm test section, the 7.5 cm side of the parallel off gas system is taken out of service using a blank-off plate at the branch point in the system (see Figure 2-19). As a result, all gas flow is diverted through the 10 cm side of the off gas system. Reduction in available flow area is required to achieve a resolvable gas flow rate through the large capacity flowmeter at the

end of the off gas system train (each flow meter has a flow capacity of 14,000 sl/min). The final filters in the system (4 individual filters per filter housing, yielding a total of 8 filters for each side of the off gas system) remove any remaining particulate before venting the off gases through flowmeters to the cell atmosphere. The filters on the side of the off gas system used for CCI-2 (10 cm) are equipped with a passive counter-weighted check valve set to open at a nominal differential pressure of 7 kPa. The bypass valve is provided in the event that the filters become plugged during the experiment.

2.6 Cover Gas System

During the test a uniform flow rate of helium is fed into the test section to suppress burning of combustible concrete decomposition gases (H_2 and CO) and protect test section internals. An illustration of the cover gas system is shown in Figure 2-20. Cover gas flow is modulated by a total of three Hastings Flow Controllers (FC's). One 0-200 slpm FC provides cover gas to the lid camera and light port penetrations, while a second 0-350 slpm FC provides dedicated cover gas flow to the lid camera to prevent aerosol deposition on the camera quartz window through which the melt upper surface is viewed. A third 0-100 slpm FC is used to inert the apparatus on the evening prior to the test.

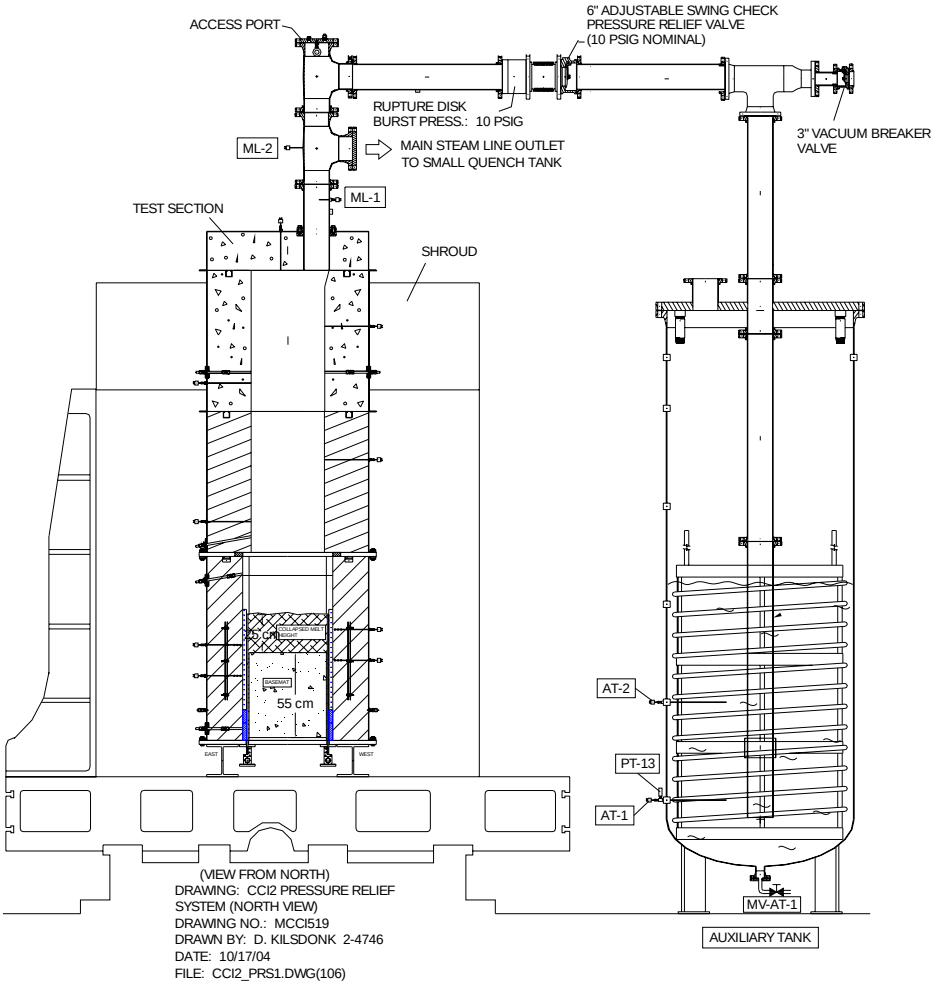

Figure 2-18. CCI-2 Test Section Pressure Relief System.

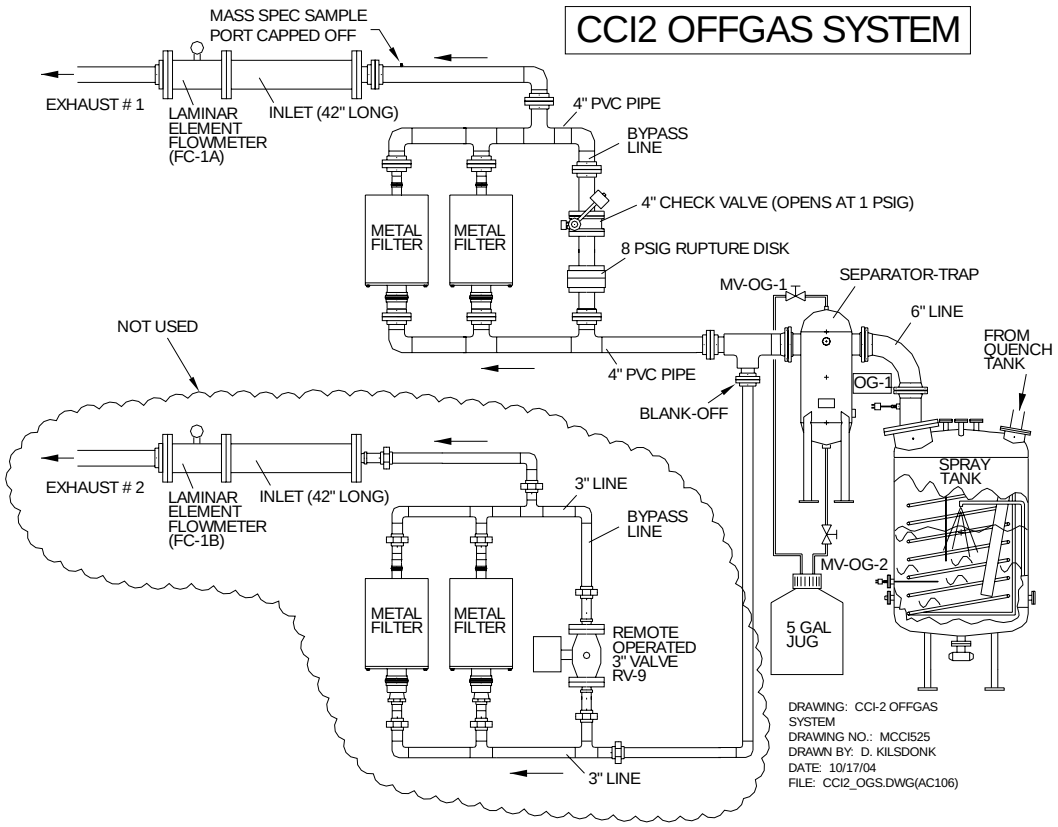

Figure 2-19. CCI-2 Off Gas System.

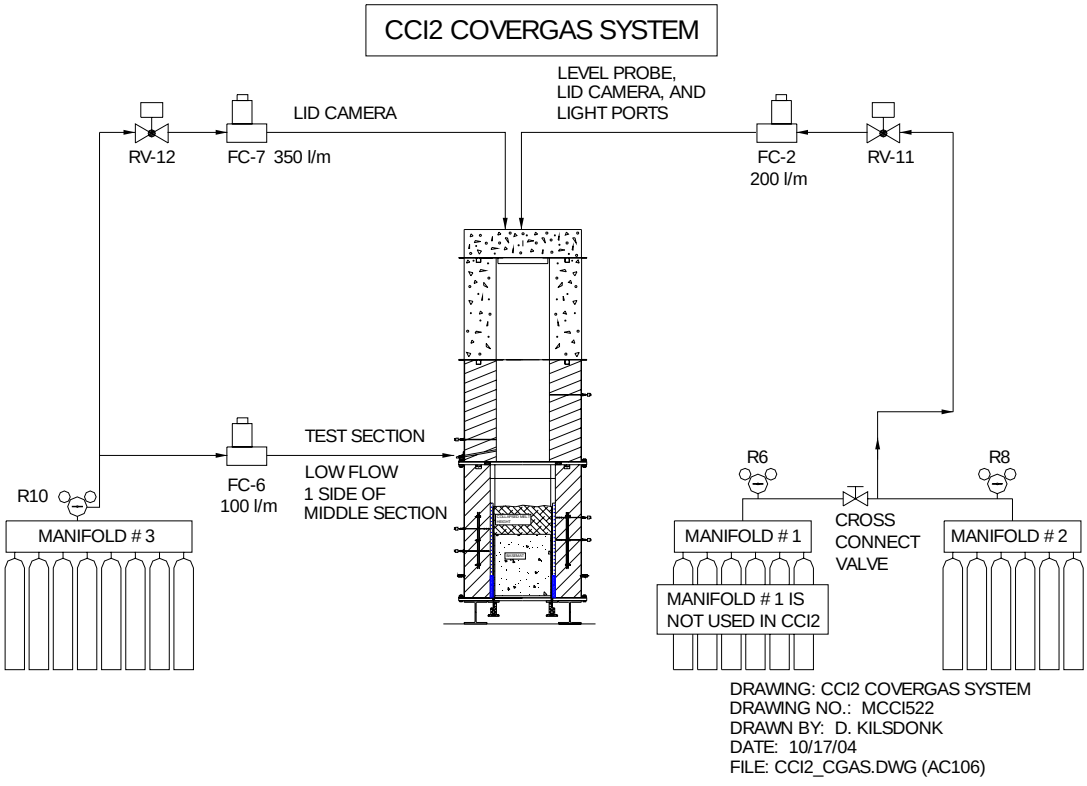

Figure 2-20. CCI-2 Cover Gas System.

2.7 Power Supply

The power for Direct Electrical Heating (DEH) of the corium is provided by a 0.56 MW single phase AC power supply made by NWL Transformers. Output of the power supply is voltage or current controlled. The supply has four voltage/current ranges: 56.4 V/10 kA, 113 V/5 kA, 169 V/3.3 kA, and 226 V/2.5 kA. The power supply is connected to the two arrays of tungsten electrodes in the test section through water cooled copper pipes that pass through a wall of the former fuel loading compartment. The calculated total voltage drop through the water cooled copper pipes and tungsten electrodes at operational temperature and maximum current is less than 0.5 V. The leakage current through the overlying water pool during test operation has been estimated to be less than 1% of the total current.

2.8 Concrete Sidewalls and Basemat

As shown in Table 1-1, the composition of the CCI-2 concrete basemat and sidewalls is specified to be of the Limestone/Common Sand (LCS) type. The engineering composition of the CCI-2 LCS concrete is shown in Table 2-2. Sand and aggregate for the mix were obtained from Meyer Materials (McHenry, IL, U.S.A.). The chemical composition of the CCI-2 concrete is shown in Table 2-3. Note that the composition has been assumed to be identical to the ACE Test L1 LCS concrete.[2] In that test, the composition was determined by chemical analysis of a portion of the concrete archive. Chemical analysis of a sample collected from the CCI-2 concrete archive had not been completed at the time this report was issued.

To prevent downward migration and possible escape of concrete decomposition gases during the course of the experiment, the electrode penetrations through the bottom support plate are sealed using O-rings. As described in the next section, the test section was leak checked at 83 kPa differential pressure as part of pretest operations, and found to have a very low leak rate. On this basis, essentially all concrete decomposition gases migrated upwards through the melt pool during the experiment, as opposed to partial loss through the bottom support plate of the apparatus. Reinforcing rod is eliminated so that it does not mask or delay the attainment of a fully oxidized melt. To prevent thermal shock of the concrete basemat and sidewalls during the initial exothermic chemical reaction, the concrete surfaces are protected by a layer 3 mm thick layer of ZrO_2 felt insulation (density ~480 kg/m^3; thermal conductivity ~0.14 W/m•K at 1170 °C). After the exothermic reaction is complete, the felt dissolves into the melt.

The density of the LCS concrete is ~2330 kg/m^3, which is calculated on the basis of the measured mass and volume of the CCI-2 concrete archive sample. Instrumentation locations within the concrete sidewalls and basemat are described later in this section.

Table 2-2. Engineering Composition of CCI-2 LCS Concrete Basemat and Sidewalls.

Constituent	wt %
Coarse Aggregate	44.8
Common Sand	32.4
Fly Ash	2.7
Type 1 Cement	14.1
Tap Water[a]	6.0

[a]Contains 1.4 ml/l Airalon 20 Air Entraining Agent (AEA).

Table 2-3. Estimated Chemical Composition of LCS Concrete.

Constituent	Wt%
SiO_2	28.3
MgO	9.6
CaO	26.0
Al_2O_3	3.5
TiO_2	0.14
K_2O	0.6
Fe_2O_3	1.6
TiO_2	0.14
Na_2O	1.1
H_2O-free -bound	2.0 4.1
CO_2	21.4

2.9 Corium Composition

As shown in Table 2-1, the corium composition for CCI-2 is specified to contain 8 wt % calcined LCS concrete as an initial constituent. As part of the developmental work for the SSWICS-1 experiment,[3] a specific thermite was developed to produce this particular melt composition. The thermite reaction is of the form:

$$1.22U_3O_8 + 3.3Zr + 0.6Si + 0.32SiO_2 + 0.46Mg + 0.91\ CaO + 0.13Al + 2.01CrO_3 \rightarrow$$

$$3.66UO_2 + 3.3ZrO_2 + 0.92SiO_2 + 0.46MgO + 0.91CaO + 0.065Al_2O_3 + 2.01Cr;$$

$$Q = -262.2\ \text{kJ/mole}\ (1.816\ \text{MJ/kg});$$

$$T_{adiabatic} = 2568\ ^\circ\text{C}$$

$$T_{actual} \sim 2100\ ^\circ\text{C}$$

The composition of the melt produced from this reaction is summarized in Table 2-4, while the detailed pre- and post-reaction compositions are provided in Table 2-5. Note that the pre- and post-reaction compositions shown in these tables do not include an additional 338.56 kg UO_2 that is in the form of crushed pellets. The pellets serve as a protective layer for the cast MgO sidewalls behind the two banks of tungsten electrodes (see Figures 2-4 and 2-5). This material will not participate in the initial exothermic chemical reaction, and will remain essentially intact as a protective layer during the ensuing core-concrete interaction. The actual mass of UO_2 that dissolves into the over the course of the experiment is determined as part of the posttest examination activities.

As shown in Figure 2-8, the thermite powders (i.e., 400 kg) are packed into the test section in a large, 1.7 mil aluminized Saran bag that is pre-installed over the basemat. The total weight of bagging material for CCI-2 is 156.6 g, which amounts to an average contaminant level of 0.039 wt % in the thermite based on the entire charge mass of 400 kg. The thermite is packed in the bag to prevent water absorption by CrO_3 and concrete oxides (principally CaO and SiO_2), since these constituents are hygroscopic. As an additional measure to prevent moisture infiltration into the thermite from the concrete, the basemat and sidewalls are completely covered with continuous sheets of Saran film before the thermite is loaded. See Figure 2-9 for a photograph showing the film installed over the concrete basemat.

Table 2-4. Post-Reaction Bulk Composition for CCI-2 Thermite.

Constituent	Wt%
UO_2	60.62
ZrO_2	24.90
Calcined Concrete	8.07[a]
Cr	6.41

[a]Calcined limestone/common sand concrete, consisting of 42.0/14.1/38.8/5.1 wt% SiO_2/MgO/CaO/Al_2O_3

Table 2-5. Detailed Pre- and Post-Reaction Compositions for CCI-2 Thermite.

Constituent	Reactant		Product	
	Wt %	Mass, kg	Wt %	Mass, kg
U_3O_8	63.01	252.04	-	-
UO_2	-	-	60.62	242.48
Zr	18.42	73.68	-	-
ZrO_2	-	-	24.90	99.60
Si	1.03	4.12	-	-
SiO_2	1.18	4.72	3.39	13.56
Mg	0.69	2.76	-	-
MgO	-	-	1.14	4.56
Al	0.22	0.88	-	-
Al_2O_3	-	-	0.41	1.64
CaO	3.13	12.52	3.13	12.52
CrO_3	12.32	49.28	-	-
Cr	-	-	6.41	25.64
Total	100.00	400.00	100.00	400.00

The powder composition shown in Table 2-5 packed to a height of ~55 cm above the surface of the concrete during loading for CCI-2. Thus, the average packing density is evaluated as ~2900 kg/m^3, which yields an average void fraction of ~48% for the entire charge assuming a theoretical density of 5550 kg/m^3.

2.10 Instrumentation and Data Acquisition

The CCI-2 facility is instrumented to monitor and guide experiment operation and to log data for subsequent evaluation. Principal parameters which are monitored during the course of the test include the power supply voltage, current, and gross input power to the melt; melt temperature and temperatures within the concrete basemat and sidewalls; crust lance position and applied load; supply water flow rate; water volume and temperature within the test apparatus, and water volume and temperature within the quench system tanks. Other key data recorded by the DAS includes temperatures within test section structural sidewalls, off gas temperature and flow rate, and pressures at various locations within the system.

All data acquisition and process control tasks are managed by a PC executing LabVIEW 6.i under Windows XP. Sensor output terminals are connected inside the test cell to model HP E1345A 16-channel multiplexers, which are integrated into a mainframe chassis in groups of eight. An illustration of the DAS setup is provided in Figure 2-21. The multiplexers direct signals to an HP E1326B 5 ½ digit multimeter incorporated into each chassis. Three independent 128 channel systems are used for a total capacity of 384 channels. The detailed channel assignment lists for each of the three systems is provided in Appendix A.

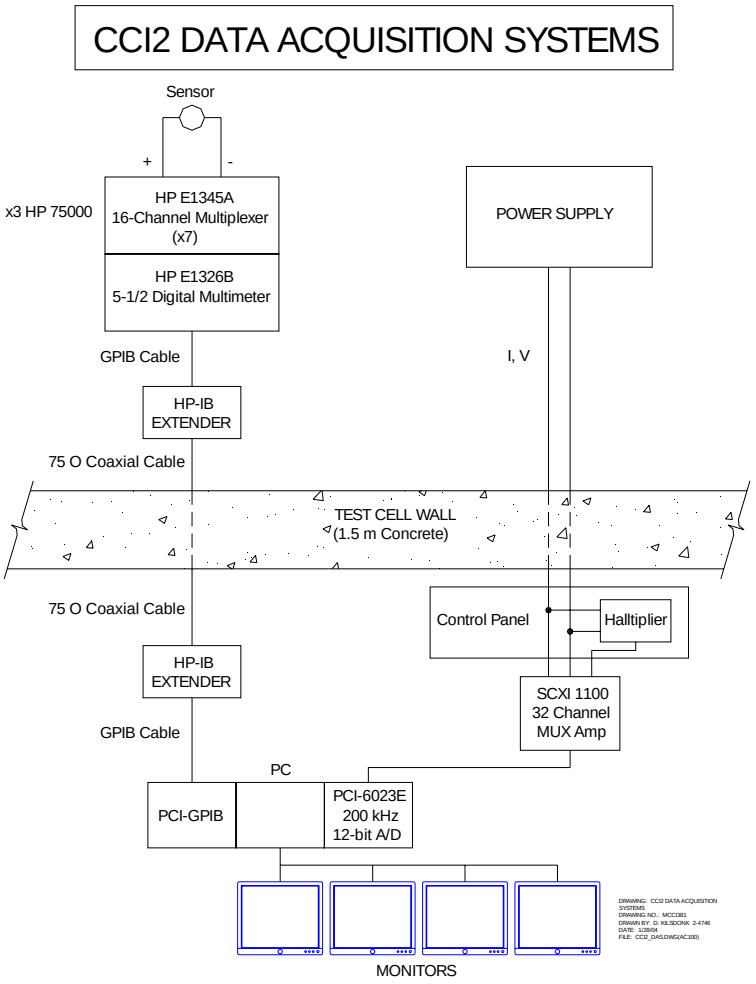

Figure 2-21. Data Acquisition System Setup for CCI-2.

Signal noise is reduced by the digitizer through integration over a single power line cycle (16.7 ms). The digitized sensor readings are routed from the test cell to the PC in the control room via two HP-IB extenders. The extenders allow the ASCII data from the HP to be sent through the cell wall over a BNC cable. The extender within the control room then communicates with a GPIB card within the PC. This configuration also permits remote control of the multimeter through LabVIEW.

Integration of the signal over the period of a power line cycle limits the speed with which the multiplexer can scan the channel list. The minimum time for the digitizer to scan the channel list is ~1.7 s (16.7 ms • 100 channels/chassis for this test). Though the three systems operate independently, implying the ability to update all 300 channels in roughly two seconds, the actual time required for the update is about 5.5 s.

Instrumentation is selected to provide the necessary measurements to determine the time-dependent 2-D concrete ablation profile and the melt temperature distribution. Detailed plan and elevation views of the basemat thermocouple layout are provided in Figures 2-22 and 2-23, respectively, while the concrete sidewall instrumentation locations are shown in Figure 2-24. The thermocouple elevations shown in these figures are all taken with respect to the original height of the basemat surface (Z = 0). Both the concrete sidewalls and basemat are

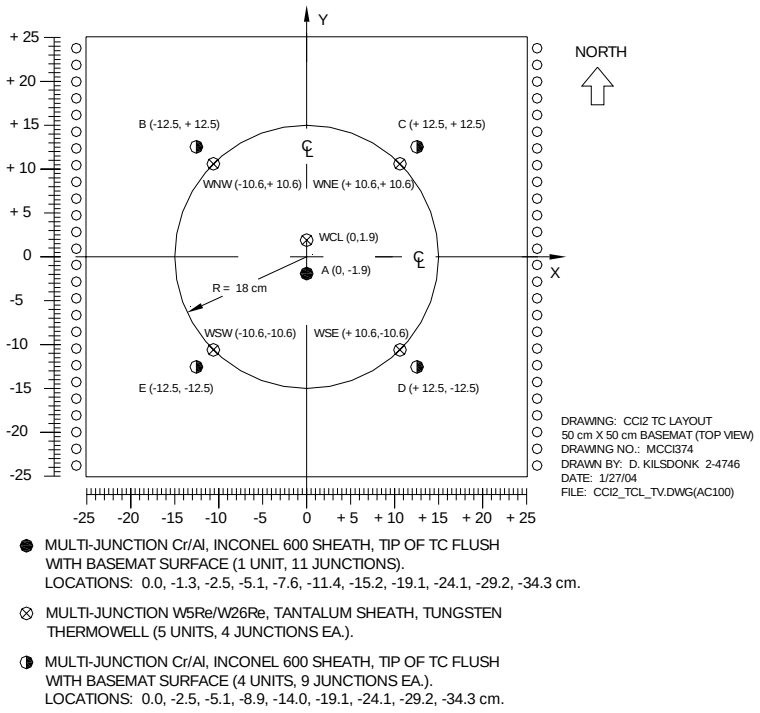

Figure 2-22. Plan View of Basemat Instrumentation Layout (dimensions are in cm).

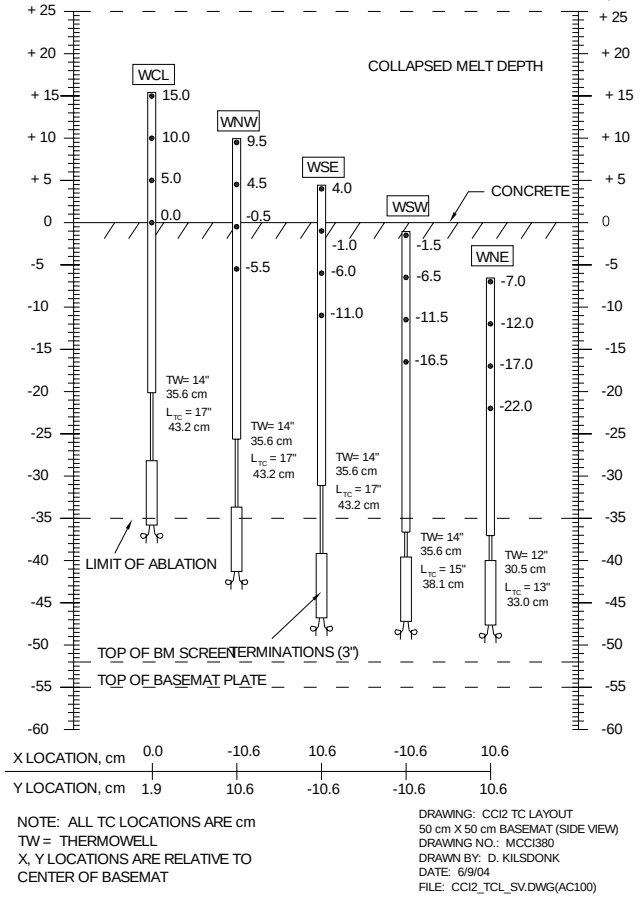

Figure 2-23. Elevation View of Basemat Type C Thermocouple Locations.

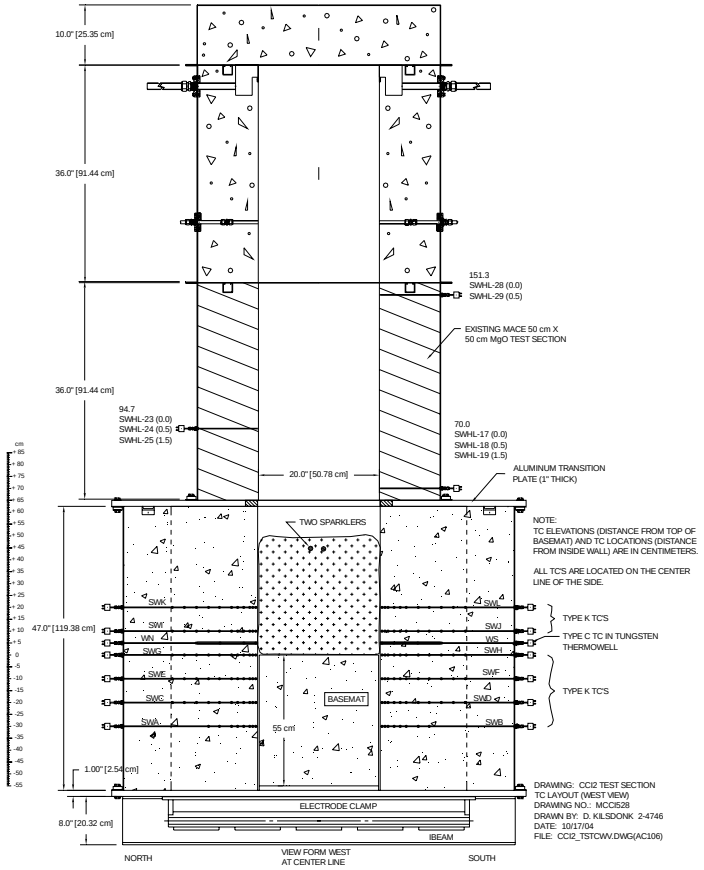

Figure 2-24. CCI-2 Test Section Sidewall Instrumentation (View From West).

instrumented with multi-junction Type K thermocouple assemblies to determine the 2-D ablation profile as a function of time. In addition, Type C thermocouple assemblies in 9.5 mm diameter long-body tungsten thermowells protrude upwards from the basemat and radially inwards from the concrete sidewalls in several locations. The purpose of these instruments is to provide data on the axial and radial melt temperature distribution as a function of time. A total of five four-junction (basemat) and two eight-junction (sidewalls) Type C arrays (36 junctions total) in tungsten thermowells were used in the test. A photograph showing the thermocouple assemblies installed in the basemat form prior to placement of the concrete is provide in Figure 2-25.

The test section sidewalls and upper lid are also instrumented with a total of 32 Type K and Type C thermocouples to measure the sidewall heat up both prior to and after water addition, and also to measure the sidewall quench rate above the melt surface after water is added. Illustrations of the TC locations in the sidewalls of the test section are provided in Figure 2-24 and 2-26.

One method for monitoring water level in the test section is provided by a differential level probe which is inserted through a sealed penetration in the lid. The probe is maintained in a retracted position during the initial heat up phase until water is added to the test section. After water is added, the probe is inserted to a distance of 50 cm from the initial basemat surface (25 cm from the initial collapsed melt surface). The probe tip is instrumented with two 1.6 mm diameter ungrounded junction Type K TC's which monitor the plenum gas temperature prior to water addition; thereafter, the TC's monitor the water temperature over the melt surface. The probe tip location above the melt surface after insertion is shown in Figure 2-27.

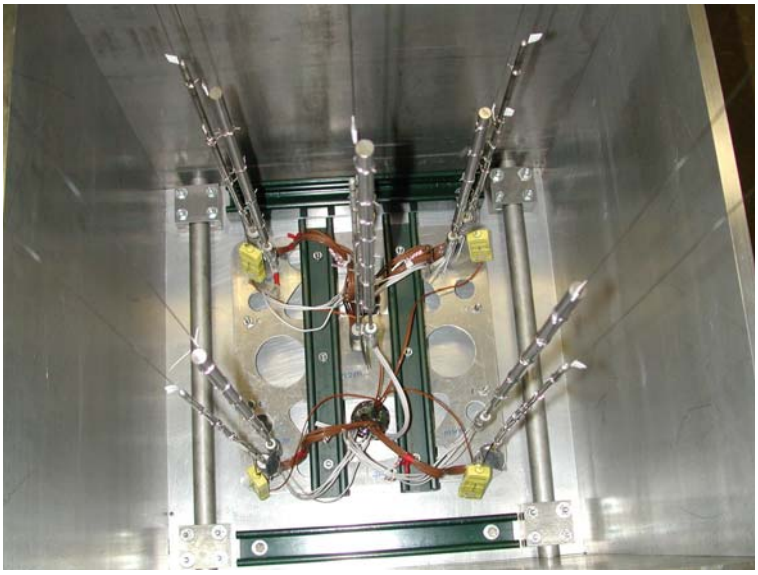

Figure 2-25. Thermocouple Arrays Installed in Basemat Concrete Form.

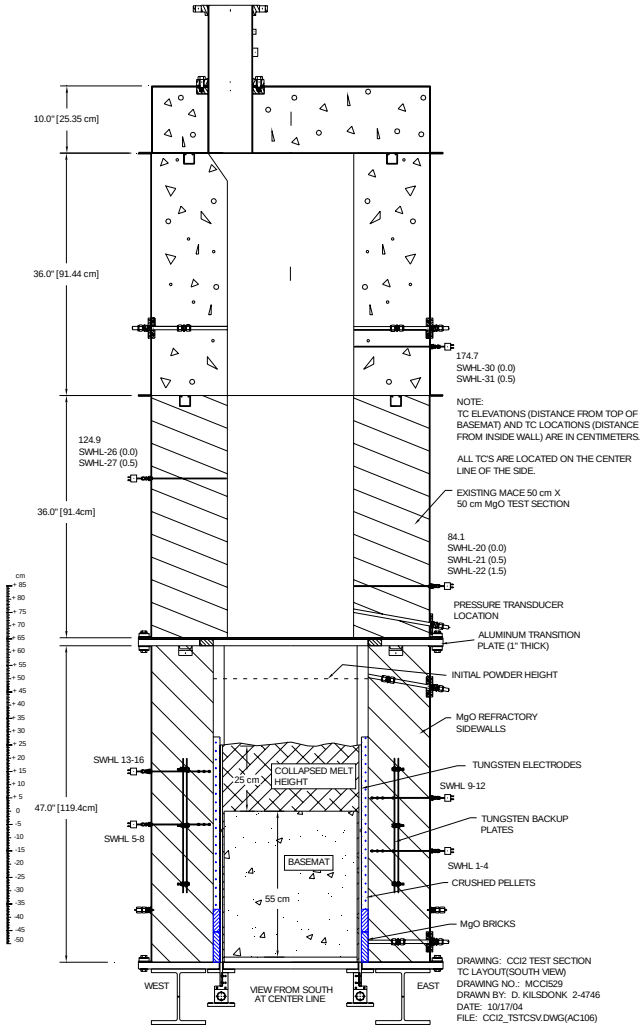

Figure 2-26. CCI-2 Test Section Sidewall Instrumentation (View From South).

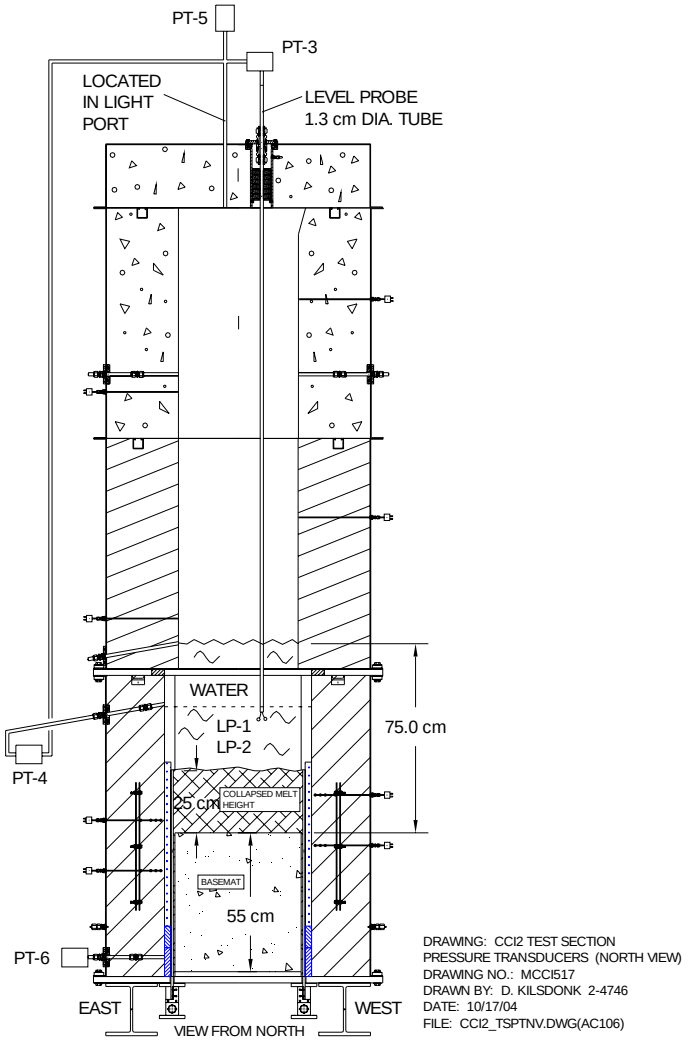

Figure 2-27. CCI-2 Test Section Pressure Transducer Layout.

Aside from the insertable water level probe, two additional methods are provided to monitor the water volume in the test section. The first is a static water level port located in the North sidewall 55 cm from the initial basemat surface (30 cm from the initial collapsed melt surface). The port location is shown in Figure 2-27. The second redundant method is provided by an on-line calculation of the water volume in the test section based on conservation of mass; i.e., the water volume in the test section at any time is equal to the initial volume in the supply/quench systems minus the volume in the supply/quench systems at the current time.

The water supply tank is equipped with a magnetic float to measure the time-dependent water level. As a redundant level measurement technique, the supply tank is also equipped with a differential PT. Water flow rate to the test section is monitored by a paddlewheel flowmeter. The location of the supply system instrumentation is shown in Figure 2-15.

The quench, overflow, and spray tanks are instrumented to measure the transient energy deposition due to steam generation from corium quenching in the test section. The quench and overflow tank instruments are shown in Figure 2-16, while the spray tank instrumentation is shown in Figure 2-17. Each tank is equipped with a magnetic float and (redundant) differential PT to measure the accumulated water volume due to steam condensation. Transient water temperatures in all tanks are monitored using Type K TC's (four in the quench tank, and one

each in the spray tank and overflow tanks). Water flow rate and temperature differential across the quench tank cooling coil are monitored with a paddlewheel flowmeter and Type K TC's, respectively, thus providing a measurement of the time-dependent energy extraction rate from the water mass in the tank. The main steamline between the test section and quench tank is instrumented with Type K TC's to measure the local gas and pipe structure temperatures. The steamline thermocouple locations are shown in Figure 2-13. The outlet noncondensable gas flow rate from the spray tank is monitored by a Hastings mass flow transducer. The location of the off gas system instrumentation is shown in Figure 2-19.

Key system pressures are monitored with strain-gauge type pressure transducers manufactured by Sensym, Inc. As shown in Figures 2-15 through 2-17 and 2-27, the pressure in all system tanks is monitored, as is the test section plenum pressure. An Additional PT is located in the lower test section to monitor the pressure beneath the melt upper surface. This transducer is mounted on the east sidewall of the test section at an elevation of 45 cm beneath the initial concrete surface. The gap between the MgO sidewalls and the electrodes is packed with crushed UO_2 pellets during loading of the corium charge. Thus, this PT will sense the pressure beneath the melt surface as long as the gap does not plug during the test.

In terms of the power supply operating parameters, voltage drop across the tungsten electrode bank is monitored with the DAS voltmeter, while current input is monitored with two parallel 5000:1 current transformers. Power input to the melt is monitored with two Hall Effect meters. At the 5th PRG meeting, the PRG requested that the project attempt to devise a method for monitoring the current through selected tungsten electrodes to determine if non-uniformities in the DEH power input occurred during the test. Clearly, the optimal method for doing this would be to use small current transformers placed around the selected electrodes. However, there was insufficient space to incorporate these devices into the existing test section design. As a result, an attempt was made to monitor the voltage drop across the lower 15 cm of selected electrodes using lacquer-insulated 14 gauge wires that were passed through potted seals into the test section along the bottom support plate and clamped at the 15 cm elevation. Given the resistivity of tungsten, then a voltage drop of ~ 20 mV should develop over the 15 cm length for every 200 Amps of current drawn. Figure 2-28 provides a drawing that shows the electrodes that were wired for current monitoring in CCI-2.

In addition to the above instrumentation, visual information regarding the core-concrete interaction and melt quenching behavior is provided by a video camera mounted on the upper lid of the apparatus. The camera location and field of view is shown in Figure 2-3. Five area video monitors are also used in the cell to monitor for leaks, and also to record any disruptive events (i.e., steam explosion) should one occur. Finally, the crust lance is equipped with load and displacement transducers to provide data on the crust load vs. time during the crust failure sequence.

.

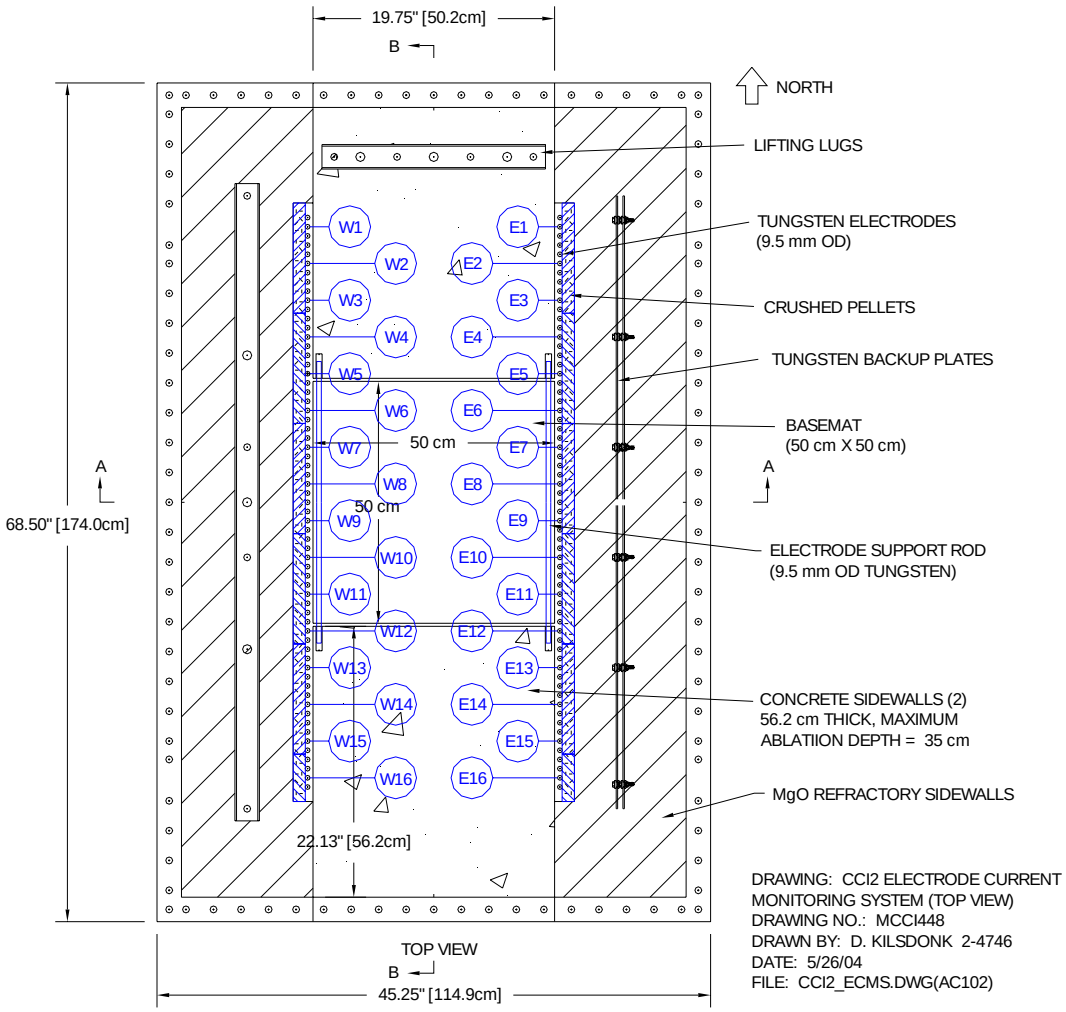

Figure 2-28. Illustration of CCI-2 Electrode Current Monitoring System Layout.

3.0 TEST PROCEDURES

3.1 Pretest Operations

Assembly of the apparatus began by installing the tungsten electrodes (126 total; 63 per side) into machined copper electrode clamps. The electrode clamps were then attached to the bottom of the 2.54 cm thick aluminum support plate which served as the foundation for the entire apparatus. With the electrode clamps installed, the support plate was moved into position on the ZPR-9 reactor bed. The concrete basemat was then placed atop the support plate. The top surface of the basemat was insulated with a 3 mm thick layer of low density ZrO_2 felt. The basemat was then completely covered with a continuous sheet of 1.7 mil aluminized Saran film to prevent moisture contamination of the thermite powders from the basemat once the powders were loaded into the test section. The lower test section concrete and MgO sidewalls were then set in place. The concrete sidewalls were also covered with ZrO_2 felt and aluminized Saran before placement to prevent moisture contamination of the thermite from these components once the powders were loaded. The lower section flange bolts and clamping bars were then installed and torqued according to an approved procedure.

In parallel with test section assembly, the thermite powders were mixed in preparation for corium loading. As a precursor for initiating mixing, a gas sample test[a] was conducted to verify that the initial level of volatile impurities in a sample prepared from the CCI-2 thermite constituents was sufficiently low to preclude excessive gas release during the burn. The results of this test indicated moisture and nitrogen contents well within acceptable limits. On this basis, mixing was initiated.

Once the lower section was assembled, preparations for loading of the corium charge began. A single, large 1.7 mil aluminized Saran bag was preinstalled over the basemat. During loading, the 400 kg thermite charge was placed within this bag in order to reduce the amount of bagging material present in the thermite. As the powders were placed in the test section, the basemat melt temperature thermocouples were monitored to detect any localized heating in the corium powders. If heating was observed, the cell was to be immediately evacuated. As the thermite was placed, the gap between the tungsten electrodes and MgO sidewalls was filled with crushed UO_2 pellets. The crushed pellets served as a protective layer against excessive chemical/thermal attack by the corium during the test. Once loading was completed, two sparkler igniters were placed a few centimeters below the top of the powders near the center of the test section, and then the bag was folded and sealed. An illustration of the loading scheme is provided in Figure 2-8. As described in Section 2.9, the use of the single large bag for containment of the thermite resulted in a low bagging material contaminant level of 0.039 wt % present in the charge at the time of ignition.

Once loading was completed, a removable sample train containing an individual, 2.0 kg bagged sample of thermite was installed over the powder bed; an illustration is provided in Figure 3-1. The sample train was removed weekly and the sample weighed to monitor the moisture pickup by the thermite during the period between loading and test initiation. Note from Figure 3-1 that the top portion of the train also contained a 4.5 kg canister of desiccant. The

[a] The gas sample test procedure consists of igniting a representative sample of the thermite in a closed vessel. The amount of noncondensable gas produced is determined from the ideal gas law; the composition of the evolved gases is determined using gas mass spectroscopy.

desiccant was provided to maintain the plenum gas as dry as possible during pretest operations. As an additional measure to prevent moisture accumulation in the powder bed, the lower test section was continuously purged with argon (2 slpm) from the time loading was completed until the test was initiated.

After installation of the sample train, the remainder of the test apparatus was assembled. This included installation of the transition plate, two upper sidewall sections, and finally the enclosure lid. Peripheral instrumentation was then installed on the lid and sidewalls of the test section. The main steamline run from the test section to the primary quench tank was completed, as well as the pressure relief line from the test section to the auxiliary tank. (The main steamline was closed off from the test section using an insertable blank-off plate throughout pretest operations to preclude moisture migration from the quench tank into the test section).

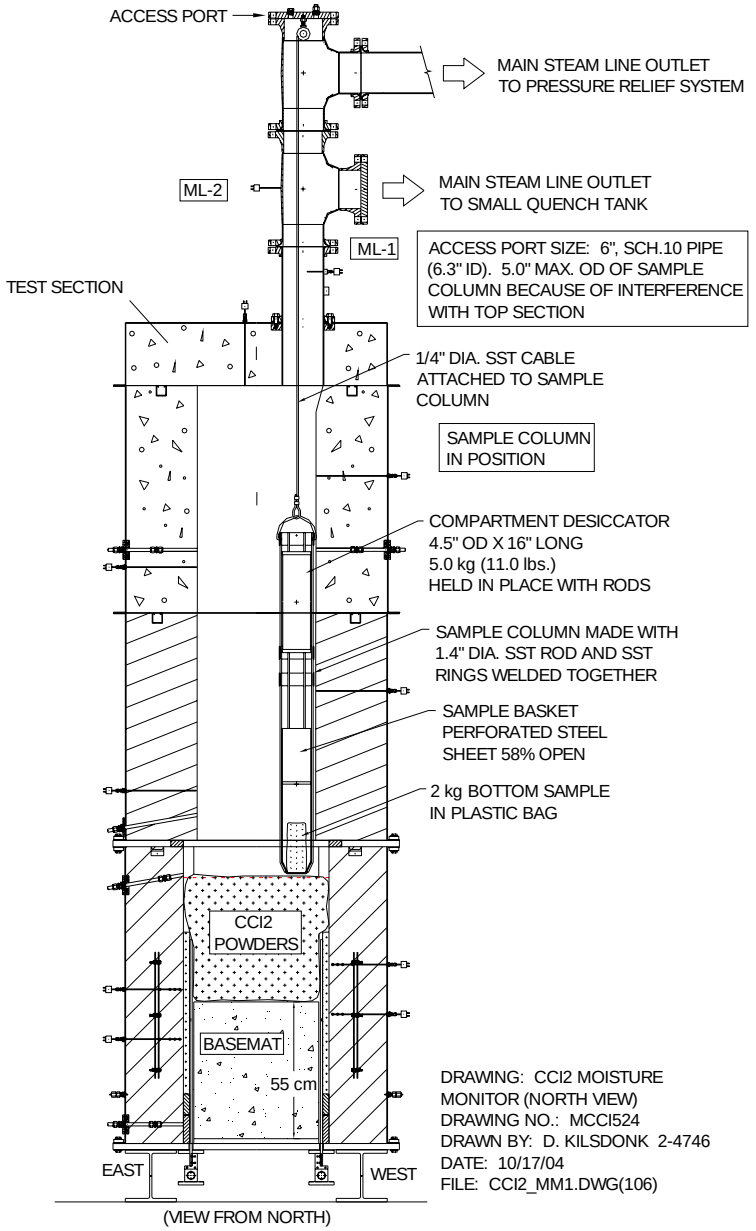

Figure 3-1. Illustration of Thermite Sample Train Installed in Test Section.

After assembly was completed, extensive system checkout procedures were performed to ensure that the facility was in proper working order. This included a proof test of the test section at 83 kPad, which is 20 % in excess of the pressure relief system activation pressure of 69 kPad. The pressurization gas for this test was argon. An insertable blind flange was installed upstream of the rupture disk in the pressure relief line to isolate this system. During the test, the apparatus was gradually pressurized to the proof pressure of 83 kPad. After a 1 minute hold at this pressure, the system was isolated to determine the leak rate. The leak rate of the CCI-2 test section was found to be 2.3 kPa/min (10 slpm at a nominal pressure of 55 kPad, which was significantly below the acceptable leak rate of the fully assembled test section (i.e., < 2 % of the expected peak gas/vapor generation rate during the test).

Pretest preparations for CCI-2 culminated with a final full system checkout that involved remotely running all equipment with the power supply in operation across a water cooled dummy load. Once the full system check was completed, final system preparations were carried out. These efforts included: (i) hookup of the power supply to the tungsten electrodes through water cooled buss bars, (ii) installation of the final piping connection between the water supply tank and the test section, and (iii) removal of the sample train from within the test section. Following connection of the power supply to the electrode clamps, the key for the power supply lockout located in the cell, as well as the key for the interlock located on the control room console, were assigned to a custodian who kept the keys in their possession until the test was initiated. This step was taken to preclude inadvertent activation of the power supply.

Over the four week time interval spanning pretest operations, the moisture content of the removable sample of bagged thermite increased gradually from 0.169 wt % to 0.190 wt %. The final moisture content was well below the maximum permissible level of 0.3 wt %. On the basis of this information, final approval was granted to proceed with the execution of Test CCI-2.

3.2 Test Operations

Test specifications for CCI-2 are summarized in Table 1-1. The planned operating procedure is described first, followed by presentation of the actual test operating procedure.

The target input power, simulated by Direct Electrical Heating (DEH), was 120 kW. After melt formation, the input power would be held constant at the 120 kW target for 5.5 hours of dry core-concrete interaction, or until a 30 cm ablation depth was reached in either the radial or axial directions. After one of these two criteria was met, the cavity would then be flooded. However, if a crust was present at the melt upper surface, the crust lance would be used to fail the crust prior to flooding so that the water would be able to contact the underlying melt. Following water addition, the power supply operation would be switched from constant power at 120 kW to a constant voltage operating mode. (With constant voltage, the input power density *in the melt zone* would remain relatively constant if a significant quench front developed). Forty five minutes after water addition, or after the debris cooling rate had been reduced to a relatively low level, the crust would be failed with the lance to obtain data on the transient crust breach cooling mechanism. After breach, power supply operations would continue for an additional 45 minutes, yielding a total operating period of 90 minutes with water present in the cavity, or until the ablation limit of 35 cm was reached in either the radial or axial directions. At this point, the input power would be turned off and the test terminated.

CCI-2 was performed on 24 August 2004. On the evening prior to the experiment, the apparatus was inerted with a slow bleed of helium into the test section. On the day of the experiment, the apparatus was brought up to operating conditions, a final walk through

inspection was performed by operating personnel, the thermite igniter was hooked up, and finally the power supply was energized before the containment was evacuated and sealed. Data acquisition was initiated at approximately 5:13 pm. Coolant and cover gas flows were brought up to design conditions, and the cell ventilation system was closed and sealed per test procedures.

The event sequence for CCI-2 is provided in Table 3-1. In the discussion that follows, time t = 0 corresponds to the point at which the thermite burn was completed. This also corresponds to the time at which the melt made initial contact with the concrete basemat of the apparatus. The criteria used to define the onset of concrete ablation at a given location was that the local temperature reached the LCS concrete liquidus temperature of 1295 °C.[2]

As shown in Table 3-1, data acquisition began at -7.57 minutes relative to initial melt contact with the basemat. As shown in Figure 3-2, power was applied to the nichrome wire/sparkler located at the top of the powder charge at -0.77 minutes. Based on video camera data from the test section, the off gas system flowmeter reading, and system pressure transducer readings, thermite ignition was announced and logged in the control room at -0.59 minutes. Based on readings from thermocouples located near the bottom of the charge, the burn front reached the bottom of the bed of powders at 0.0 minutes, yielding an overall burn time of ~ 37 seconds, which was within the planning basis for the experiment. The readings from selected melt temperature thermocouples are shown in Figure 3-3 over the first 5 minutes of the interaction. As is evident from this collection of data, the average melt temperature at the end of the burn was ~2000 °C. Onset of ablation was detected at all five basemat thermocouple array locations (see Figure 2-22), as well as all six sidewall array locations on the North and South sidewalls initially exposed to corium (i.e., at the 0.0 cm, +10.0 cm, and +20.0 cm elevations; see Figure 2-6) within the first 0.38 minutes of the interaction.

At completion of the burn, a power supply current ramp up to the target power of 120 kW was initiated. This power level was reached at 1.56 minutes, where it was essentially maintained for the balance of the test involving dry cavity operations. At 1.16 minutes, aerosols within the test section plenum cleared to the point that the melt surface could be seen with the lid video camera. This view revealed a melt pool covered by crust segments that were not rigidly bonded to each other.

Over the first five minutes of the interaction, the average melt temperature fell rapidly before stabilizing at ~1800 °C. During the next 18 minutes, the melt pool was quiescent, and the average melt temperature gradually climbed back to ~1910 °C during this interval. At 23.07 minutes, sudden chaotic melt interaction was observed, and the view of the melt surface was rapidly occluded by aerosol. Over the next 32 minutes, ablation increased rapidly, reaching a peak radial rate of 1.6 cm/min on the North sidewall at the +10.0 cm elevation, and a peak axial rate of 0.5 cm/min at the basemat centerline. However, these rapid ablation rates were not sustained; after an ablation depth of 7.6 cm was reached in both the radial and axial directions, the ablation rate slowed dramatically. During this time interval (i.e., from 23.07-55.00 minutes), the crust at the melt upper surface remelted, revealing substantial melt convection and churning by the sparging concrete decomposition gases. As the interaction progressed, stable mantles of crust material were evident, growing steadily outwards from both inert MgO sidewalls. The melt temperature steadily declined from ~1910 °C at the start of this period to ~1800 °C. At 55.41 minutes, aerosols in the plenum cleared sufficiently to reveal the debris upper surface which was again covered by a continuous crust.

Table 3-1. CCI-2 Event Sequence (times relative to melt contact with basemat).

Time (Minutes)	Event
-7.57	DAS started.
-0.77	Power applied to thermite igniter wire.
-0.59	Thermite burn initiated.
0.00	Thermite burn completed (burn time ~ 37 seconds); initial melt temperature ~2000 °C
-0.1 - 0.38	Onset of basemat ablation detected at centerline, in all four basemat quadrants, and at 0.0 cm, +10.0 cm, and +20.0 cm elevations on both North and South concrete sidewalls.
1.16	Aerosol clears in test section plenum revealing crusted melt upper surface.
1.56	Target input power of 120 kW reached.
5.00-23.00	Quiescent period; average melt temperature falls rapidly to ~1800 °C at 5:00 minutes before stabilizing and then gradually increasing back up to ~1910 °C at 23:00 minutes.
23.07	Initiation of sudden interaction observed on video; view is occluded by aerosols.
23.00-55.00	Average melt temperature peaks at the start of the period, and then steadily declines to ~1800 °C at the end of the period.
34.94 - 35.62	Melt eruption near North sidewall; aerosols gradually block view.
35.30 - 38.40	Ablation burst detected at + 10 cm elevation on North sidewall (SWI-Array). Local ablation depth proceeds from 2.5 to 7.6 cm; average ablation rate = 1.6 cm/min.
37.41 - 40.91	Aerosols gradually clear to reveal chaotic melt churning. View gradually deteriorates again.
42.74 - 43.58	Aerosols gradually clear again, melt churning is still evident. Large crust mantles evident on East and West walls. View is eventually blocked again by aerosols.
42.18 - 52.81	Axial ablation picks up dramatically, proceeding from 2.5 to 7.6 cm; average ablation rate =0.5 cm/min.
53.90	Voltage limit of 56 volts reached on tap 1 of the power supply; changed to Tap 2 (112 volt) voltage tap.
55.41	Aerosols clear slightly to reveal upper crust. A single opening exists near the North sidewall.
62.74 - 66.66 67.23 - 67.56 68.07 - 69.96 70.53 - 85.66	Eruption through holes in crust near Northeast corner.
146.80 - 148.02 149.26 - 151.20 152.26 - 154.99	Eruptions through holes in crust in Southwest corner.
165.43 169.25	Large volume, short duration lava flows occur near South wall.
177.38 - 178.89 178.82 - 179.10 182.60 - 189.26	Eruption begins near South wall, and eventually a large hole develops through the crust near the centerline. The latter two eruptions are intense, and they culminate with a single vent hole still open near the Southwest corner.
195.68 - 199.6	Minor intermittent eruptions through Southwest crust opening.
202.35 - 204.26 212.60 - 215.33 220.68 - 229.80	Eruptions through vent hole in Southwest corner. Additional hole develops near South wall centerline but this hole eventually closes.
266.82 - 270.15 275.32 - 278.65	Eruptions through opening that gradually grows towards centerline. At culmination, hole in crust is present in Southeast corner.
284.80 - 285.66 286.82 - 287.49 288.49 - 289.15	Intermittent eruption activity through crust opening in Southeast corner.

Table 3.1 (Contd.) CCI-2 Event Sequence.

Time (Minutes)	Event
298.9	Crust lance probe inserted in an attempt to breach the bridge crust. Peak load of ~4.84 kN applied. Crust was not breached.
300.79	Water addition initiated, average melt temperature ~1540 ºC. Peak debris cooling rate reaches 1.4 MW. Water is evident flooding through hole in crust near Southeast corner.
301.5	Sidewall ablation reaches 29.2 cm depth in North sidewall at +10.0 cm elevation.
305.20	Quench tank water reaches saturation; steam blow over into spray tank begins.
312.6	Power supply operation in constant voltage operating mode initiated at voltage level just prior to water addition (83 volts).
320.60	Spray tank water reaches saturation; steam venting through off gas system into the cell atmosphere is evident.
325.82 - 326.82 330.49 - 332.15	Eruptions observed occurring below the bridge crust, as evidenced by luminescence through crust opening in the Southeast corner.
342.6	Quench tank water falls below saturation temperature, indicating that debris cooling rate has fallen below quench tank coil capacity of ~ 170 kW.
346.0	Crust lance used in an attempt to breach the bridge crust. Peak load of 3.35 kN applied. Crust was not breached.
423.1	Test terminated on the basis that concrete temperatures had stabilized and input power had fallen below 15 % of initial value.
423.1	Power supply operations and data acquisition terminated.

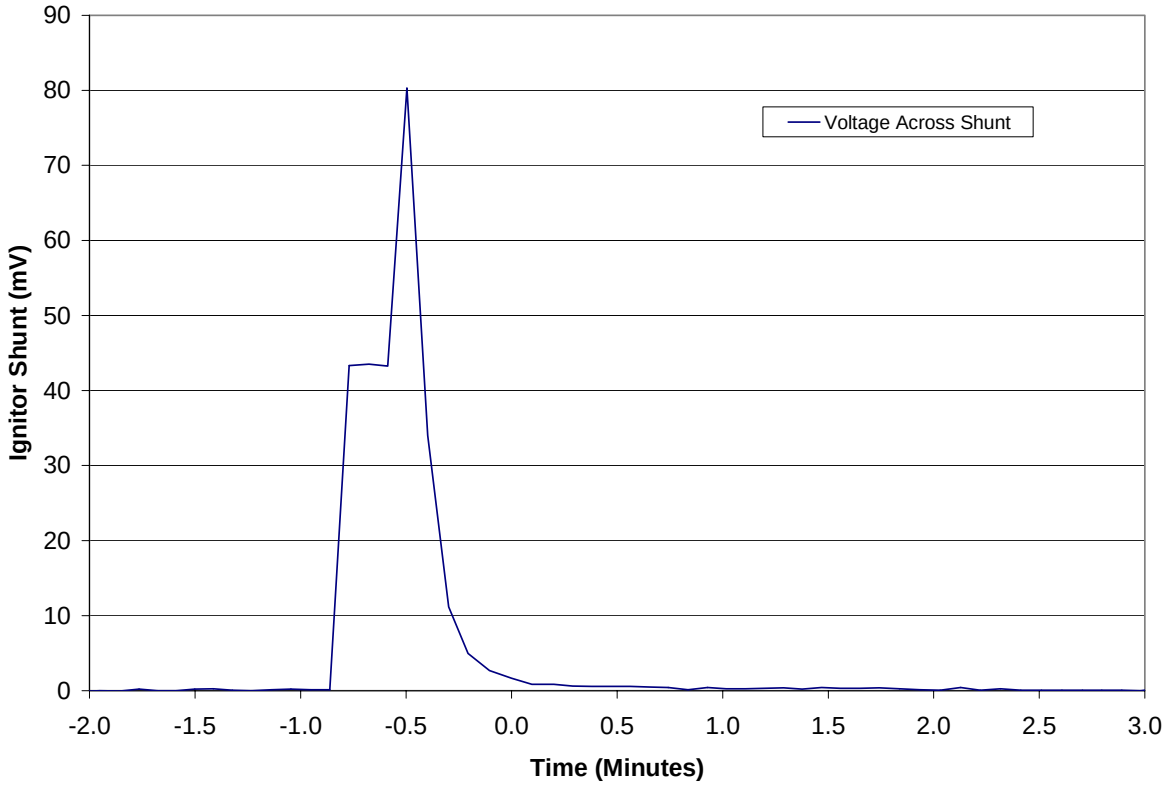

Figure 3-2. Voltage Reading Across Thermite Igniter Shunt.

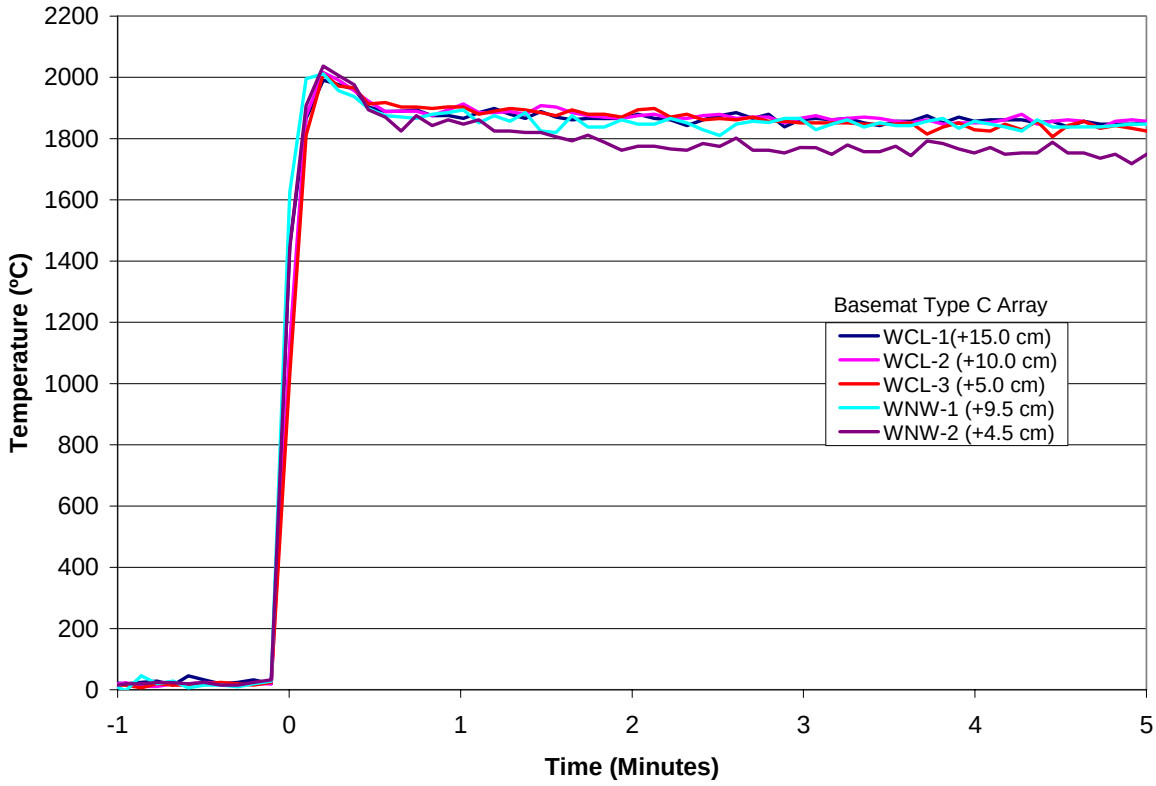

Figure 3-3. Bulk Melt Temperature Data Over the First 5 Minutes of the Interaction.

Over the next four hours, the core-concrete interaction progressed steadily in both the radial and axial directions. The average melt temperature declined steadily from ~1800 °C to ~1600 °C during this interval. A total of 21 discrete eruptive events occurred periodically through vent holes in the crust that formed at various locations. Several of these eruptions were extensive, the longest of which lasting more than 10 minutes.

At 290 minutes, it became apparent that the cavity would soon be flooded based on the criterion of reaching the 30 cm ablation depth in the North sidewall. The view of the melt upper surface indicated the continued presence of a stable crust. On this basis, the crust lance was inserted in an attempt to breach the crust at 298.9 minutes. Although the lance delivered the full load capacity of nearly 4.5 kN to the crust surface, the crust was not breached. However, the lid video camera indicated the presence of a large opening (e.g., several centimeters wide) in the southeast quadrant of crust at this time. On this basis, water addition to the cavity was initiated at 300.79 minutes. The official criterion for water addition was reached at 301.50 minutes (or just after cavity flooding was initiated), at which time the concrete liquidus temperature of 1295 °C was reached at the 29.2 cm ablation depth in the North sidewall at the +10.0 cm elevation. The cavity was flooded with 125 liters of water to bring the water level over the melt to ~ 50 cm. The peak debris cooling rate reached ~ 1.4 MW during the initial flooding stage. Makeup water was added periodically as the test progressed to maintain the water level over the melt in the range of 50 ± 5 cm.

Following cavity flooding, power supply operation was switched from constant power to constant voltage mode per the normal test operating procedure. Subsequently, the input power fell precipitously, which is consistent with substantial debris quenching. Moreover, the steaming rate from the quench process was so significant that the quench tank coil (capacity of 170 kW)

was overwhelmed, and the quench tank water inventory reached saturation at 305.20 minutes. Steam blow over into the secondary spray tank began at this time. The water inventory in the spray tank subsequently saturated at 320.6 minutes. After this time, steam was vented directly into the cell through the final off gas system until the corium quench rate fell below the quench tank coil capacity at 342.6 minutes. After this time, the quench tank water inventory fell below saturation temperature and all steam from the quench process was once again captured in that tank. During this time interval, two significant melt eruptions occurred below the bridge crust, as evidenced by luminescence observed through the crust opening in the southeastern quadrant.

Per the normal test procedure, the crust lance was reinserted ~ 45 minutes after cavity flooding in an attempt to breach the bridge crust. However, this attempt was not successful, despite delivering a peak load of 3.35 kN to the crust surface.

After this time, the input power continued to fall dramatically while the debris quenching rate remained significant. Several surviving melt temperature thermocouples indicated local debris quench to the water saturation temperature. In addition, virtually all concrete thermocouples indicated that local concrete temperatures had stabilized, and at several locations, the concrete had been cooled to water saturation temperature. On this basis, the test was terminated at 423.1 minutes, or ~ 2 hours after cavity flooding, on the basis that the input power had fallen below ~ 15 % of the initial value. Normal shutdown procedures were followed, and the DAS was restarted to record the long-term cool down data. The experiment was left unattended to cool down overnight.

4.0 TEST RESULTS

A summary description of the principal experiment results from CCI-2 is provided in this section. A complete list of instruments used in the test is provided in Appendix A, while plots of all test data are provided in Appendix B.

4.1.1 Electric Power

The DEH power supply voltage, current, and total input power for CCI-2 are shown in Figures 4-1 through 4-3, respectively. At completion of the thermite burn, the power supply voltage was steadily increased until the input power reached the target level of 120 kW at 1.56 minutes. Thereafter, input power was held constant in the range of 120 ± 10 kW over the balance of dry cavity operations. A power supply range change was made at 53.90 minutes due to the fact that the voltage limit of 56 volts had been reached on Tap 1 of the supply. In general, the power supply voltage increased and total current decreased over the course of the test. This is due to the fact that the melt becomes more resistive as concrete oxides from ablation are gradually incorporated into the melt.

Soon after cavity flooding at 300.79 minutes, power supply control was switched from constant power at the 120 kW level to a constant voltage operating mode. Operation in this manner maintains the power density constant in the molten (i.e., electrically conductive) region should a quench front develop. As is evident from Figure 4-3, input power dropped steadily after the cavity was flooded, which is indicative of extensive debris cooling. Power supply operations were terminated at 423.1 minutes after input power had dropped to < 15 % of the initial value.

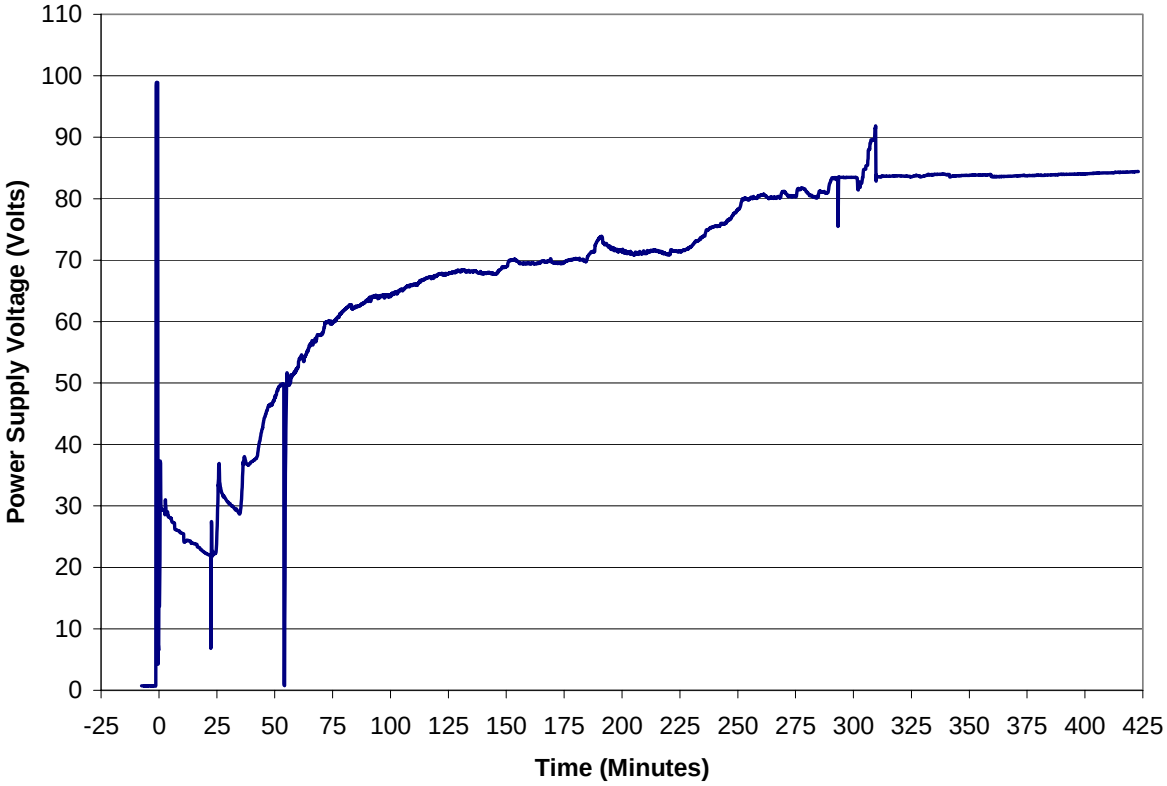

Figure 4-1. Power Supply Voltage.

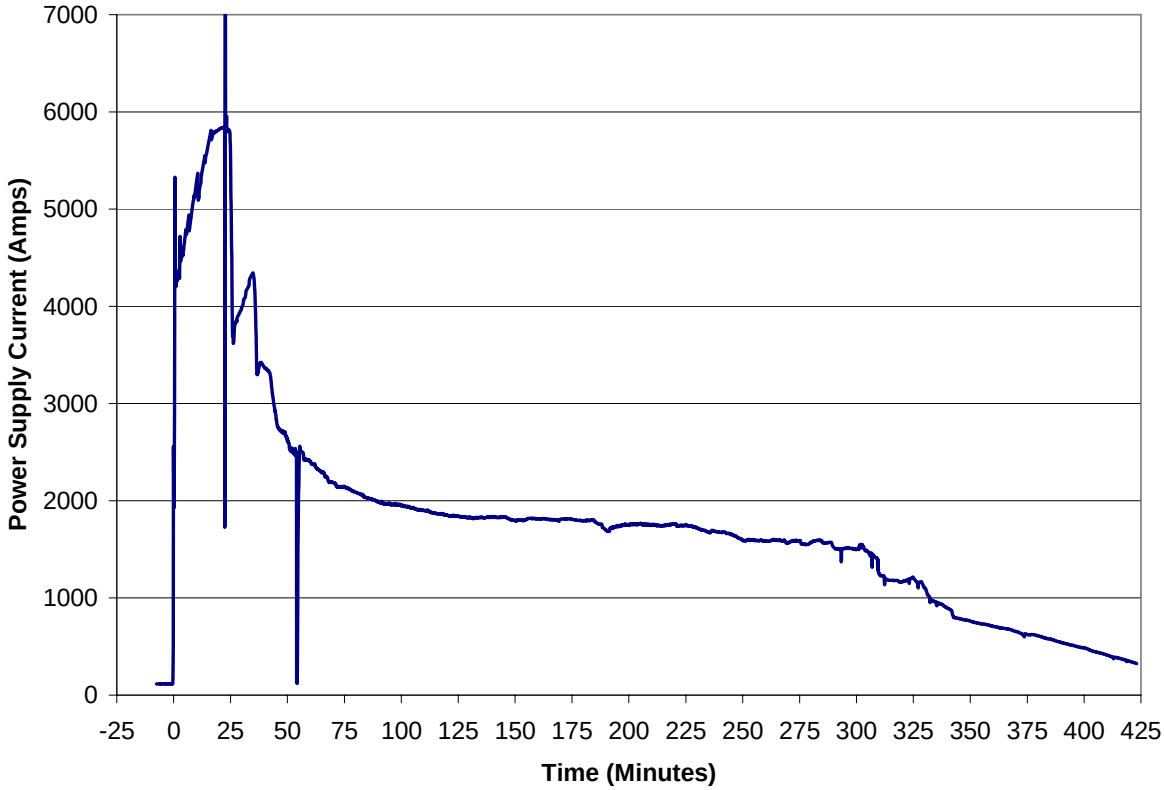

Figure 4-2. Power Supply Current.

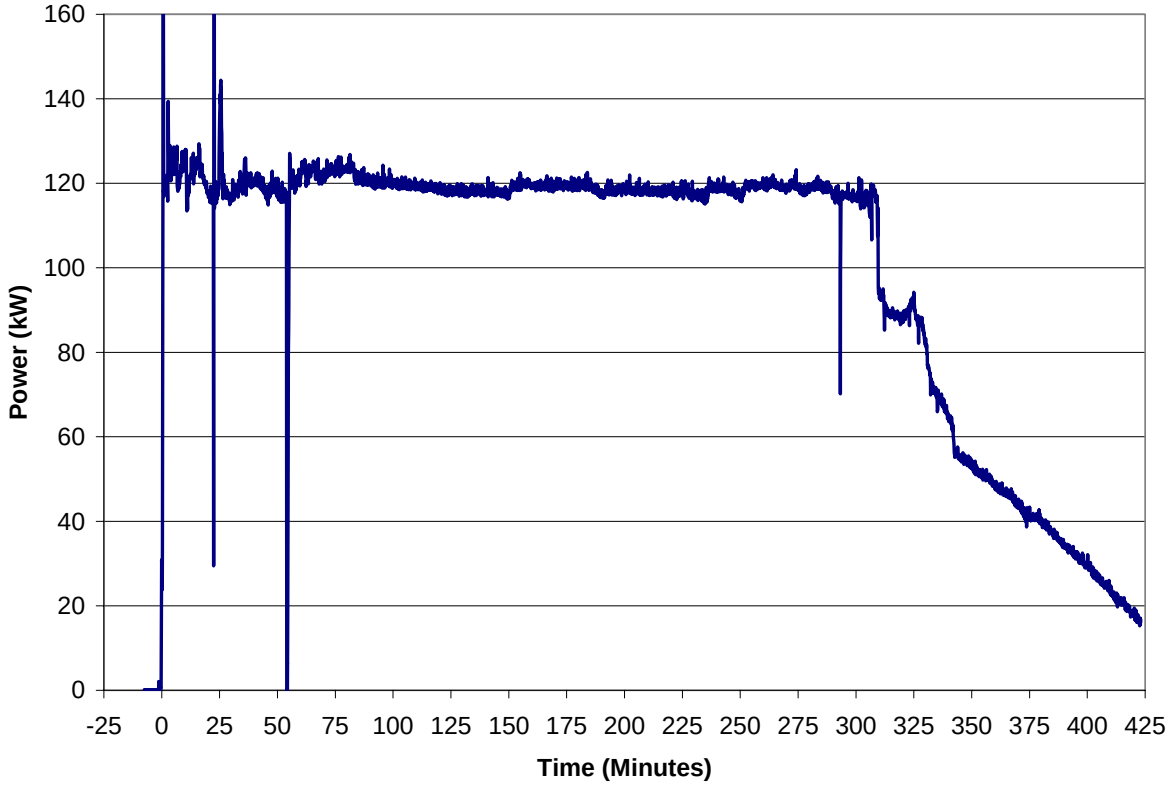

Figure 4-3. Total DEH Input Power.

4.2 Melt Temperatures

A total of thirty six W5%Re/W26%Re (Type C) thermocouple junctions were used to monitor melt temperatures at various axial and radial locations in CCI-2. The junction locations for these thermocouples are shown in Figures 2-6, 2-22, and 2-23. The thermocouples were configured within five four-junction and two eight-junction thermocouple arrays. The five four-junction units were all located in the concrete basemat; each of these arrays was protected by a 0.95 cm diameter tungsten thermowell. The two eight-junction arrays were radially configured in the two concrete sidewalls; each of these units was protected by a 1.27 cm tungsten thermowell. Data from the five Type C arrays in the basemat are provided in Figures 4-4 through 4-8, while data from the two sidewall arrays are provided in Figures 4-9 and 4-10. To provide an indication of the overall melt temperature behavior during the course of the test, a graph including the readings from all thirty six thermocouples is provided in Figure 4-11. To improve the readability of this data, two steps have been taken: i) the data have been one-minute averaged, and ii) only data preceding the first off-scale reading by the thermocouples are shown.

Examination of the data in Figure 4-11 indicates that: i) the average melt temperature declined from ~1900 ˚C during the first hour of the interaction, to ~ 1550 ˚C at the time the cavity was flooded, and ii) melt temperatures are fairly uniform across the extent of the interaction, generally clustering within a band of approximately ± 50˚C of the average melt temperature at any given time. Furthermore, the data in Figures 4-9 and 4-10 indicate that water was able to penetrate into the corium, possibly along the core-concrete interface, as the interaction progressed. This observation is supported by the response of Type K thermocouples cast into the concrete sidewalls. This information is provided later in this section.

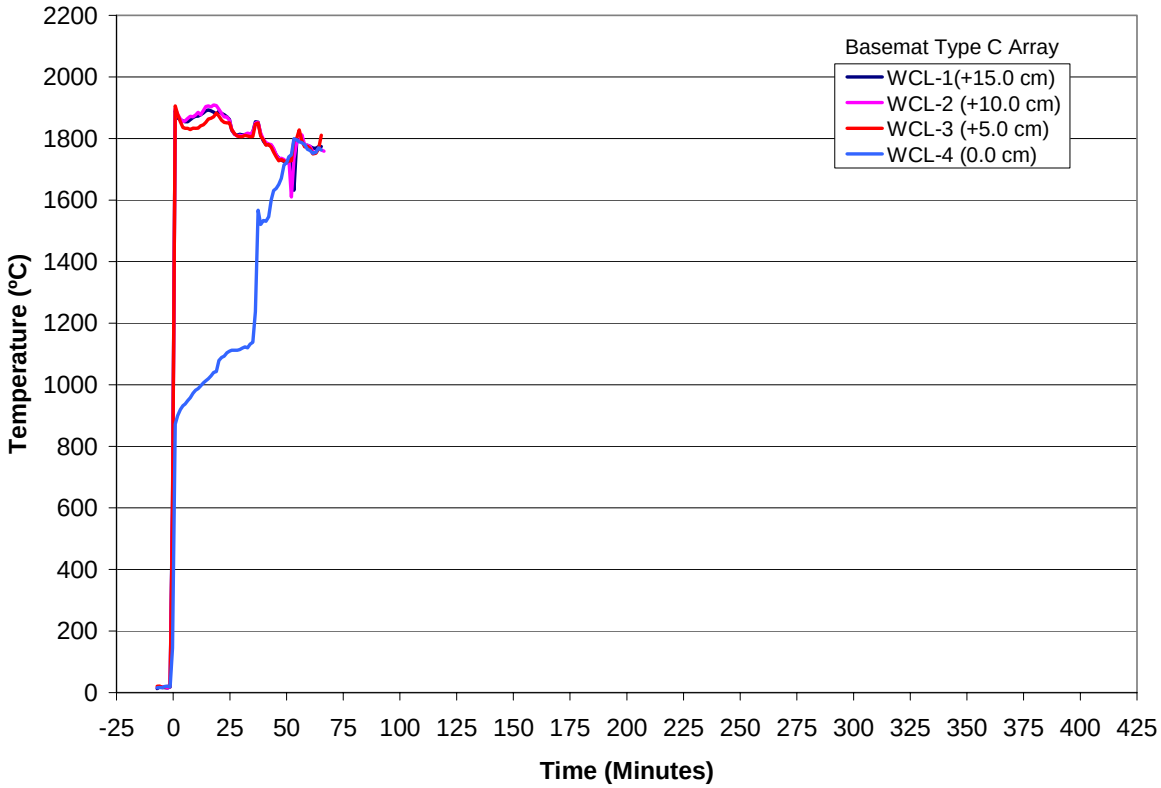

Figure 4-4. Melt Temperature Data From Basemat Type C "WCL" Array.

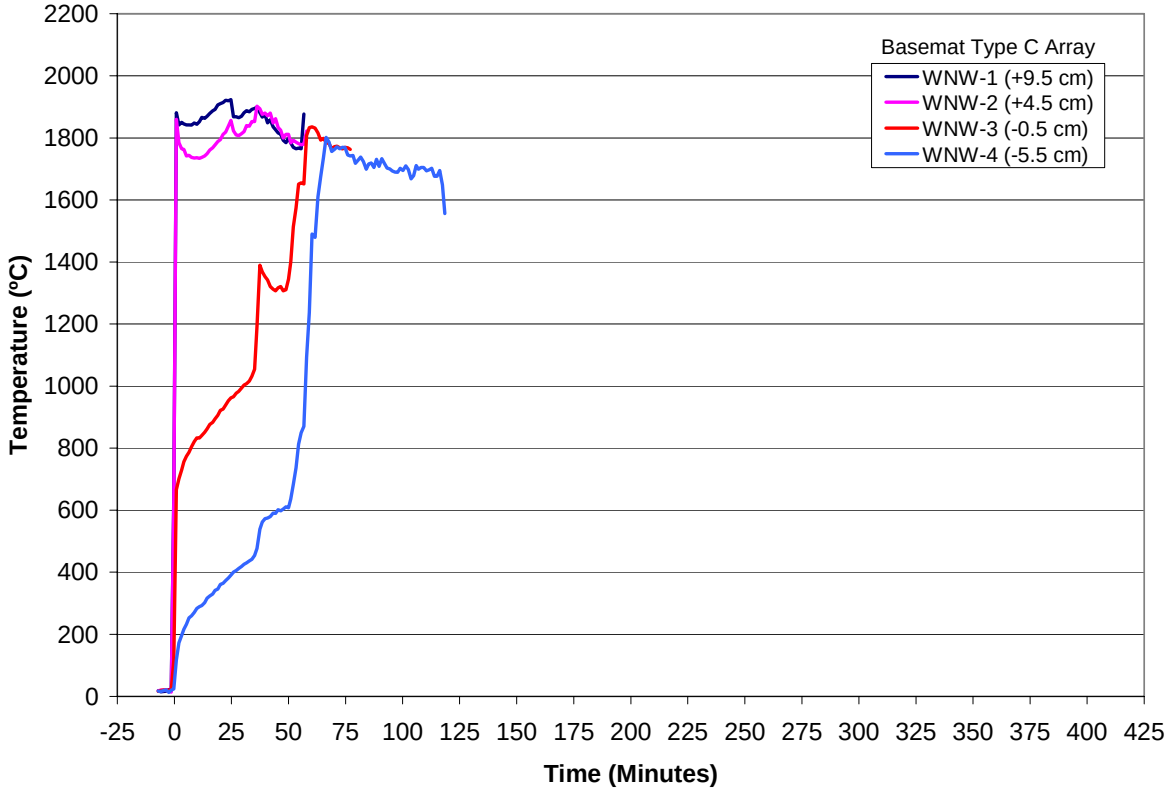

Figure 4-5. Melt Temperature Data From Basemat Type C "WNW" Array.

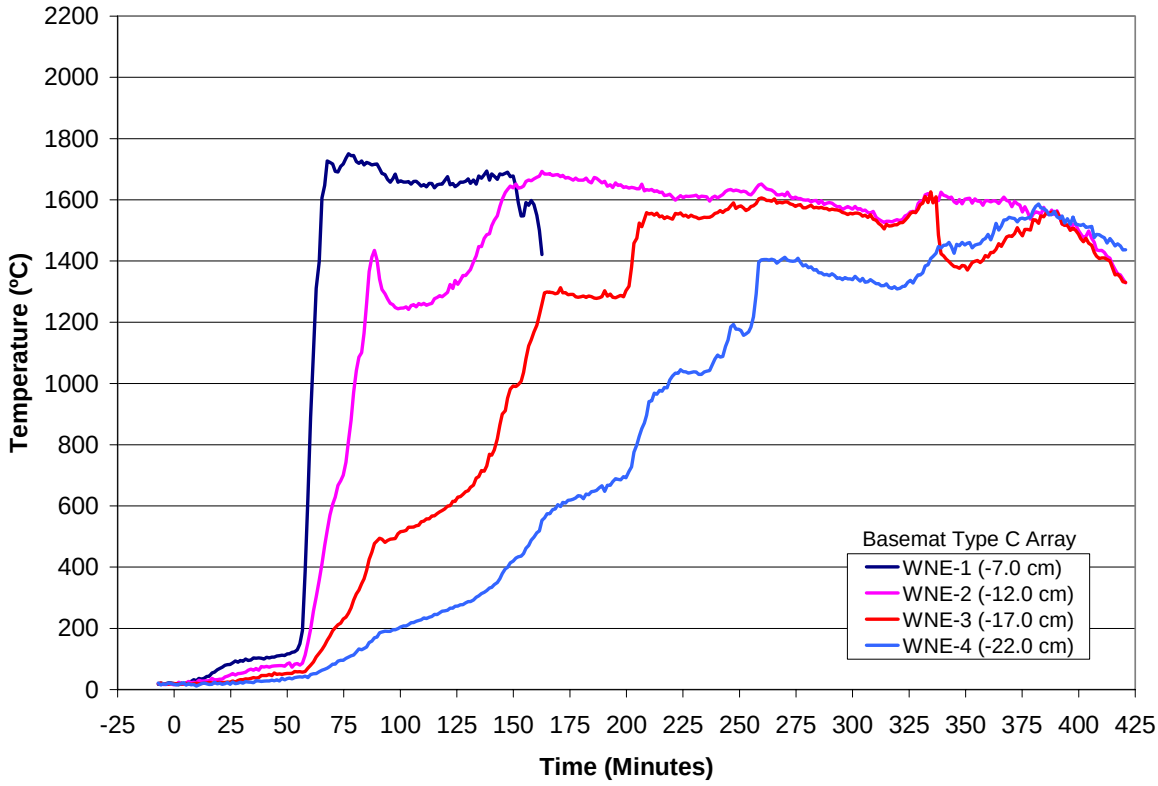

Figure 4-6. Melt Temperature Data From Basemat Type C "WNE" Array.

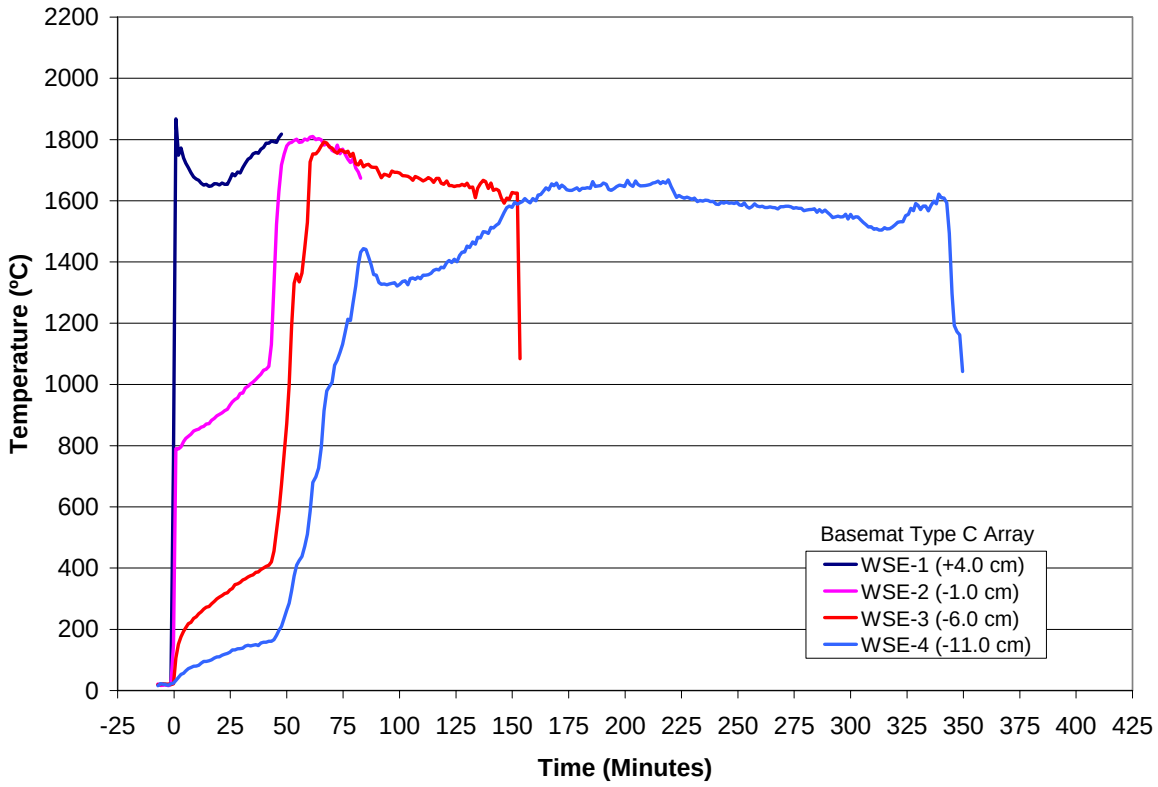

Figure 4-7. Melt Temperature Data From Basemat Type C "WSE" Array.

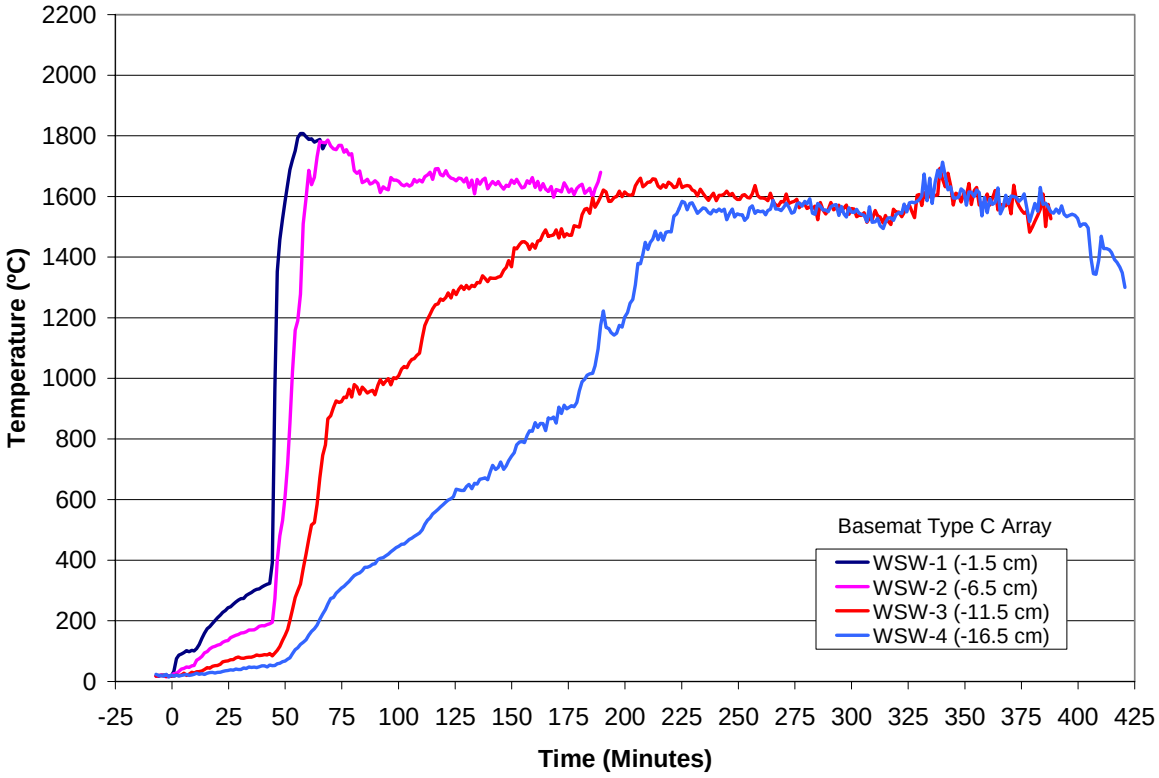

Figure 4-8. Melt Temperature Data From Basemat Type C "WSW" Array.

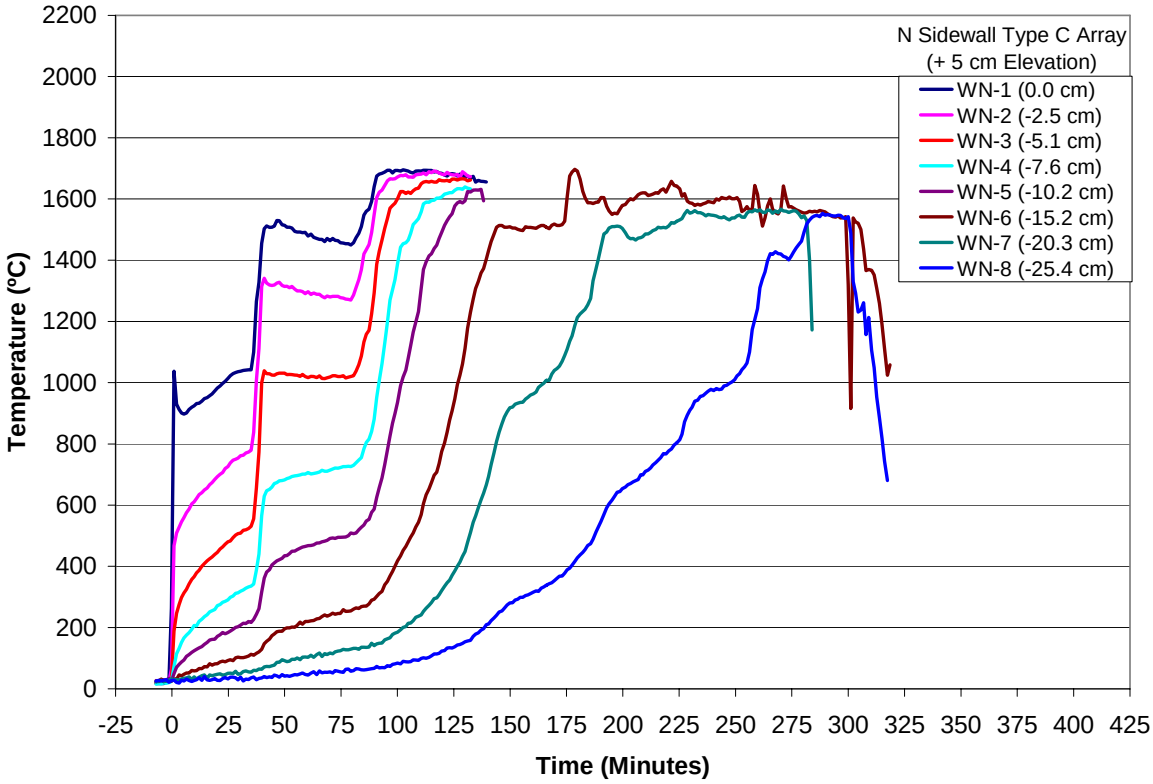

Figure 4-9. Melt Temperature Data From North Sidewall Type C "WN" Array.

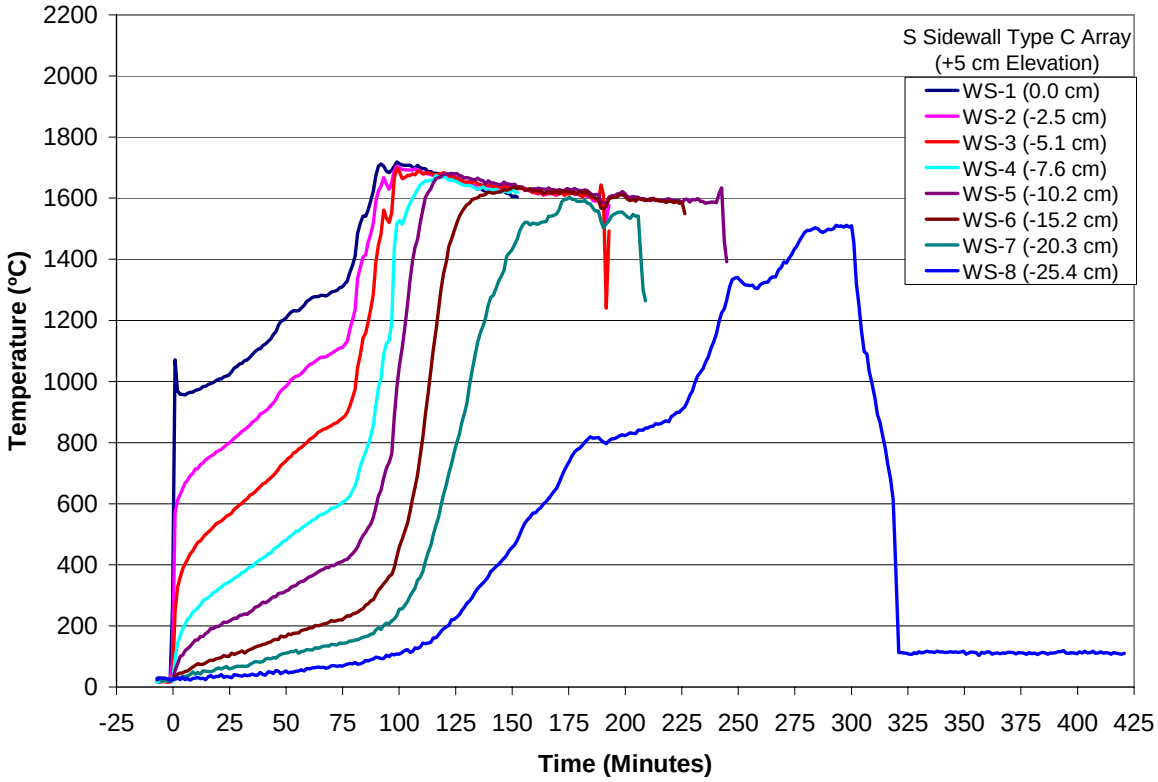

Figure 4-10. Melt Temperature Data From North Sidewall Type C "WS" Array.

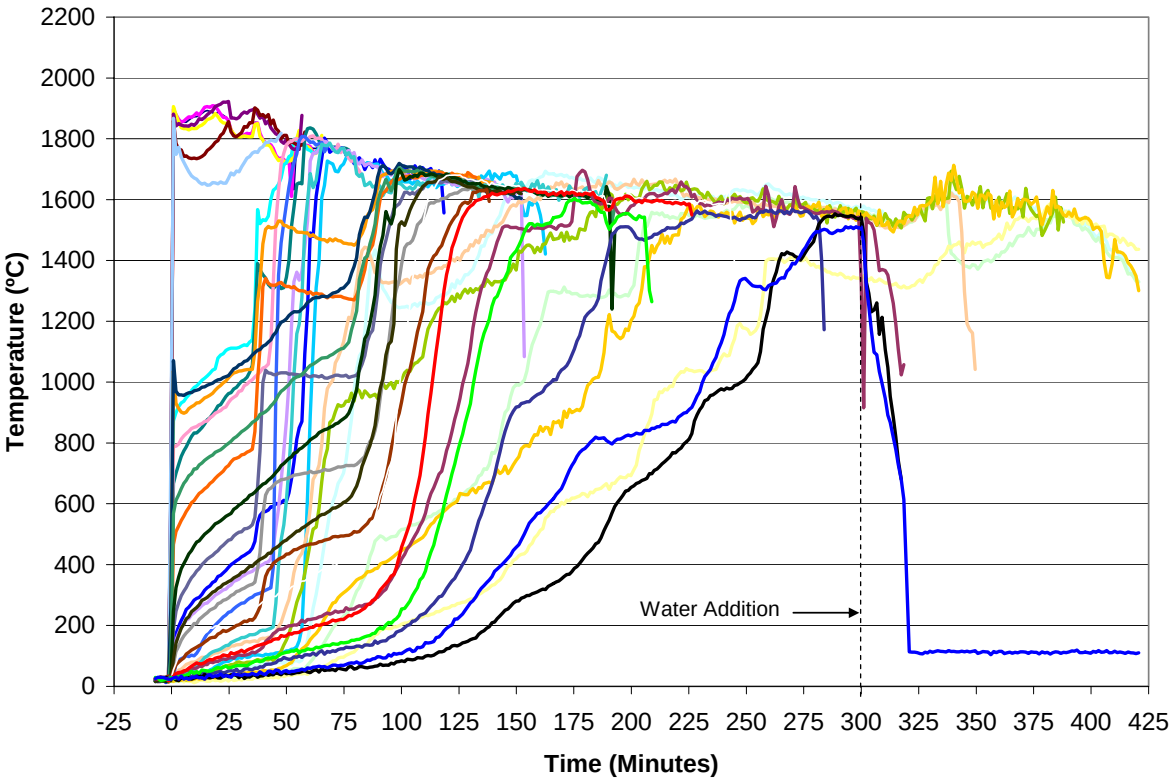

Figure 4-11. Data From all 36 Melt Temperature Thermocouples.

4.3 Concrete Basemat and Sidewall Ablation Rates

The basemat was instrumented with five multi-junction Type K thermocouple arrays to monitor the axial progression of the ablation front, while each concrete sidewall was instrumented with six arrays to monitor the radial ablation front progression at six different elevations. The location and identification of these thermocouple assemblies are shown in Figures 2-6, 2-22, and 2-23. The first junction of each array was mounted flush with the concrete surface. When a thermocouple reached the LCS concrete liquidus temperature of 1295 ºC,[2] the melt was considered to be in contact with the thermocouple at the junction location.

The sequential rise in signals from the basemat centerline array as the test progressed is shown in Figure 4-12. As noted earlier, only data preceding the first off-scale reading by the thermocouples are shown in this figure. The analogous plots showing the thermal response in the North and South concrete sidewalls at the +10.0 cm elevation location are provided in Figures 4-13 and 4-14, respectively. Plots of the thermal response at all basemat and sidewall array locations are provided in Appendix B.

Figure 4-15 provides the axial ablation depth versus time based on the signal responses from the Type K basemat arrays, while Figures 4-16 and 4-17 provide the analogous plots of the radial ablation depth in the North and South sidewalls, respectively. Finally, Figure 4-18 provides a comparison of the peak ablation depths versus time recorded on all three concrete surfaces during the test. Examination of these figures indicates: i) no substantial incoherence between the radial ablation rates observed on the North and South sidewalls, and ii) the radial and axial ablation rates are approximately the same.

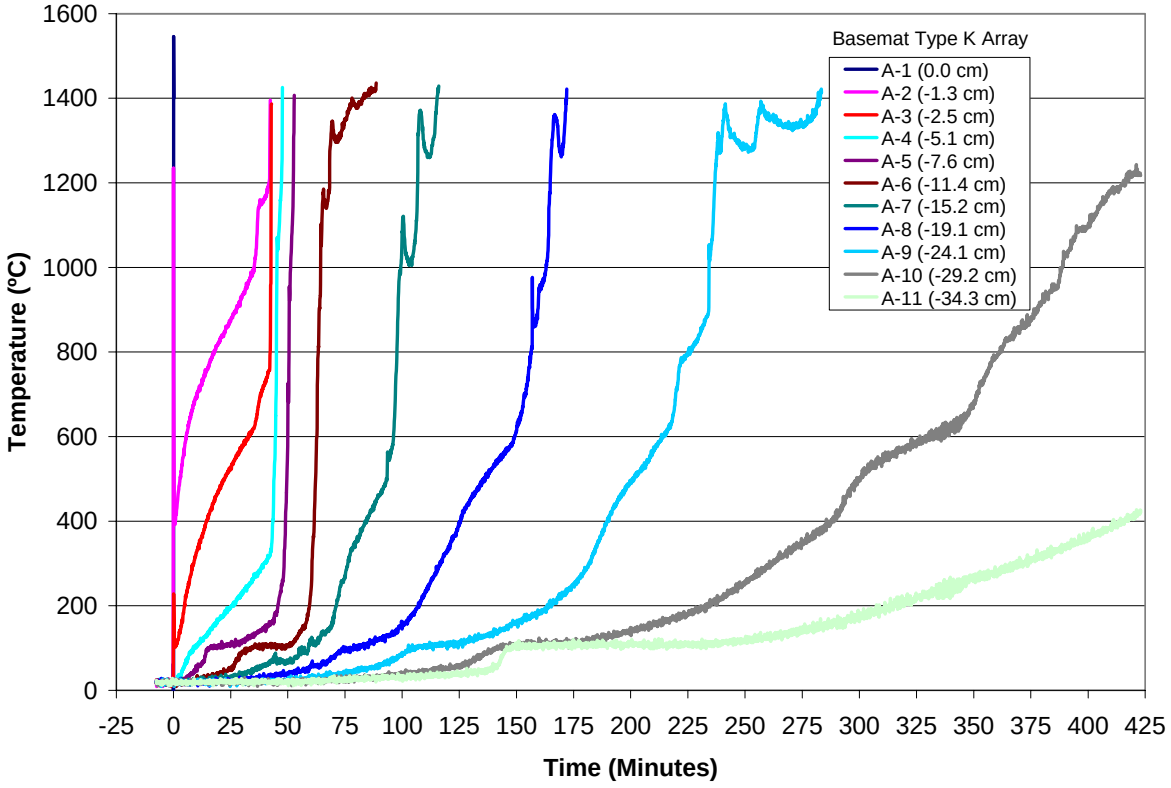

Figure 4-12. Thermal Response of the Concrete Basemat at the Centerline ("A" Array).

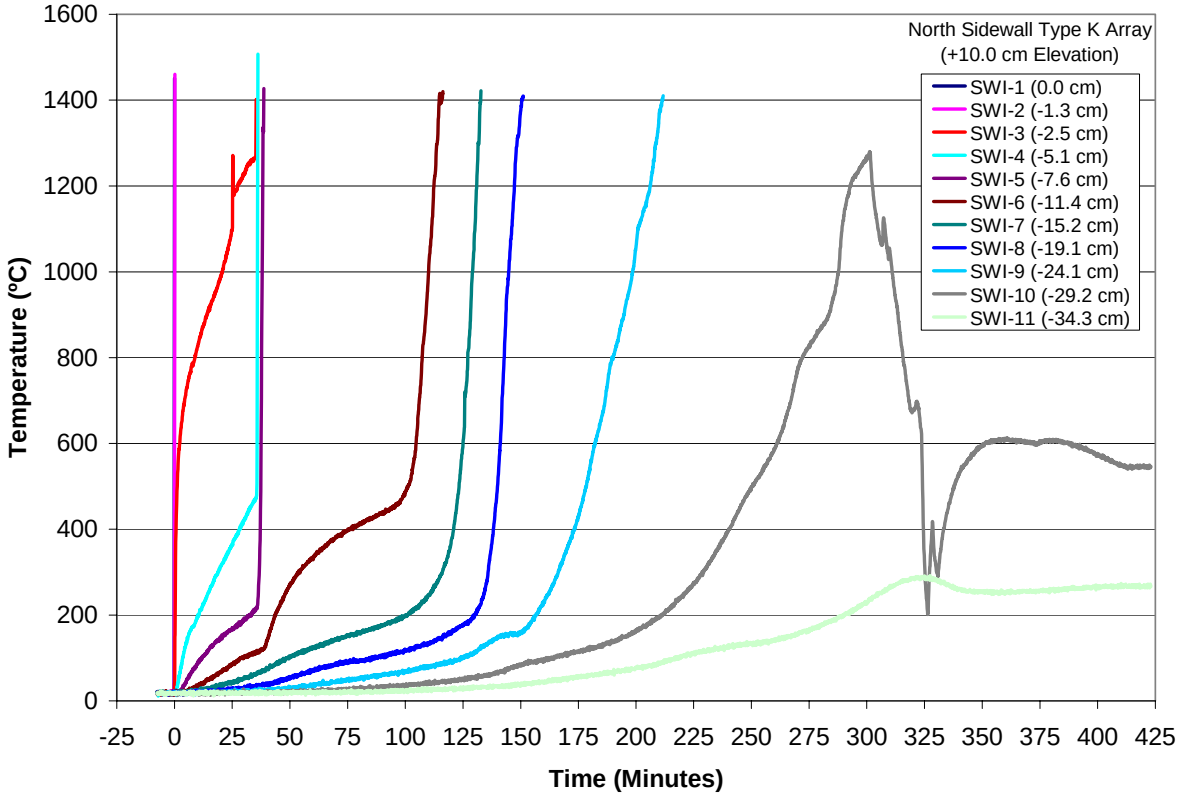

Figure 4-13. North Concrete Sidewall Thermal Response at +10.0 cm ("SWI" Array).

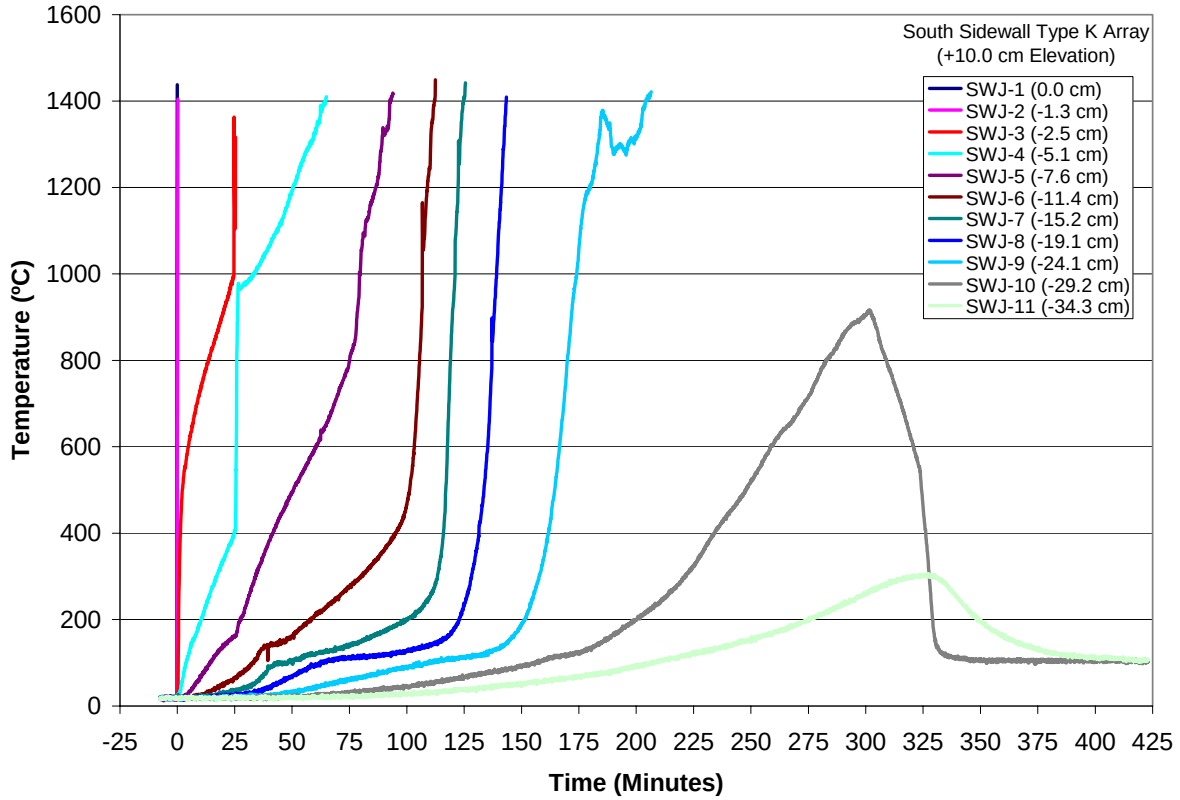

Figure 4-14. South Concrete Sidewall Thermal Response at +10.0 cm ("SWJ" Array).

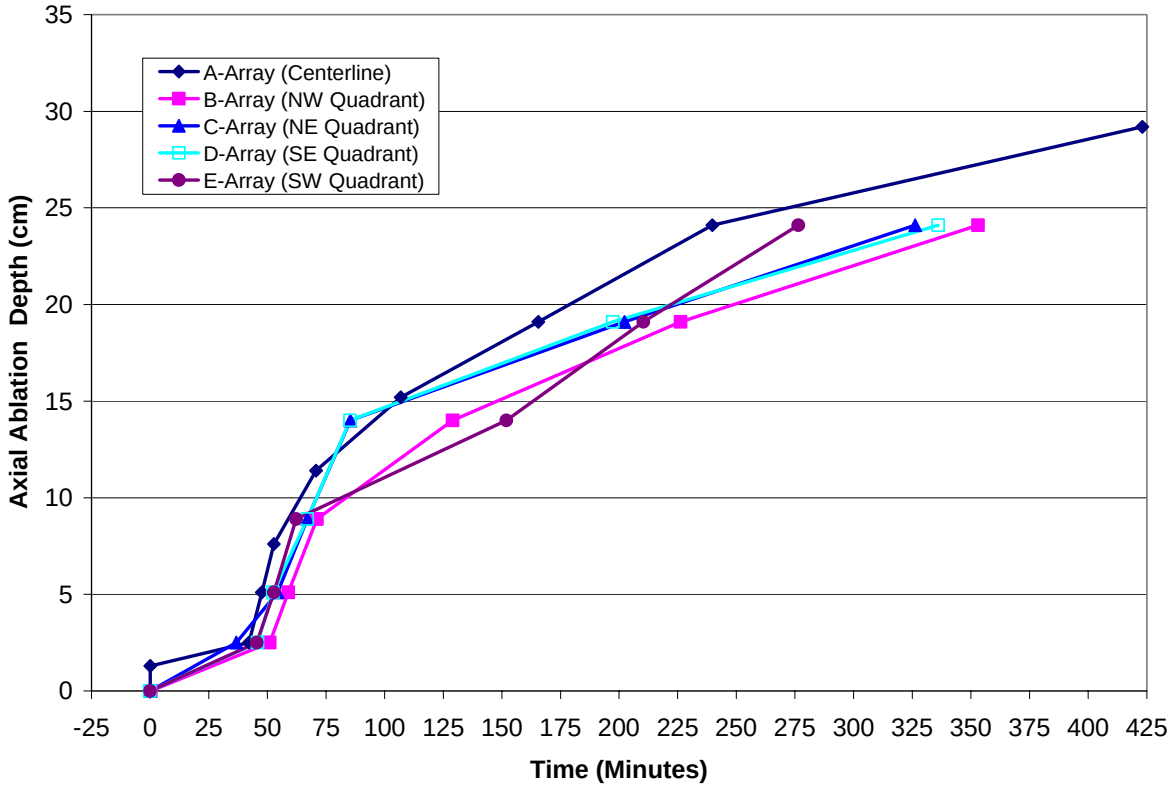

Figure 4-15. Basemat Axial Ablation Front Location.

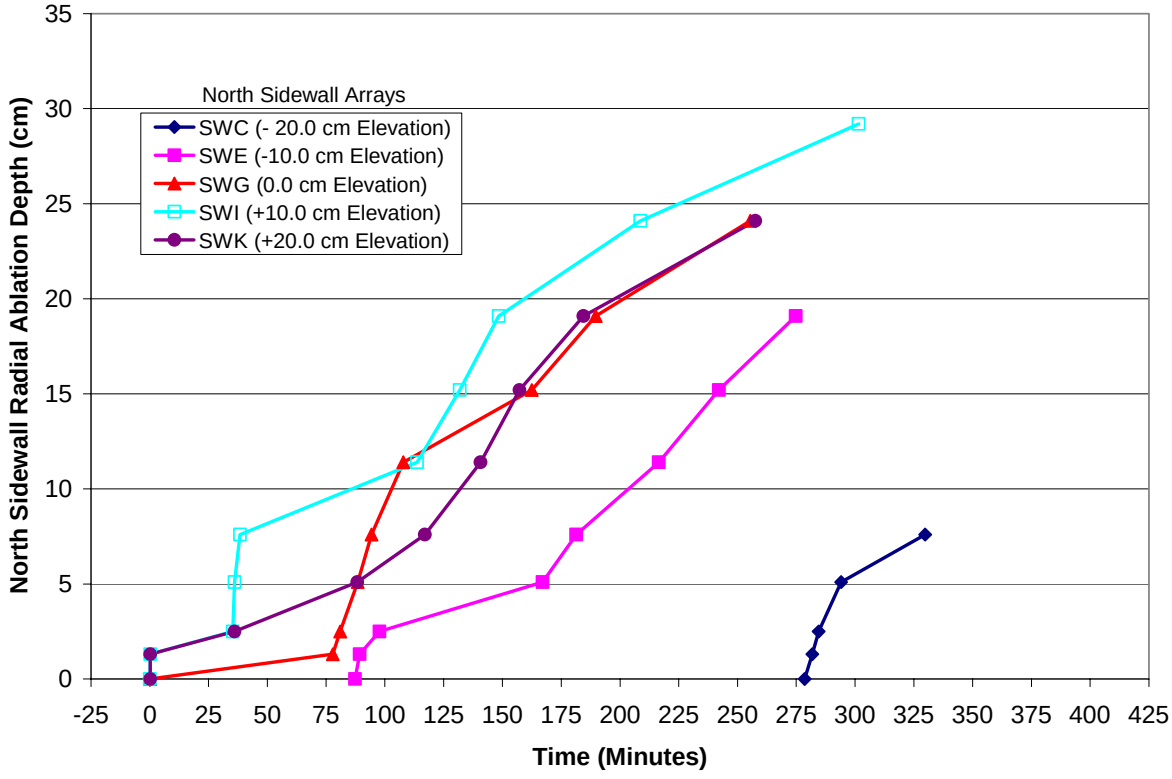

Figure 4-16. North Sidewall Radial Ablation Front Location.

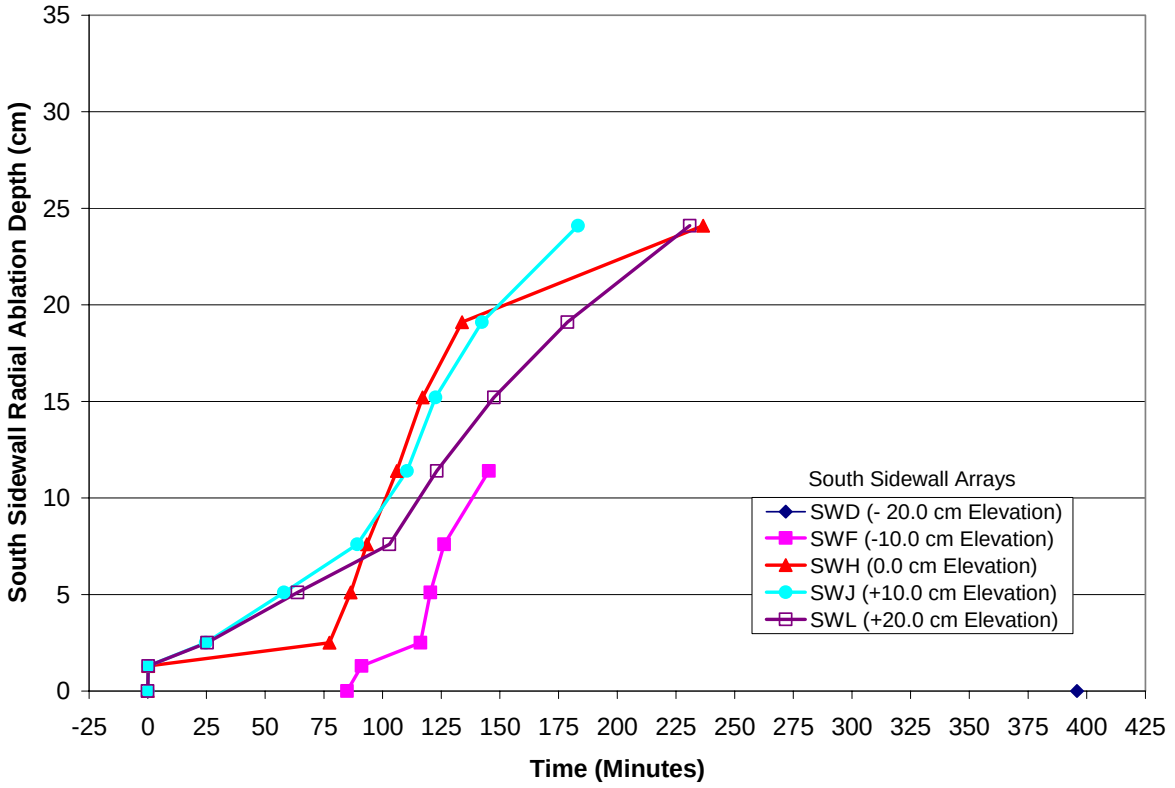

Figure 4-17. South Sidewall Radial Ablation Front Location.

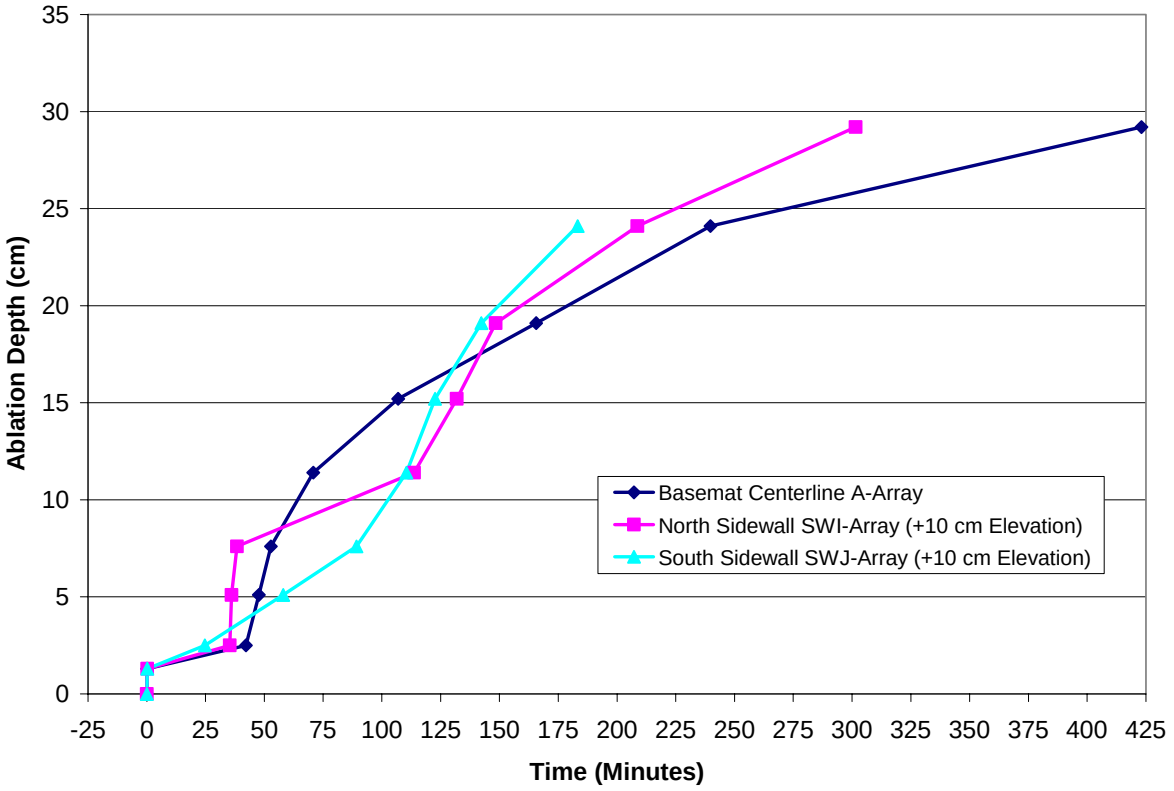

Figure 4-18. Maximum Axial and Radial Ablation Depths Versus Time.

To first order, the cavity shape can be estimated from the thermocouple data presented above. This estimate is provided in Figure 4-19. This profile was developed by performing a spline curve fit to the local ablation depth data points recorded at each basemat and sidewall thermocouple array location. Above the layer of solidified melt, the ablation profile is based on direct measurement of the cavity profile during posttest debris examinations. Additional information regarding these examinations and the debris characteristics are provided later in this section.

4.4 Test Section Water Inlet Conditions

As summarized in Table 1-1, the water supply system was designed to provide an initial water inventory of 125 l to the test section at a flow rate of nominally 120 liters/minute (2 l/sec), with makeup to maintain a constant collapsed water level (volume) of 50 ± 5 cm (125 ± 13 l) over the melt. The actual water flow rate to the test section as measured by the paddlewheel flow meter in the supply line (see Figure 2-15) is shown in Figure 4-20. As shown in the Figure, the actual flow rate ranged from 160 to 180 liters/minute. The inlet water temperature was constant at ~23 ˚C over the course of the experiment (see Appendix B). The supply tank water inventory, as measured by the magnetic level float in this tank, is shown in Figure 4-21.

The water head over the melt calculated based on conservation of mass (i.e., the water volume in the test section equals the initial supply/quench system water volumes minus the volumes in these tanks at the current time) is shown in Figure 4-22. The head measured by the two differential pressure transducers located in the test section to monitor water level (see Figure 2-27) are also shown in this figure. After cavity flooding, the actual water level in the test section[d] was maintained within the range of roughly 15 to 60 cm for most of the test.

[d] The spikes in the test section water volume observed immediately after makeup water was added are due to the fact that the introduction of the subcooled water caused steam condensation in the test section to occur. As a result, test section plenum pressure was reduced, causing water to backfill the evacuated downcomer pipe in the primary quench tank. From the conservation of mass calculation, the apparent loss of water from the quench tank was manifest as an artificial increase in the amount of water in the test section until the water became saturated. At this point, the downcomer was evacuated and normal flow conditions were reestablished.

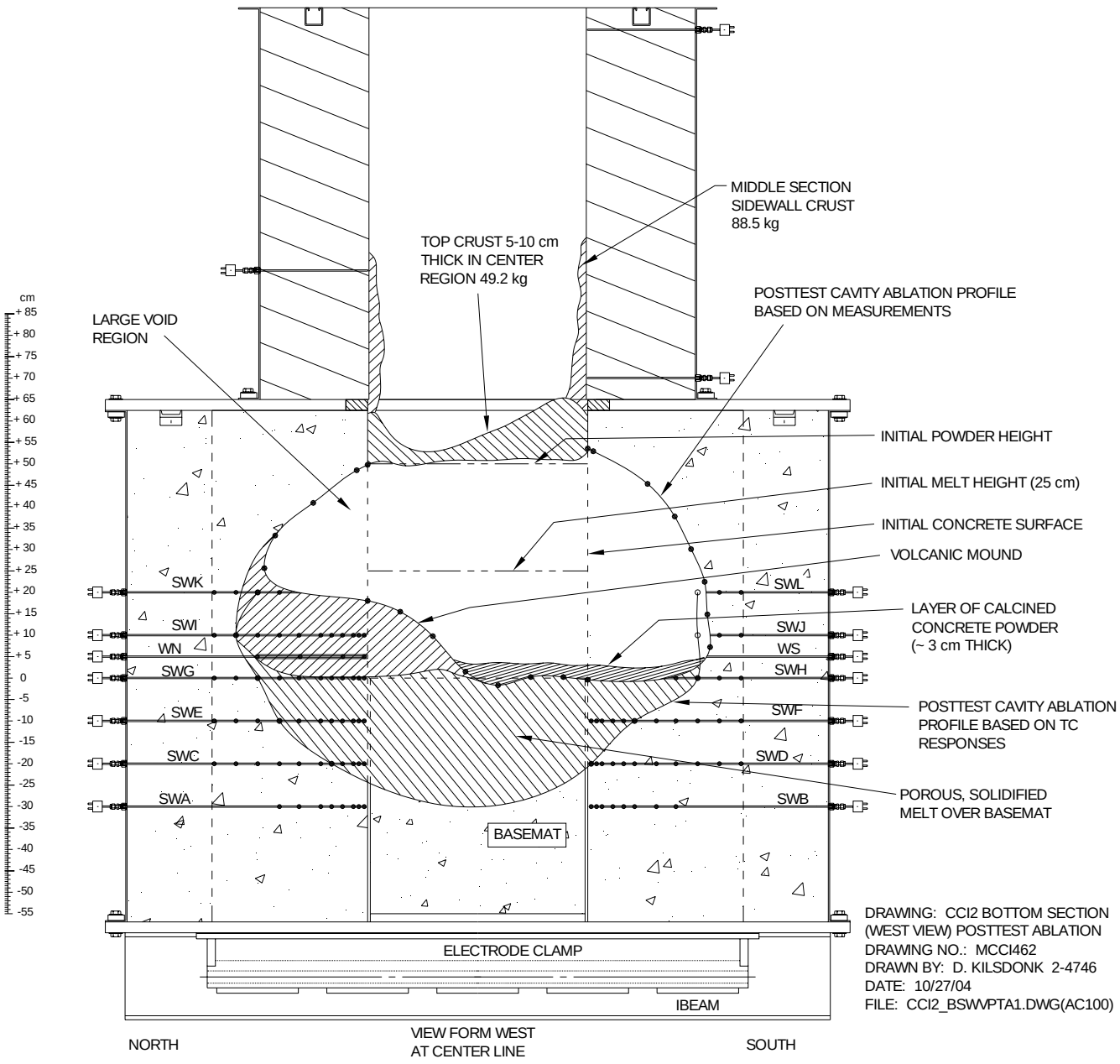

Figure 4-19. Cavity Erosion Profile Based on TC Data and Posttest Examinations.

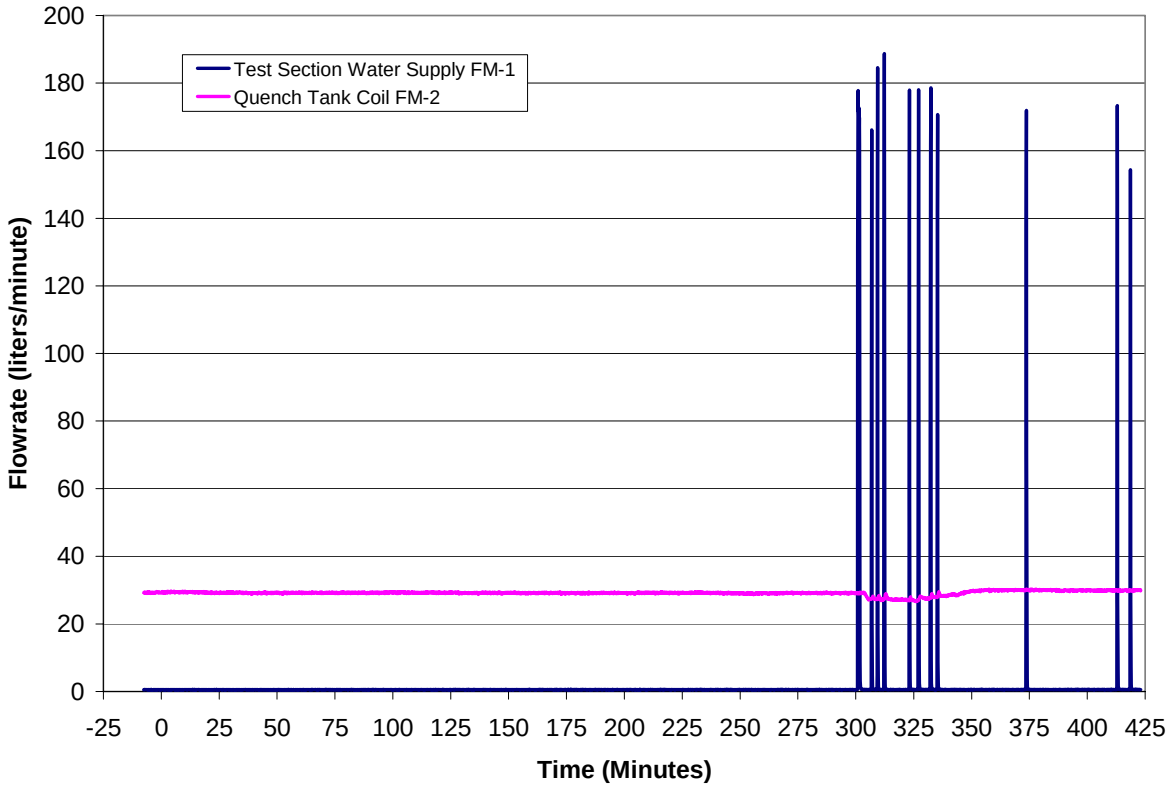

Figure 4-20. Test Section Water Inlet and Quench Tank Coil Water Flow Rates.

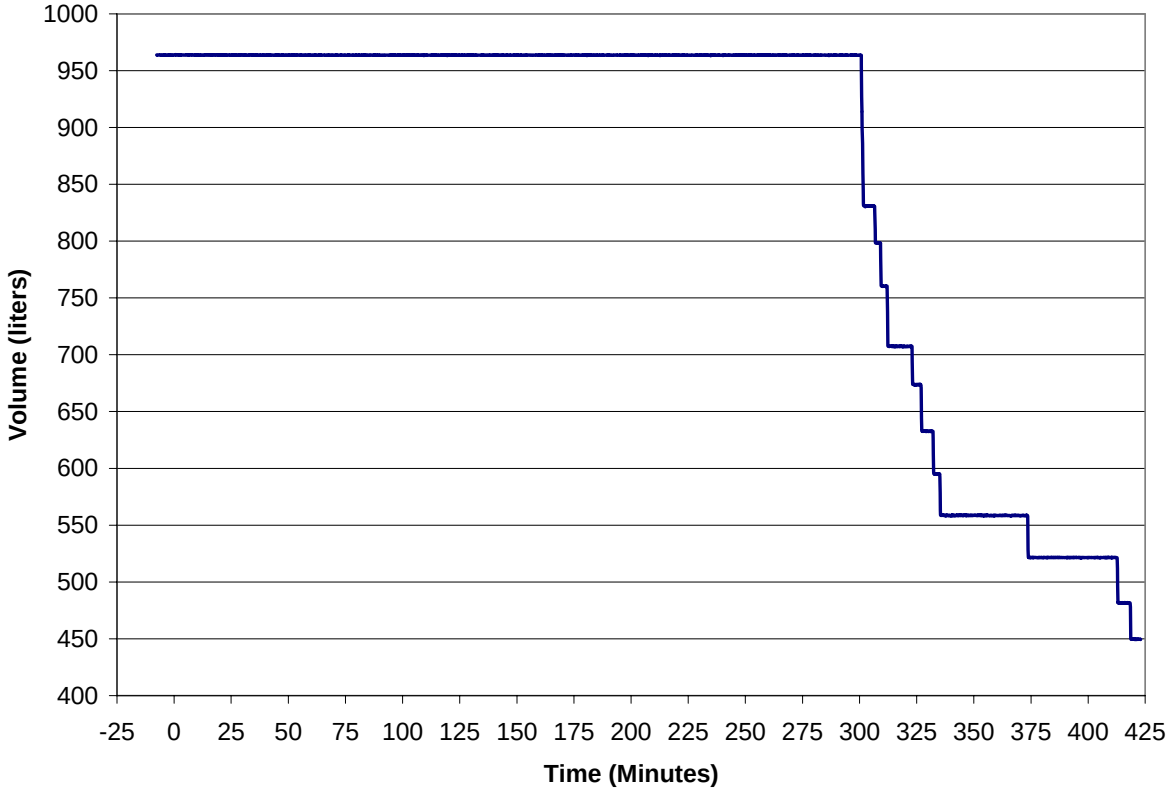

Figure 4-21. Water Supply Tank Water Volume.

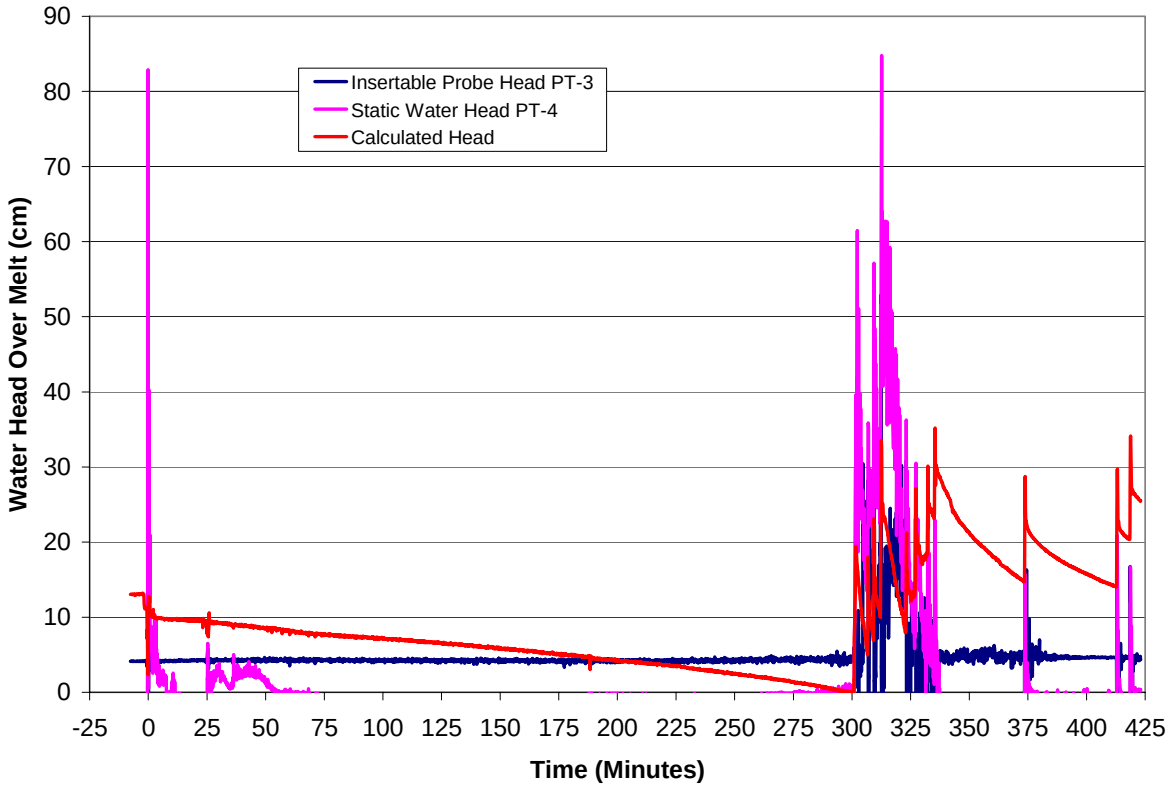

Figure 4-22. Water Head Over Melt.

4.5 Crust Lance Data

Two key test objectives for CCI-2 were to: i) obtain in-situ crust strength data to supplement the room temperature strength database being assembled as part of the SSWICS program, and ii) provide information on the nature and the extent of the debris cooling that occurs after the crust fails. This subsection provides the results of the crust strength measurement, while the debris cooling data is provided in the next subsection.

As shown in Table 3-1, the lance was inserted in an attempt to fail the crust ~ 45 minutes after the cavity was flooded, as specified in the test operating procedure. The output from the crust lance force transducer is shown in Figure 4-23, while the lance displacement transducer output is shown in Figure 4-24. This data indicates that the lance contacted the crust at 346.0 minutes. The load applied to the crust was measured as 3.35 kN; the crust upper surface elevation was at +61 cm. The crust was not breached by this contact force. The contact elevation can be compared with the initial collapsed melt height of ~ 25 cm at the start of the test. As shown in Figure 4-19, the contact elevation is consistent with the upper surface elevation of the bridge crust spanning the upper region of the test section. Subsequent posttest examinations indicated that large mantles of solidified corium were present on the east and west sidewalls of the test section at the time the lance was inserted. The applied load of 3.35 kN was insufficient to dislodge these large crust mantles, and therefore no crust strength information was obtained as part of the crust breach procedure for CCI-2.

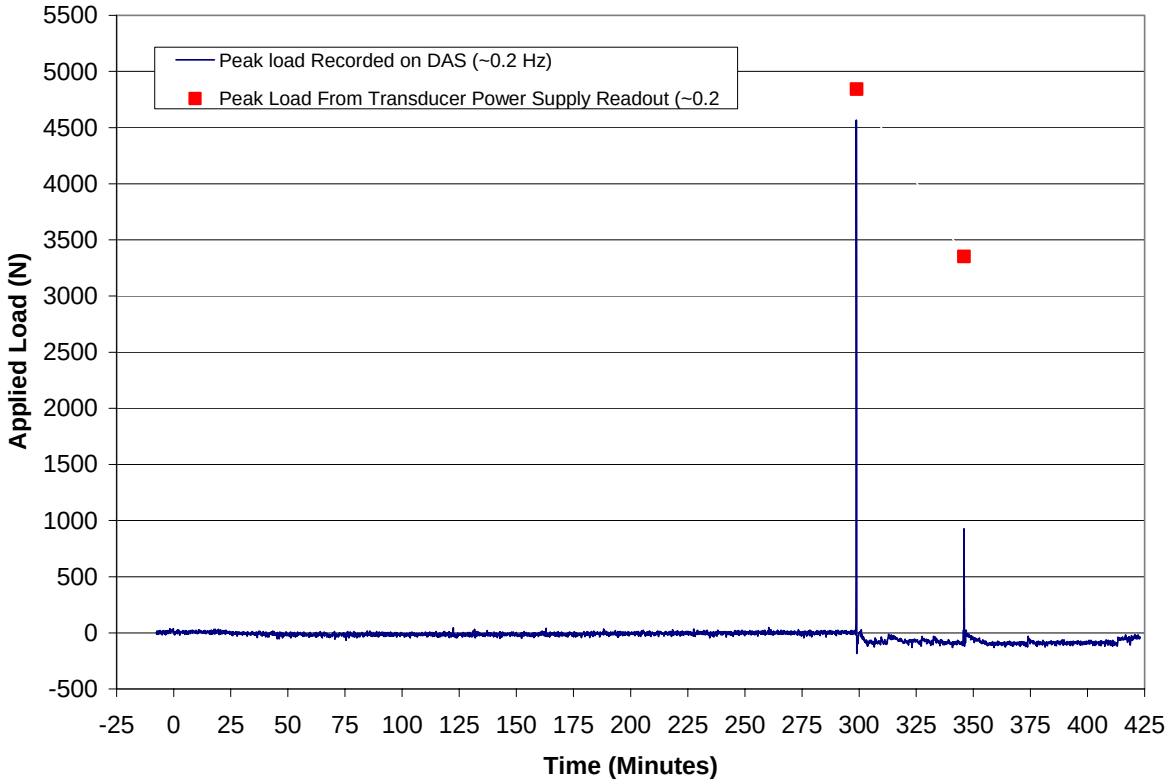

Figure 4-23. Load Force Exerted on Crust vs. Time.

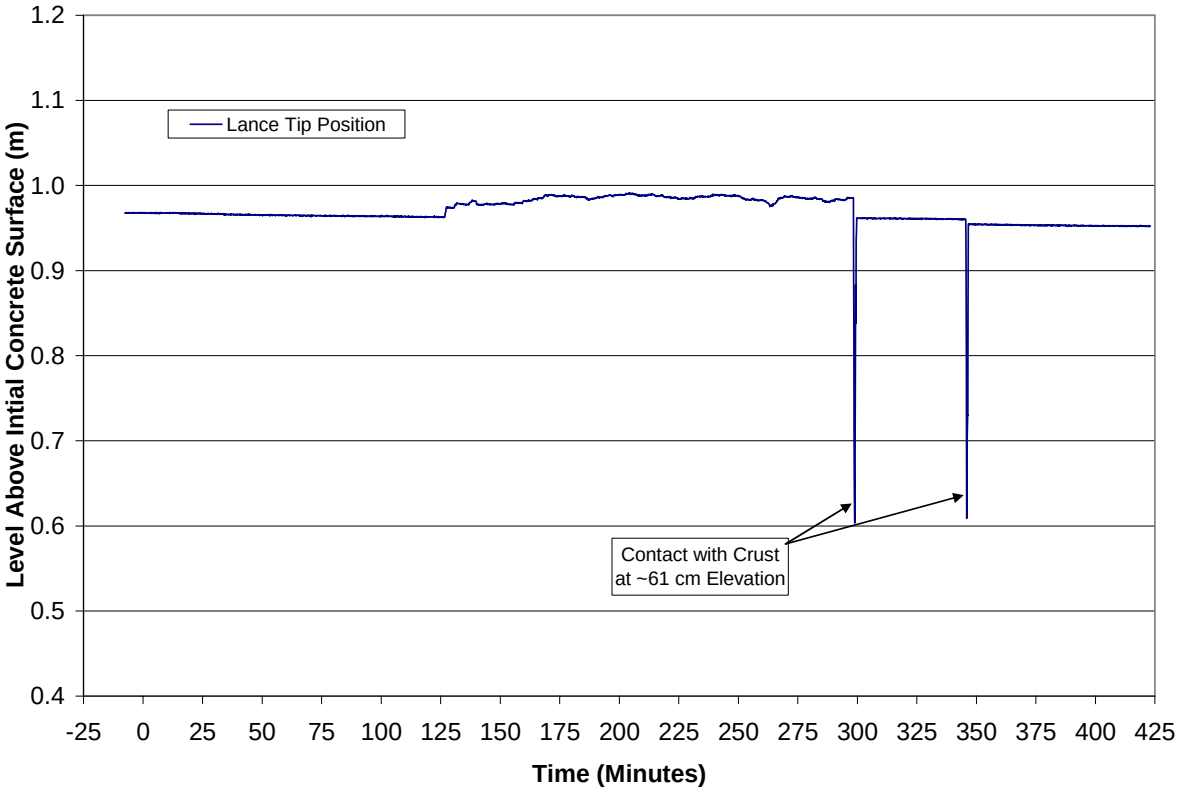

Figure 4-24. Lance Tip Elevation Over Initial Concrete Surface.

4.6 Corium Quench Rate

Another key test objective was to obtain data on the nature and extent of the corium quench process when flooding occurs late in the sequence. Given the system instrumentation layout described in Section 2, sufficient data is available to determine the corium/water heat transfer rate from the gross energy transport rate into the quench system, including the following energy source/sink terms: (i) water heat up and boil off in the test section, (ii) heat transfer from test section sidewalls, (iii) heat transfer from interconnecting piping between the test section and quench tank, (iv) sensible and latent heat transport into the quench tank (i.e., water inventory temperature change and water inventory mass), and (v) heat removal from the quench tank through the cooling coil. However, for the purposes of this data report, a first-order estimate of the heat flux is provided based on the steaming rate from the test section. The water levels in each of the three quench system tanks are shown in Figure 4-25, while the cumulative water level in all three tanks is provided in Figure 4-26. For reference, selected temperatures throughout the quench system are shown in Figure 4-27.

Given this collection of information, the overall corium cooling rate can be estimated from the equation:

$$q'' = h_{lv} \bullet \dot{m}_s$$

where h_{lv} is the water latent heat of vaporization (2.256 MJ/kg), and $\dot{m}_s$ is the steam mass flow rate. The steam flow rate is calculated by first performing a 6-point (~30 second) running average on the cumulative quench system water level data shown in Figure 4-26, and then calculating the derivative of the resultant dataset using a central differencing scheme.

The corium cooling rate calculated using this approach is shown in Figure 4-28. As shown in Table 3-1, cavity flooding was initiated at 300.79 minutes. As the figure indicates, the initial debris heat flux reached ~ 1.4 MW. Posttest debris examinations indicated that the upper surface area of the solidified corium beneath the bridge crust was ~ 0.5 m^2 (see Figure 4-19). Thus, the initial corium-water heat flux was ~ 2.8 MW/m^2. This heat flux is significantly above the CHF limitation of ~ 1 MW/m^2 at atmospheric pressure, indicating that the initial cooling transient was probably dominated by bulk (as opposed to crust-limited) cooling. After the initial interaction, the cooling rate steadily declined, but remained relatively high (i.e., above 250 kW, or ~ 500 kW/m^2) for the first 30 minutes of the interaction.

Due to large debris cooling rate, the quench tank coil (capacity of 170 kW) was not able to completely remove the energy due to condensation. Thus, the quench tank water inventory reached the saturation point at 305.20 minutes (see Figure 4-27). Steam blow over into the secondary spray tank began at this time. The spray tank water inventory subsequently reached saturation at 320.6 minutes. After this time, steam was vented directly into the cell through the final off gas system until the corium quench rate fell below the quench tank coil capacity at 342.6 minutes. After this time, the quench tank water inventory fell below the saturation point, and all steam was once again captured in that tank. During the time interval in which both tanks were saturated (i.e., 320.6 - 342.6 minutes), two melt eruptions occurred below the bridge crust (see Table 3-1). However, the augmentation in the debris cooling rate due to these eruptions could not be documented since the quench system was already at full capacity (170 kW). Furthermore, since steam was escaping from the system, the corium cooling rate shown in Figure 4-27 is thus conservative (i.e., underestimated) during the time interval from 320.6 - 342.6 minutes.

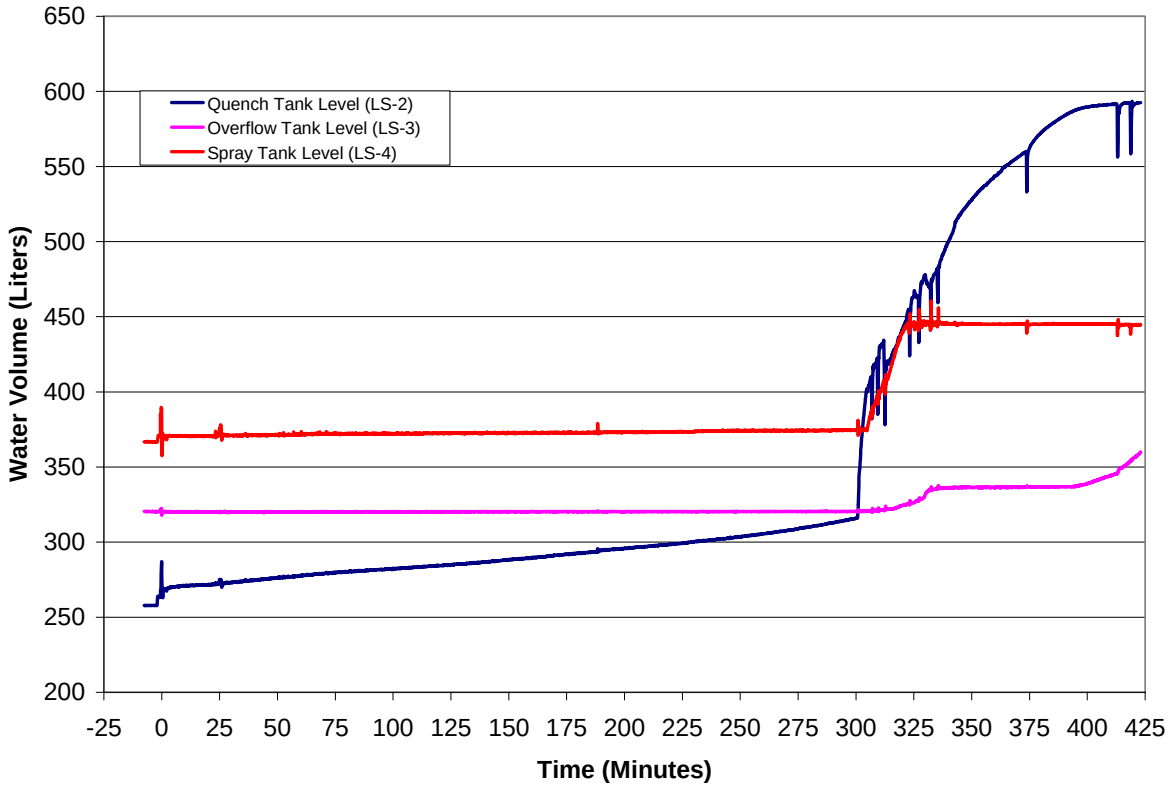

Figure 4-25. Quench System Tank Water Volume Data.

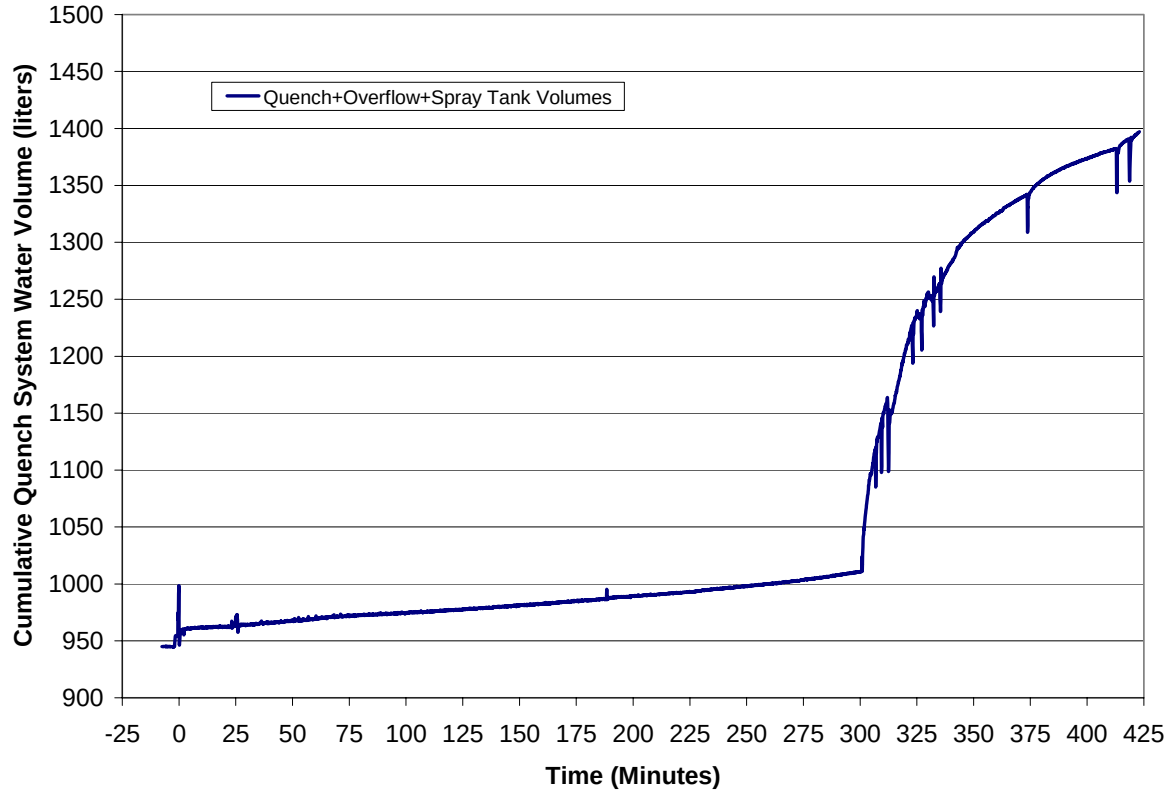

Figure 4-26. Cumulative Quench System Water Volume.

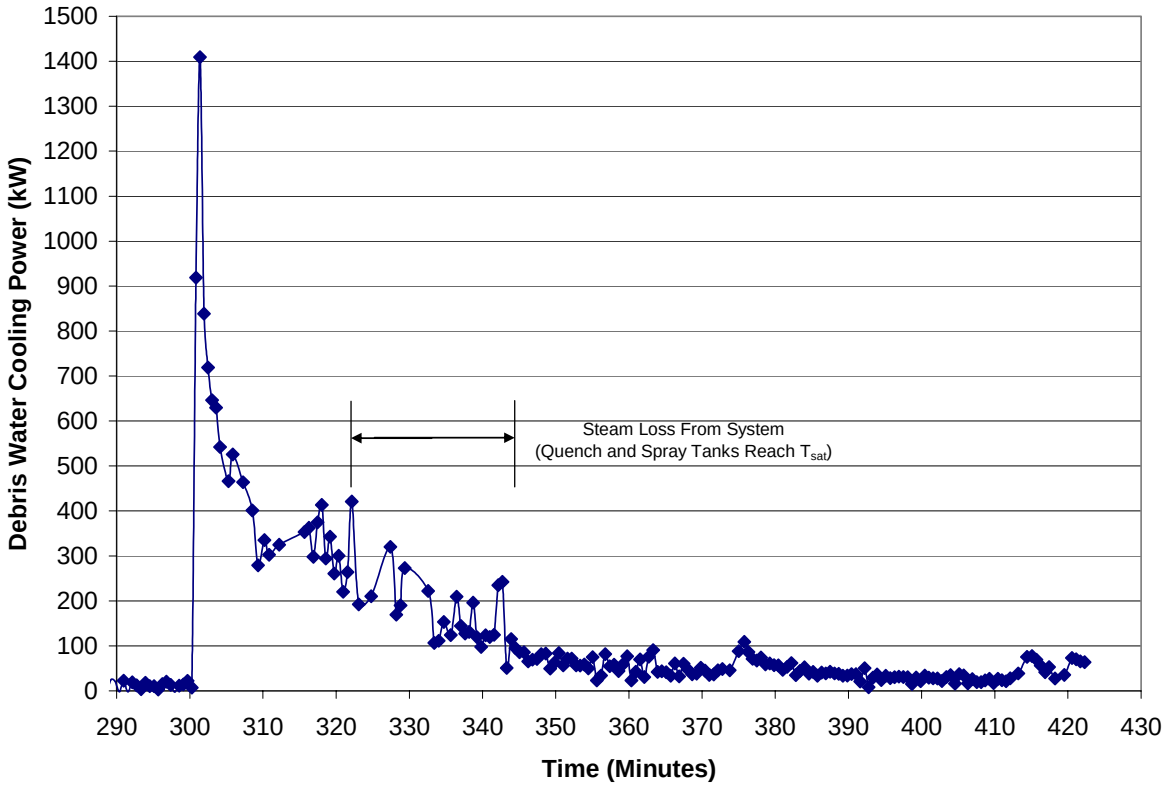

Figure 4-27. Melt-Water Heat Flux Based on Steam Formation Rate.

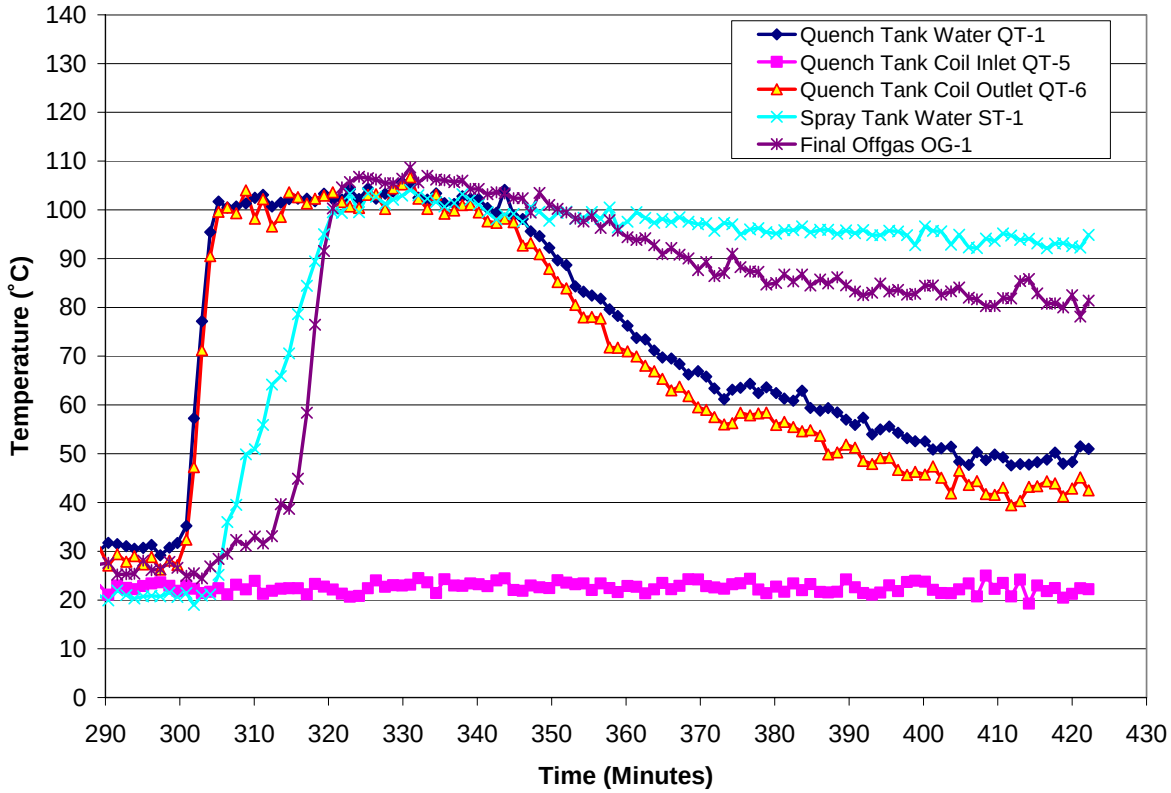

Figure 4-28. Selected Quench System Temperatures During Water Flooding Stage.

As shown in Table 3-1, the crust lance was inserted in an attempt to breach the bridge crust at 346.0 minutes, but the crust was not breached. However, the lid video camera clearly indicated the presence of a large hole through the bridge crust at initiation of cavity flooding that allowed water to pass through and flood the underlying melt. Thus, the bridge crust did not play a significant role in influencing the overall debris cooling rate.

4.7 Electrode Current Monitoring System Data

During CCI-2, an attempt was made to monitor the voltage drop across the lower 15 cm of selected tungsten electrodes using lacquer-insulated 14 gauge wires that were passed through potted seals into the test section along the bottom support plate and clamped at the 15 cm elevation. Figure 2-28 provides a drawing that shows the electrodes that were wired for current monitoring. Data obtained from the west and east electrode banks are provided in Figures 4-29 and 4-30, respectively. As shown in Figure 4-29, data from the west electrode bank indicates that most current is drawn through the central region of the test section (i.e., monitors W-6 through W-11; see Figure 2-28) during the test. In general, the data from the East electrode bank show the same trend, except for monitors E-1 and E-2, which are located deep in the electrode recessments (see Figure 2-28). Based on the well-defined progression of the radial ablation profile, these electrodes would not have been exposed to melt and drawn significant current until late in the experiment. However, the data seems to indicate that the primary current path was through these two electrodes over most of the entire test. No explanation can be offered for this trend, and therefore this data appears to be suspect.

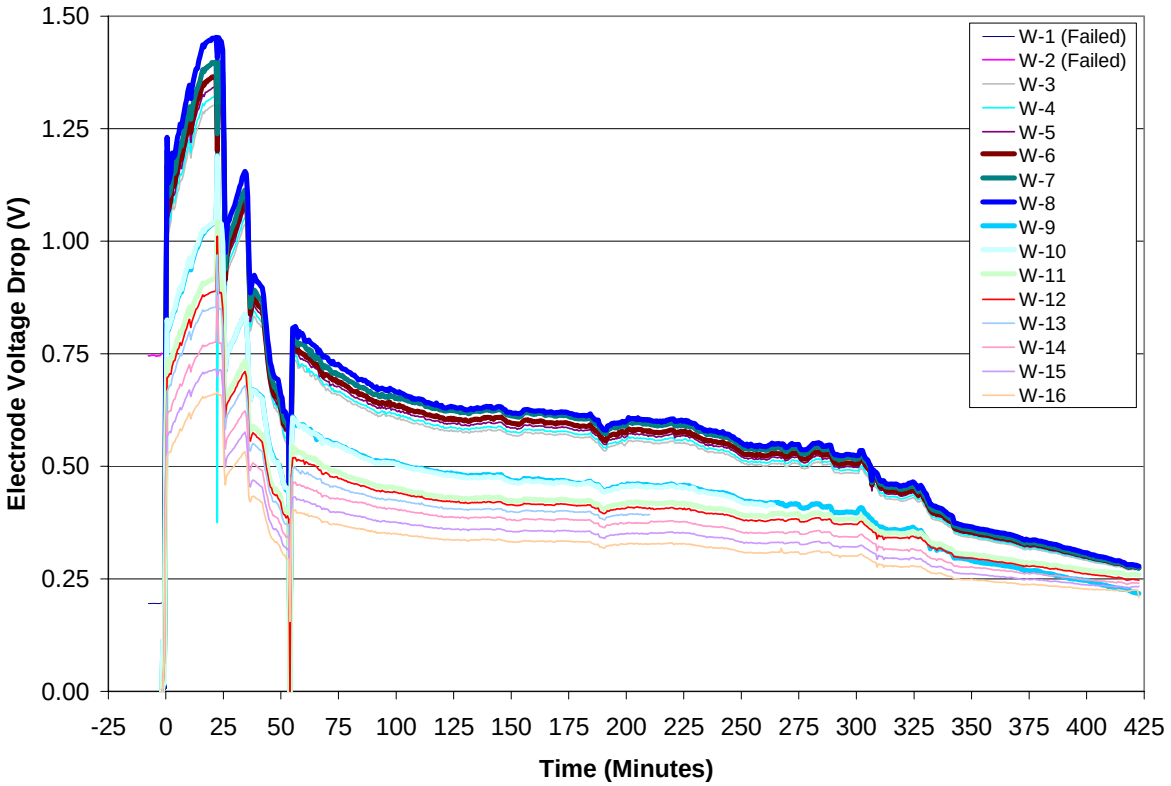

Figure 4-29. Voltage Drop Across Selected Electrodes on the West Side.

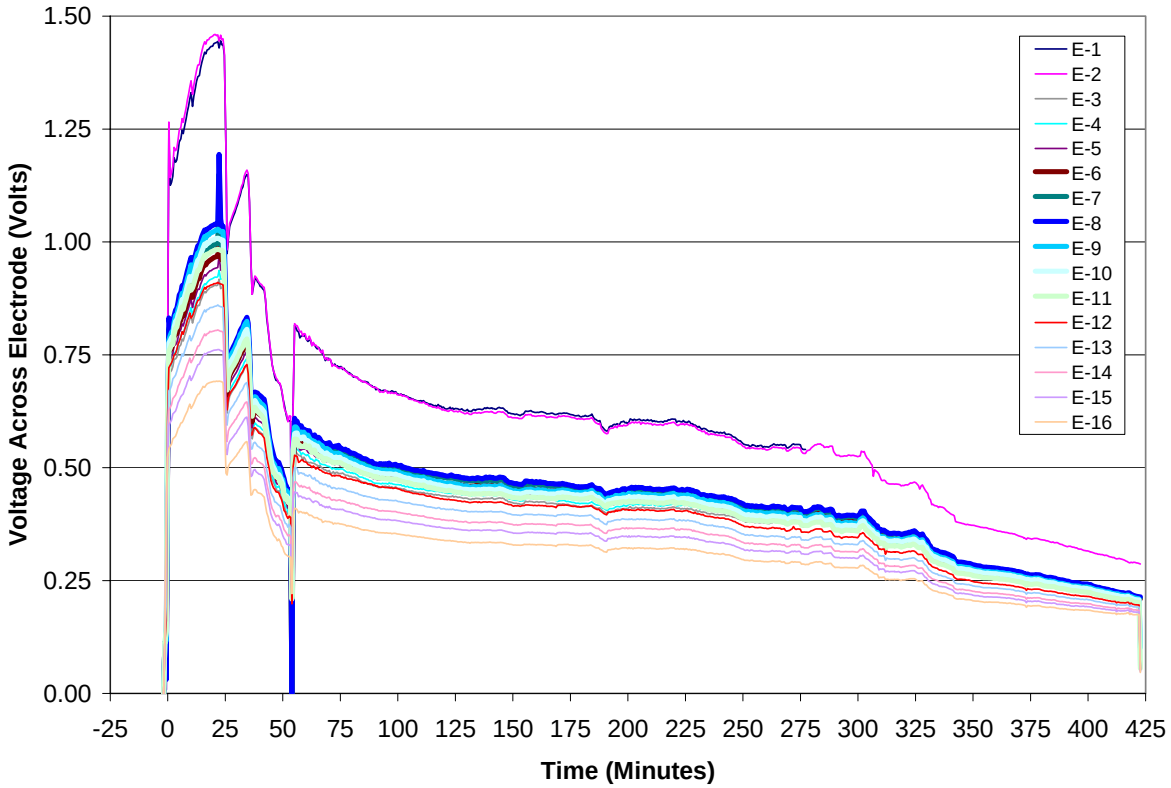

Figure 4-30. Voltage Drop Across Selected Electrodes on the East Side.

4.8 Posttest Debris Examinations

Following the experiment, the apparatus was carefully disassembled to document the posttest debris configuration. Figure 4-31 provides a picture of the top surface of the crust after removal of the middle sidewall section, while a sketch of the surface showing key elevations and features is provided in Figure 4-32. A large opening through the bridge crust is apparent in the southeast corner of the test section. The characteristic dimensions of this opening are 6 cm by 9 cm. Visual examination through the opening revealed the presence of a large void region beneath the crust. The lid video camera view of the corium surface clearly indicated that this hole provided the pathway for water to flood the underlying melt during the test. The crust upper surface elevations measured with the lance probe both prior to and after cavity flooding (see Figure 4-24) are consistent with the posttest surface elevations, indicating that the crust had not moved significantly during at least the last two hours of the experiment. In addition, video footage taken prior to cavity flooding indicates that the two-phase melt (voided) height periodically bridged this large gap, as evidenced by melt eruptions and lava flows occurring through this (and other) openings in the crust.

After key features of the bridge crust were documented, the crust was removed to gain access to the underlying void region. As shown in Figures 4-33 and 4-34, removal of this material revealed the presence of large mantles of crust protruding from both the east and west MgO sidewalls. Video data indicates that these mantles started forming as early as 42 minutes into the test sequence (see Table 3-1). The crust mantles were collected and weighed. The total mass was found to be quite large, amounting to 301.4 kg (see Figure 4-34).

Figure 4-31. West View of Debris Top Surface After Removal of the Middle Sidewall Section.

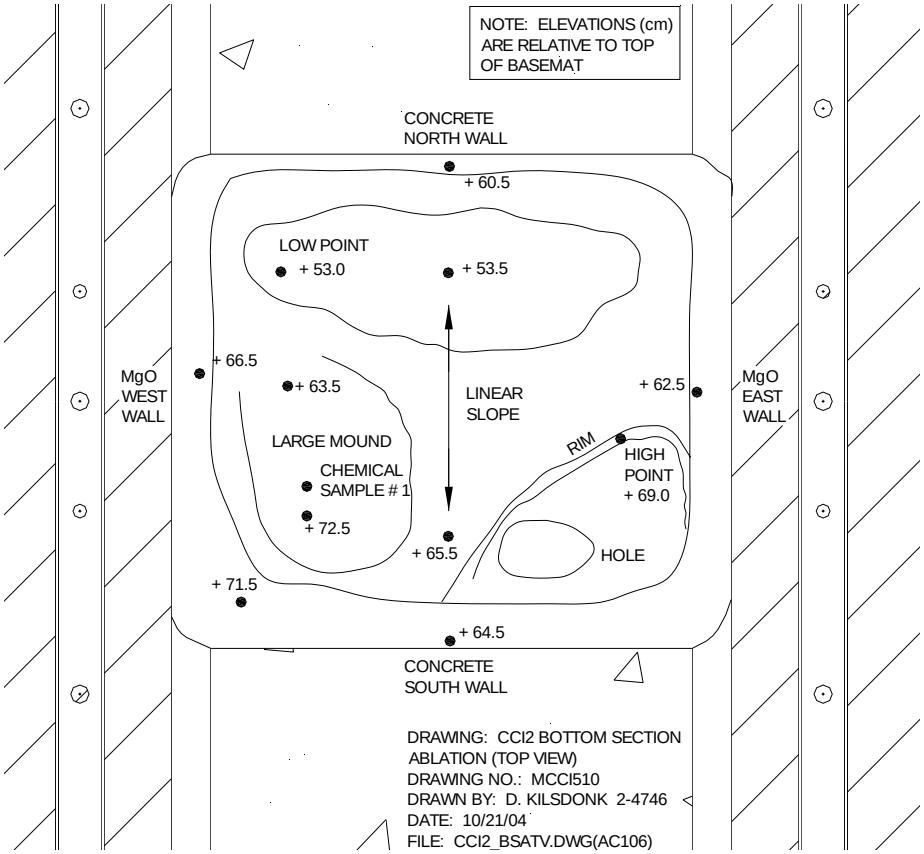

Figure 4-32. Topographical Map Showing Key Debris Upper Surface Elevations.

Figure 4-33. Crust Mantle Adhering to East Sidewall (after removal of bridge crust).

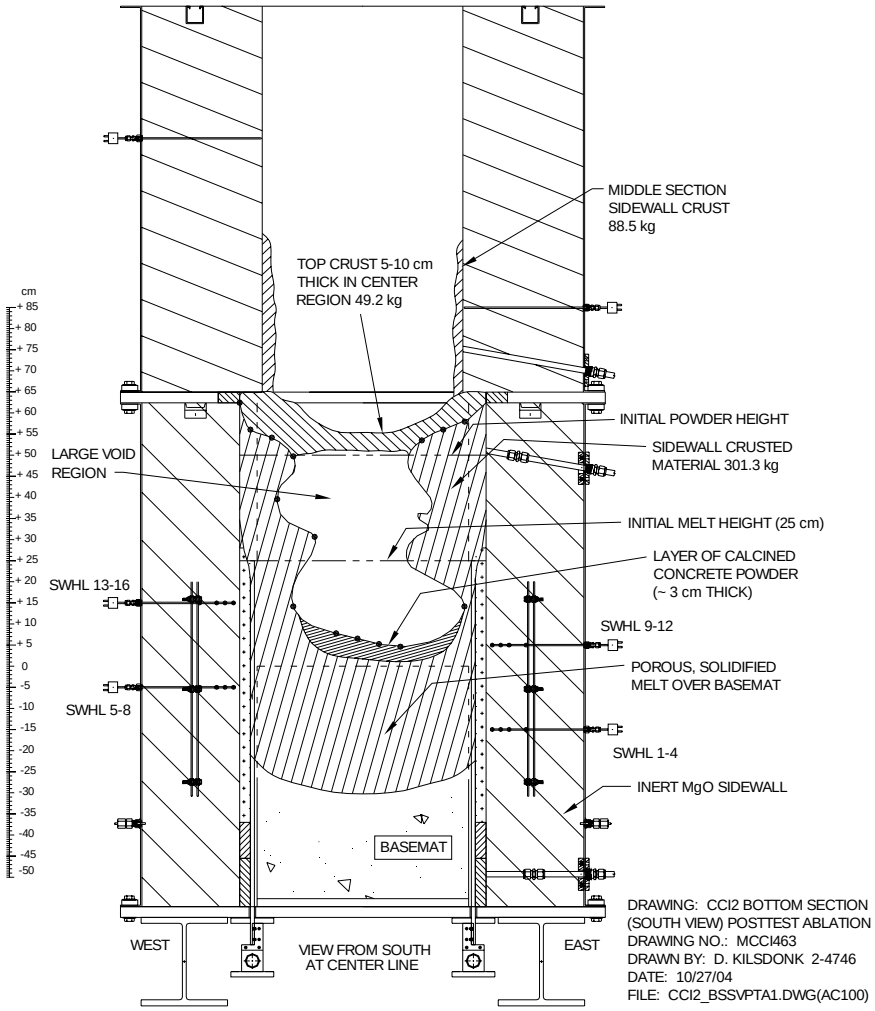

Figure 4-34. Non-Electrode Sidewall View of the Solidified Debris.

With these steps completed, the inert MgO sidewalls were removed to gain additional information regarding the shape of the cavity erosion profile. East and west profile photographs taken after the sidewalls were removed are provided in Figures 4-35 and 4-36, respectively. As is evident from these pictures, cavity erosion above the solidified debris layer was extensive. This erosion was probably driven by radiation heat transfer from the melt surface during periods in which the melt pool was collapsed, and also by convective heat transfer directly from the melt pool itself when the pool was undergoing extensive voiding (see previous discussion regarding apparent melt voiding behavior). One significant finding during this stage of the disassembly was the presence of a large mound of erupted material near the North concrete sidewall; see Figures 4-19 and 4-35. A vent opening was discovered approximately 10 cm from the eroded North concrete sidewall near the East-West centerline of the test section. The opening was ~ 1 cm in diameter.

Prior to removal of the concrete sidewalls, an axial core sample was drilled into the corium over the basemat near the test section centerline. A photograph of the hole created in the corium by the drilling process is shown in Figure 4-37, while a photograph of the core sample is provided in Figure 4-38. The core sample was used to collect specimens for chemical analysis (this data will be provided in a subsequent publication). Limited examination of the corium through this hole indicated the presence of significant porosity, but no continuous void region that would be expected if a second bridge crust had formed during the test.

After the core sample was collected, the concrete sidewalls were removed to provide more information about the posttest debris configuration. A side view of the solidified corium remaining over the basemat is provided in Figure 4-39, while a photograph of the south concrete sidewall is provided in Figure 4-40. Visual examination indicated that the corium remaining over the basemat was very porous, with pore sizes of several cm clearly evident. In fact, the porosity was so significant that one could see completely through the debris in the North-South direction. This level of porosity is consistent with the high rate of corium cooling observed when the cavity was flooded at 300.79 minutes during the test sequence (see Table 3-1).

During the disassembly, the various debris regions were carefully segregated and weighed to better document the debris distribution. The masses of these various debris regions are summarized in Table 4-1.

Table 4-1. Masses of Various Debris Regions.

Material Description	Mass (kg)	Notes(s)
Mass of Corium Recovered from Middle Section Sidewalls	88.5	-
Bridge Crust Mass in Central Region of Test Section	49.2	-
Sidewall Crust Mantles on East and West Walls	301.4	-
Recovered UO_2 pellets	295.4	The UO_2 pellet mass shown includes 245.4 kg that were physically recovered, plus ~ 50 kg of pellets that were bonded (melted) to the backs of the electrodes. A total of 338.56 kg of pellets were loaded. Thus, the difference of ~43.2 kg UO_2 dissolved into the melt.

Figure 4-35. Solidified Corium and Concrete Sidewalls (View From Southeast).

Figure 4-36. Solidified Corium and Concrete Sidewalls (View From Northwest).

Figure 4-37. Picture of the Core Hole Drilled Near the Test Section Centerline.

Figure 4-38. Core Sample Remnants (Core-concrete interface is to the right).

Figure 4-39. View of Solidified Corium Remaining Over the Basemat.

Figure 4-40. View of the South Concrete Sidewall After Removal.

5.0 REFERENCES

1. B. W. Spencer, et al., "MACE Scoping Test Data Report," ACE-TR-D03, June, 1991.

2. D. H. Thompson, M. T. Farmer, J. K. Fink, D. R. Armstrong, and B. W. Spencer, "ACE Phase C Final Report: Volume I – MCCI Thermalhydraulic Results," ACE-TR-C42 Volume I, September, 1997.

3. S. Lomperski, M. T. Farmer, D. J. Kilsdonk, and R. W. Aeschlimann, "SSWICS-1 Test Data Report – Thermalhydraulic Results," Rev. 0, OECD/MCCI-2002-TR05, September 20, 2002.

APPENDIX A
Data Acquisition System Channel Assignments

This Appendix provides the channel assignments for the three independent DAS systems that were used to record the data for CCI-2. For convenience, these three 128 channel systems were referred to the "Basemat", "Power," and "Quench" systems by operating personnel. The channel assignment lists for each of these three systems are provided in Tables A-1 through A-3. The data recorded on each of these channels is provided in Appendix B.

Table A-1. "Basemat" DAS Channel Assignments for CCI-2.

Channel	Variable	Sensor	Location	Level	Range/Limit	Accuracy	Notes
00	T	Diode Sensor	TC compensation Chs. B01-B49		130 C		
01	T	TC Type C	Basemat 0.0 cm, +1.9 cm WCL-1	+15.0 cm	2320 C	± 1%	
02	T	TC Type C	Basemat 0.0 cm, +1.9 cm WCL-2	+10.0 cm	2320 C	± 1%	
03	T	TC Type C	Basemat 0.0 cm, +1.9 cm WCL-3	+5.0 cm	2320 C	± 1%	
04	T	TC Type C	Basemat 0.0 cm, +1.9 cm WCL-4	0.0 cm	2320 C	± 1%	
05	T	TC Type C	Basemat -10.6 cm, +10.6 cm WNW-1	+9.5 cm	2320 C	± 1%	
06	T	TC Type C	Basemat -10.6 cm, +10.6 cm WNW-2	+4.5 cm	2320 C	± 1%	
07	T	TC Type C	Basemat -10.6 cm, +10.6 cm WNW-3	-0.5 cm	2320 C	± 1%	
08	T	TC Type C	Basemat -10.6 cm, +10.6 cm WNW-4	-5.5 cm	2320 C	± 1%	
09	T	TC Type C	Basemat +10.6 cm, +10.6 cm WNE-1	-7.0 cm	2320 C	± 1%	
10	T	TC Type C	Basemat +10.6 cm, +10.6 cm WNE-2	-12.0 cm	2320 C	± 1%	
11	T	TC Type C	Basemat +10.6 cm, +10.6 cm WNE-3	-17.0 cm	2320 C	± 1%	
12	T	TC Type C	Basemat +10.6 cm, +10.6 cm WNE-4	-22.0 cm	2320 C	± 1%	
13	T	TC Type C	Basemat +10.6 cm, -10.6 cm WSE-1	+4.0 cm	2320 C	± 1%	
14	T	TC Type C	Basemat +10.6 cm, -10.6 cm WSE-2	-1.0 cm	2320 C	± 1%	
15	T	TC Type C	Basemat +10.6 cm, -10.6 cm WSE-3	-6.0 cm	2320 C	± 1%	
16	T	TC Type C	Basemat +10.6 cm, -10.6 cm WSE-4	-11.0 cm	2320 C	± 1%	
17	T	TC Type C	Basemat -10.6 cm, -10.6 cm WSW-1	-1.5 cm	2320 C	± 1%	
18	T	TC Type C	Basemat -10.6 cm, -10.6 cm WSW-2	-6.5 cm	2320 C	± 1%	
19	T	TC Type C	Basemat -10.6 cm, -10.6 cm WSW-3	-11.5 cm	2320 C	± 1%	
20	T	TC Type C	Basemat -10.6 cm, -10.6 cm WSW-4	-16.5 cm	2320 C	± 1%	
21	T	TC Type C	N Sidewall, 0.0 cm deep, WN-1	+5.0 cm	2320 C	± 1%	
22	T	TC Type C	N Sidewall, 2.5 cm deep, WN-2	+5.0 cm	2320 C	± 1%	
23	T	TC Type C	N Sidewall, 5.1 cm deep, WN-3	+5.0 cm	2320 C	± 1%	
24	T	TC Type C	N Sidewall, 7.6 cm deep, WN-4	+5.0 cm	2320 C	± 1%	
25	T	TC Type C	S Sidewall, 0.0 cm deep, WS-1	+5.0 cm	2320 C	± 1%	
26	T	TC Type C	S Sidewall, 2.5 cm deep, WS-2	+5.0 cm	2320 C	± 1%	

27	T	TC Type C	S Sidewall, 5.1 cm deep, WS-3	+5.0 cm	2320 C	± 1%	
28	T	TC Type C	S Sidewall, 7.6 cm deep, WS-4	+5.0 cm	2320 C	± 1%	
29	T	TC Type K	Basemat 0.0 cm, -1.9 cm A-1	0.0 cm	1400 C	± 0.75%	
30	T	TC Type K	Basemat 0.0 cm, -1.9 cm A-2	-1.3 cm	1400 C	± 0.75%	
31	T	TC Type K	Basemat 0.0 cm, -1.9 cm A-3	-2.5 cm	1400 C	± 0.75%	
32	T	TC Type K	Basemat 0.0 cm, -1.9 cm A-4	-5.1 cm	1400 C	± 0.75%	
33	T	TC Type K	Basemat 0.0 cm, -1.9 cm A-5	-7.6 cm	1400 C	± 0.75%	
34	T	TC Type K	Basemat 0.0 cm, -1.9 cm A-6	-11.4 cm	1400 C	± 0.75%	
35	T	TC Type K	Basemat 0.0 cm, -1.9 cm A-7	-15.2 cm	1400 C	± 0.75%	
36	T	TC Type K	Basemat 0.0 cm, -1.9 cm A-8	-19.1 cm	1400 C	± 0.75%	
37	T	TC Type K	Basemat 0.0 cm, -1.9 cm A-9	24.1 cm	1400 C	± 0.75%	
38	T	TC Type K	Basemat 0.0 cm, -1.9 cm A-10	-29.2 cm	1400 C	± 0.75%	
39	T	TC Type K	Basemat 0.0 cm, -1.9 cm A-11	-34.3 cm	1400 C	± 0.75%	
40	T	TC Type K	Basemat –12.5 cm, +12.5 cm B-1	0.0 cm	1400 C	± 0.75%	
41	T	TC Type K	Basemat –12.5 cm, +12.5 cm B-2	-2.5 cm	1400 C	± 0.75%	
42	T	TC Type K	Basemat –12.5 cm, +12.5 cm B-3	-5.1 cm	1400 C	± 0.75%	
43	T	TC Type K	Basemat –12.5 cm, +12.5 cm B-4	-8.9 cm	1400 C	± 0.75%	
44	T	TC Type K	Basemat –12.5 cm, +12.5 cm B-5	-14.0 cm	1400 C	± 0.75%	
45	T	TC Type K	Basemat –12.5 cm, +12.5 cm B-6	-19.1 cm	1400 C	± 0.75%	
46	T	TC Type K	Basemat –12.5 cm, +12.5 cm B-7	-24.1 cm	1400 C	± 0.75%	
47	T	TC Type K	Basemat –12.5 cm, +12.5 cm B-8	-29.2 cm	1400 C	± 0.75%	
48	T	TC Type K	Basemat –12.5 cm, +12. 5 cm B-9	-34.3 cm	1400 C	± 0.75%	
49	T	TC Type K	N Sidewall 24.1 cm deep SWK-9	+20.0 cm	1400 C	± 0.75%	
50	T	Diode Sensor	TC compensation Chs. B51-B99		130 C		
51	T	TC Type K	Basemat +12.5 cm, +12.5 cm C-1	0.0 cm	1400 C	± 0.75%	
52	T	TC Type K	Basemat +12.5 cm, +12.5 cm C-2	-2.5 cm	1400 C	± 0.75%	
53	T	TC Type K	Basemat +12.5 cm, +12.5 cm C-3	-5.1 cm	1400 C	± 0.75%	
54	T	TC Type K	Basemat +12.5 cm, +12.5 cm C-4	-8.9 cm	1400 C	± 0.75%	

55	T	TC Type K	Basemat +12.5 cm, +12.5 cm C-5	-14.0 cm	1400 C	± 0.75%	
56	T	TC Type K	Basemat +12.5 cm, +12.5 cm C-6	-19.1 cm	1400 C	± 0.75%	
57	T	TC Type K	Basemat +12.5 cm, +12.5 cm C-7	-24.1 cm	1400 C	± 0.75%	
58	T	TC Type K	Basemat +12.5 cm, +12.5 cm C-8	-29.2 cm	1400 C	± 0.75%	
59	T	TC Type K	Basemat +12.5 cm, +12. 5 cm C-9	-34.3 cm	1400 C	± 0.75%	
60	T	TC Type K	N Sidewall 29.2 cm deep SWK-10	+20.0 cm	1400 C	± 0.75%	
61	T	TC Type K	Basemat +12.5 cm, -12.5 cm D-1	0.0 cm	1400 C	± 0.75%	
62	T	TC Type K	Basemat +12.5 cm, -12.5 cm D-2	-2.5 cm	1400 C	± 0.75%	
63	T	TC Type K	Basemat +12.5 cm, -12.5 cm D-3	-5.1 cm	1400 C	± 0.75%	
64	T	TC Type K	Basemat +12.5 cm, -12.5 cm D-4	-8.9 cm	1400 C	± 0.75%	
65	T	TC Type K	Basemat +12.5 cm, -12.5 cm D-5	-14.0 cm	1400 C	± 0.75%	
66	T	TC Type K	Basemat +12.5 cm, -12.5 cm D-6	-19.1 cm	1400 C	± 0.75%	
67	T	TC Type K	Basemat +12.5 cm, -12.5 cm D-7	-24.1 cm	1400 C	± 0.75%	
68	T	TC Type K	Basemat +12.5 cm, -12.5 cm D-8	-29.2 cm	1400 C	± 0.75%	
69	T	TC Type K	Basemat +12.5 cm, -12. 5 cm D-9	-34.3 cm	1400 C	± 0.75%	
70	T	TC Type K	N Sidewall 34.3 cm deep SWK-11	+20.0 cm	1400 C	± 0.75%	
71	T	TC Type K	Basemat -12.5 cm, -12.5 cm E-1	0.0 cm	1400 C	± 0.75%	
72	T	TC Type K	Basemat -12.5 cm, -12.5 cm E-2	-2.5 cm	1400 C	± 0.75%	
73	T	TC Type K	Basemat -12.5 cm, -12.5 cm E-3	-5.1 cm	1400 C	± 0.75%	
74	T	TC Type K	Basemat -12.5 cm, -12.5 cm E-4	-8.9 cm	1400 C	± 0.75%	
75	T	TC Type K	Basemat -12.5 cm, -12.5 cm E-5	-14.0 cm	1400 C	± 0.75%	
76	T	TC Type K	Basemat -12.5 cm, -12.5 cm E-6	-19.1 cm	1400 C	± 0.75%	
77	T	TC Type K	Basemat -12.5 cm, -12.5 cm E-7	-24.1 cm	1400 C	± 0.75%	
78	T	TC Type K	Basemat -12.5 cm, -12.5 cm E-8	-29.2 cm	1400 C	± 0.75%	
79	T	TC Type K	Basemat -12.5 cm, -12. 5 cm E-9	-34.3 cm	1400 C	± 0.75%	
80	T	TC Type K	S Sidewall 24.1 cm deep SWL-9	+20.0 cm	1400 C	± 0.75%	
81	T	TC Type K	N Sidewall 0.0 cm deep SWA-1	-30.0 cm	1400 C	± 0.75%	
82	T	TC Type K	N Sidewall 1.3 cm deep SWA-2	-30.0 cm	1400 C	± 0.75%	

83	T	TC Type K	N Sidewall 2.5 cm deep SWA-3	-30.0 cm	1400 C	± 0.75%	
84	T	TC Type K	N Sidewall 5.1 cm deep SWA-4	-30.0 cm	1400 C	± 0.75%	
85	T	TC Type K	N Sidewall 7.6 cm deep SWA-5	-30.0 cm	1400 C	± 0.75%	
86	T	TC Type K	N Sidewall 11.5 cm deep SWA-6	-30.0 cm	1400 C	± 0.75%	
87	T	TC Type K	N Sidewall 15.2 cm deep SWA-7	-30.0 cm	1400 C	± 0.75%	
88	T	TC Type K	N Sidewall 17.8 cm deep SWA-8	-30.0 cm	1400 C	± 0.75%	
89	T	TC Type K	S Sidewall 0.0 cm deep SWB-1	-30.0 cm	1400 C	± 0.75%	
90	T	TC Type K	S Sidewall 1.3 cm deep SWB-2	-30.0 cm	1400 C	± 0.75%	
91	T	TC Type K	S Sidewall 2.5 cm deep SWB-3	-30.0 cm	1400 C	± 0.75%	
92	T	TC Type K	S Sidewall 5.1 cm deep SWB-4	-30.0 cm	1400 C	± 0.75%	
93	T	TC Type K	S Sidewall 7.6 cm deep SWB-5	-30.0 cm	1400 C	± 0.75%	
94	T	TC Type K	S Sidewall 11.5 cm deep SWB-6	-30.0 cm	1400 C	± 0.75%	
95	T	TC Type K	S Sidewall 15.2 cm deep SWB-7	-30.0 cm	1400 C	± 0.75%	
96	T	TC Type K	S Sidewall 17.8 cm deep SWB-8	-30.0 cm	1400 C	± 0.75%	
97	T	TC Type K	N Sidewall 0.0 cm deep SWC-1	-20.0 cm	1400 C	± 0.75%	
98	T	TC Type K	N Sidewall 1.3 cm deep SWC-2	-20.0 cm	1400 C	± 0.75%	
99	T	TC Type K	N Sidewall 2.5 cm deep SWC-3	-20.0 cm	1400 C	± 0.75%	

Explanation of Variable Notations
T = temperature

Table A-2. "Power" DAS Channel Assignments for CCI-2.

Channel	Variable	Sensor	Location	Level	Range/Limit	Accuracy	Notes
00	T	TC Type K	S Sidewall 29.2 cm deep SWL-10	+20.0 cm	1400 C	± 0.75%	
01	T	TC Type K	N Sidewall 5.1 cm deep SWC-4	-20.0 cm	1400 C	± 0.75%	
02	T	TC Type K	N Sidewall 7.6 cm deep SWC-5	-20.0 cm	1400 C	± 0.75%	
03	T	TC Type K	N Sidewall 11.4 cm deep SWC-6	-20.0 cm	1400 C	± 0.75%	
04	T	TC Type K	N Sidewall 15.2 cm deep SWC-7	-20.0 cm	1400 C	± 0.75%	
05	T	TC Type K	N Sidewall 19.1 cm deep SWC-8	-20.0 cm	1400 C	± 0.75%	
06	T	TC Type K	N Sidewall 24.1 cm deep SWC-9	-20.0 cm	1400 C	± 0.75%	
07	T	TC Type K	N Sidewall 29.2 cm deep SWC-10	-20.0 cm	1400 C	± 0.75%	
08	T	TC Type K	N Sidewall 34.3 cm deep SWC-11	-20.0 cm	1400 C	± 0.75%	
09	T	TC Type K	S Sidewall 0.0 cm deep SWD-1	-20.0 cm	1400 C	± 0.75%	
10	T	TC Type K	S Sidewall 1.3 cm deep SWD-2	-20.0 cm	1400 C	± 0.75%	
11	T	TC Type K	S Sidewall 2.5 cm deep SWD-3	-20.0 cm	1400 C	± 0.75%	
12	T	TC Type K	S Sidewall 5.1 cm deep SWD-4	-20.0 cm	1400 C	± 0.75%	
13	T	TC Type K	S Sidewall 7.6 cm deep SWD-5	-20.0 cm	1400 C	± 0.75%	
14	T	TC Type K	S Sidewall 11.4 cm deep SWD-6	-20.0 cm	1400 C	± 0.75%	
15	T	TC Type K	S Sidewall 15.2 cm deep SWD-7	-20.0 cm	1400 C	± 0.75%	
16	T	TC Type K	S Sidewall 19.1 cm deep SWD-8	-20.0 cm	1400 C	± 0.75%	
17	T	TC Type K	S Sidewall 24.1 cm deep SWD-9	-20.0 cm	1400 C	± 0.75%	
18	T	TC Type K	S Sidewall 29.2 cm deep SWD-10	-20.0 cm	1400 C	± 0.75%	
19	T	TC Type K	S Sidewall 34.3 cm deep SWD-11	-20.0 cm	1400 C	± 0.75%	
20	T	TC Type K	N Sidewall 0.0 cm deep SWE-1	-10.0 cm	1400 C	± 0.75%	
21	T	TC Type K	N Sidewall 1.3 cm deep SWE-2	-10.0 cm	1400 C	± 0.75%	
22	T	TC Type K	N Sidewall 2.5 cm deep SWE-3	-10.0 cm	1400 C	± 0.75%	
23	T	TC Type K	N Sidewall 5.1 cm deep SWE-4	-10.0 cm	1400 C	± 0.75%	
24	T	TC Type K	N Sidewall 7.6 cm deep SWE-5	-10.0 cm	1400 C	± 0.75%	
25	T	TC Type K	N Sidewall 11.4 cm deep SWE-6	-10.0 cm	1400 C	± 0.75%	
26	T	TC Type K	N Sidewall 15.2 cm deep SWE-7	-10.0 cm	1400 C	± 0.75%	

27	T	TC Type K	N Sidewall 19.1 cm deep SWE-8	-10.0 cm	1400 C	± 0.75%	
28	T	TC Type K	N Sidewall 24.1 cm deep SWE-9	-10.0 cm	1400 C	± 0.75%	
29	T	TC Type K	N Sidewall 29.2 cm deep SWE-10	-10.0 cm	1400 C	± 0.75%	
30	T	TC Type K	N Sidewall 34.3 cm deep SWE-11	-10.0 cm	1400 C	± 0.75%	
31	T	TC Type K	S Sidewall 0.0 cm deep SWF-1	-10.0 cm	1400 C	± 0.75%	
32	T	TC Type K	S Sidewall 1.3 cm deep SWF-2	-10.0 cm	1400 C	± 0.75%	
33	T	TC Type K	S Sidewall 2.5 cm deep SWF-3	-10.0 cm	1400 C	± 0.75%	
34	T	TC Type K	S Sidewall 5.1 cm deep SWF-4	-10.0 cm	1400 C	± 0.75%	
35	T	TC Type K	S Sidewall 7.6 cm deep SWF-5	-10.0 cm	1400 C	± 0.75%	
36	T	TC Type K	S Sidewall 11.4 cm deep SWF-6	-10.0 cm	1400 C	± 0.75%	
37	T	TC Type K	S Sidewall 15.2 cm deep SWF-7	-10.0 cm	1400 C	± 0.75%	
38	T	TC Type K	S Sidewall 19.1 cm deep SWF-8	-10.0 cm	1400 C	± 0.75%	
39	T	TC Type K	S Sidewall 24.1 cm deep SWF-9	-10.0 cm	1400 C	± 0.75%	
40	T	TC Type K	S Sidewall 29.2 cm deep SWF-10	-10.0 cm	1400 C	± 0.75%	
41	T	TC Type K	S Sidewall 34.3 cm deep SWF-11	-10.0 cm	1400 C	± 0.75%	
42	T	TC Type K	N Sidewall 0.0 cm deep SWG-1	0.0 cm	1400 C	± 0.75%	
43	T	TC Type K	N Sidewall 1.3 cm deep SWG-2	0.0 cm	1400 C	± 0.75%	
44	T	TC Type K	N Sidewall 2.5 cm deep SWG-3	0.0 cm	1400 C	± 0.75%	
45	T	TC Type K	N Sidewall 5.1 cm deep SWG-4	0.0 cm	1400 C	± 0.75%	
46	T	TC Type K	N Sidewall 7.6 cm deep SWG-5	0.0 cm	1400 C	± 0.75%	
47	T	TC Type K	N Sidewall 11.4 cm deep SWG-6	0.0 cm	1400 C	± 0.75%	
48	T	TC Type K	N Sidewall 15.2 cm deep SWG-7	0.0 cm	1400 C	± 0.75%	
49	T	TC Type K	N Sidewall 19.1 cm deep SWG-8	0.0 cm	1400 C	± 0.75%	
50	T	TC Type K	S Sidewall 34.3 cm deep SWL-11	+20.0 cm	1400 C	± 0.75%	
51	T	TC Type K	N Sidewall 24.1 cm deep SWG-9	0.0 cm	1400 C	± 0.75%	
52	T	TC Type K	N Sidewall 29.2 cm deep SWG-10	0.0 cm	1400 C	± 0.75%	
53	T	TC Type K	N Sidewall 34.3 cm deep SWG-11	0.0 cm	1400 C	± 0.75%	
54	T	TC Type K	S Sidewall 0.0 cm deep SWH-1	0.0 cm	1400 C	± 0.75%	

55	T	TC Type K	S Sidewall 1.3 cm deep SWH-2	0.0 cm	1400 C	± 0.75%	
56	T	TC Type K	S Sidewall 2.5 cm deep SWH-3	0.0 cm	1400 C	± 0.75%	
57	T	TC Type K	S Sidewall 5.1 cm deep SWH-4	0.0 cm	1400 C	± 0.75%	
58	T	TC Type K	S Sidewall 7.6 cm deep SWH-5	0.0 cm	1400 C	± 0.75%	
59	T	TC Type K	S Sidewall 11.4 cm deep SWH-6	0.0 cm	1400 C	± 0.75%	
60	T	TC Type K	S Sidewall 15.2 cm deep SWH-7	0.0 cm	1400 C	± 0.75%	
61	T	TC Type K	S Sidewall 19.1 cm deep SWH-8	0.0 cm	1400 C	± 0.75%	
62	T	TC Type K	S Sidewall 24.1 cm deep SWH-9	0.0 cm	1400 C	± 0.75%	
63	T	TC Type K	S Sidewall 29.2 cm deep SWH-10	0.0 cm	1400 C	± 0.75%	
64	T	TC Type K	S Sidewall 34.3 cm deep SWH-11	0.0 cm	1400 C	± 0.75%	
65	T	TC Type K	N Sidewall 0.0 cm deep SWI-1	+10.0 cm	1400 C	± 0.75%	
66	T	TC Type K	N Sidewall 1.3 cm deep SWI-2	+10.0 cm	1400 C	± 0.75%	
67	T	TC Type K	N Sidewall 2.5 cm deep SWI-3	+10.0 cm	1400 C	± 0.75%	
68	T	TC Type K	N Sidewall 5.1 cm deep SWI-4	+10.0 cm	1400 C	± 0.75%	
69	T	TC Type K	N Sidewall 7.6 cm deep SWI-5	+10.0 cm	1400 C	± 0.75%	
70	T	TC Type K	N Sidewall 11.4 cm deep SWI-6	+10.0 cm	1400 C	± 0.75%	
71	T	TC Type K	N Sidewall 15.2 cm deep SWI-7	+10.0 cm	1400 C	± 0.75%	
72	T	TC Type K	N Sidewall 19.1 cm deep SWI-8	+10.0 cm	1400 C	± 0.75%	
73	T	TC Type K	N Sidewall 24.1 cm deep SWI-9	+10.0 cm	1400 C	± 0.75%	
74	T	TC Type K	N Sidewall 29.2 cm deep SWI-10	+10.0 cm	1400 C	± 0.75%	
75	T	TC Type K	N Sidewall 34.3 cm deep SWI-11	+10.0 cm	1400 C	± 0.75%	
76	T	TC Type K	S Sidewall 0.0 cm deep SWJ-1	+10.0 cm	1400 C	± 0.75%	
77	T	TC Type K	S Sidewall 1.3 cm deep SWJ-2	+10.0 cm	1400 C	± 0.75%	
78	T	TC Type K	S Sidewall 2.5 cm deep SWJ-3	+10.0 cm	1400 C	± 0.75%	
79	T	TC Type K	S Sidewall 5.1 cm deep SWJ-4	+10.0 cm	1400 C	± 0.75%	
80	T	TC Type K	S Sidewall 7.6 cm deep SWJ-5	+10.0 cm	1400 C	± 0.75%	
81	T	TC Type K	S Sidewall 11.4 cm deep SJI-6	+10.0 cm	1400 C	± 0.75%	
82	T	TC Type K	S Sidewall 15.2 cm deep SWJ-7	+10.0 cm	1400 C	± 0.75%	

83	T	TC Type K	S Sidewall 19.1 cm deep SWJ-8	+10.0 cm	1400 C	± 0.75%	
84	T	TC Type K	S Sidewall 24.1 cm deep SWJ-9	+10.0 cm	1400 C	± 0.75%	
85	T	TC Type K	S Sidewall 29.2 cm deep SWJ-10	+10.0 cm	1400 C	± 0.75%	
86	T	TC Type K	S Sidewall 34.3 cm deep SWJ-11	+10.0 cm	1400 C	± 0.75%	
87	T	TC Type K	N Sidewall 0.0 cm deep SWK-1	+20.0 cm	1400 C	± 0.75%	
88	T	TC Type K	N Sidewall 1.3 cm deep SWK-2	+20.0 cm	1400 C	± 0.75%	
89	T	TC Type K	N Sidewall 2.5 cm deep SWK-3	+20.0 cm	1400 C	± 0.75%	
90	T	TC Type K	N Sidewall 5.1 cm deep SWK-4	+20.0 cm	1400 C	± 0.75%	
91	T	TC Type K	N Sidewall 7.6 cm deep SWK-5	+20.0 cm	1400 C	± 0.75%	
92	T	TC Type K	N Sidewall 11.5 cm deep SWK-6	+20.0 cm	1400 C	± 0.75%	
93	T	TC Type K	N Sidewall 15.2 cm deep SWK-7	+20.0 cm	1400 C	± 0.75%	
94	T	TC Type K	N Sidewall 17.8 cm deep SWK-8	+20.0 cm	1400 C	± 0.75%	
95	T	TC Type K	S Sidewall 0.0 cm deep SWL-1	+20.0 cm	1400 C	± 0.75%	
96	T	TC Type K	S Sidewall 1.3 cm deep SWL-2	+20.0 cm	1400 C	± 0.75%	
97	T	TC Type K	S Sidewall 2.5 cm deep SWL-3	+20.0 cm	1400 C	± 0.75%	
98	T	TC Type K	S Sidewall 5.1 cm deep SWL-4	+20.0 cm	1400 C	± 0.75%	
99	T	TC Type K	S Sidewall 7.6 cm deep SWL-5	+20.0 cm	1400 C	± 0.75%	

Explanation of Variable Notations
T = temperature

Table A-3. "Quench" DAS Channel Assignments for CCI-2.

Channel	Variable	Sensor	Location	Level	Range/Limit	Accuracy	Notes
00	T	Diode Sensor	TC Compensation CH Q00-Q49		130 C		
01	T	TC Type K	S Sidewall 11.5 cm deep SWL-6	+20.0 cm	1400 C	± 0.75%	
02	T	TC Type K	S Sidewall 15.2 cm deep SWL-7	+20.0 cm	1400 C	± 0.75%	
03	T	TC Type K	S Sidewall 17.8 cm deep SWL-8	+20.0 cm	1400 C	± 0.75%	
04	T	TC Type C	E Sidewall 1.0 cm deep SWHL-1	-15.0 cm	2320 C	± 1.0%	
05	T	TC Type C	E Sidewall 2.0 cm deep SWHL-2	-15.0 cm	2320 C	± 1.0%	
06	T	TC Type C	E Sidewall 4.0 cm deep SWHL-3	-15.0 cm	2320 C	± 1.0%	
07	T	TC Type C	E Sidewall 8.0 cm deep SWHL-4	-15.0 cm	2320 C	± 1.0%	
08	T	TC Type C	W Sidewall 1.0 cm deep SWHL-5	-5.0 cm	2320 C	± 1.0%	
09	T	TC Type C	W Sidewall 2.0 cm deep SWHL-6	-5.0 cm	2320 C	± 1.0%	
10	T	TC Type C	W Sidewall 4.0 cm deep SWHL-7	-5.0 cm	2320 C	± 1.0%	
11	T	TC Type C	W Sidewall 8.0 cm deep SWHL-8	-5.0 cm	2320 C	± 1.0%	
12	T	TC Type C	E Sidewall 1.0 cm deep SWHL-9	+5.0 cm	2320 C	± 1.0%	
13	T	TC Type C	E Sidewall 2.0 cm deep SWHL-10	+5.0 cm	2320 C	± 1.0%	
14	T	TC Type C	E Sidewall 4.0 cm deep SWHL-11	+5.0 cm	2320 C	± 1.0%	
15	T	TC Type C	E Sidewall 8.0 cm deep SWHL-12	+5.0 cm	2320 C	± 1.0%	
16	T	TC Type C	W Sidewall 1.0 cm deep SWHL-13	+15.0 cm	2320 C	± 1.0%	
17	T	TC Type C	W Sidewall 2.0 cm deep SWHL-14	+15.0 cm	2320 C	± 1.0%	
18	T	TC Type C	W Sidewall 4.0 cm deep SWHL-15	+15.0 cm	2320 C	± 1.0%	
19	T	TC Type C	W Sidewall 8.0 cm deep SWHL-16	+15.0 cm	2320 C	± 1.0%	
20	L	Potentiometer	Lance Position Indicator		0-127 cm		
21	T	TC Type K	Steamline internal vertical run from vessel ML-1		1400 C	± 0.75%	
22	T	TC Type K	Steamline external vertical run from vessel ML-2		1400 C	± 0.75%	
23	T	TC Type K	Steamline external lateral run from vessel ML-3		1400 C	± 0.75%	
24	T	TC Type K	Steamline external vertical run to quench tank ML-4		1400 C	± 0.75%	
25	T	TC Type C	S Sidewall 0.0 cm deep SWHL-17	+70.0 cm	2320 C	± 1.0%	
26	T	TC Type C	S Sidewall 0.5 cm deep SWHL-18	+70.0 cm	2320 C	± 1.0%	

27	T	TC Type C	S Sidewall 1.5 cm deep SWHL -19	+70.0 cm	2320 C	± 1.0%	
28	FOR	Strain	Crust Force Load		0-44.6 kN		
29	T	TC Type K	Quench tank internal QT-1	21 cm	1400 C	± 0.75%	
30	T	TC Type K	Quench tank internal QT-2	55 cm	1400 C	± 0.75%	
31	T	TC Type C	N Sidewall, 10.2 cm deep, WN-5	+5.0 cm	2320 C	± 1%	
32	T	TC Type C	N Sidewall, 15.2 cm deep, WN-6	+5.0 cm	2320 C	± 1%	
33	T	TC Type K	E Sidewall 0.0 cm deep SWHL-30	+174.7 cm	1400 C	± 0.75%	
34	T	TC Type K	E Sidewall 0.5 cm deep SWHL-31	+174.7 cm	1400 C	± 0.75%	
35	T	TC Type K	Quench tank coil inlet QT-5		1400 C	± 0.75%	
36	T	TC Type K	Quench tank coil outlet QT-6		1400 C	± 0.75%	
37	T	TC Type K	Quench tank coil outlet QT-7		1400 C	± 0.75%	
38	T	TC Type K	Overflow tank internal OT-1	16 cm	1400 C	± 0.75%	
39	T	Voltage	Igniter Current		100 mV		
40	T	TC Type K	Spray tank internal ST-1	10 cm	1400 C	± 0.75%	
41	T	TC Type C	N Sidewall, 20.3 cm deep, WN-7	+5.0 cm	2320 C	± 1%	
42	T	TC Type K	E Sidewall 0.0 cm deep SWHL-20	+84.1 cm	1400 C	± 0.75%	
43	T	TC Type K	E Sidewall 0.5 cm deep SWHL-21	84.1 cm	1400 C	± 0.75%	
44	T	TC Type K	E Sidewall 1.5 cm deep SWHL-22	84.1 cm	1400 C	± 0.75%	
45	T	TC Type K	N Sidewall 0.0 cm deep SWHL-23	+94.7 cm	1400 C	± 0.75%	
46	T	TC Type K	N Sidewall 0.5 cm deep SWHL-24	+94.7 cm	1400 C	± 0.75%	
47	T	TC Type K	N Sidewall 1.5 cm deep SWHL-25	+94.7 cm	1400 C	± 0.75%	
48	T	TC Type K	W Sidewall 0.0 cm deep SWHL-26	+124.9 cm	1400 C	± 0.75%	
49	T	TC Type K	W Sidewall 0.5 cm deep SWHL-27	+124.9 cm	1400 C	± 0.75%	
50	T	Diode Sensor	TC Compensation CH Q50-Q99		130 C		
51	T	TC Type K	S Sidewall 0.0 cm deep SWHL-28	+151.3 cm	1400 C	± 0.75%	
52	T	TC Type K	S Sidewall 0.5 cm deep SWHL-29	+151.3 cm	1400 C	± 0.75%	
53	T	TC Type C	N Sidewall, 25.4 cm deep, WN-8	+5.0 cm	2320 C	± 1%	
54	T	TC Type K	Internal, exhaust line OG-1		1400 C	± 0.75%	

55	T	TC Type K	Water supply tank internal WS-1	45 cm	1400 C	± 0.75%	
56	T	TC Type K	Upper lid, 0.0 cm deep VL-1	247.8 cm	1400 C	± 0.75%	
57	T	TC Type K	Water level probe LP-1	169/50 cm	1400 C	± 0.75%	
58	T	TC Type K	Water level probe LP-2	169/50 cm	1400 C	± 0.75%	
59	T	TC Type K	Test vessel plenum gas TS-1	225.5 cm	1400 C	± 0.75%	
60	L	Strain	Supply tank head PT-1		350-2000 l		D-6
61	P	Strain	Supply tank pressure PT-2		0-204 kPa		A-17
62	L	Strain	Test vessel head, insertion probe PT-3		63-150 l		D-3
63	L	Strain	Test vessel head, static probe PT-4		32-150 l		D-1
64	P	Strain	Test vessel plenum pressure PT-5		0-204 kPa		A-16
65	P	Strain	Basemat side pressure PT-6		0-204 kPa		A-3
66	Unused						
67	L	Strain	Quench tank head PT-8		80-590 l		D-2
68	P	Strain	Quench/overflow tank pressure PT-9		0-204 kPa		A-10
69	L	Strain	Overflow tank head PT-10		200-900 l		D-8
70	L	Strain	Spray tank head PT-11		240-1290 l		D-5
71	P	Strain	Spray tank pressure PT-12		0-204 kPa		A-1
72	L	Magnetic Float	Supply tank volume LS-1		350-2000 l		
73	L	Magnetic Float	Quench tank volume LS-2		80-590 l		
74	L	Magnetic Float	Overflow tank volume LS-3		200-900 l		
75	L	Magnetic Float	Spray tank volume LS-4		240-1290 l		
76	F	Paddlewheel	Water supply flow rate FM-1		680 lpm		
77	F	Paddlewheel	Quench tank coil flow rate FM-2		190 lpm		
78	Unused						
79	T	TC Type C	S Sidewall, 10.2 cm deep, WS-5	+5.0 cm	2320 C	± 1%	
80	T	TC Type C	S Sidewall, 15.2 cm deep, WS-6	+5.0 cm	2320 C	± 1%	
81	FC	Flowcontroller	Final Off gas Flow rate FC1a		0-15,000 lpm		
82		-	Calculated Water Volume in Test Section		0-150 l		

83	FC	Flowcontroller	Lid lights & camera cover gas flow rate FC-2		0-200 lpm		
84	Unused						
85		-	Calculated Total Current (Q92+Q93)		0 -10,000 A		
86	Unused	-	Calculated Total Power (Q94+Q95)		0-500 kW		
87	FC	Flowcontroller	Test vessel cover gas flow rate FC-6		0-100 lpm		
88	FC	Flowcontroller	Lid camera cover gas flow rate FC-7		0-350 lpm		
89	V		Pressure transducer power supply #1 voltage		0-30 V		
90	V		Pressure transducer power supply #2 voltage		0-30 V		
91	V	Voltmeter	Power supply voltage		0-200 V		
92	A	Transformer	Power supply current #2		5000 A		
93	A	Transformer	Power supply current #1		5000 A		
94	W	Hall Meter	Power supply power #2		1100 kW		
95	W	Hall Meter	Power supply power #1		1100 kW		
96	L	Strain	Auxiliary Tank Head PT-13		366-4080		D-10
97	T	TC Type K	Auxiliary Tank Internal AT-1	43 cm	1400 C	± 0.75%	
98	T	TC Type C	S Sidewall, 20.3 cm deep, WS-7	+5.0 cm	2320 C	± 1%	
99	T	TC Type C	S Sidewall, 25.4 cm deep, WS-8	+5.0 cm	2320 C	± 1%	

Explanation of variable notations

T = temperature P = Pressure FOR=Force L = Level V = Voltage F = Flow rate A = Current W = Power FC = Flow Controller

APPENDIX B
Test Data

This Appendix provides plots of all data recorded during Test CCI-2. The complete channel assignment list is provided in Appendix A. Time t = 0 in all plots is referenced to the time at which the melt made initial contact with the concrete basemat. This corresponds to 7.57 minutes after onset of data acquisition; see Table 3-1.

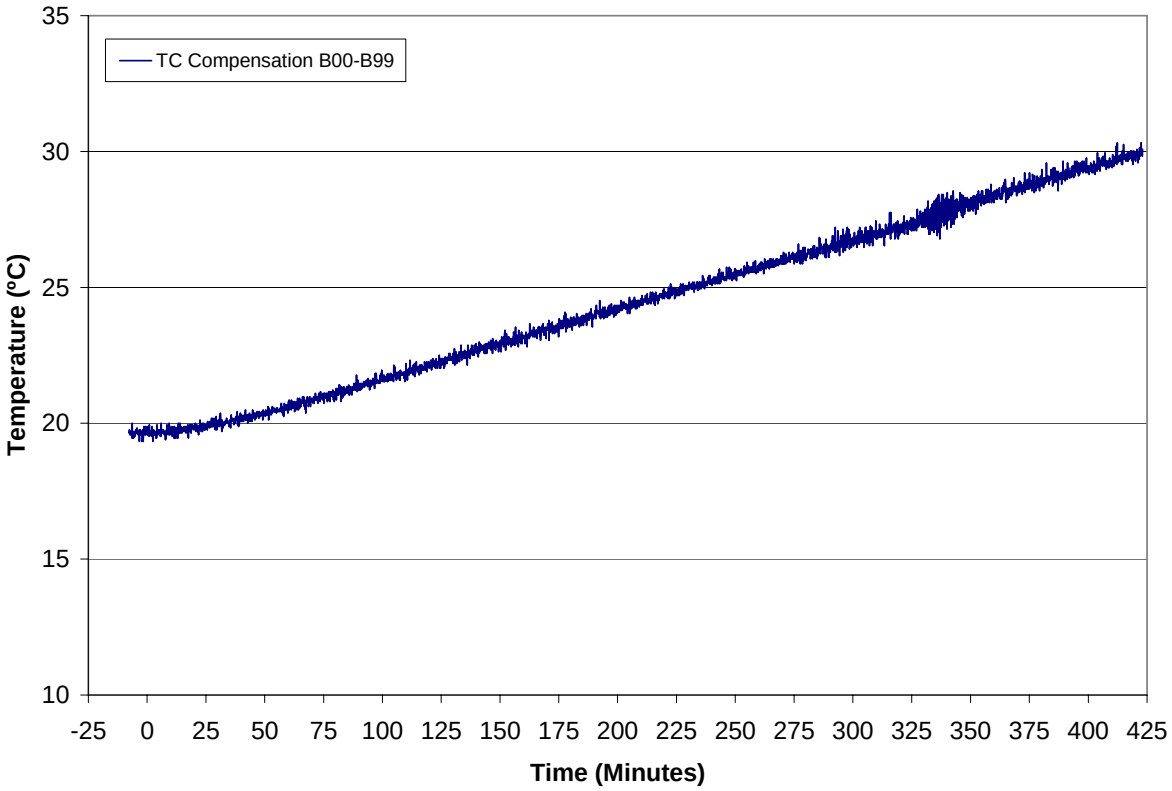

Figure B-1. Compensator Temperature, Channels B01-B49 and B50-B99.

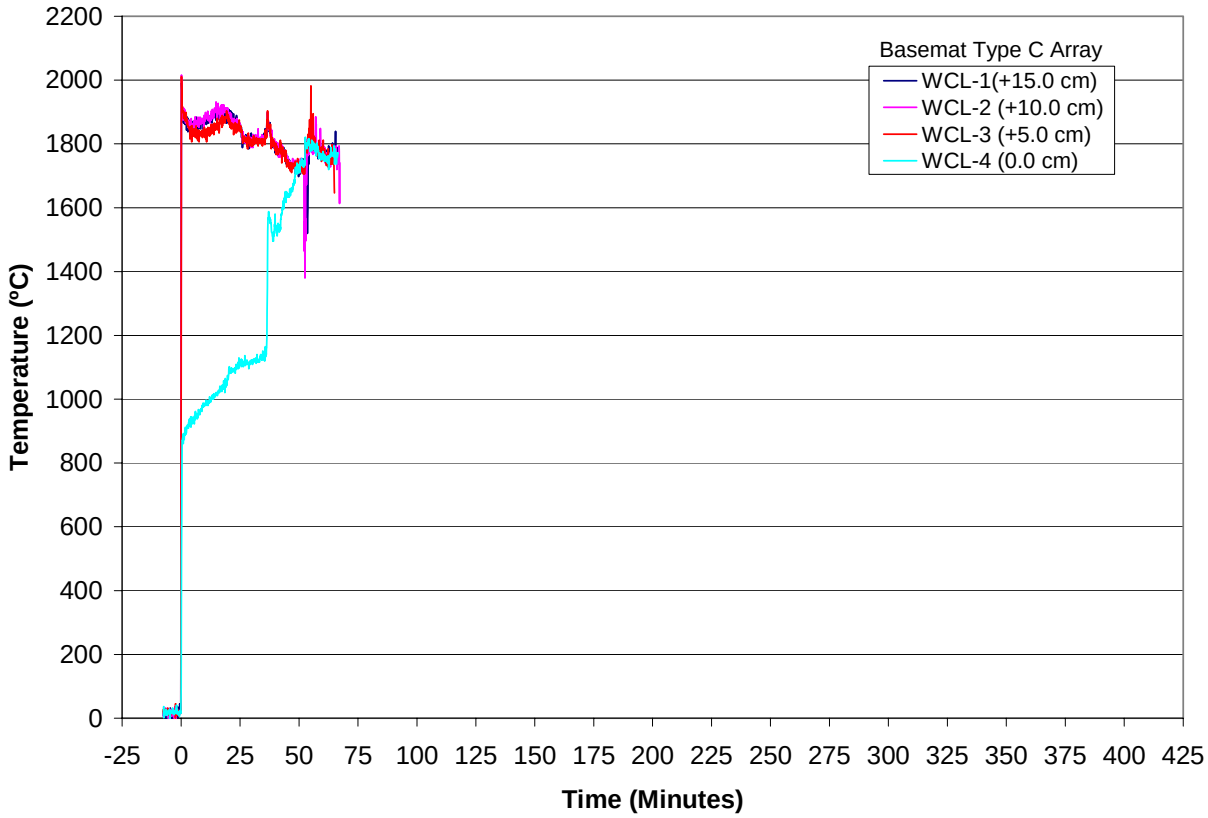

Figure B-2. Basemat Type C "WCL" Array Data.

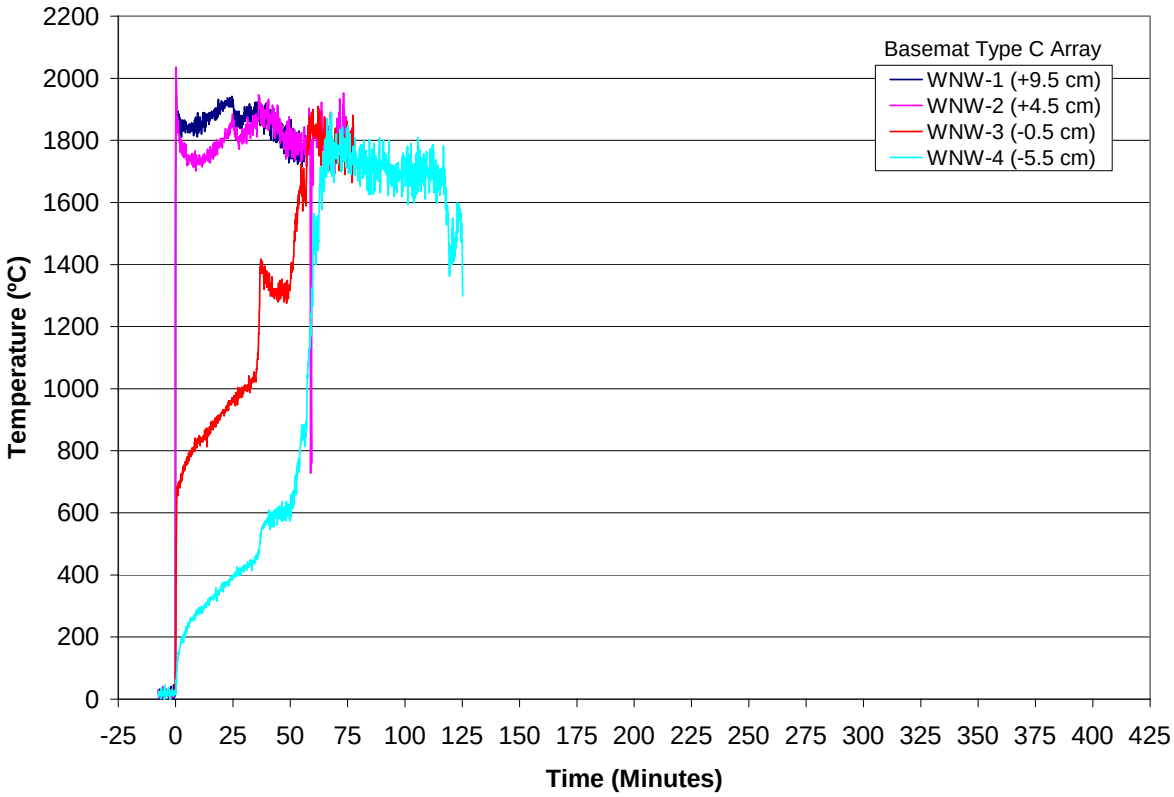

Figure B-3. Basemat Type C "WNW" Array Data.

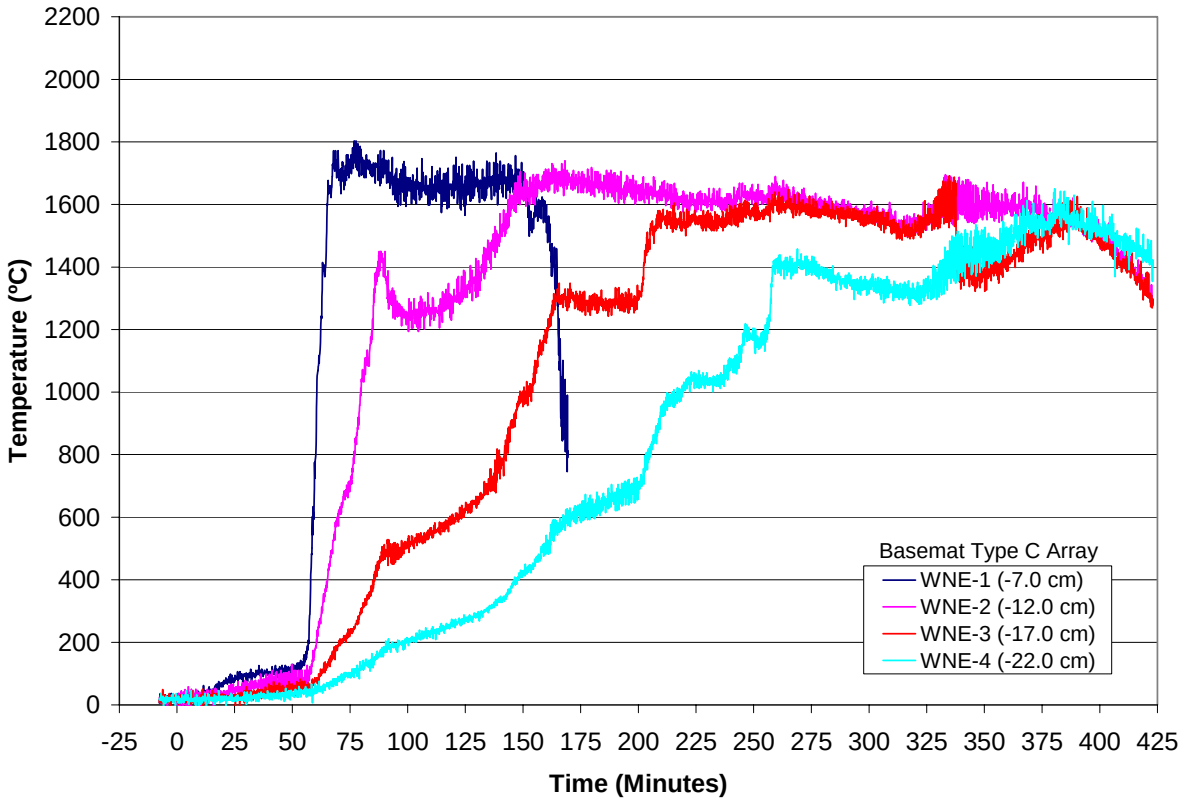

Figure B-4. Basemat Type C "WNE" Array Data.

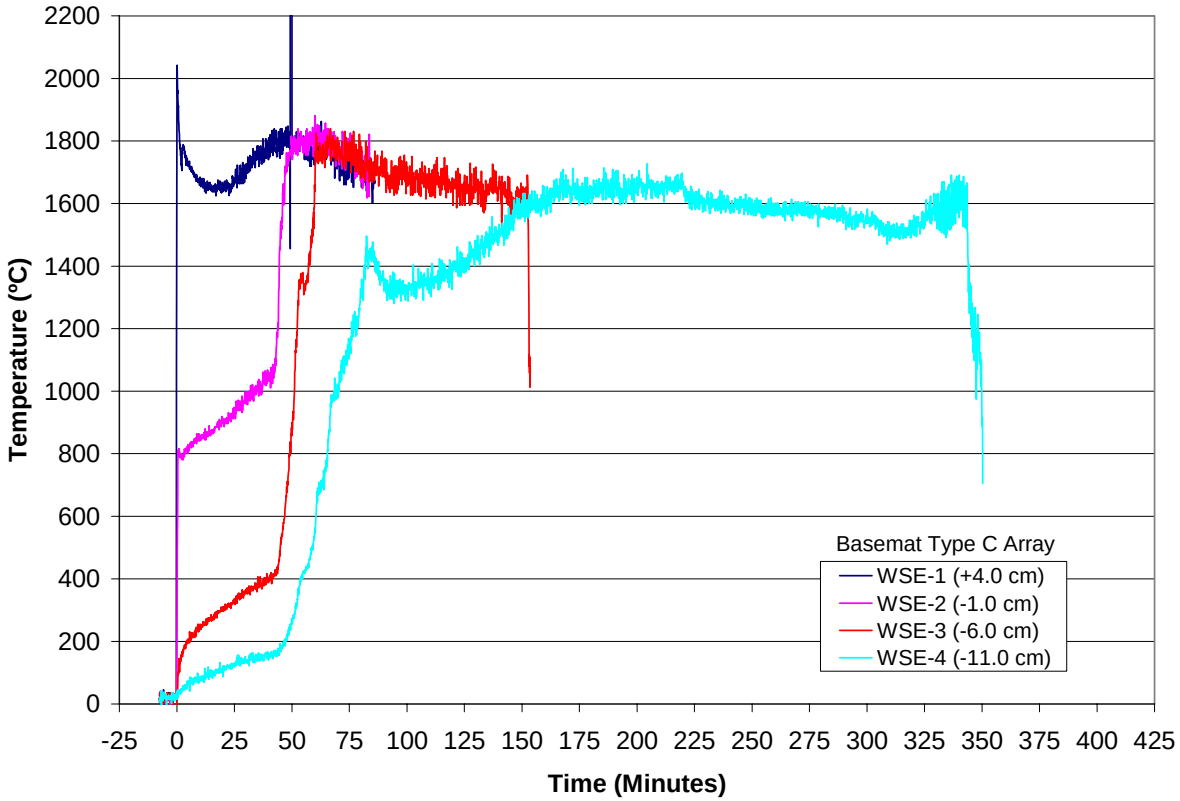

Figure B-5. Basemat Type C "WSE" Array Data.

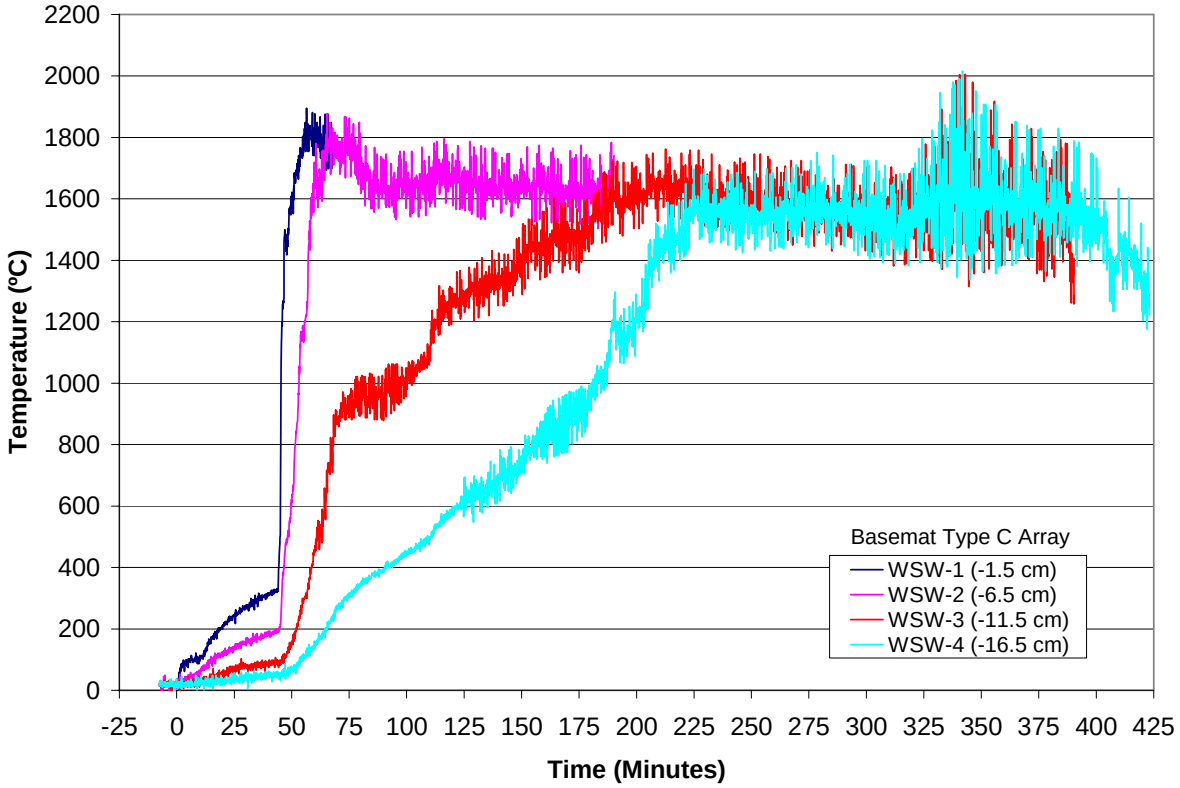

Figure B-6. Basemat Type C "WSW" Array Data.

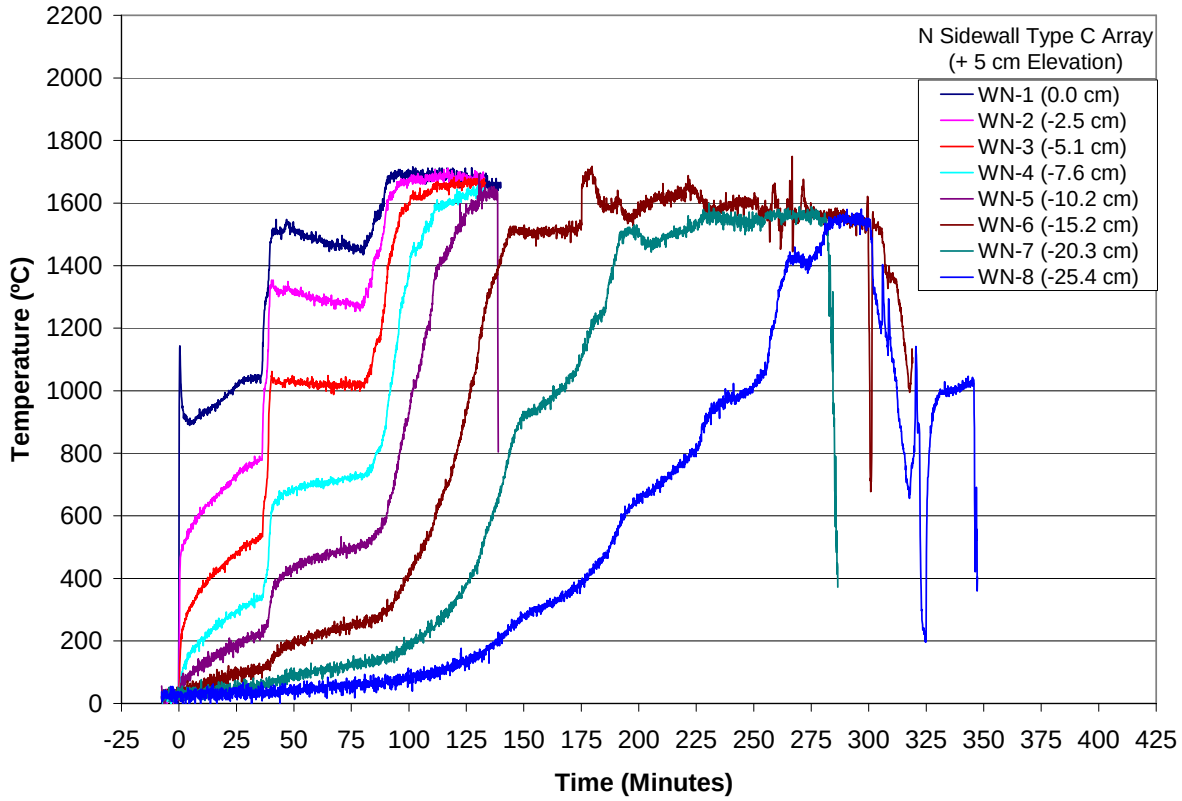

Figure B-7. North Sidewall Type C "NW" Array Data.

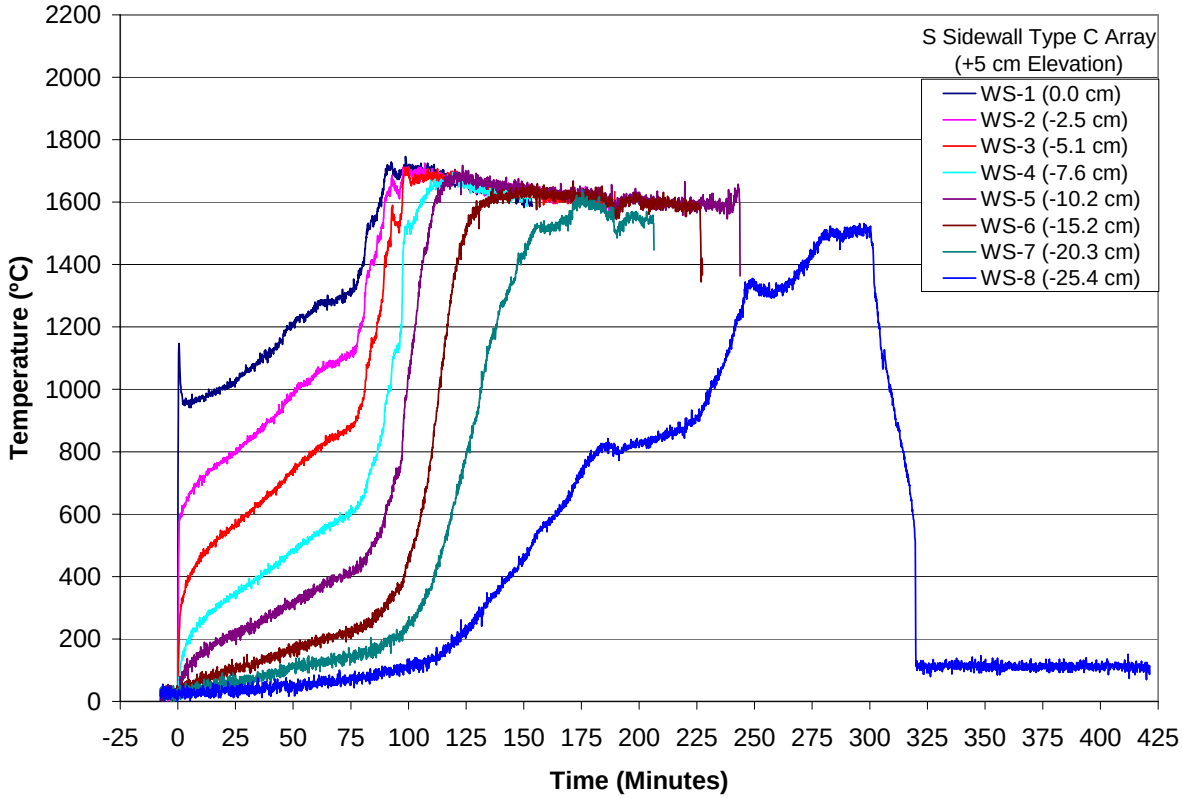

Figure B-8. South Sidewall Type C "WS" Array Data.

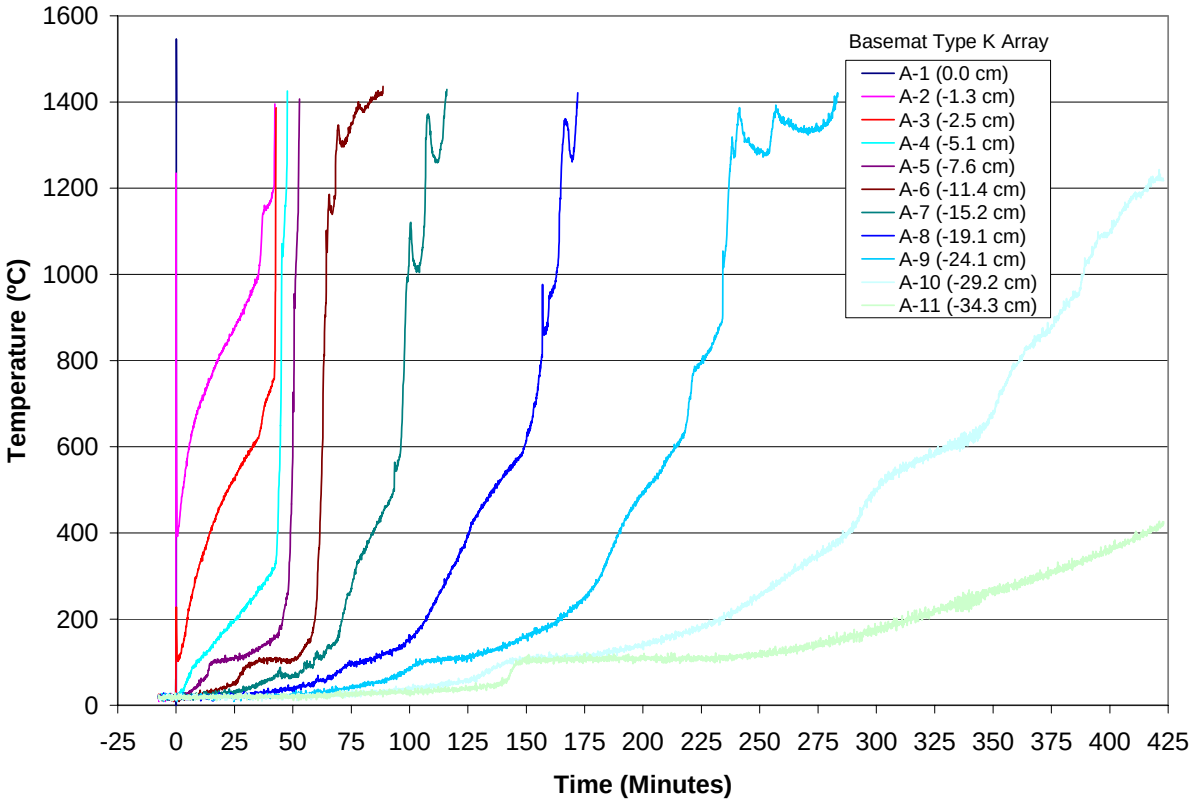

Figure B-9. Basemat Type K "A" Array Data.

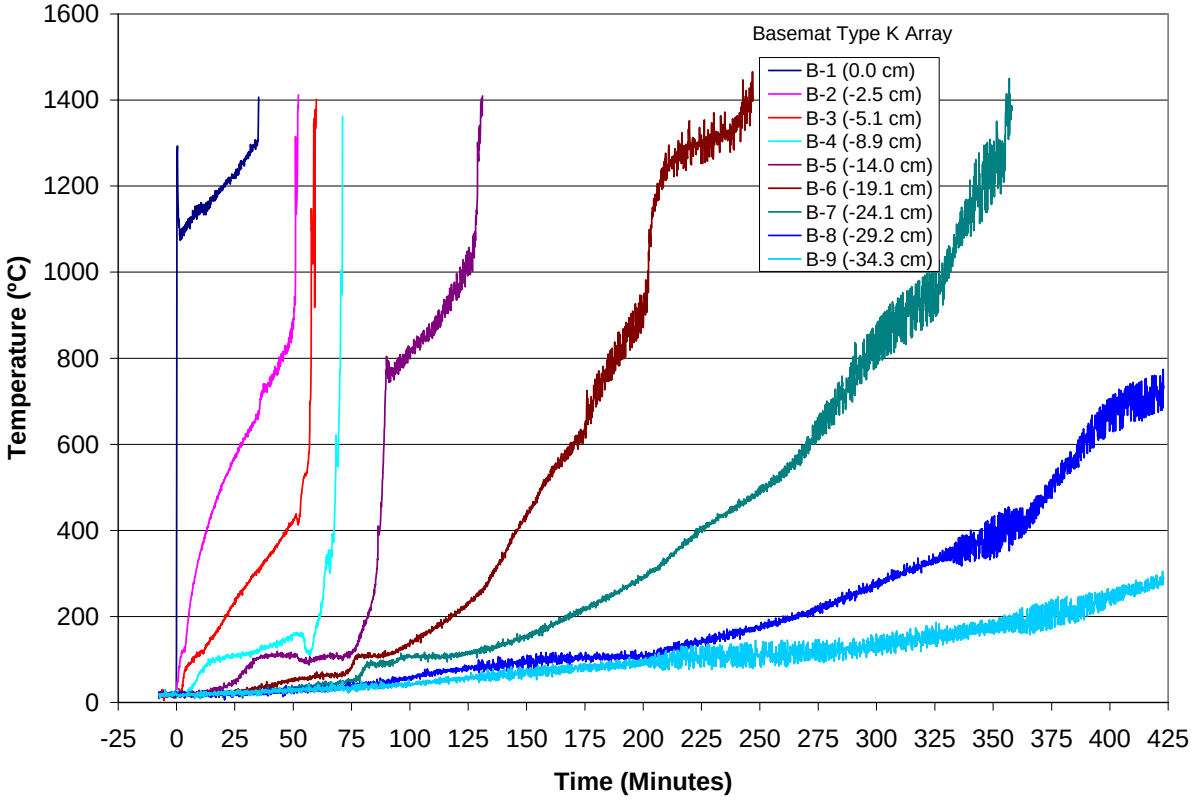

Figure B-10. Basemat Type K "B" Array Data.

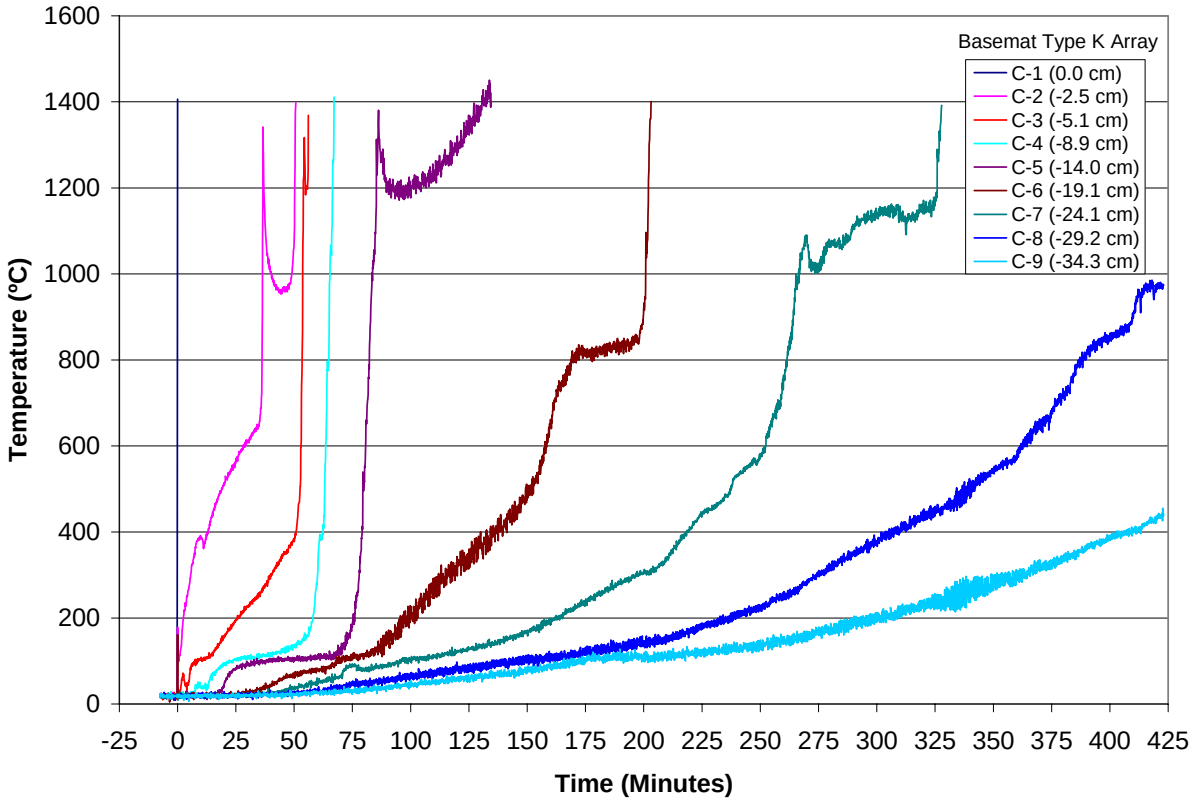

Figure B-11. Basemat Type K "C" Array Data.

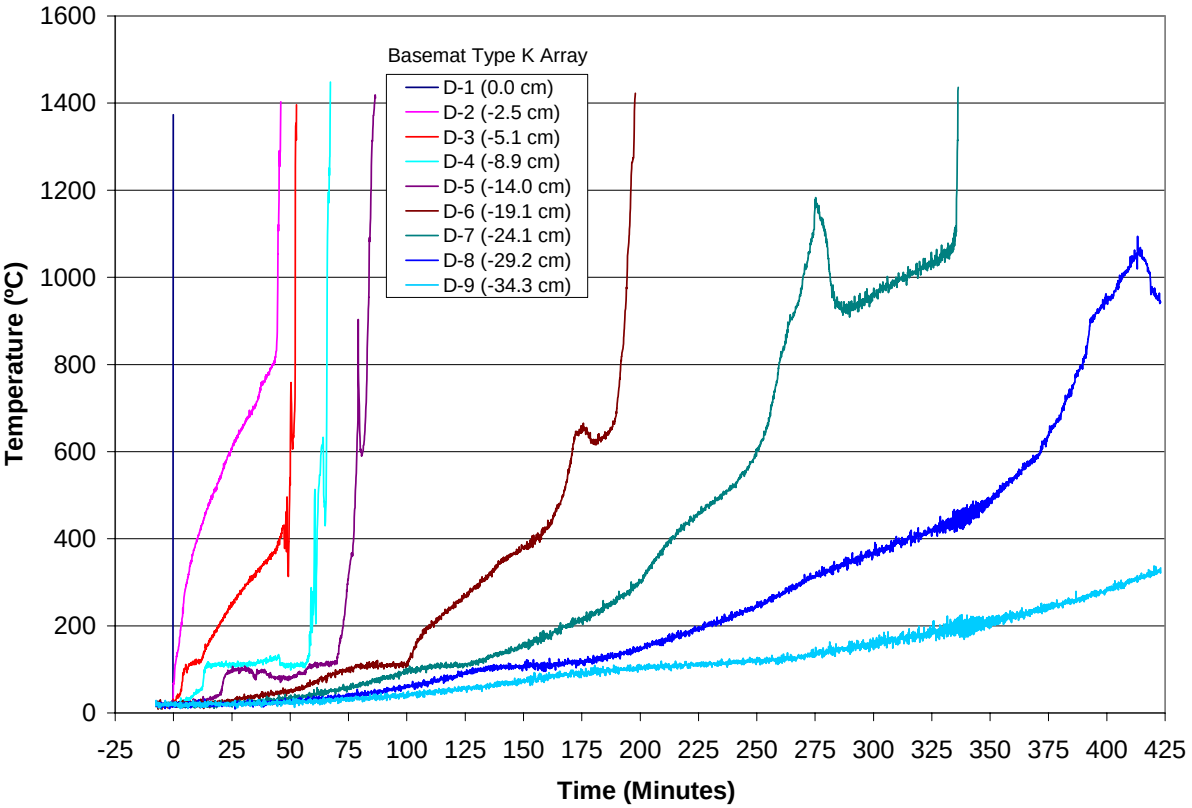

Figure B-12. Basemat Type K "D" Array Data.

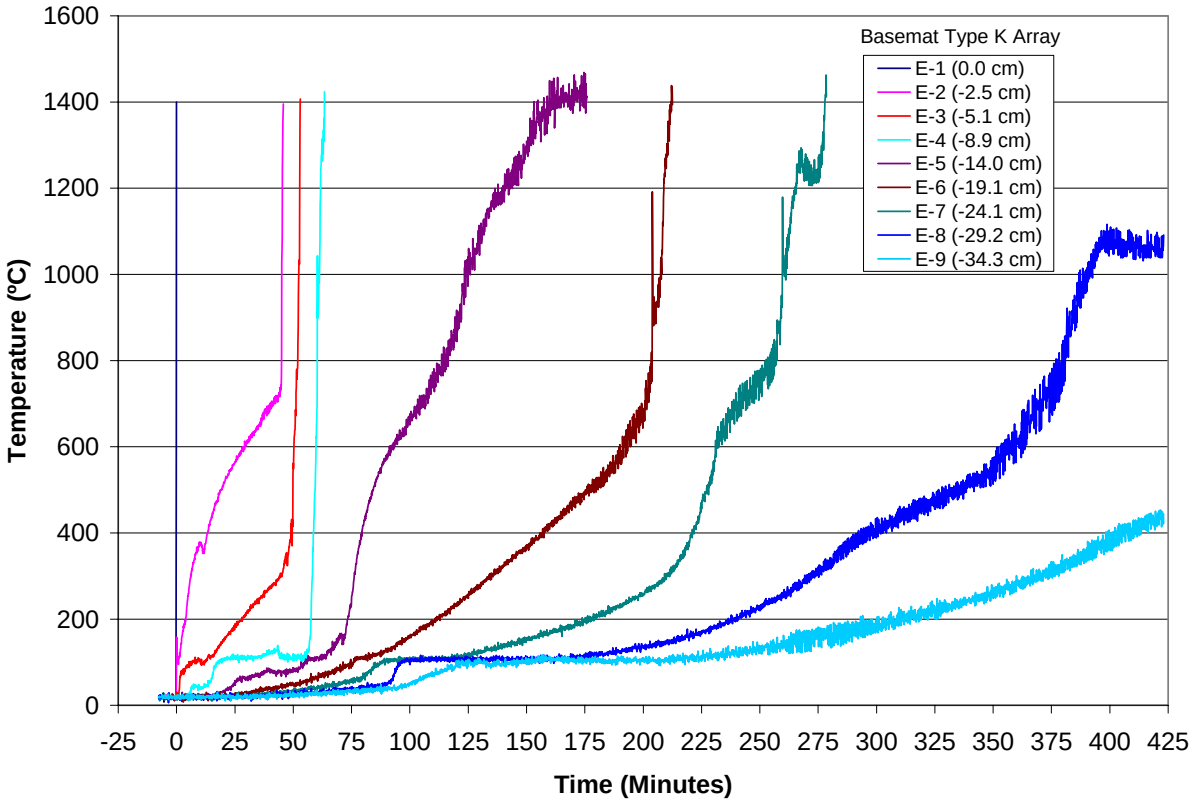

Figure B-13. Basemat Type K "E" Array Data.

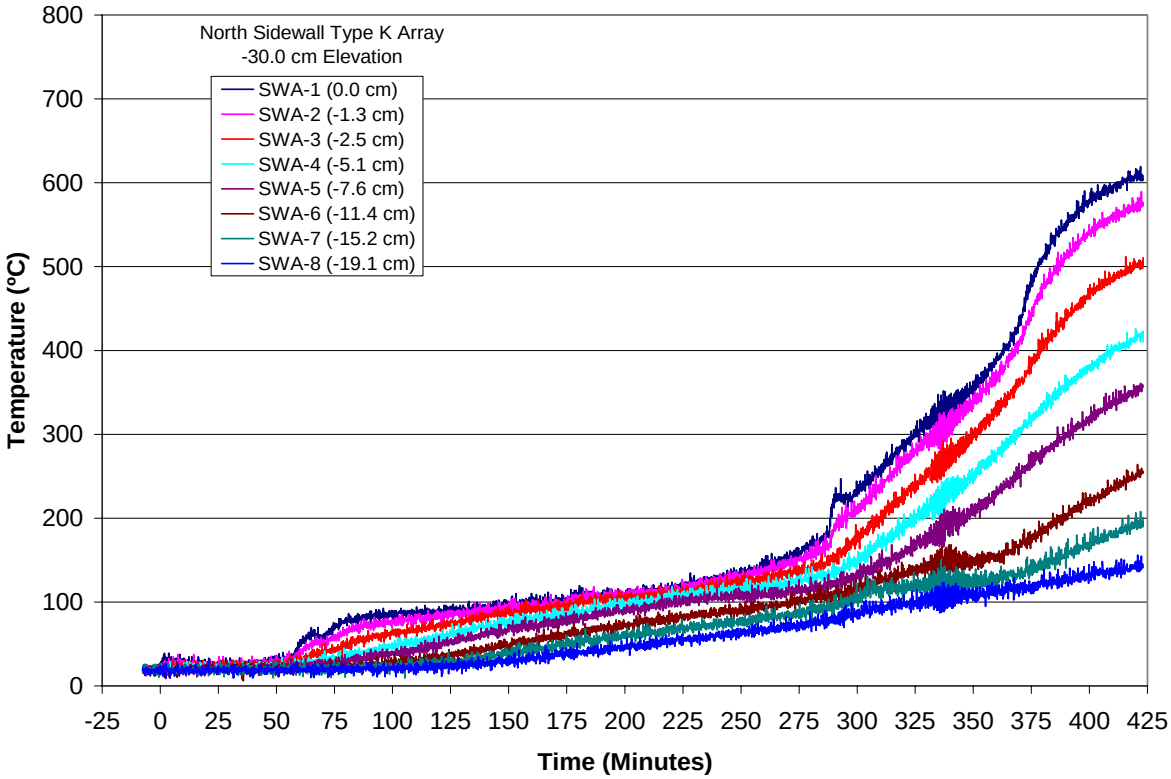

Figure B-14. North Sidewall Type K "SWA" Array Data.

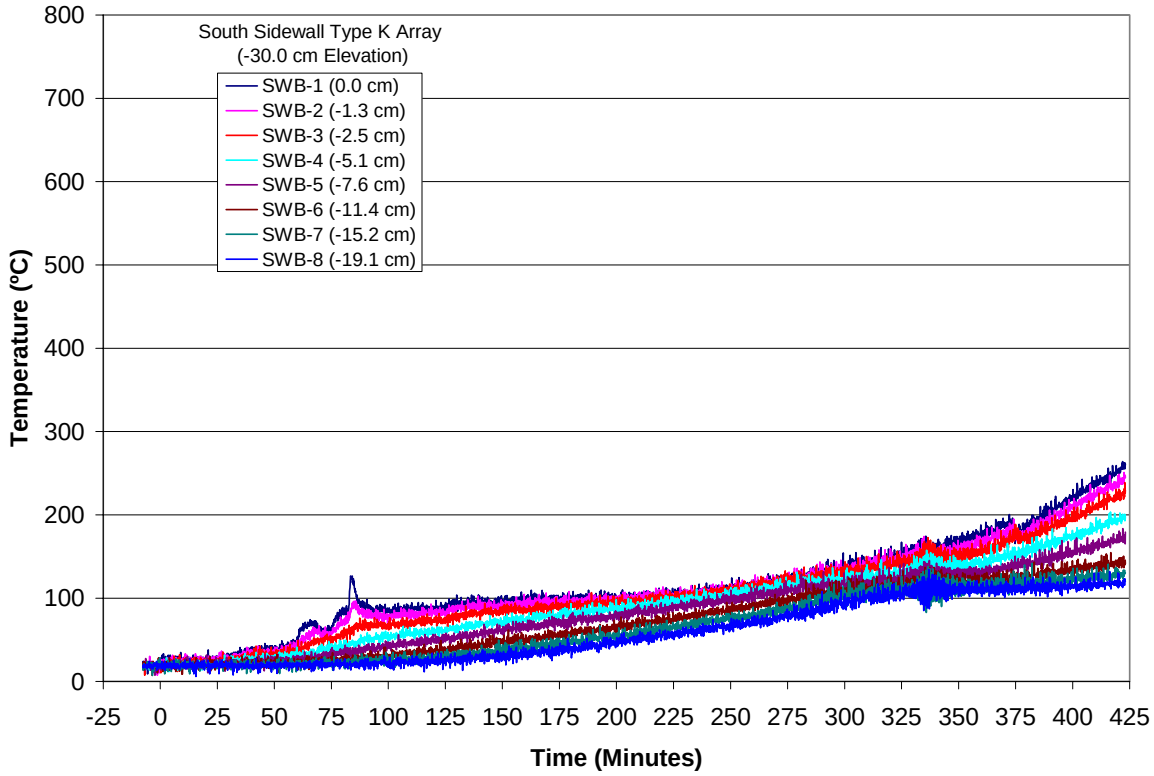

Figure B-15. South Sidewall Type K "SWB" Array Data.

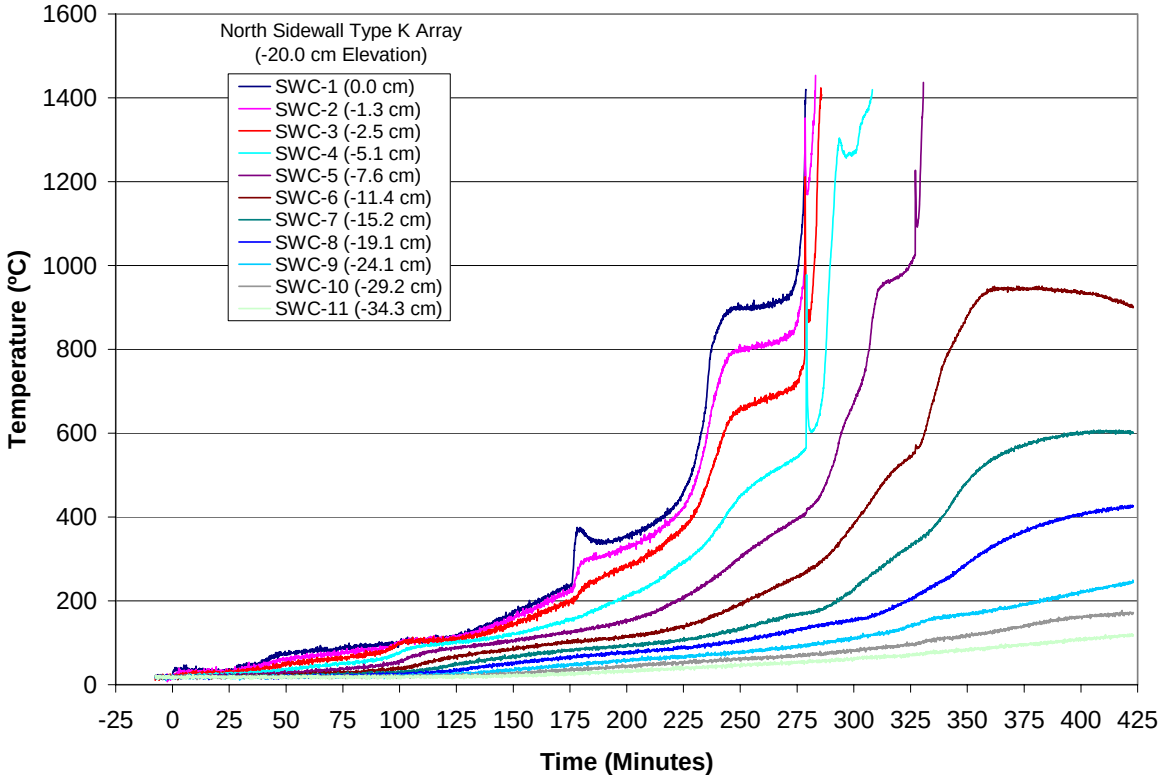

Figure B-16. North Sidewall Type K "SWC" Array Data.

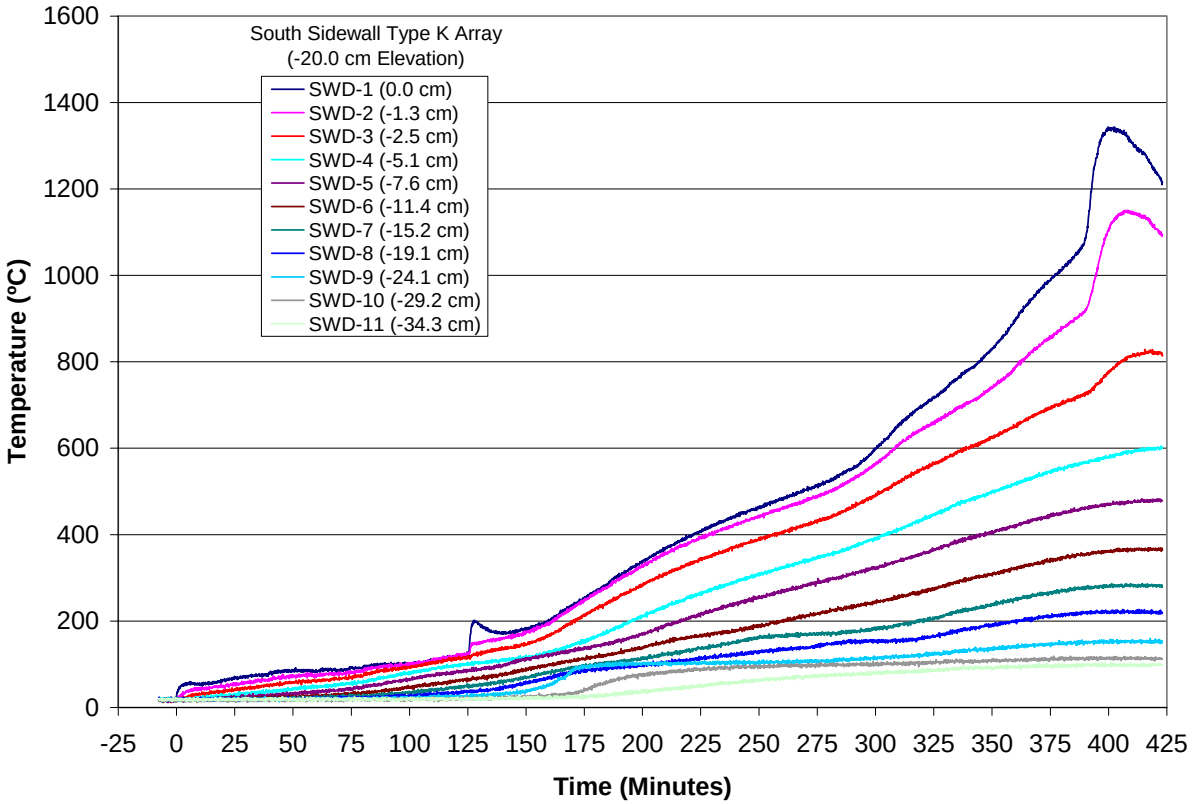

Figure B-17. South Sidewall Type K "SWD" Array Data.

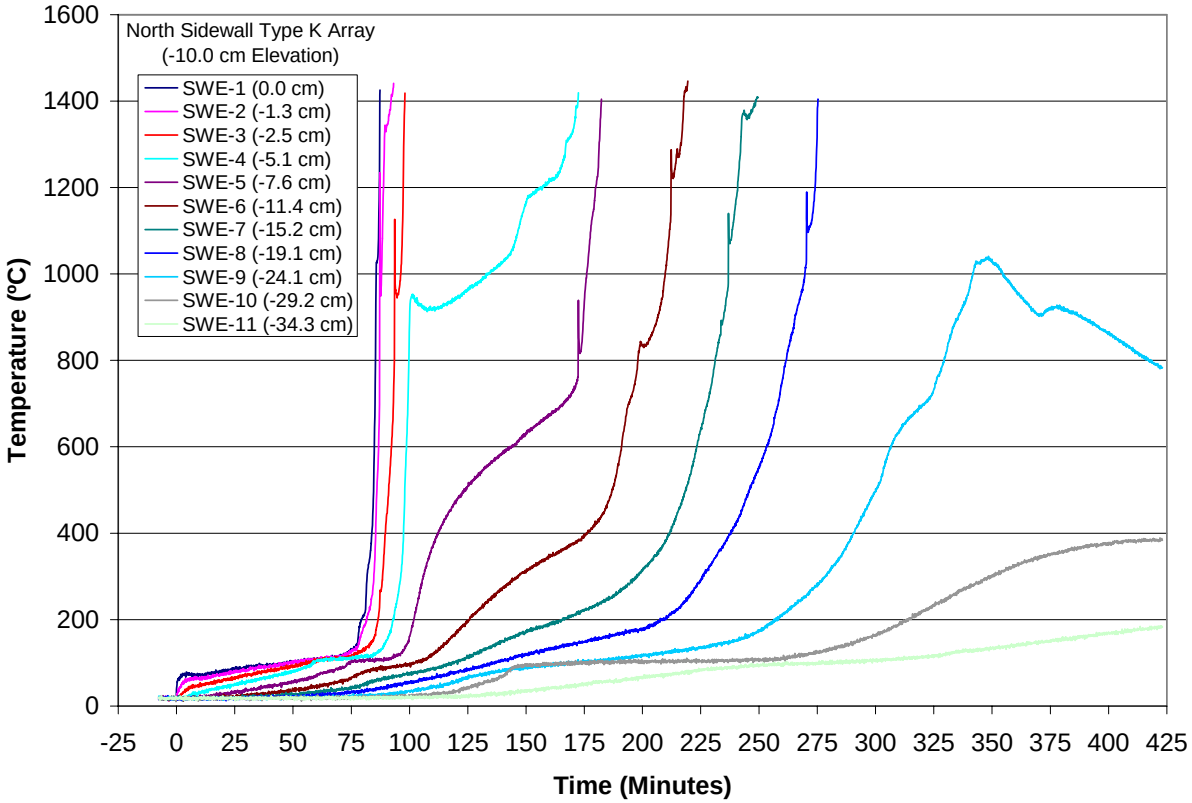

Figure B-18. North Sidewall Type K "SWE" Array Data.

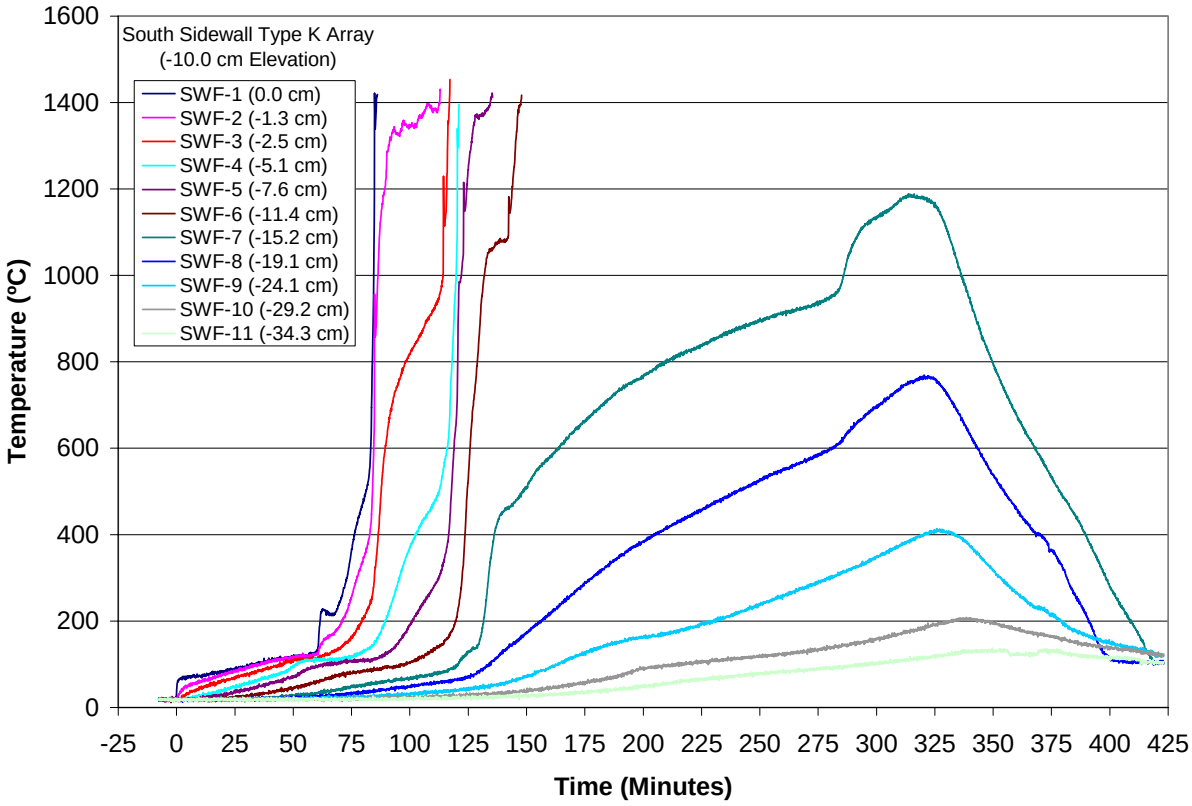

Figure B-19. South Sidewall Type K "SWF" Array Data.

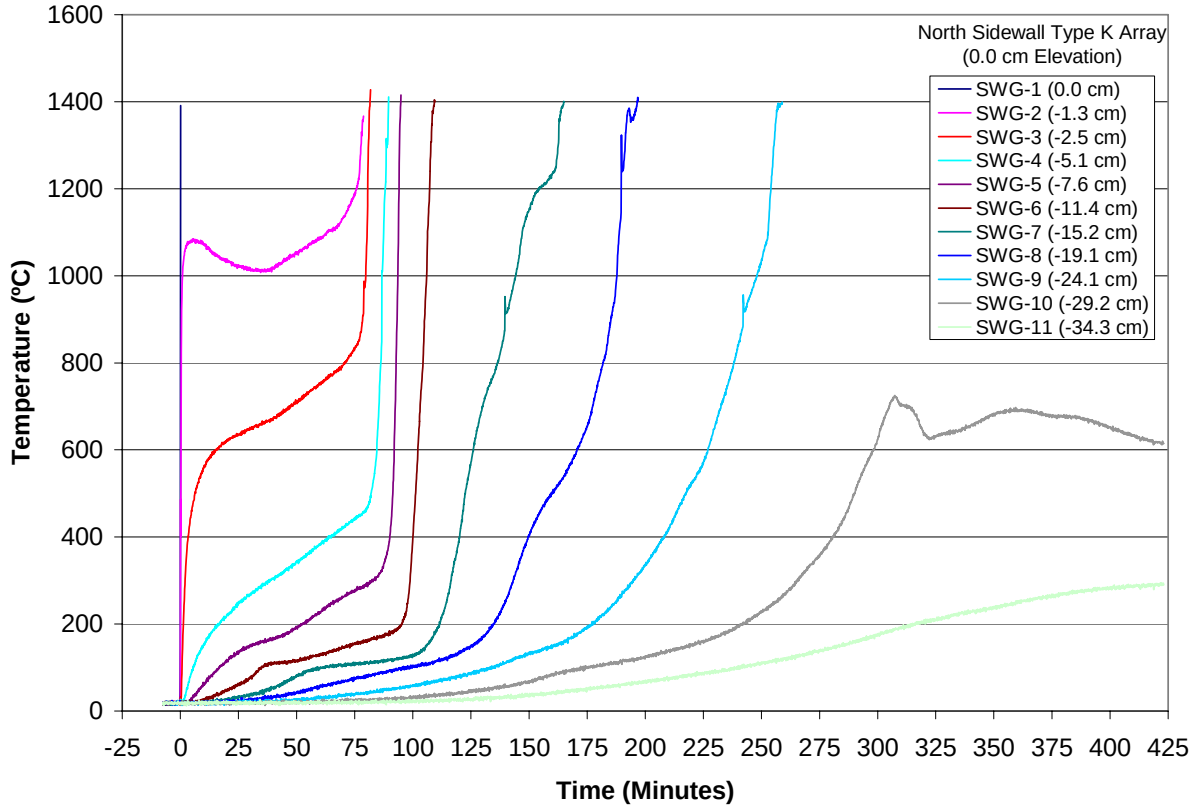

Figure B-20. North Sidewall Type K "SWG" Array Data.

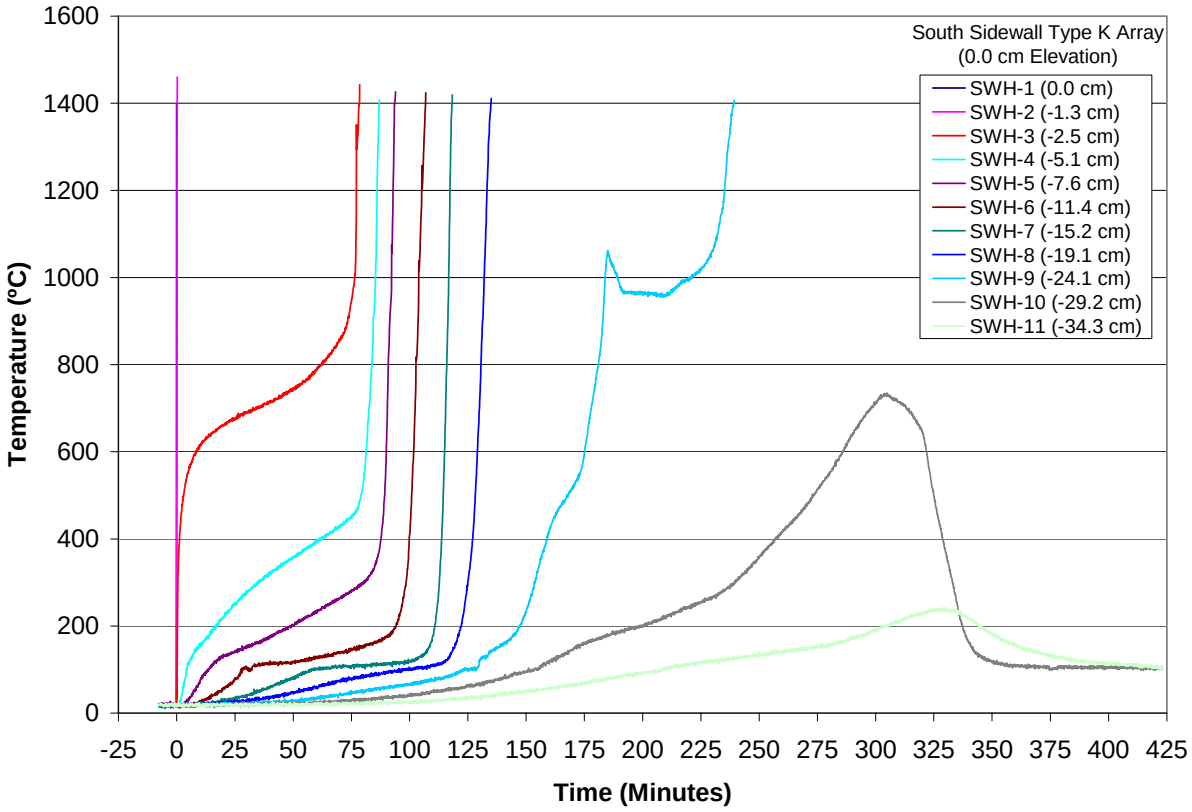

Figure B-21. South Sidewall Type K "SWH" Array Data.

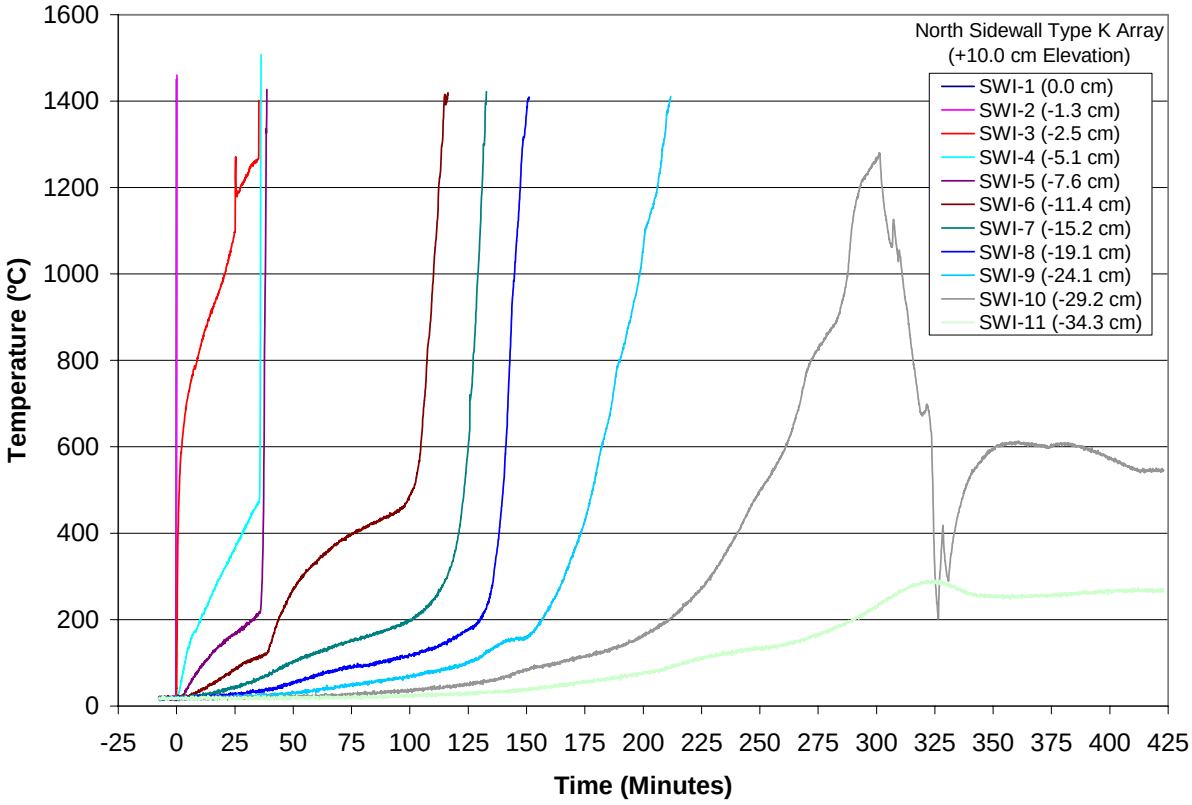

Figure B-22. North Sidewall Type K "SWI" Array Data.

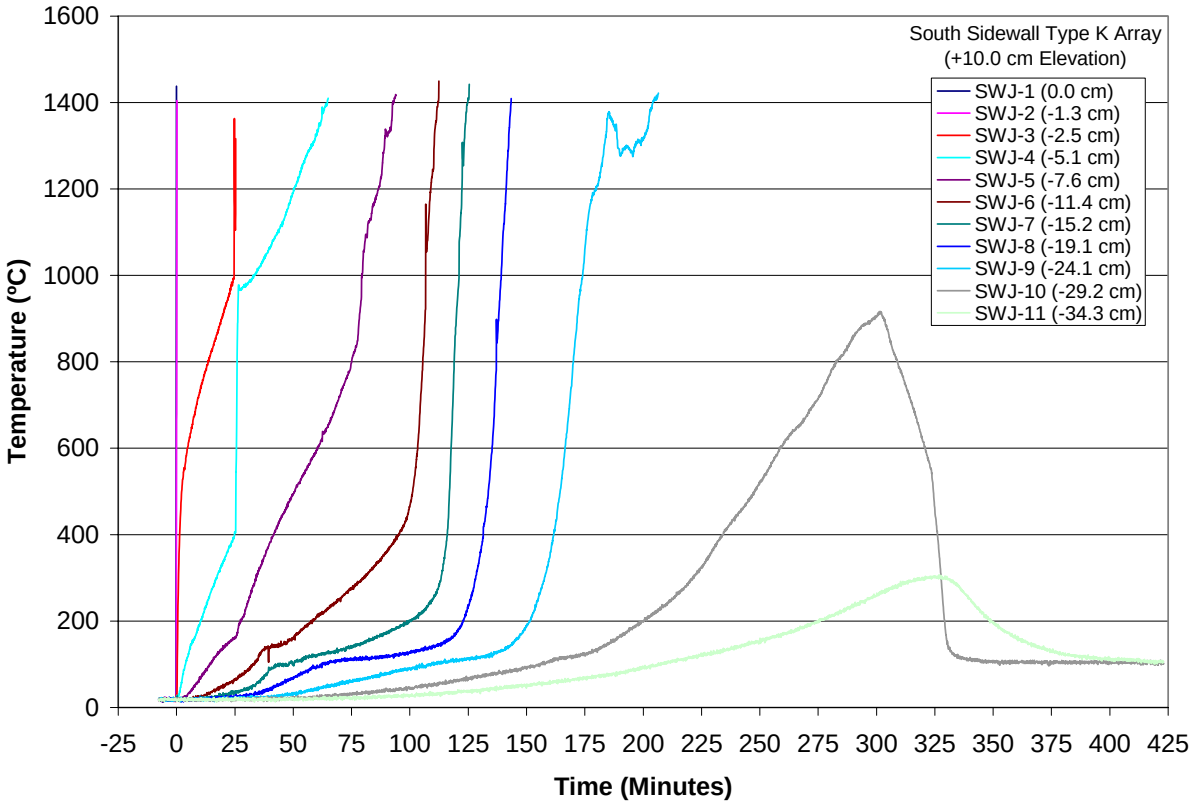

Figure B-23. South Sidewall Type K "SWJ" Array Data.

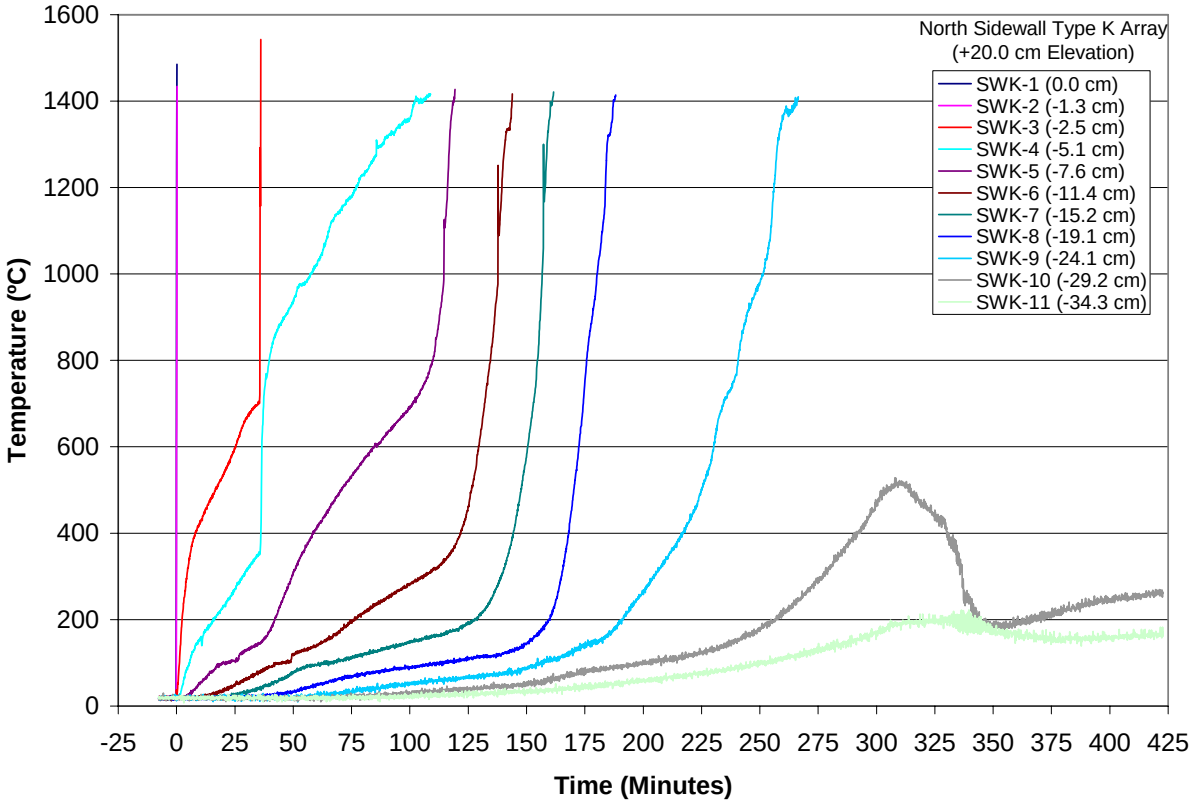

Figure B-24. North Sidewall Type K "SWK" Array Data.

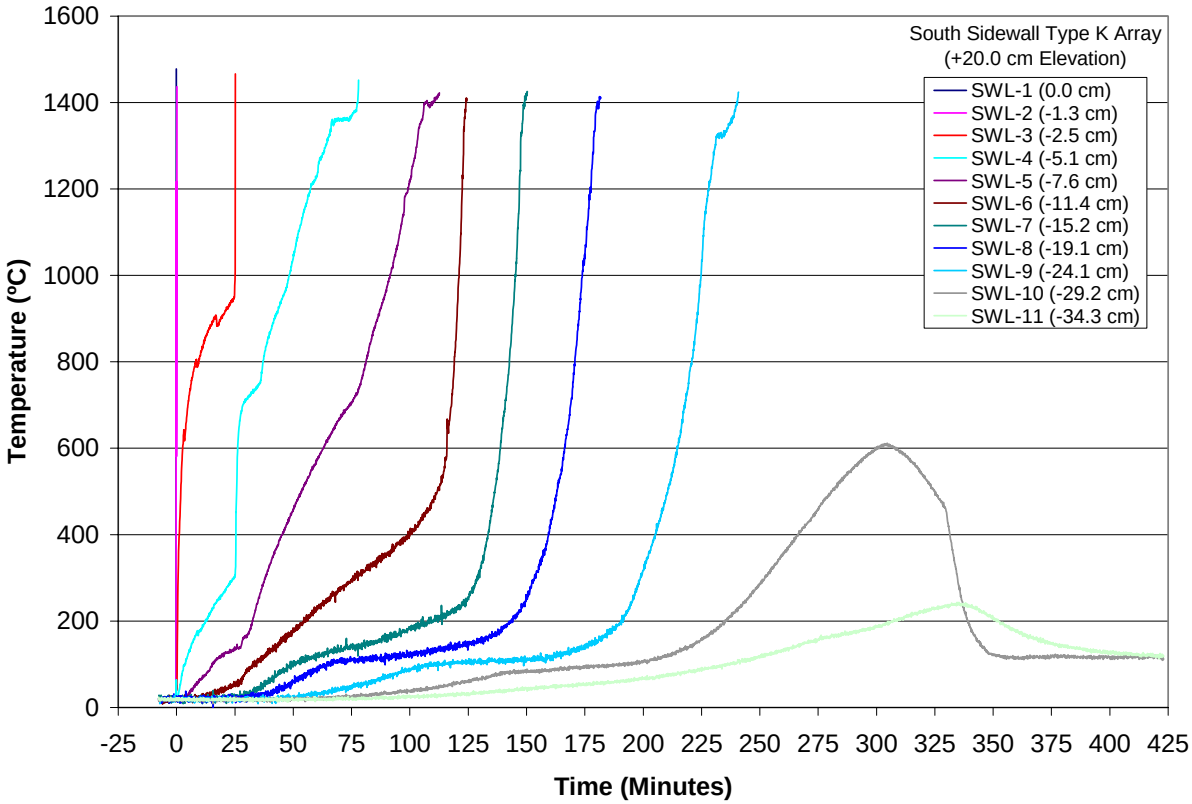

Figure B-25. South Sidewall Type K "SWL" Array Data.

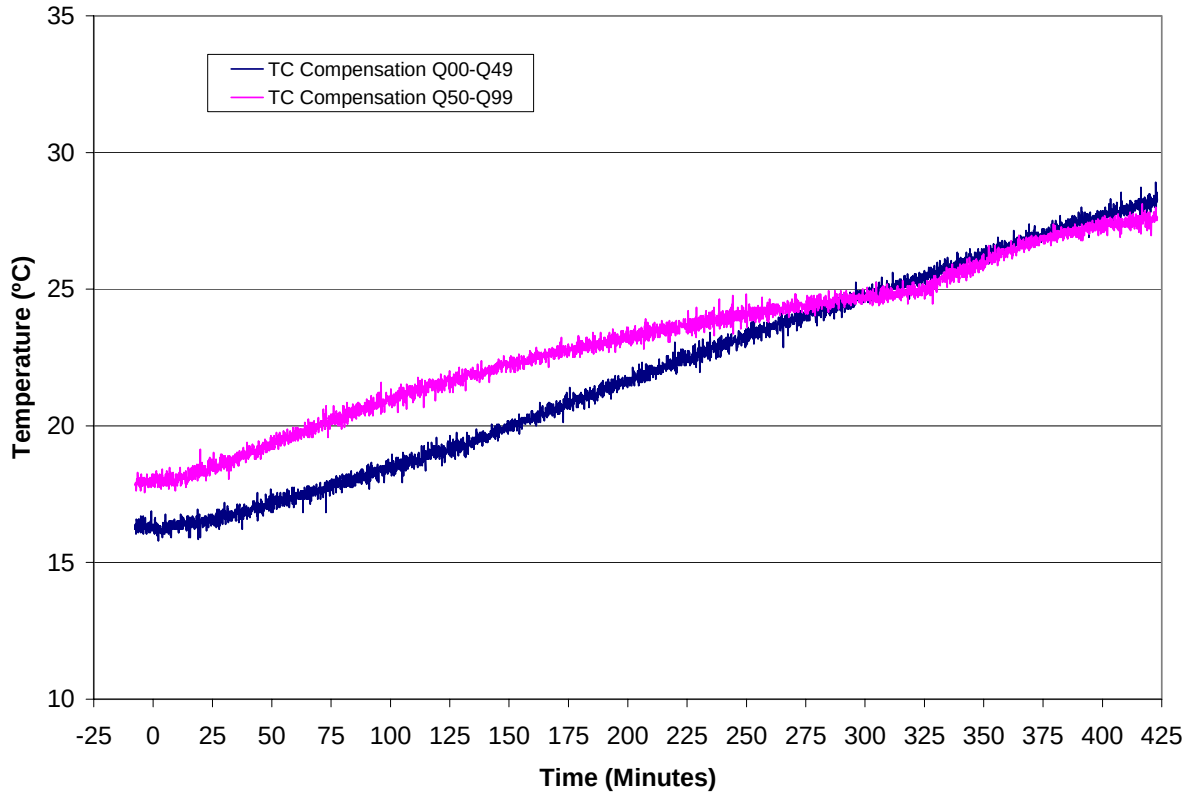

Figure B-26. Thermocouple Compensator Data for Channels Q01-Q49 and Q50-Q99.

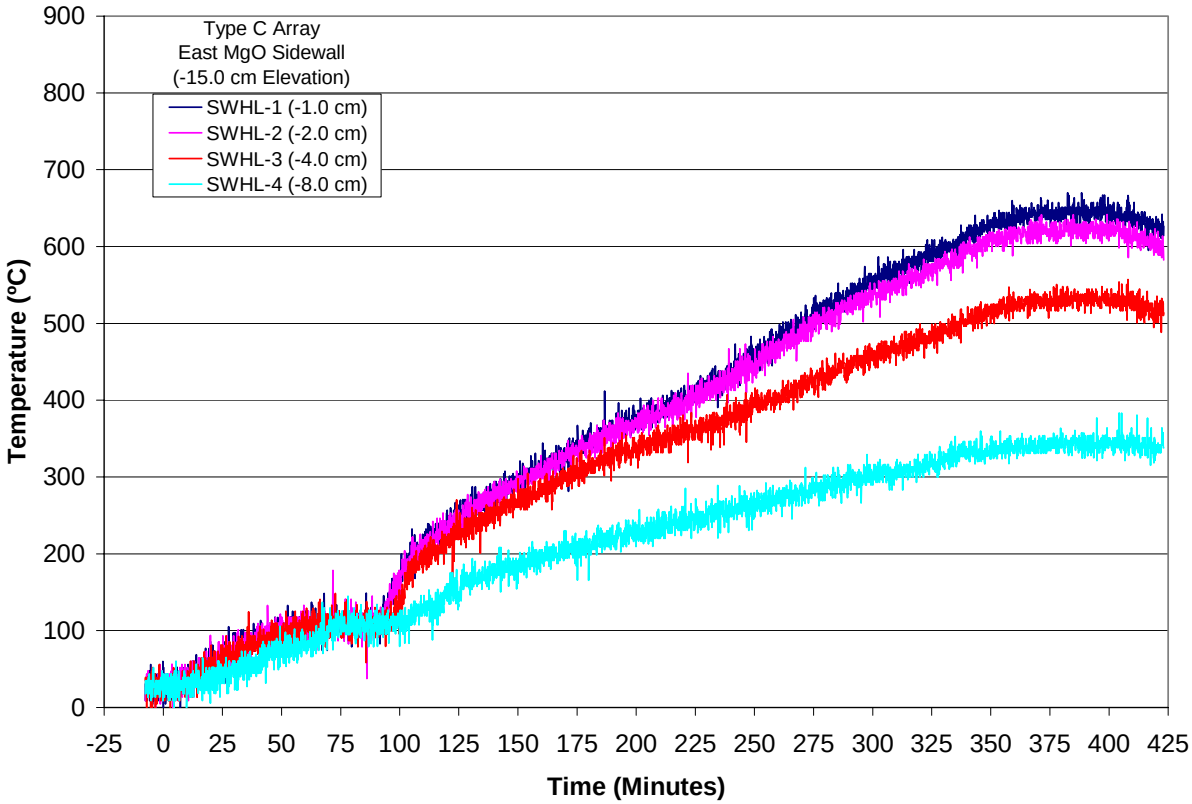

Figure B-27. Test Section Sidewall Heat Loss Data at -15.0 cm Elevation.

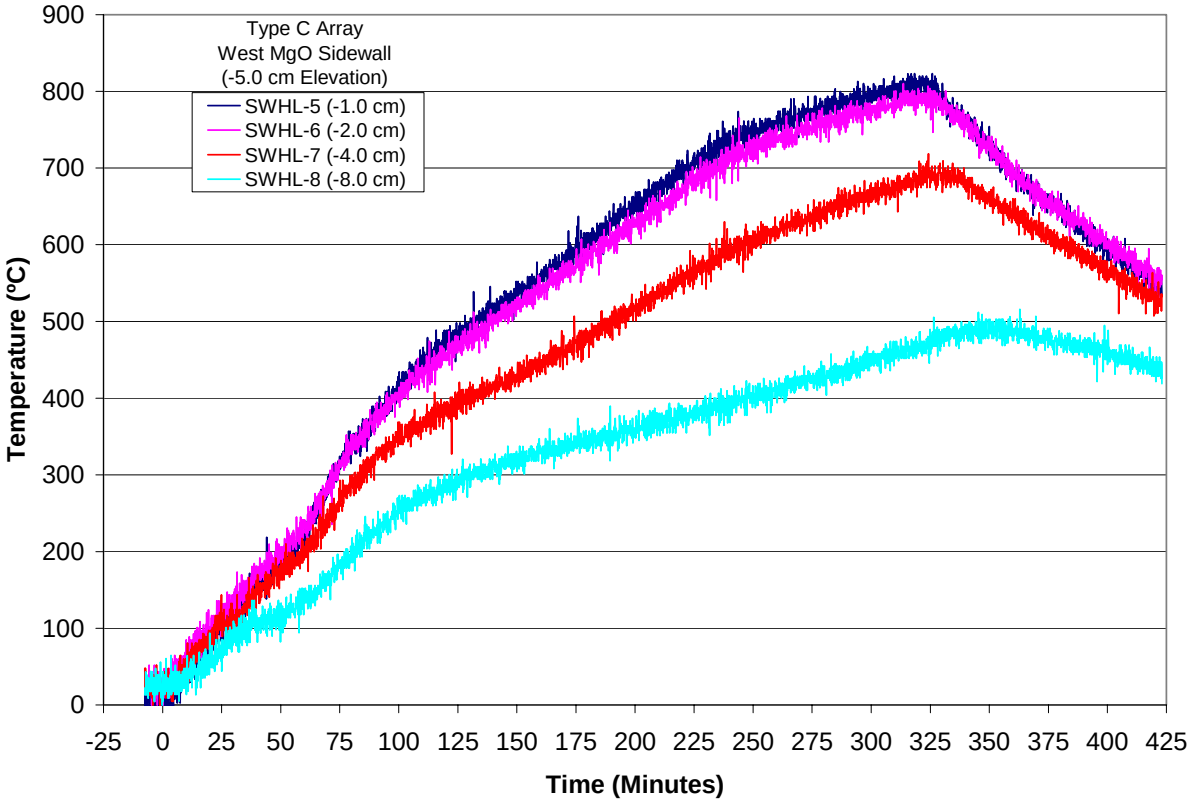

Figure B-28. Test Section Sidewall Heat Loss Data at -5.0 cm Elevation.

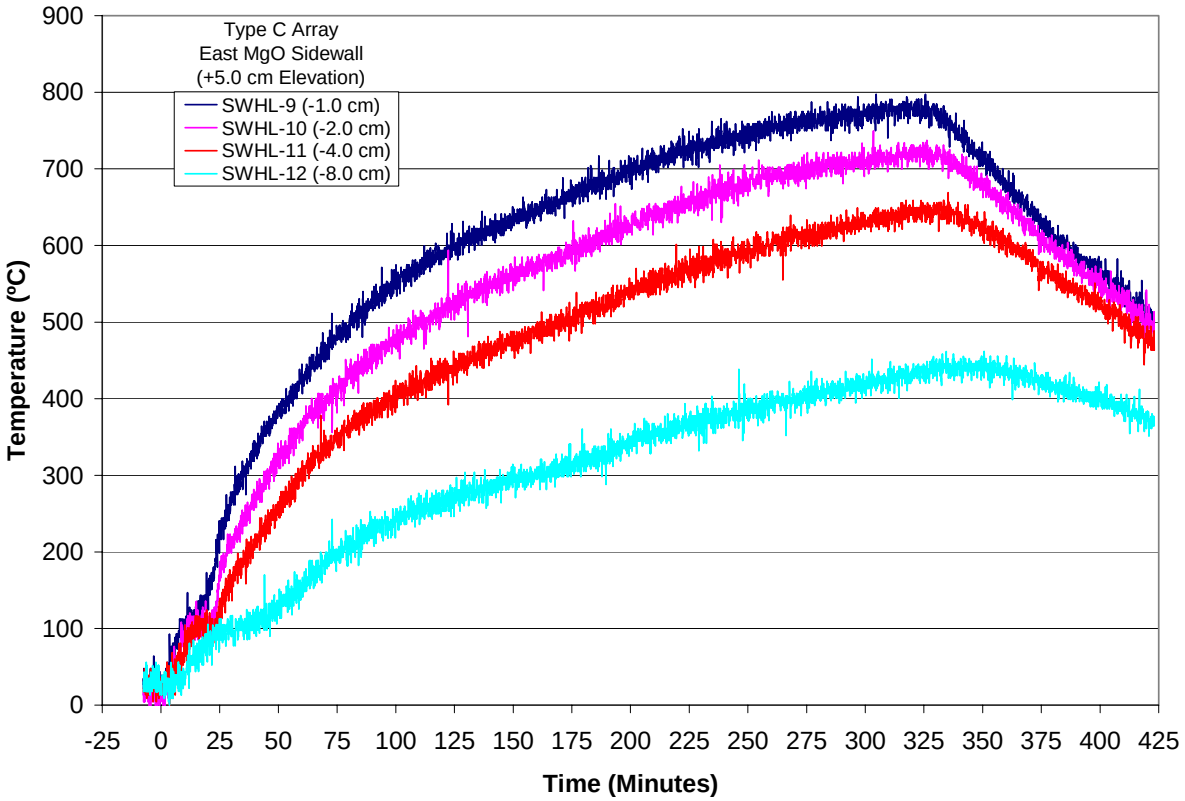

Figure B-29. Test Section Sidewall Heat Loss Data at +5.0 cm Elevation.

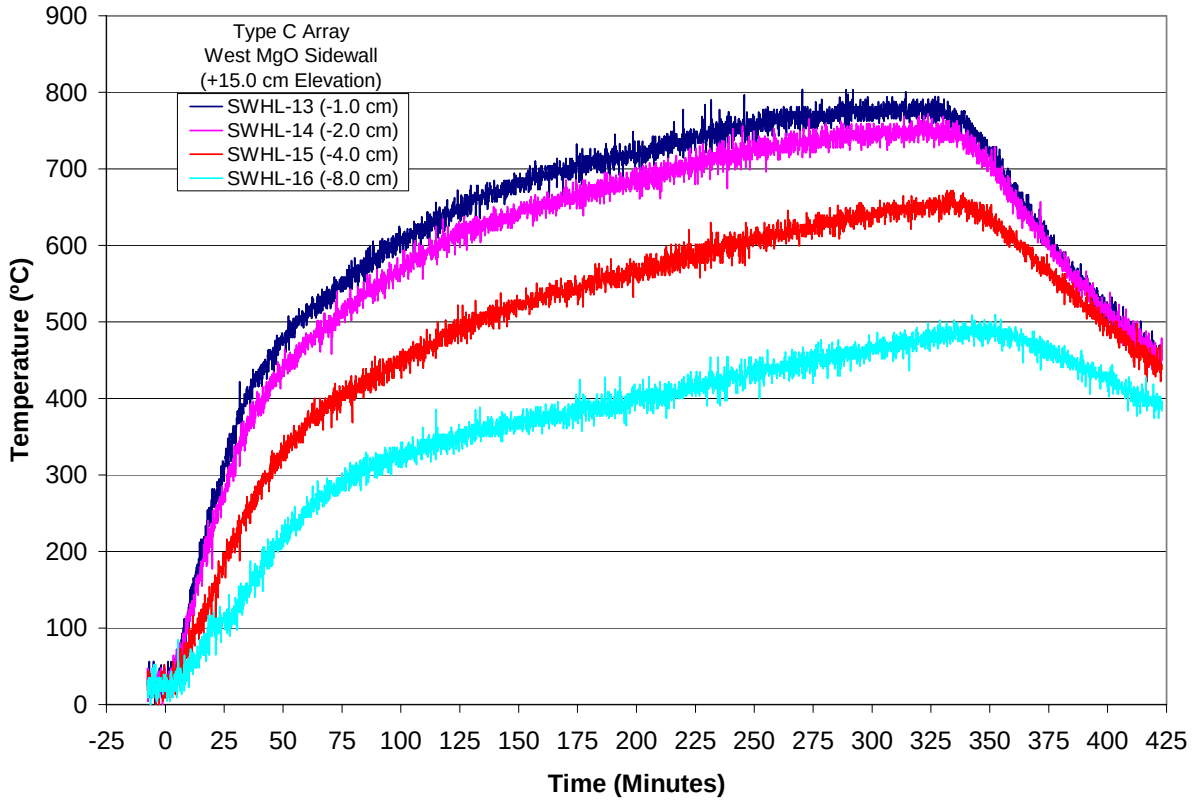

Figure B-30. Test Section Sidewall Heat Loss Data at +15.0 cm Elevation.

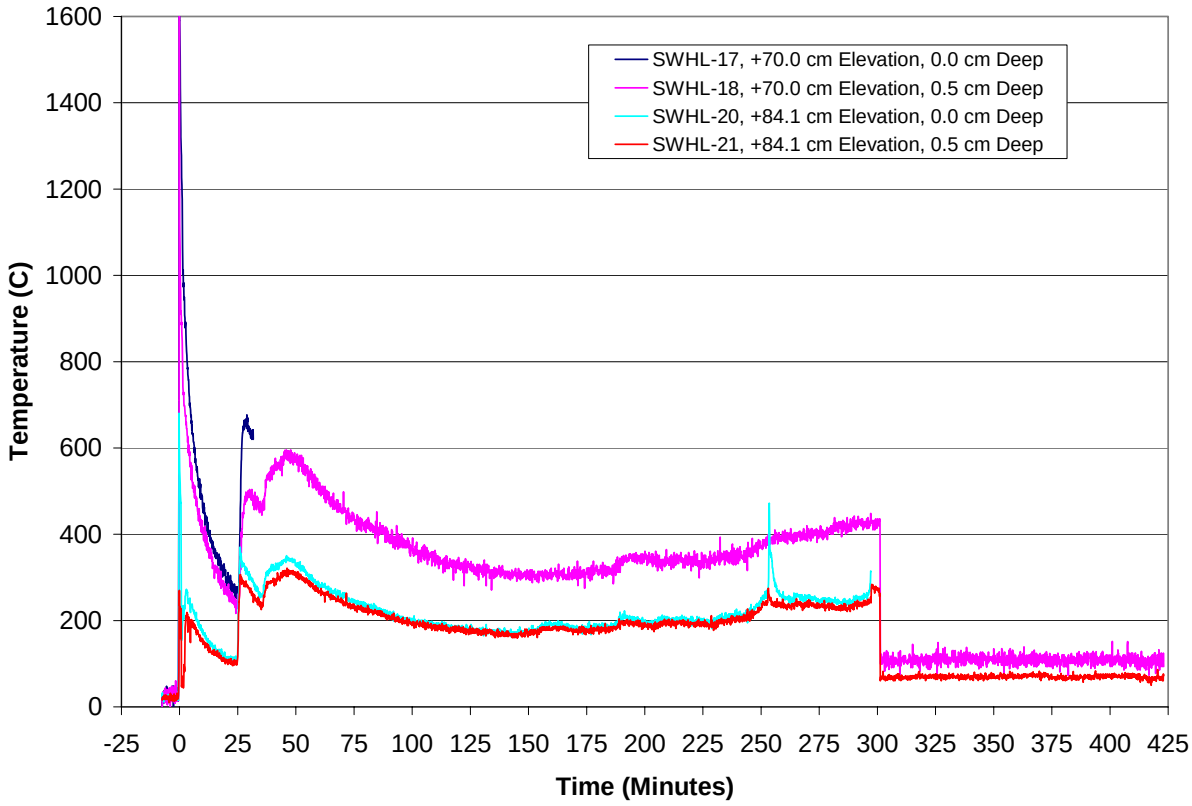

Figure B-31. Test Section Sidewall Heat Loss Data at +70.0 cm and +84.7 cm Elevations.

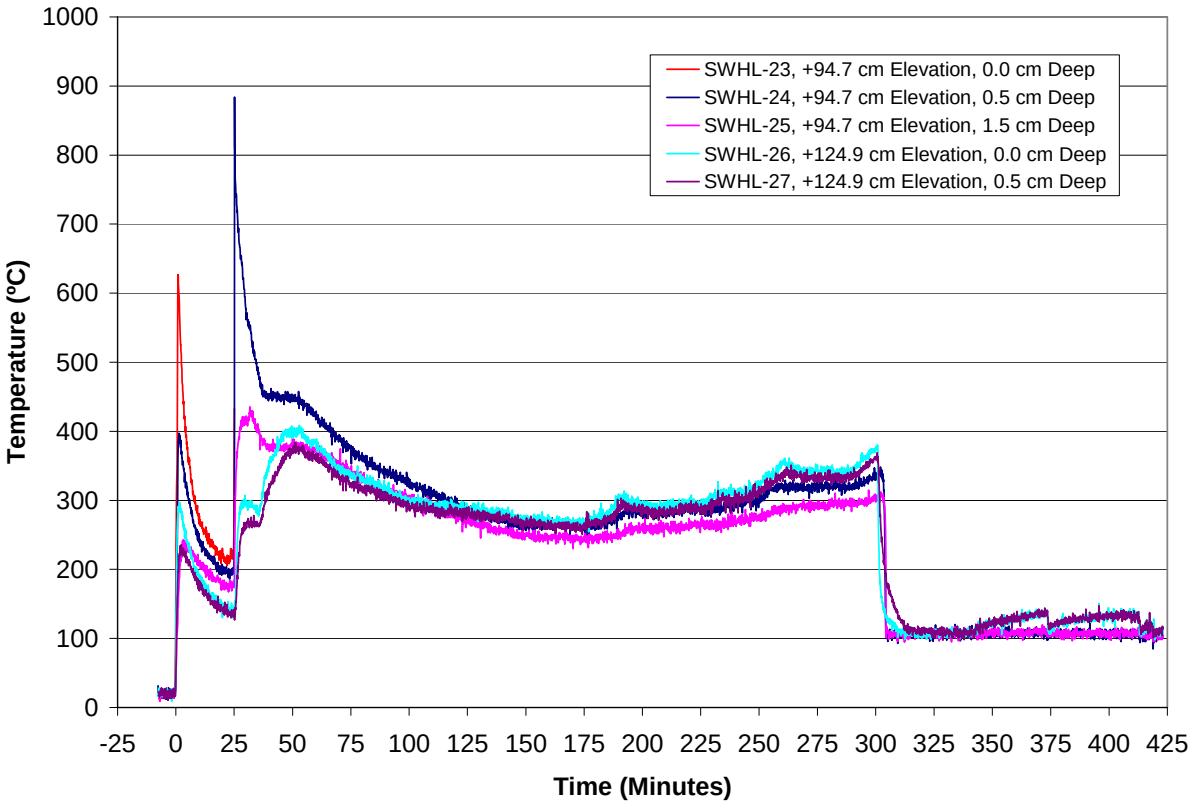

Figure B-32. Test Section Sidewall Heat Loss Data at +94.7 cm and +124.9 cm Elevations.

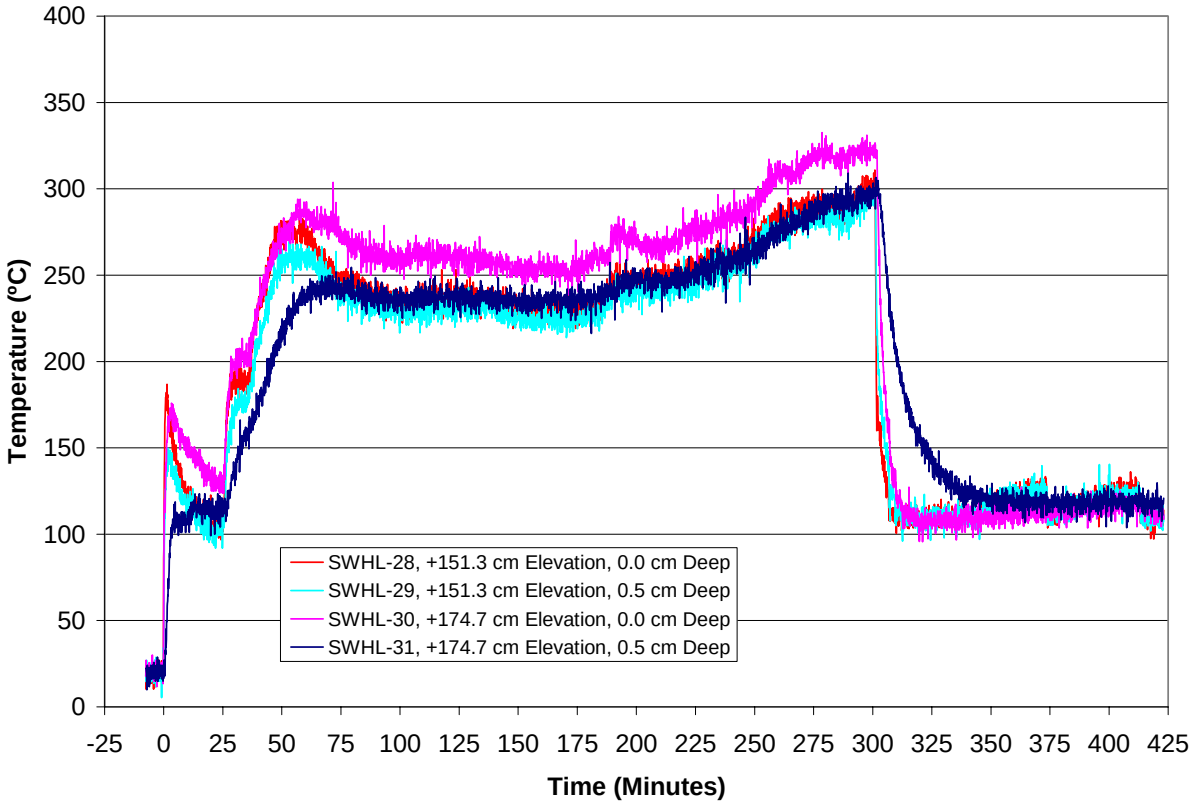

Figure B-33. Test Section Sidewall Heat Loss Data at +151.3 cm and +174.7 cm Elevations.

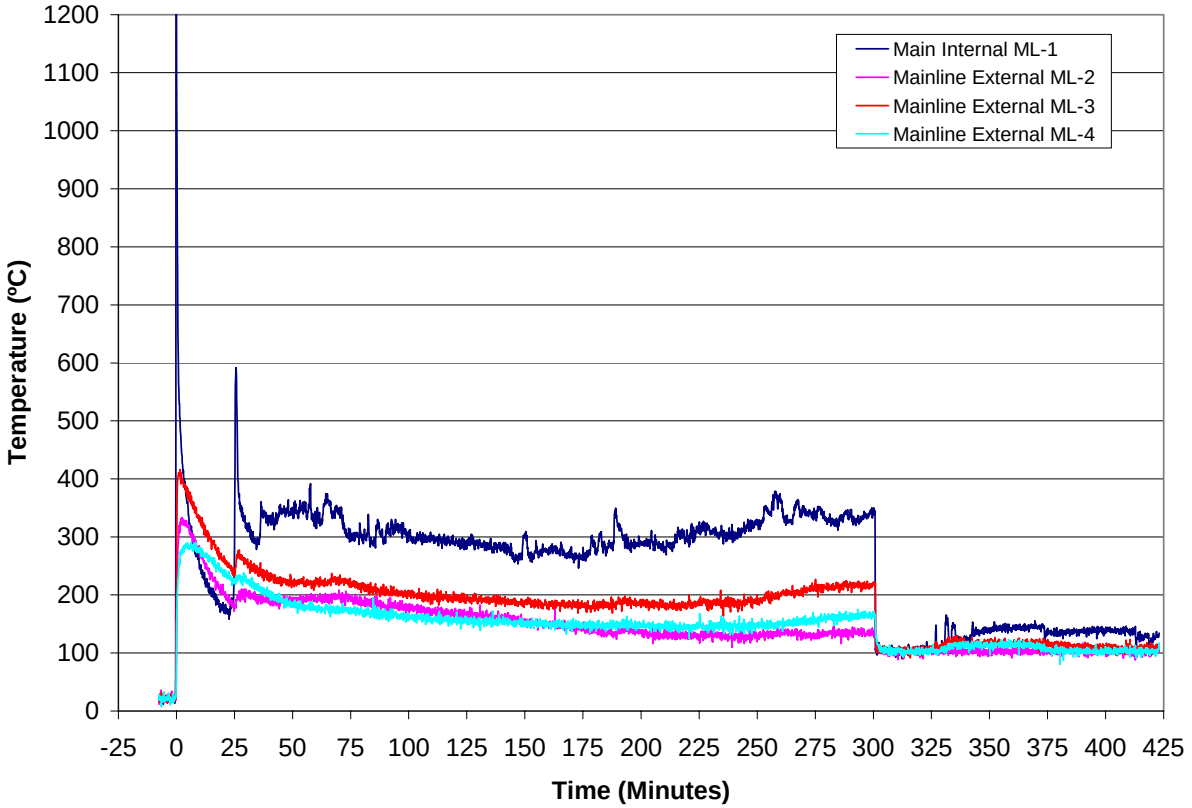

Figure B-34. Test Section Mainline Thermocouple Data.

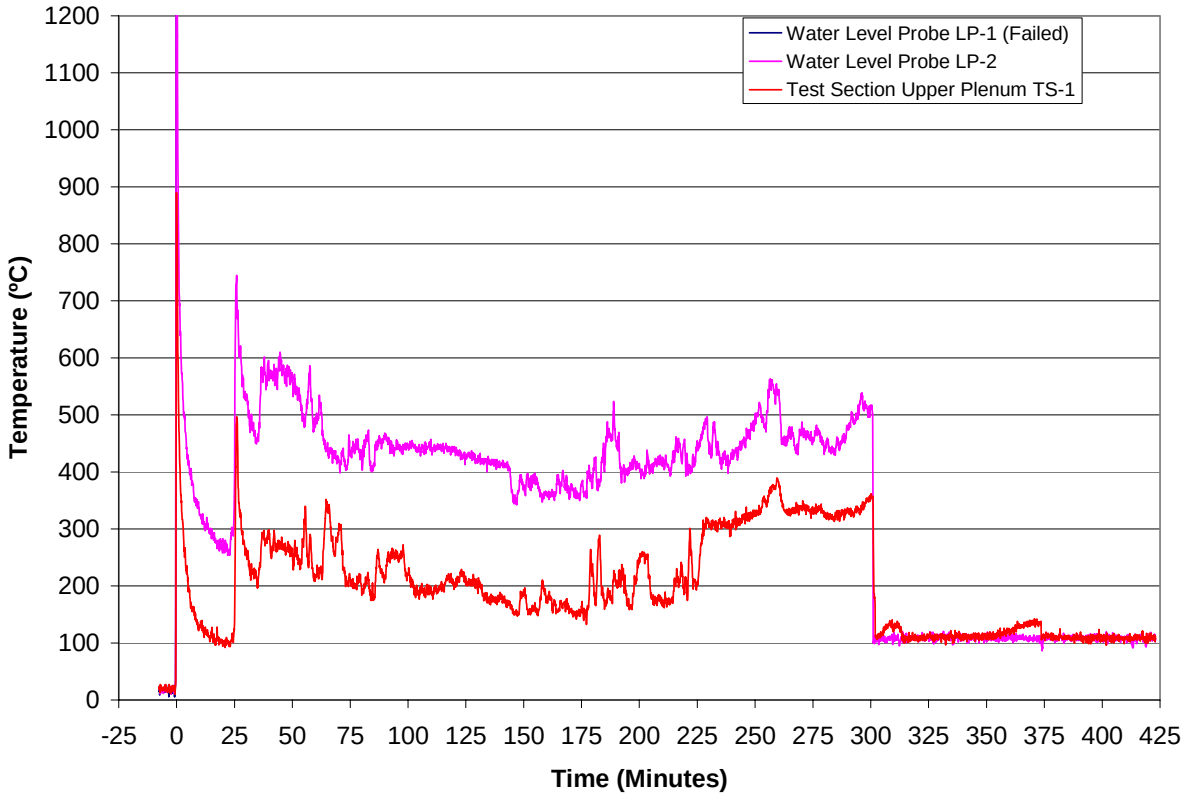

Figure B-35. Test Section Plenum and Insertable Water Level Probe Thermocouple Data.

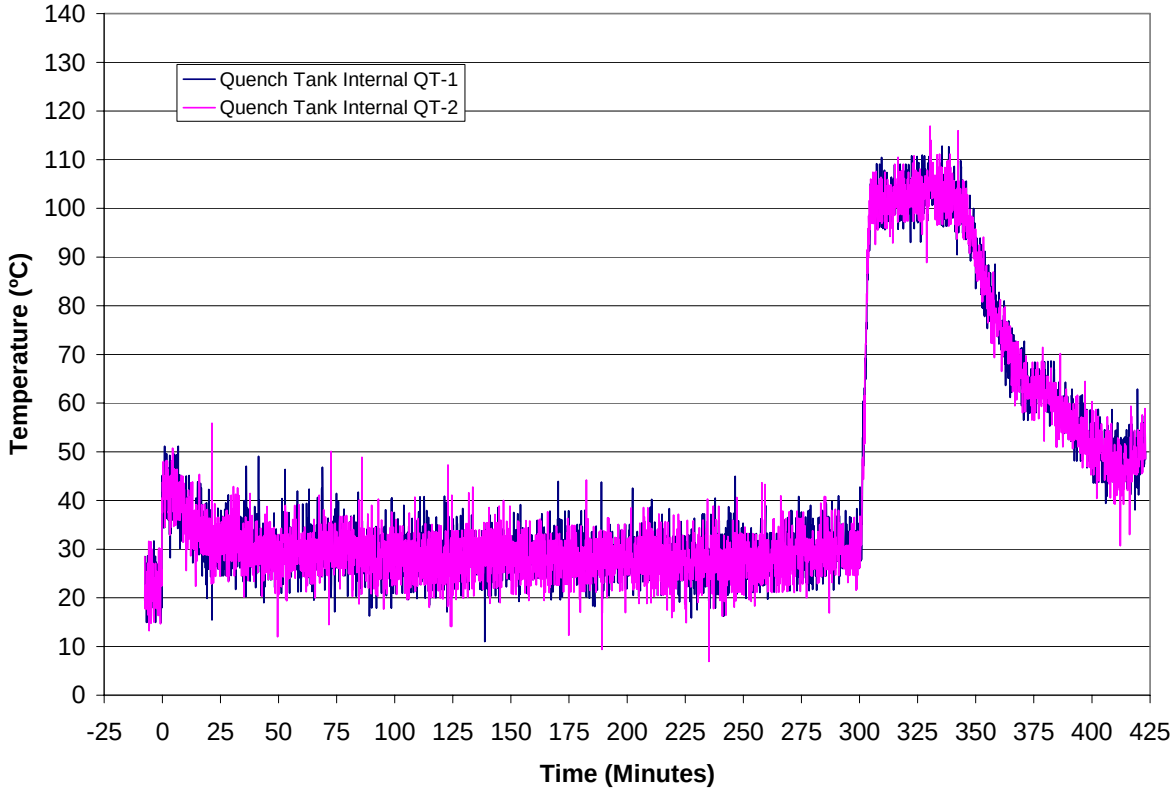

Figure B-36. Quench Tank Water Temperature Data.

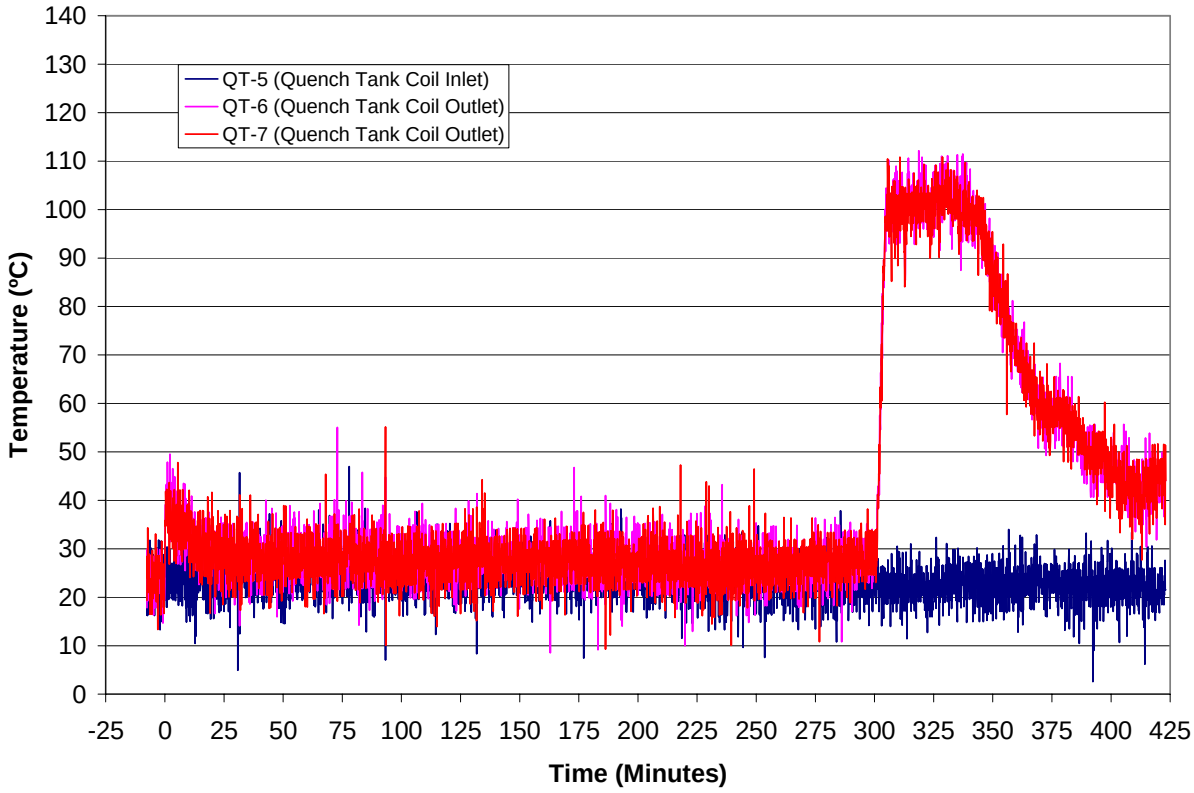

Figure B-37. Quench Tank Coil Inlet and Outlet Temperature Data.

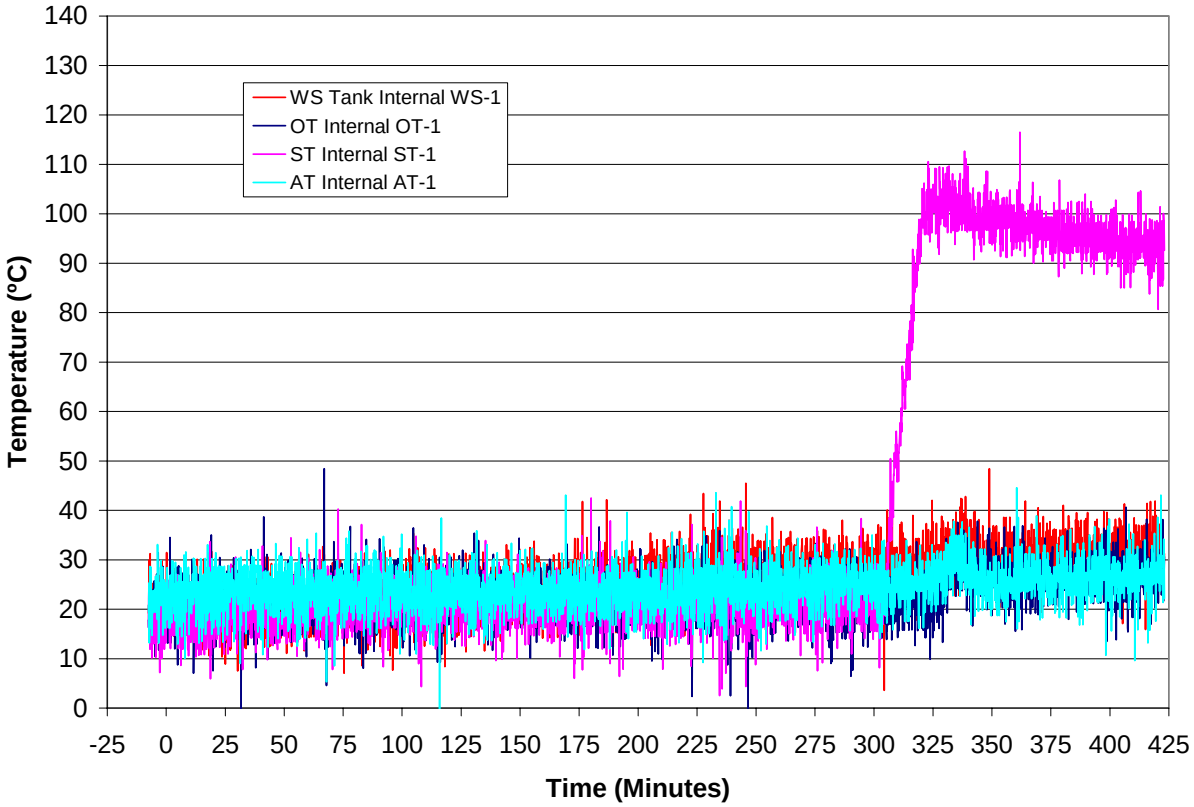

Figure B-38. Supply, Overflow, Spray, and Auxiliary Tank Water Temperature Data.

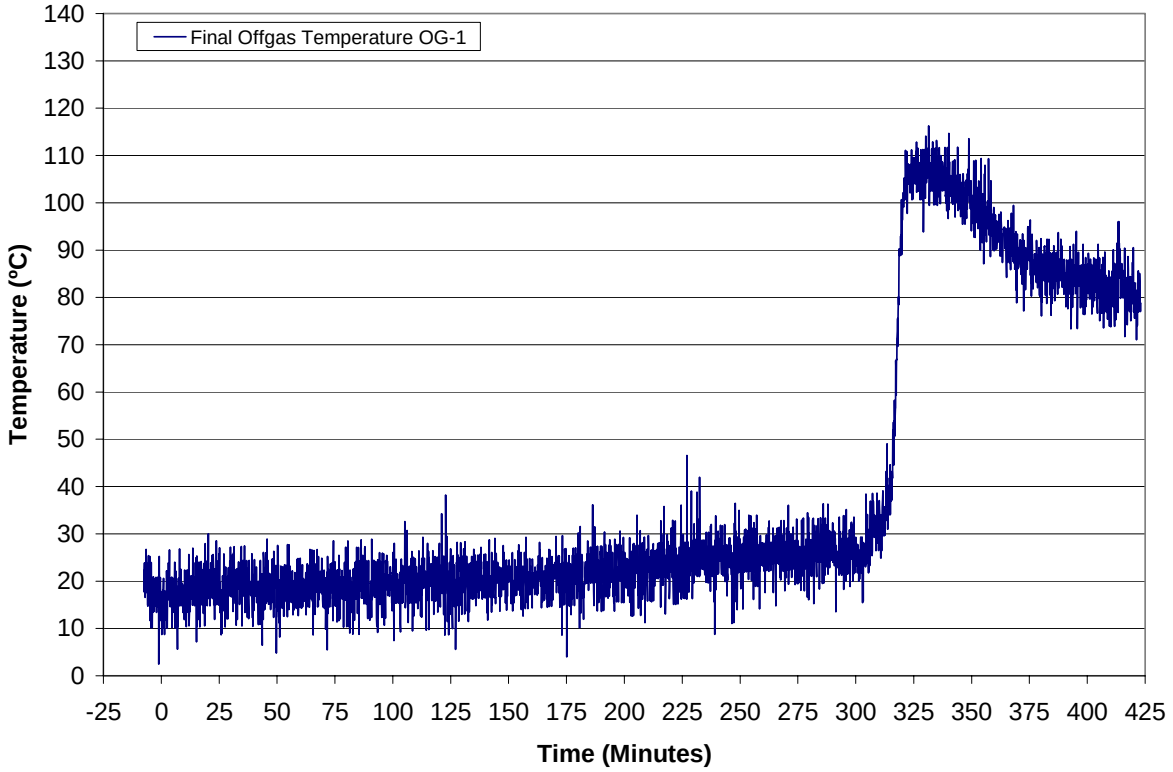

Figure B-39. Gas Temperature in Off Gas System.

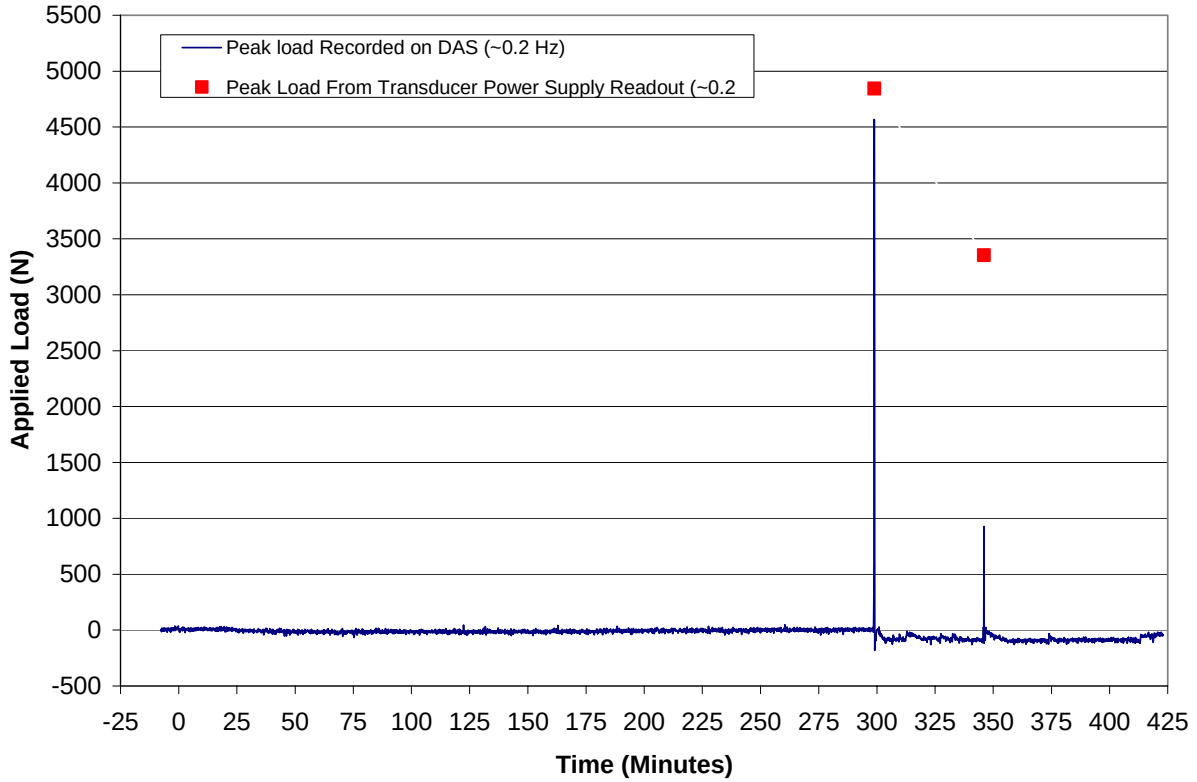

Figure B-40. Crust Lance Load Cell Data.

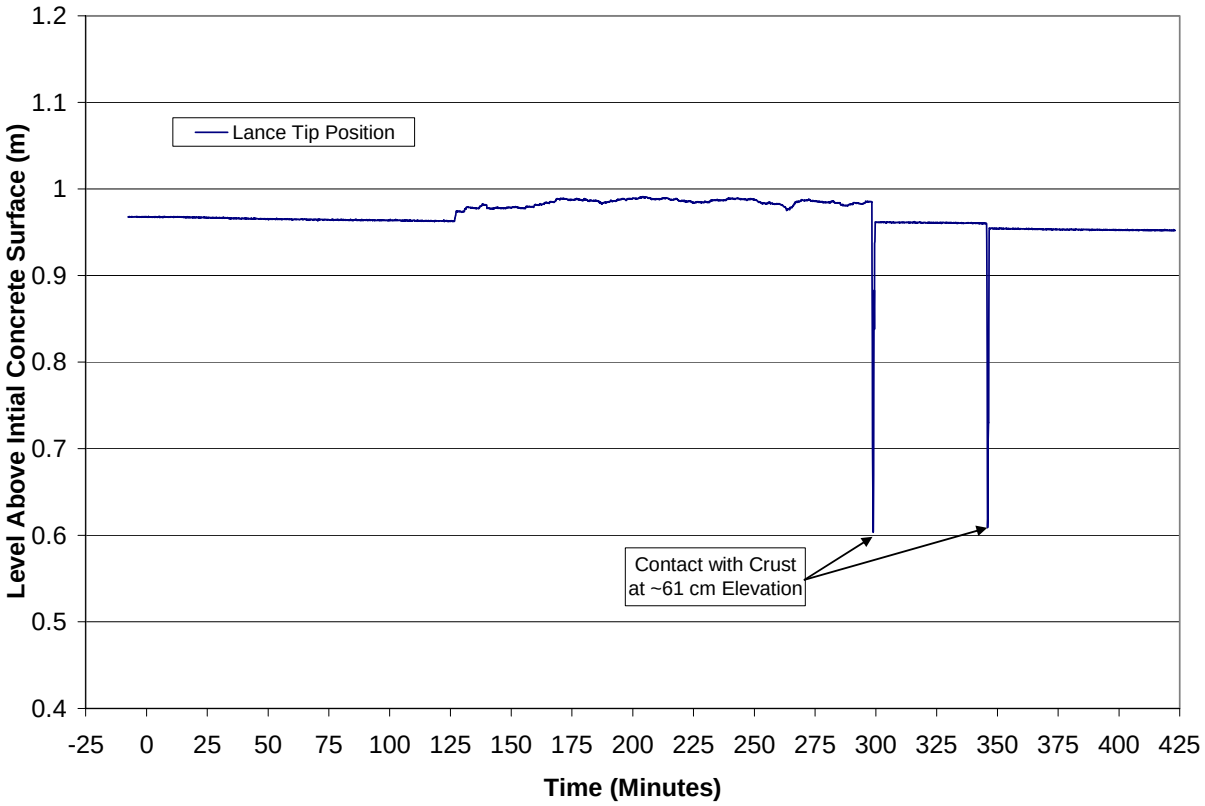

Figure B-41. Lance Position Indicator Data.

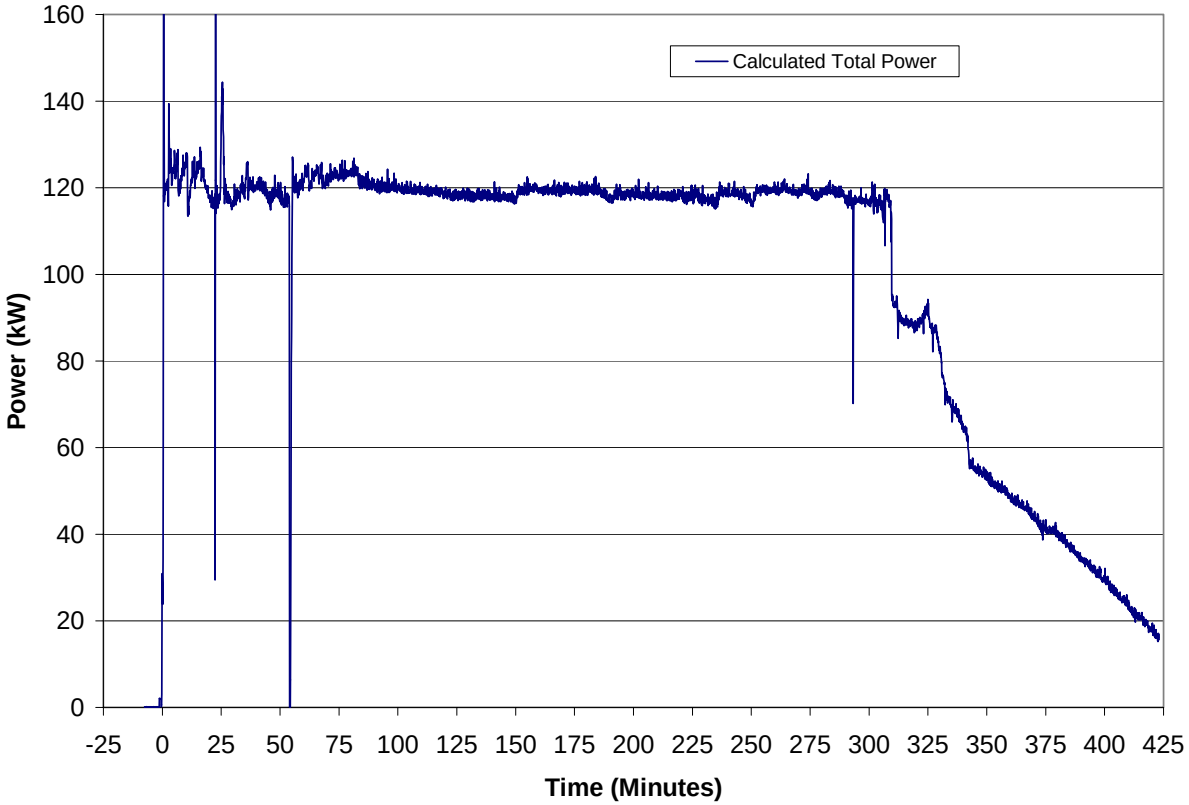

Figure B-42. Total Power Supply Power.

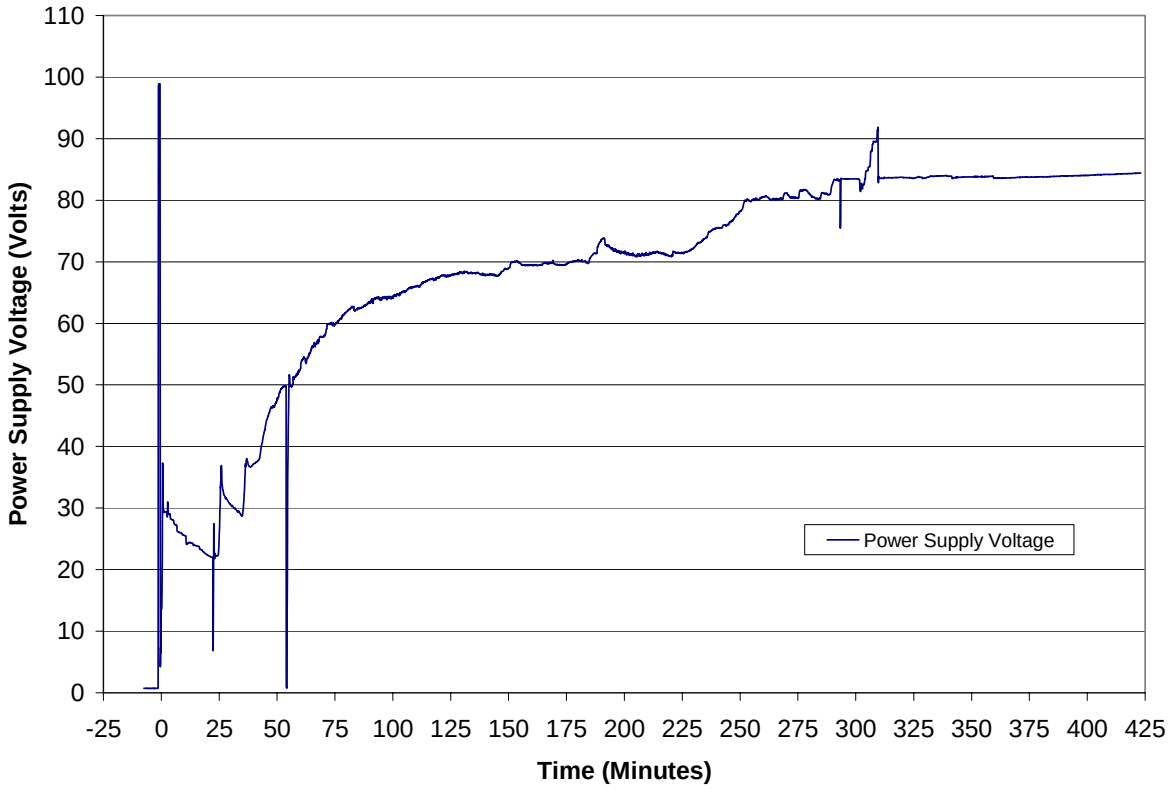

Figure B-43. Power Supply Voltage Data.

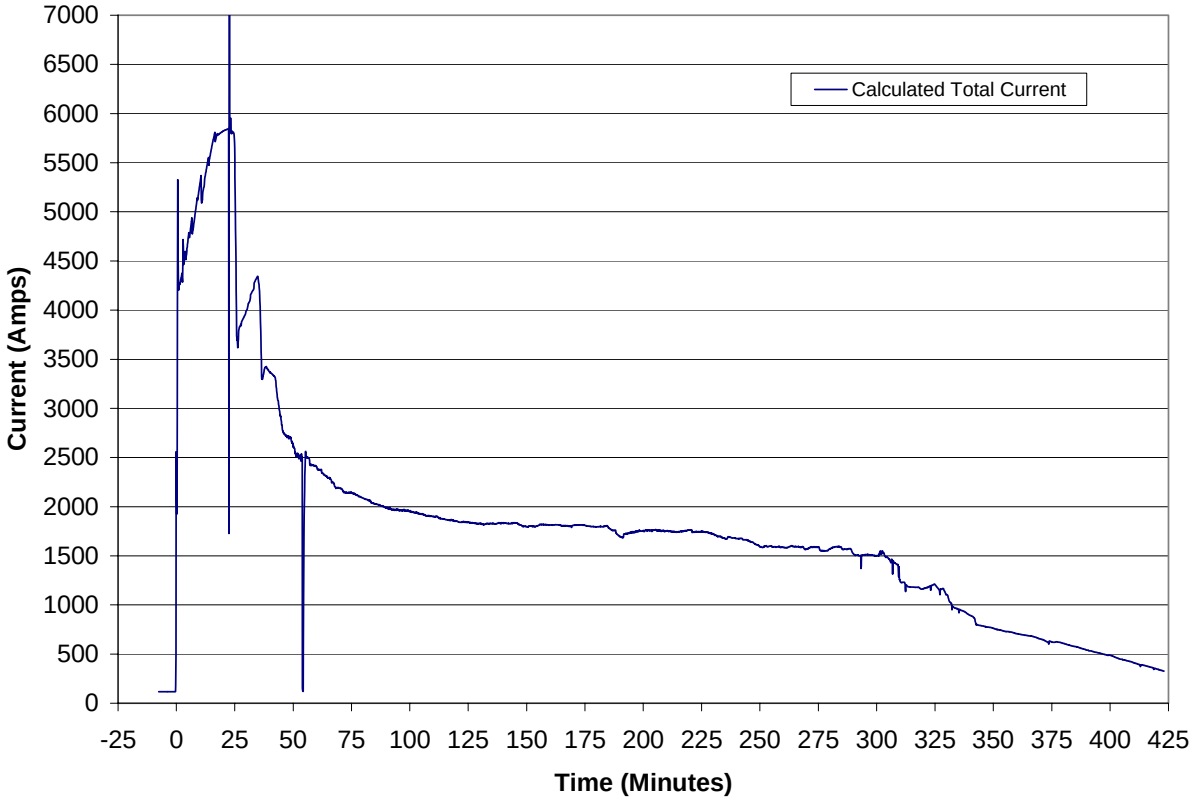

Figure B-44. Total Power Supply Current Data.

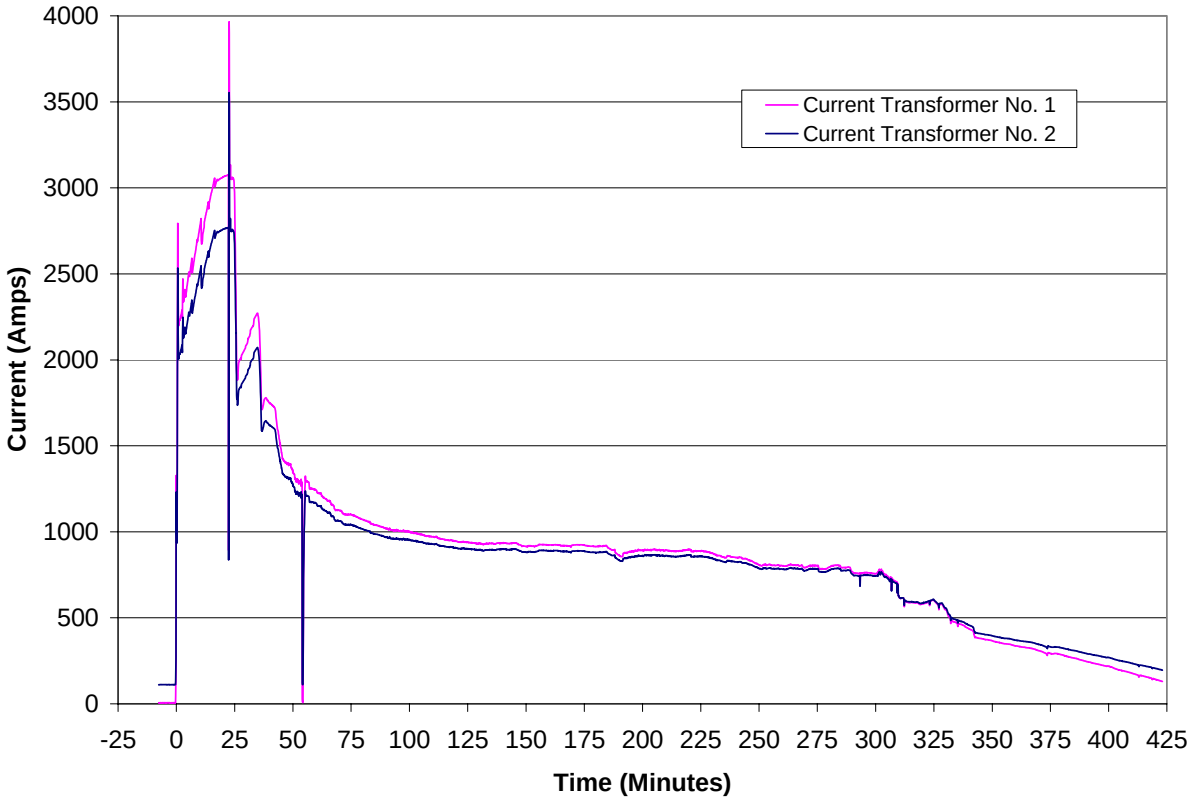

Figure B-45. Power Supply Current Transformer Data.

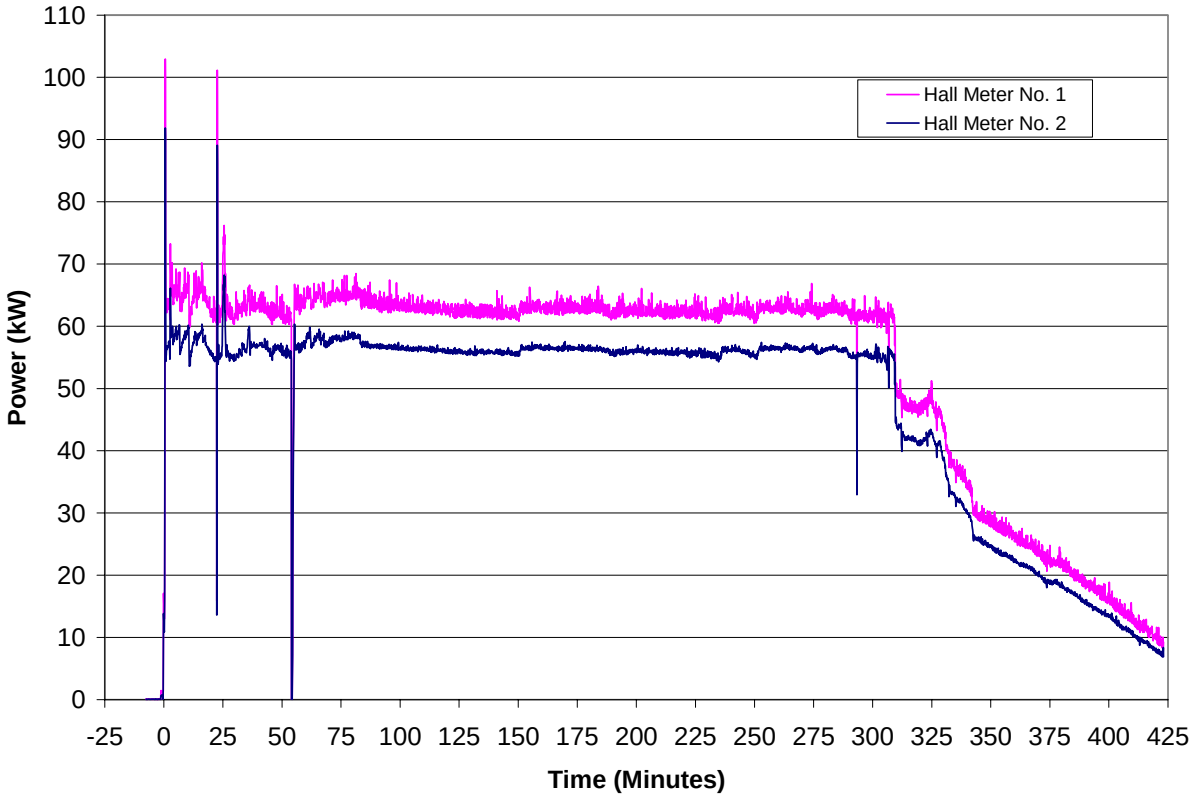

Figure B-46. Hall Effect Meter Data.

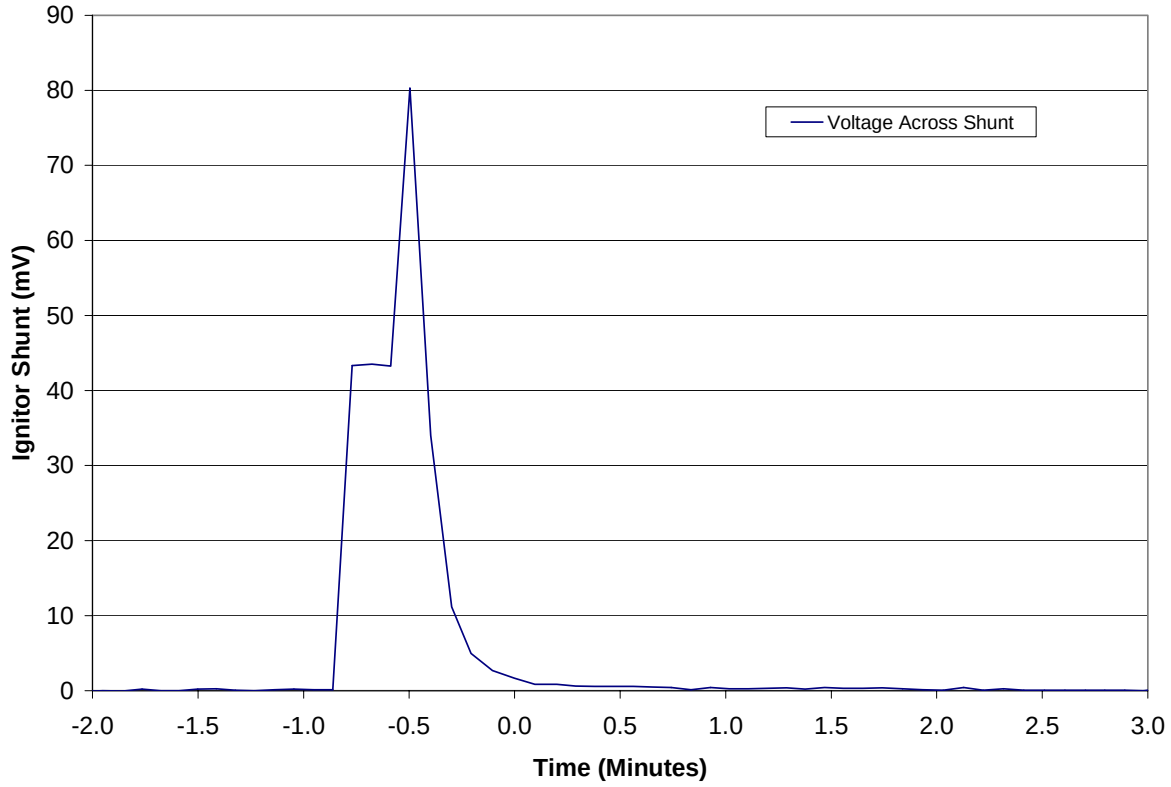

Figure B-47. Voltage across Igniter Shunt.

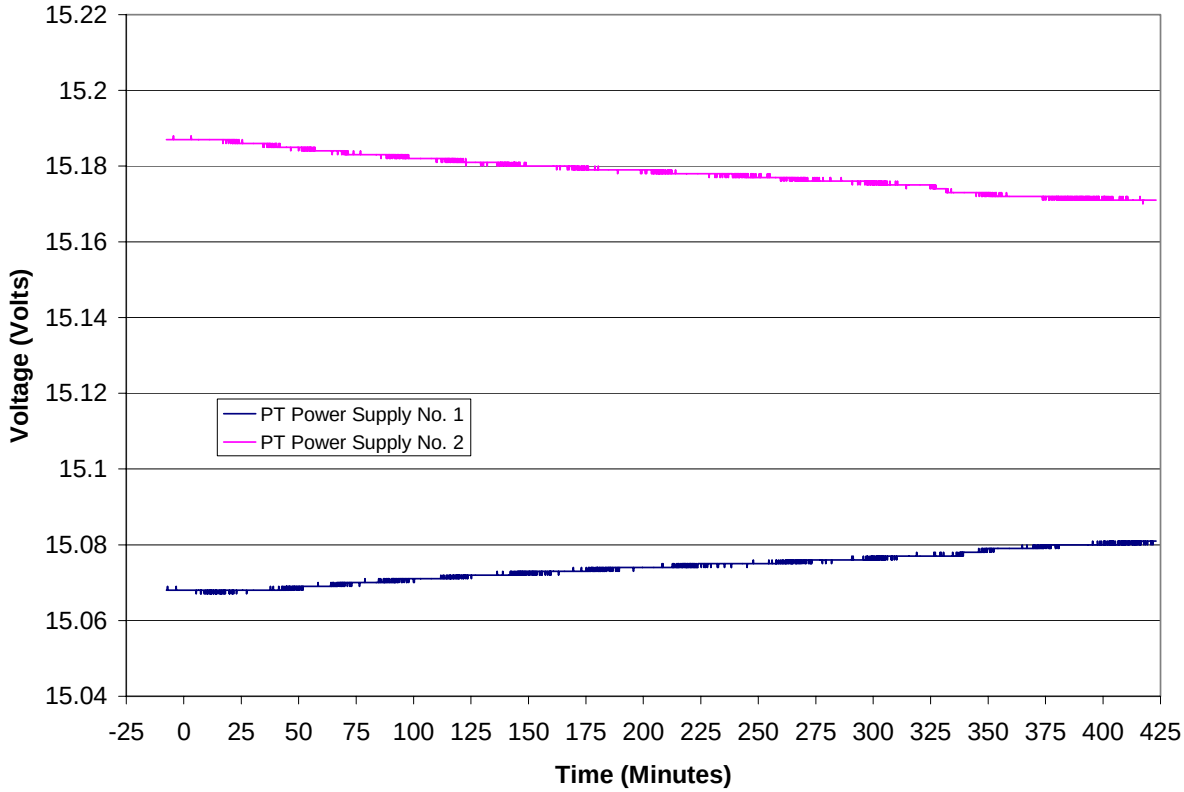

Figure B-48. Pressure Transducer Power Supply Voltages.

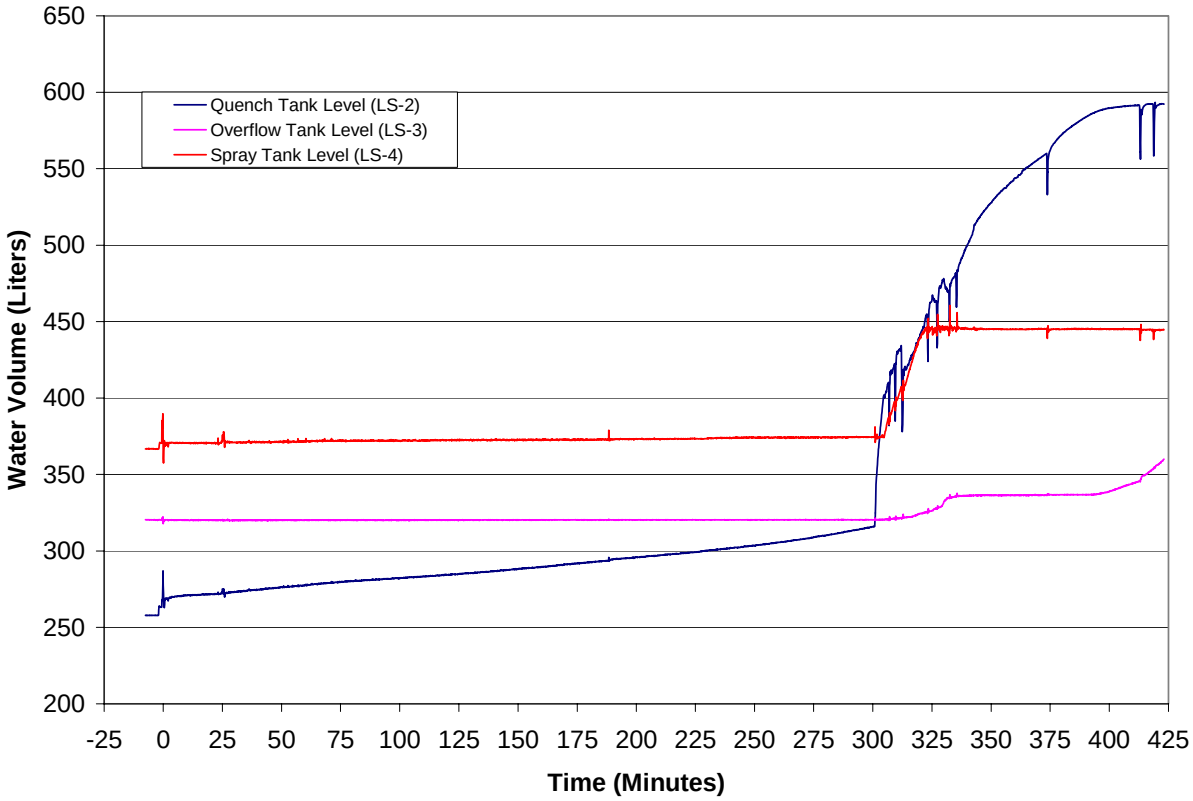

Figure B-49. Quench System Tank Water Volume Data.

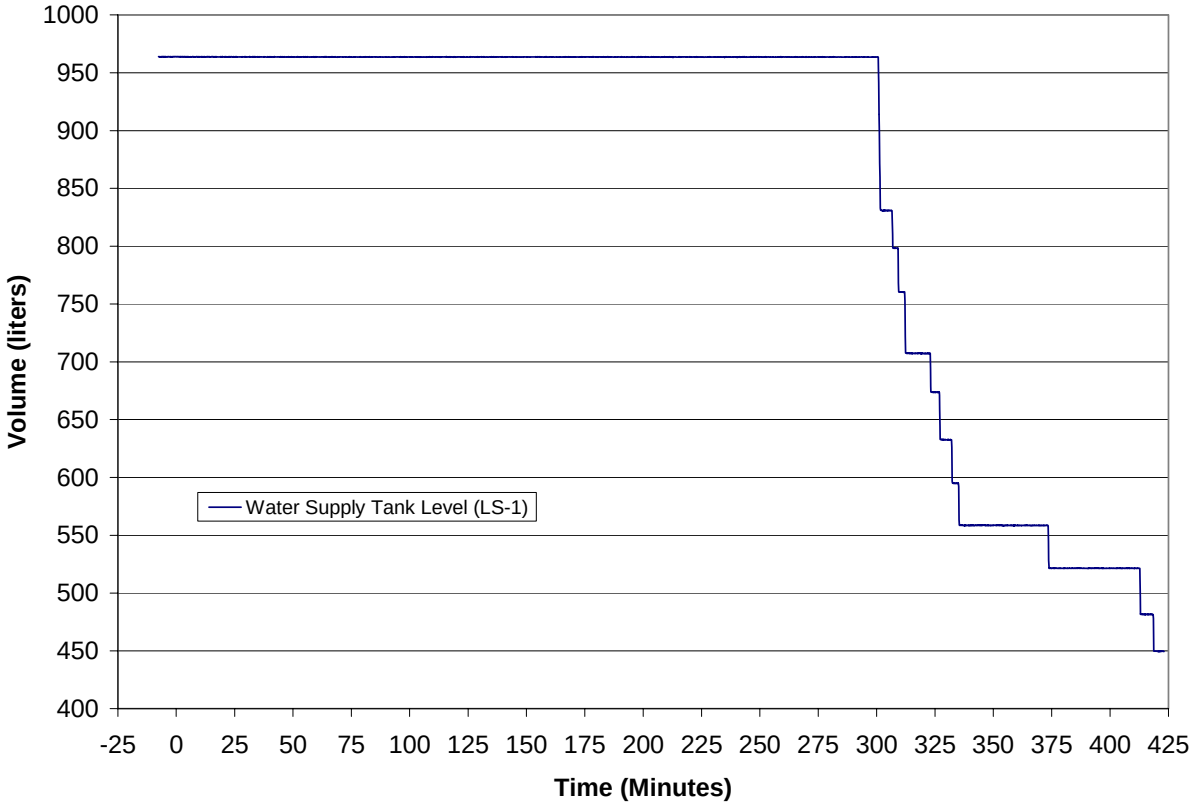

Figure B-50. Water Supply Tank Water Volume Data.

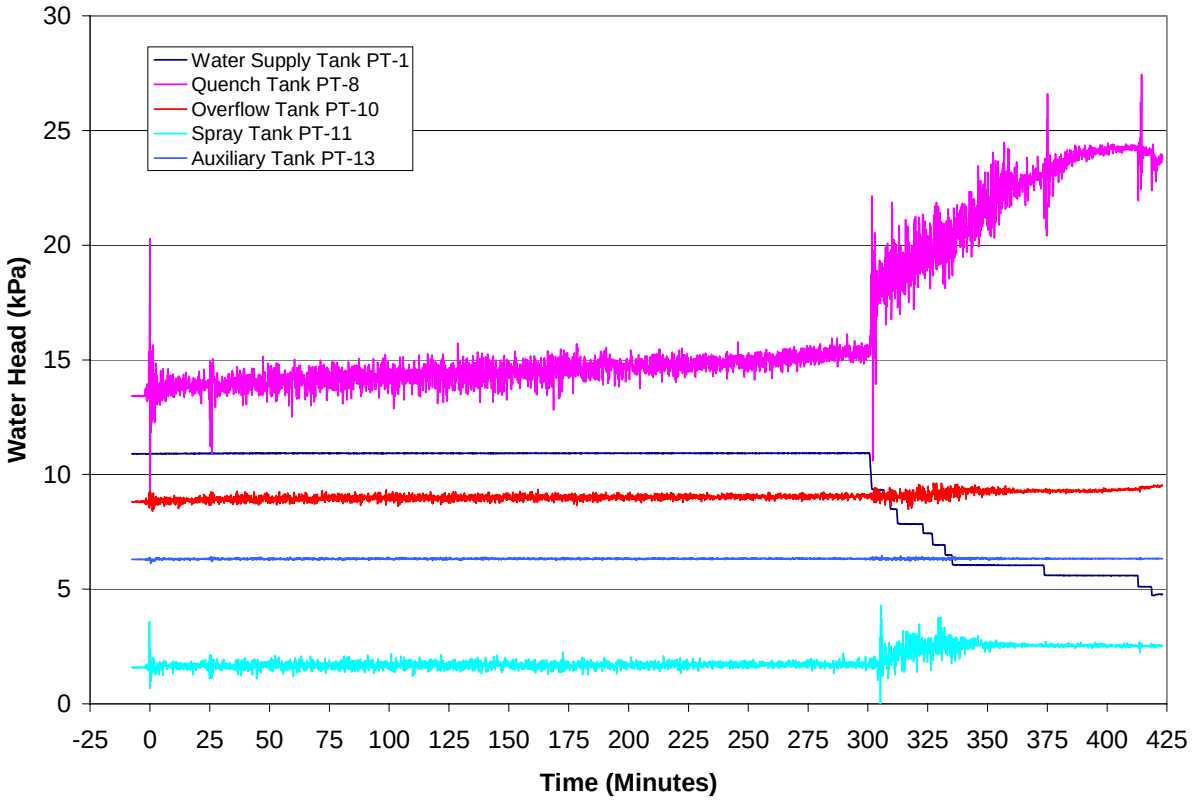

Figure B-51. Supply and Quench System Tank Head Data (Backup).

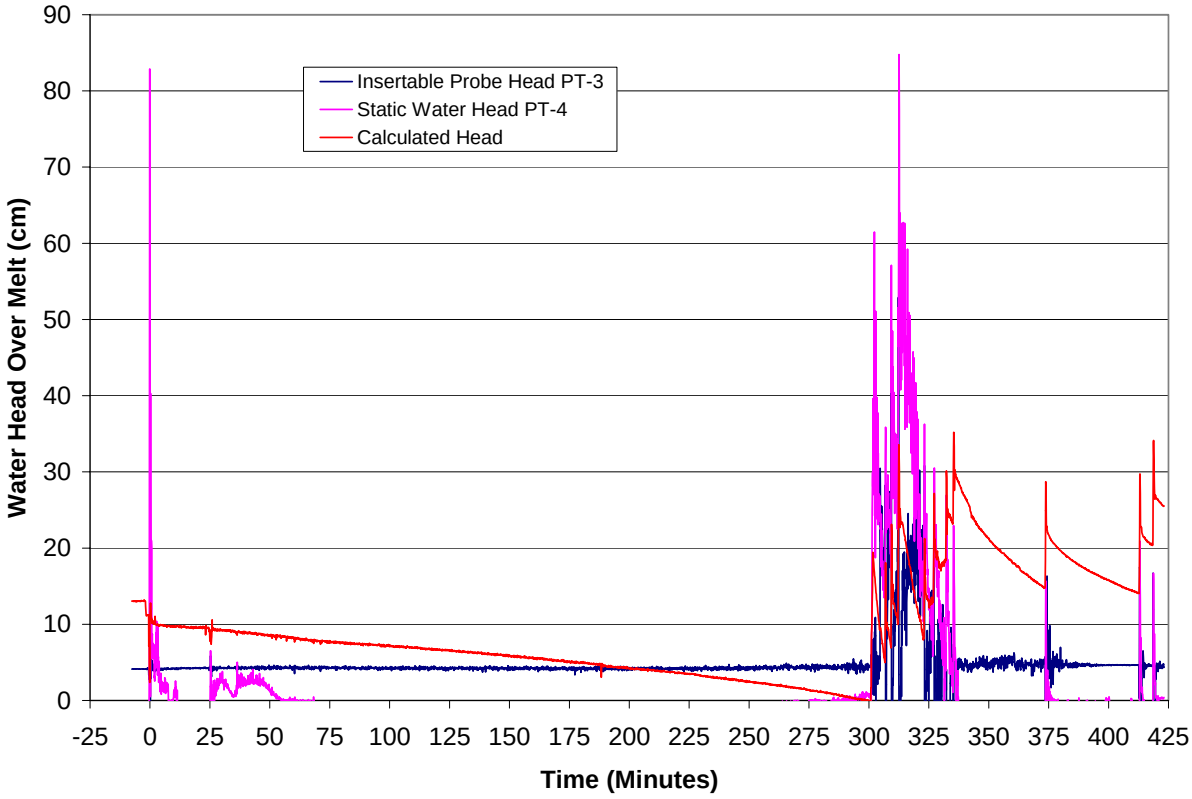

Figure B-52. Water Head over Melt.

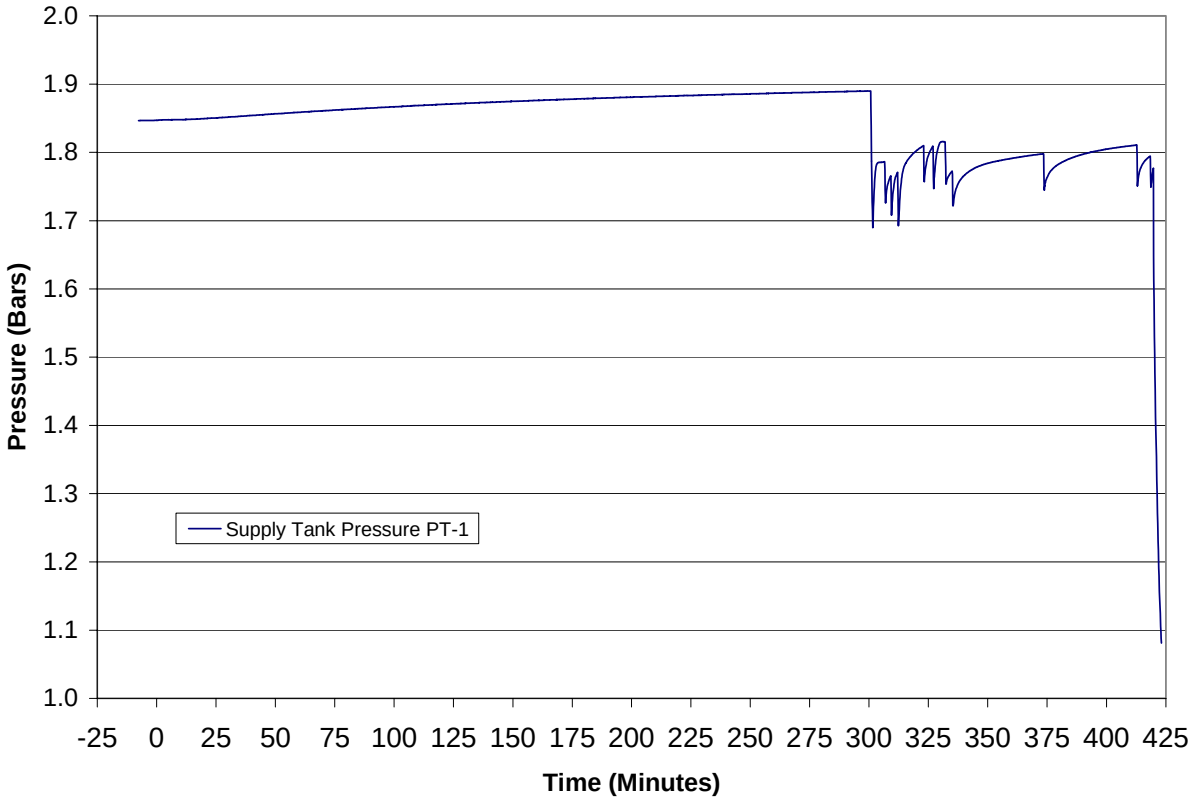

Figure B-53. Water Supply Tank Pressure.

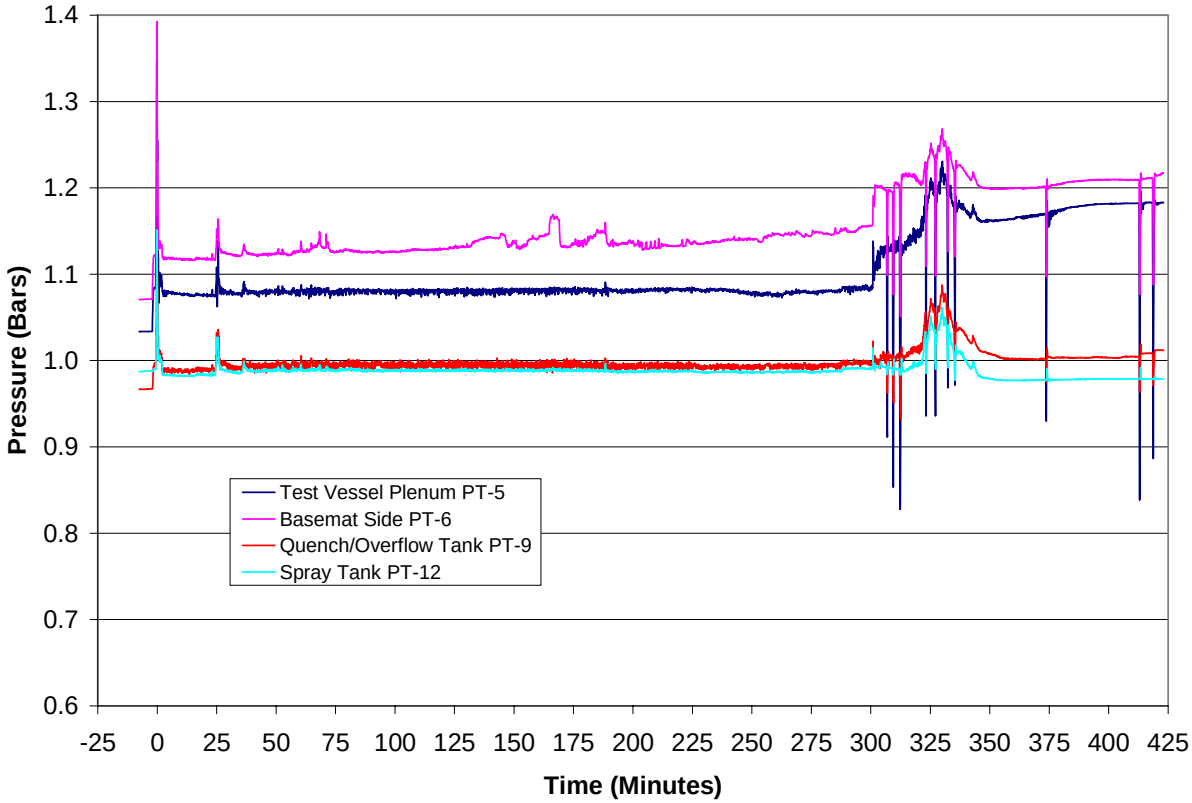

Figure B-54. Various System Pressures.

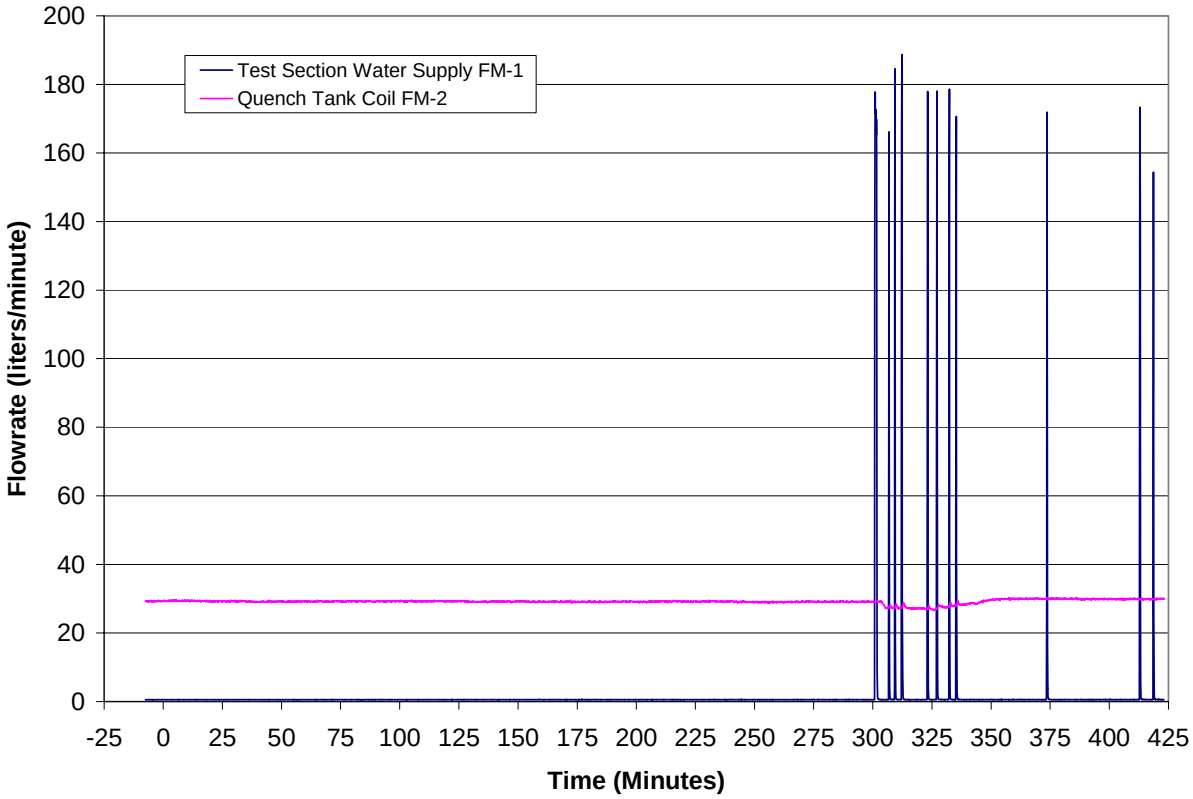

Figure B-55. Water Flow Rates.

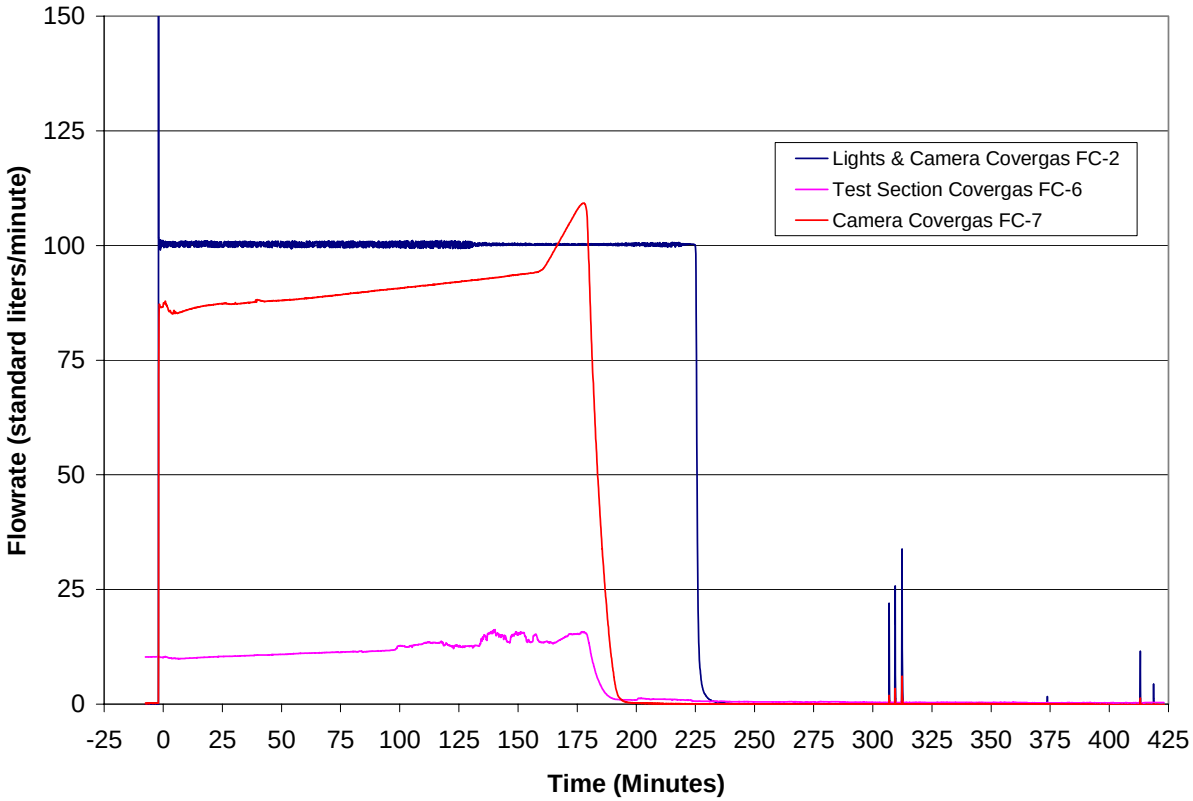

Figure B-56. Test Section Helium Cover Gas Flow Rates.

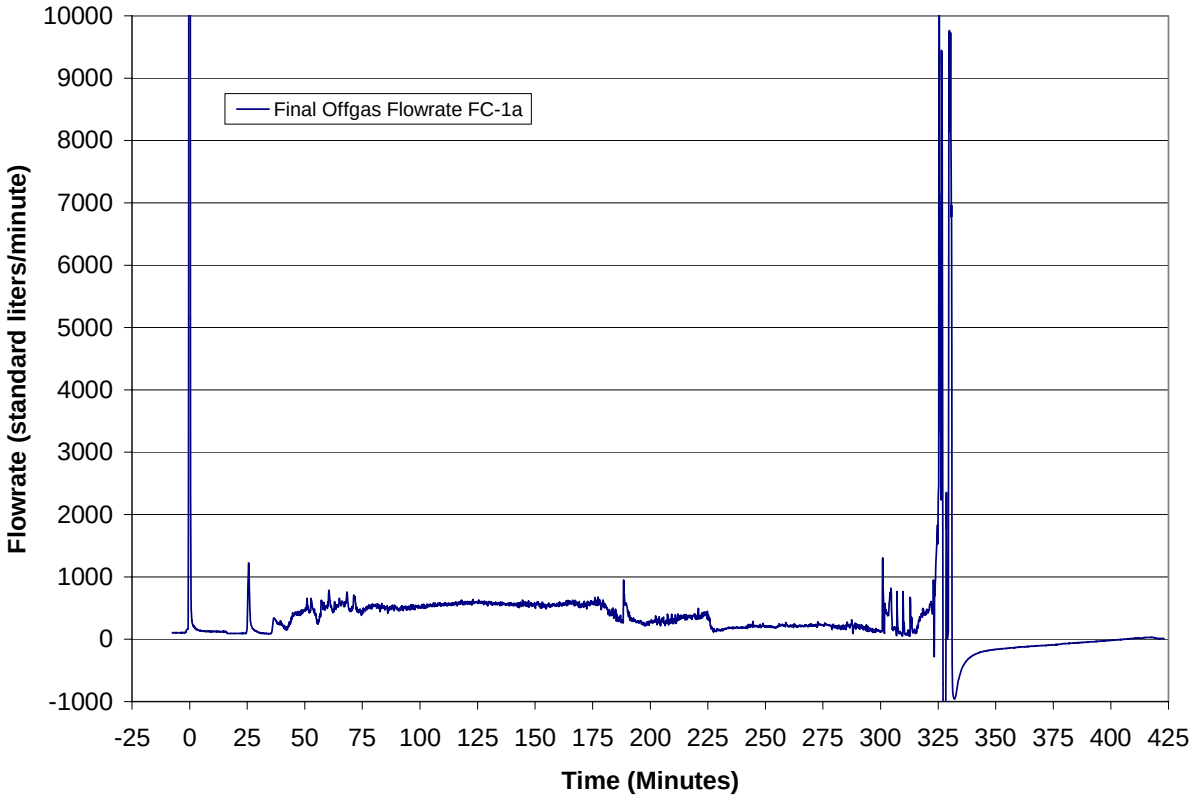

Figure B-57. Final Off Gas Flow Rate.